

Design Optimisation of a Safety Relief Valve to Meet ASME BPVC Section I Performance Requirements

Steven Taggart

Thesis presented in fulfilment of the requirements for the degree of
Doctor of Philosophy

Declaration

This thesis is the result of the author's original research. It has been composed by the author and has not been previously submitted for examination which has led to the award of a degree.

Signed: *Steven Taggart*

Date: 12/05/2021

Acknowledgements

I would like to express my gratitude to Dr. William Dempster for his guidance and encouragement, without him this research would not have been possible. I would also like to thank Andy Mowforth for his help throughout the last 4 years, his knowledge of relief valves and manufacture has been invaluable.

Finally I would like to acknowledge both Broady Flow Control Ltd and Strathclyde University for the resources provided for this research.

Contents

Declaration.....	ii
Acknowledgements.....	iii
Abstract.....	vi
Nomenclature	vii
1. Introduction	1
1.1 Overview	1
1.2 Design Tools	3
1.3 Objectives.....	5
1.4 Thesis Structure	7
2. Background Studies and Literature Review	10
2.1 Introduction	10
2.2 Background Studies.....	10
2.2.1 Standards	10
2.2.2 Operation.....	14
2.2.3 Working Fluid	21
2.2.4 Pressure Scaling	22
2.2.5 Dynamics.....	24
2.2.6 Design Methodology.....	25
2.3 Literature Review	33
2.3.1 Working Fluid	33
2.3.2 Pressure Scaling	35
2.3.3 Dynamics.....	36
2.3.4 CFD Literature Review.....	40
2.4 Summary	45
3. Mathematical Models	49
3.1 Computational Fluid Dynamics	49
3.1.1 CFD Configuration	53
3.1.2 CFD Verification and Validation	58
3.2 Description of Low-order Valve Model.....	95
3.2.1 Low-order Valve Model Governing Equations.....	95
3.2.2 Low-order Valve Model Verification and Validation.....	98
3.3 Discussion.....	109
4. Safety Relief Valve Operation	111

4.1	Experimental and CFD Analysis.....	111
4.1.1	Opening Process.....	112
4.1.2	Closing Process.....	121
4.2	Pressure Scaling	124
4.2.1	Low Lift Pressure Scaling.....	125
4.2.2	High Lift Pressure Scaling	138
4.3	Discussion.....	150
5.	Design methodology	156
6.	Optimisation	165
6.1	Optimisation Methods	165
6.1.1	Low-Order Valve Model Optimisation	165
6.1.2	Geometrical Optimisation.....	171
6.2	Optimisation Results	178
6.2.1	Force-lift Curve Optimisation.....	178
6.2.2	Geometrical Optimisation.....	180
7.	Optimisation Validation	189
7.1	Validation at 5 barg set pressure.	190
7.2	Validation at 9 barg set pressure.	192
7.3	Assessment at a 50 barg set pressure.....	194
8.	Discussion and Conclusion	198
8.1	Discussion.....	198
8.1.1	CFD Modelling.....	198
8.1.2	Pressure Scaling	200
8.1.3	Optimisation.....	201
8.2	Conclusion and Recommendations for Future Work.....	205
8.2.1	Conclusion.....	205
8.2.2	Recommendations for Future Work	206
9.	References	208
10.	Appendices.....	214
A.1	Low-lift Design Space Exploration	214
A.2	High-lift Design Space Exploration.....	219
A.3	Low-order Valve Model Matlab Code.....	222
A.4	Quasi-Steady Flow	225

Abstract

The understanding of fluid flow behaviour within safety relief valves invariably requires knowledge of strong pressure and velocity gradients with significant levels of turbulence in three-dimensional flow environments. In the case of gas service valves - the focus of this thesis - these flows will be super-sonic with multidimensional shock formations resulting in challenging design conditions. This thesis takes advantage of the development and validation of computational fluid dynamic (CFD) techniques in recent years to reliably predict such flows and investigate how the techniques can be used to produce better performing safety valves. Historically OEMs will have relied on an experimental based design approach using feedback from test data to guide the evolution of a valve design. Unfortunately, due to the complexity of these devices this method could require much iteration. However, it is now possible to combine CFD techniques and optimisation algorithms to search for improved designs with reduced development times. To date these techniques have had limited exposure within valve design studies.

This thesis investigates the development of a numerical based design procedure by combining validated CFD models optimisation techniques to seek valve trim geometries that improve opening and closing behaviour. The approach is applied to an ASME Section VIII certified valve and seeks to modify the internal trim to satisfy the improved performance requirements stipulated in Section I of the ASME Boiler and Pressure Vessel Code.

Nomenclature

Letter	Description
A	Area
d,D	Diameter
f,F	Force
F_s	Factor of safety
h	Cell height / dimension
H	Hessian matrix
J	Jacobian matrix
k	Spring stiffness
l	Litres
m	meters / mass
M	Metric thread
Ma	Mach number
N	Newtons
p,P	Pressure
r	Radius / non-integer level of refinement
s,S	Seconds
t	Time
u	Velocity vector component
v	Velocity vector component
x,X	Distance / displacement

Greek Letter	Description
Γ	Diffusivity
Δ	Small difference
ε	Turbulent kinetic energy dissipation / relative error
κ	Viscosity ratio

λ	Lagrangian multiplier
μ	Dynamic viscosity
ρ	Density
Σ	Sum
τ	Shear stress
∇^2	Lagrangian operator

Acronym	Description
API	American Petroleum Institute
ASME	American Society of Mechanical Engineers
CFD	Computational fluid dynamics
DAQ	Data acquisition
DN	Nominal Diameter
GCI	Grid convergence index
LVM	Low-order valve model
ODE	Ordinary differential equation
PDE	Partial differential equation
PRV	Pressure relief valve
PSI	Pound per square inch
PTC	Performance test code
SRV	Safety relief valve
SST	Shear stress transport

Term	Definition
Normalised Pressure	$\frac{p}{p(gauge)}$
Normalised Force	$\frac{Force}{P(gauge) \times Area}$ where area refers to the sealing face area.

1.Introduction

1.1 Overview

Fluids are ubiquitous throughout industry with applications from transporting materials to cooling nuclear reactors. Fluid systems generally operate above atmospheric pressure which introduces a risk that requires close observation. A pressure increase could lead to a loss of structural integrity and would have dire consequences. Such an increase could result from a breakdown of a cooling system, external heating of a pressure vessel or a runaway chemical reaction. Consequently, safeguards must be established to protect these systems from this type of incident - one of the most common pieces of equipment used is a pressure relief valve. Fluid behaviour within these devices can contain complex turbulent flows with high velocity and pressure gradients; understanding these flows and their impact on design can present significant challenges for a manufacturer. Pressure relief valves are self-actuating devices that function by acting as a weak point in a pressurised system. A typical spring loaded safety relief valve is presented in figure 1.1. They are designed to open and release fluid at a specified pressure and this will remain open until the system returns to safe working pressure levels. These devices are often the last line of defence against overpressure events, thus their reliability and performance is crucial to the structural integrity of a pressurised system. Unfortunately, the complexity of these devices is often underestimated, resulting in an ineffective design which could lead to industrial accidents.

Historically, manufacturers relied solely on physical testing to assess their products, however numerical modelling offers another technique to gain insight to their operation.

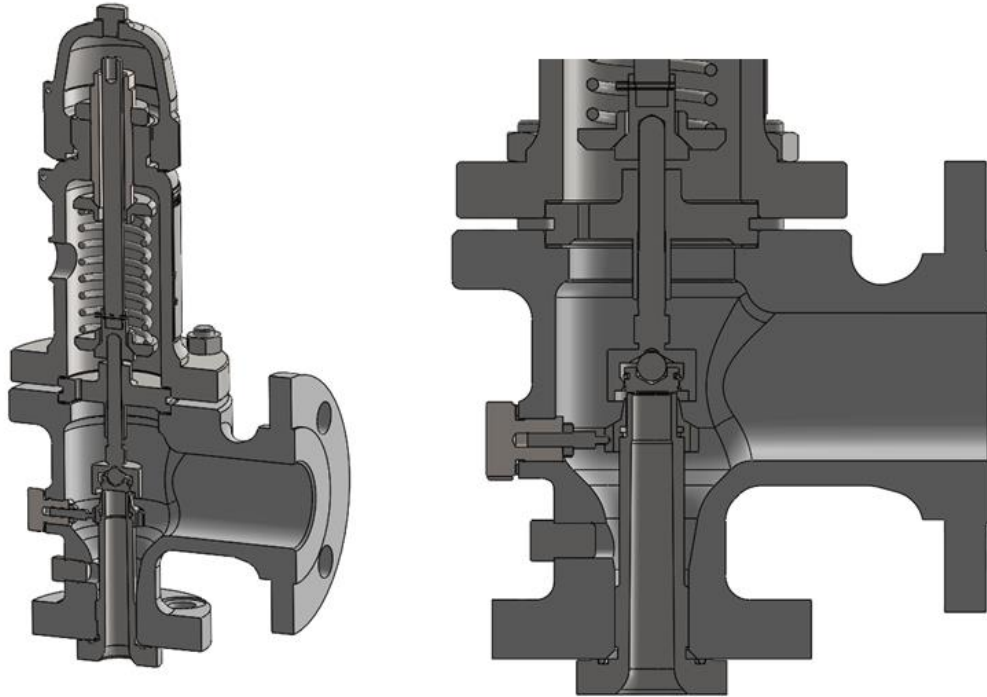


Figure 1.1 – CAD image of a typical ASME type safety relief valve.

Numerical modelling is nonintrusive thus it provides a means of studying fluid behaviour within a valve without affecting the flow in anyway; achieving this experimentally would be extremely difficult. The information obtained from such a numerical method could have a significant impact on the design process and potentially reduce the lead time to get new products to market.

There are many relief valve failures documented throughout industry, Lochbaum (2015) highlighted events in the nuclear industry, focusing on two main issues, failure to opening when required and failure to reclose after opening. In his report, the Pilgrim Boiling Water Reactor (BWR) (Massachusetts, USA) was going through a planned cooldown event and a safety relief valve (SRV) failed to operate when manually actuated. On the same site another SRV was unable to operate manually after an unplanned shutdown. During a planned

shutdown at the Browns Ferry BWR (Alabama, USA), 8 of 13 valves required significantly higher pressures to open. Furthermore, at Pilgrim, the BWR was shut down due to a leaking SRV, upon dismantling the device no clear indication was found to the cause of failure (Lochbaum, 2015). In the research report RR162 (NEL, 2003) compiled for the Health and Safety Executive, an analysis of all valve related hydrocarbon releases was undertaken. Of these incidents 12% were a result of relief valves and the working fluid was predominantly gas. It was reported that six incidents occurred above the maximum allowable working pressure rating with one being over 150% of the pressure rating.

NEL reported that the primary issues of these devices were mainly due to mechanical fatigue and failure, it was reasoned that this is due to faulty design in the original device. From the small number of incidents listed, it is shown that relief valve operation can be unreliable, supporting the notion that these valves are difficult to design. Considering that they are one of the last lines of defence of an overpressure incident it is crucial that they work as intended under all conditions.

1.2 Design Tools

Traditionally relief valve design would have been undertaken using experimental methods. This experimental approach would rely on physical data as a means of measuring the suitability of a given design. This feedback approach to design could result in numerous iterations to obtain an optimal geometry whilst offering little opportunity to gain an understanding to the fluid behaviour within a device. The primary benefit of experimental techniques is that they are a direct measurement of the way a valve would operate under

those conditions - the data obtained at test conditions would be more accurate representation of how each device would operate in the field. However, the weakness of this approach is that the test conditions are generally limited. As valves are frequently required to operate at high pressures or high flow rates, it is difficult to recreate these conditions in a laboratory. Moreover, the measurement process is generally intrusive, so obtaining data can affect the valve behaviour and give a false representation of a given configuration.

Numerical modelling introduces an alternative to physical testing, once the preserve of large corporations and research institutes, these techniques are now common place throughout industry. Driven by the exponential increase in computing power, mathematical modelling tools are now becoming an essential instrument for all design and analysis. The vast applications available coupled with an increasingly user-friendly software has resulted in its adoption in many different fields. Computational fluid dynamics (CFD) is a branch of numerical modelling that solves the governing equations of fluid flow. The output of this technique is a numerical representation of the fluid behaviour throughout a given domain. The calculated field offers significantly more information than that available through physical experiments. Having a numerical representation of the fluid behaviour throughout an entire system significantly increases the understanding of the underlying physics, gaining this level of detail experimentally would be near impossible.

Whilst CFD analysis could decrease the development time of a relief valve it could still involve many iterations to reach a given goal. Due to the often-counterintuitive behaviour of fluids it can be difficult to make geometry change decisions in the design process. This can be further complicated by the complex flow path that is found within a relief valve. When faced with such a task it is common to utilise optimisation algorithms as these can help guide parameter changes to attain target behaviour. In the context of CFD analysis, these algorithms could be utilised to change the shape of the geometry and guide the design towards one of improved performance. The application of these techniques to valve design is the main focus of this research study.

1.3 Objectives

Currently the design techniques used for safety relief valves rely on a feedback approach and results in extensive design & development time. It is proposed that significant improvements to the design process could be realised by introducing numerical methods from the initial design conception. The following objectives should be able to address the accuracy of this hypothesis.

- Undertake a review of the current literature on SRV design. This process should give insight into recent progress being made within SRV design and analysis. Also, by consulting the relevant standards and specifications, the performance requirements could be obtained and this will provide a target for performance improvements.
- Determine the capabilities of CFD modelling in SRVs. If these methods are to be utilised to improve the design process, their accuracy and robustness needs to be

quantified. In doing so the data obtained will be examined to provide a thorough explanation of SRV operation and the fluid behaviour within them.

- Asses the reliability of the quasi-steady state assumption to SRV analysis. It is a common approach that the behaviour of an SRV can be modelled using several steady state calculations to represent the transient opening process, this assumption needs to be evaluated before use throughout this research.
- Undertake an investigation into the capabilities of a low-order valve model (LVM) of the dynamics of an SRV. If appropriate, this method can provide a computationally efficient model to evaluate the opening and closing behaviour of a relief valve. This will be used in conjunction with CFD modelling to produce a dual model technique in valve design.
- Develop an effective optimisation process that can be used in SRV design. This is the main objective of this research and will focus on optimising the internal components of an SRV to improve the opening and closing performance.
- Carry out a geometrical optimisation of the internal components of an SRV using the developed optimisation process. This process should be able to demonstrate the capabilities of the developed optimisation method and whither it can provide any improvements to the lead time in SRV design and development. The technique will be validated by manufacturing the optimised valve and undertaking a series of experiments to measure its performance.

1.4 Thesis Structure

An overview of the issues involved in relief valve design has been presented and potential opportunities for improvement through numerical modelling have been highlighted. This research aims to evaluate the suitability of numerical optimisation techniques in the context of relief valve design. The thesis chapters comprise of the following:

1. Introduction

Overview of research, context and objectives.

2. Background Studies and Literature Review

Review of safety relief valve operation and the current literature in safety relief valve design. This will provide a basis for the knowledge and understanding that can be built upon to improve the design process.

3. Mathematical Models

A review of the mathematical models used for studying SRV behaviour is undertaken and an explanation of the different techniques used throughout this research is made. Also included is a verification and validation of these techniques. This is necessary to prove that the physics and models in use are applicable to the research being undertaken.

4. Safety Relief Valve Operation

This chapter provides a description of SRV operation paying particular interest to the fluid mechanics within the device, the effects of pressure variation will also be discussed. This chapter will build upon the discussion presented in the previous chapter and give a description of the physics involved specifically for the SRV used in this study.

5. Design Methodology

Presented within chapter 5 is the choice of design parameters used for the optimisation process. From the previous work undertaken in chapter 4, the key parameters to control the behaviour of an SRV will have been exposed. A justification to the choice of parameters will be included alongside a CAD model of the base valve prior to optimisation.

6. Optimisation

Chapter 6 will cover the optimisation process and the choice of models used, included within this chapter are the results obtained from the optimisation process. The design obtained through the numerical optimisation will be shown and a full CFD simulation of the final valve geometry will be included.

7. Optimisation Validation

Chapter 7 will present the results from validating the optimisation process through physical testing. From this data, the capabilities of the optimisation process will become clear. Using several different measurement methods, the accuracy of the optimisation process will be measured, this will include disc force measurements, dynamic behaviour and also opening and closing performance of the device.

8. Discussion

Chapter 8 will discuss the outcome of the optimisation procedure, evaluating it against the initial objectives. Here the final result can be compared with the initial target for this research.

9. Conclusion & Recommendations

Finally, the thesis will close with a conclusion of all the work undertaken within this research and include any future recommendations that could build upon this research.

10. Appendices

The data obtained throughout the design space exploration stage will be included and also a copy of the low-order valve model code.

2. Background Studies and Literature Review

2.1 Introduction

This chapter will present a review of the current literature on safety relief valve design and operation. To begin, an introduction to the governing standards for relief valves shall be presented, this will be followed with a brief outline of pressure relieving devices and how they operate. The main body of this chapter will review the key aspects involved in relief valve design, and using the currently available literature, the technical status and progress made in these areas shall be evaluated. Recent progress in advanced modelling approaches - particularly computational fluid dynamics (CFD) - provides an opportunity to understand valve flow physics more deeply and the relationships between design geometry and performance. Since the basis of this study is to develop and apply modelling techniques effectively, this chapter will emphasise the progress made in using numerical modelling methods in the design process and if they have offered any increase in design efficiency.

2.2 Background Studies

2.2.1 Standards

Pressure relief valves are required to be installed on most pressurised systems; this is a regulatory requirement to protect the structural integrity of the components in the event of an overpressure incident. In an effort to provide some standardisation and consistency across the field of pressure system design, standards and certifications have been developed by governing bodies to ensure that manufacturers supply products that are suitable for the desired application. One such body is the American Society of Mechanical

Engineers (ASME), a non-profit organisation that has produced a code of conduct for pressurised systems. Their Boiler and Pressure Vessel Code (BPVC) was developed in response to several accidents from boiler explosions in the early 1900s when it was recognised that some level of standardisation was required.

There are 12 sections to the BPVC which cover a range of different pressurised system requirements. For a pressure relief device to be classed as compliant under the BPVC, certain performance requirements must be met, this is verified by physical testing of the devices carried out by the National Board of Boiler and Pressure Vessel Inspectors (NB). The specifications cover a wide range of structural and performance criteria and dictate how the device should perform under different conditions. Certain BVPC sections have specific performance requirements for pressure relief devices, these are specified as a maximum allowable overpressure and blowdown. The most stringent of these being BVPC Section I – Rules for Construction of Power Boilers. This code specifies the requirements for power boilers, steam generators and super heaters. As a consequence of the vast span of pressures that these systems could operate under, a range of overpressure and blowdown limits are specified rather than one value. Presented below in table 2.1 are the performance requirements given in ASME Section I for pressure relief devices. The maximum allowable blowdown figure varies over the full pressure range, however the minimum blowdown is a constant 2 psi or 2% of set pressure (whichever is greater), similarly the maximum overpressure figure is 3% over the full pressure range.

Set Pressure (psi)	Minimum Blowdown	Maximum Blowdown	Overpressure
< 67	2 psi or 2%	4 psi	3%
≥ 67 and ≤ 250	2 psi or 2%	6 %	3%
> 250 and < 375	2 psi or 2%	15 psi	3%
≥ 375	2 psi or 2%	4 %	3%

Table 2.1 – ASME Section I pressure relief device performance criteria.

The manufacture and construction of safety relief valves also complies with further codes in addition to ASME certification. The American Petroleum Institute (API) provides the globally adopted recommended practice (RP) for sizing and manufacture of pressure relieving devices used throughout the oil and gas industry. API RP 526 (API, 2017) is a standard pertaining to flanged steel pressure relief valves, the document covers both direct-spring loaded and pilot operated devices. Requirements are provided for the following:

- i. Orifice designation and area.
- ii. Valve size and pressure rating, inlet and outlet.
- iii. Materials.
- iv. Pressure-temperature limits.
- v. Centre-to-face dimensions, inlet and outlet.

The benefit of having standardisation in industry is that it provides geometrical consistency across many manufacturers and devices. API RP 520 (API, 2000) provides a recommended orifice area size that is adopted throughout industry. In doing so, this allows manufacturers

to adopt specified orifice areas and provides customers with a means to compare products from different companies. Similarly, specifying centre to face dimensions for pressure relief devices has the benefit of simplifying pipework design for each application. Being of a set size gives a customer the option to swap out one manufacturer's valve for another whenever needed. This ability causes the pipework design process to be more flexible in that the exact valve does not need to be specified during the design phase.

API RP 526 also covers pressure-temperature limits and valve size and pressure ratings. These remaining topics are concerned with the structural integrity of the devices. The pressure-temperature limits are directly connected to the designated material being used; from this information a customer can obtain the correct material for their application. Provided in API RP 526 are the required flange ratings for each application covering all sizes and pressures, further information on flange rating can be obtained in ASME B16.5 (ASME, 2017). The API recommended practices are adopted globally throughout the process industry; however, the ASME codes are law within the USA and must be used. Other standards exist throughout the world which provides similar specifications to the ASME codes, for example, the European Community is covered by the Pressure Equipment Directive (PED).

From the information presented it is shown that although a significant number of standards and specifications governing pressure relief valve design exist, the design and manufacture of the internal trim (valve disc, nozzle and disc adjustment rings, etc.) are not defined and are the responsibility of the manufacturer. As the design of the components around the disc

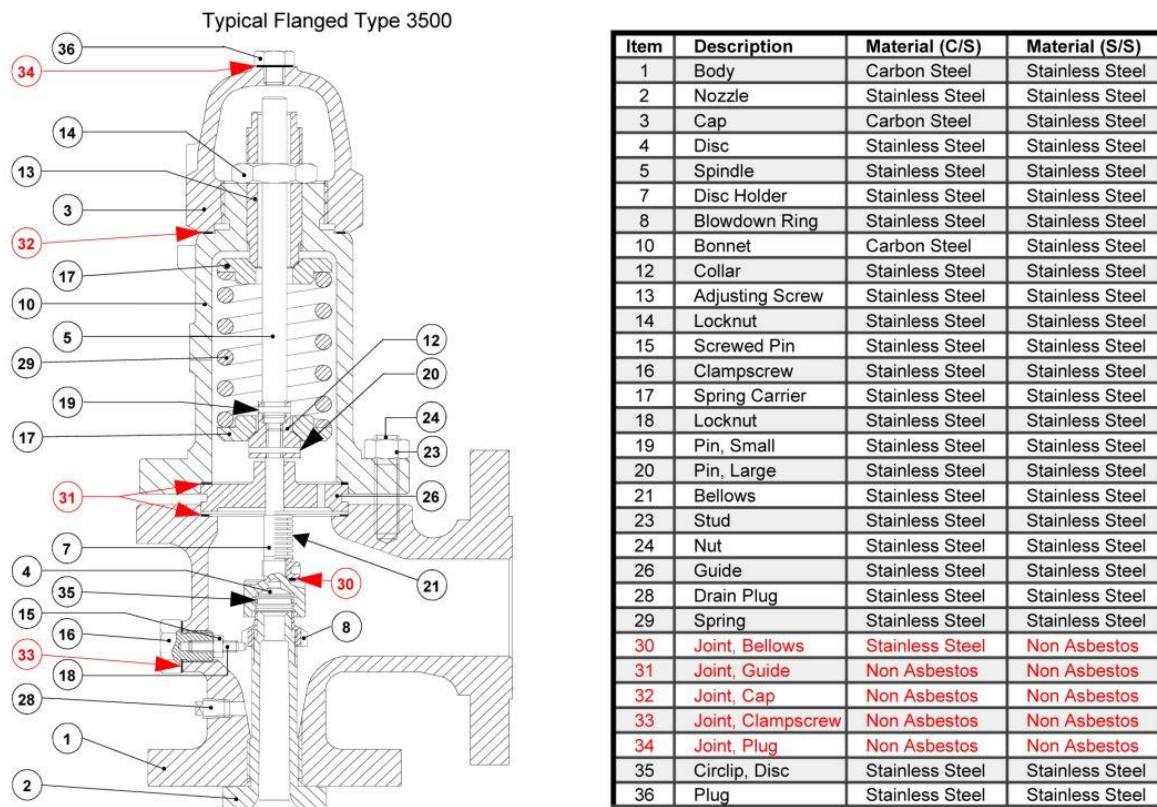
face and nozzle exit control the performance of each device, the devices may appear similar externally but produce vastly different operational characteristics.

2.2.2 Operation

Pressure relief devices come in many different forms, their one common feature is that they act as a controlled weak point in a pressurised system and are designed to open at a specific pressure. Pressure relieving devices can be categorised into two different types, non-reclosing and reclosing. Non-reclosing devices - like rupture discs - open at a set pressure to release contained fluid but cannot reclose after they have opened. Reclosing type devices are able to recover a seal once they have opened and return a pressurised system back to a normal working condition. Within reclosing type devices are pressure relief valves (PRV) and safety relief valves (SRV), the difference between these types is in the way they operate and the system pressure that they are designed to open at. PRVs are designed to open proportionally to the degree of pressure increase within a system, thus a small level of pressure increase would result in a PRV only opening the required amount to return the system to safe working levels. In the event of a PRV not providing adequate protection against a pressure increase, an SRV would operate, these devices are characterised by a faster action than PRVs as they are the last line of defence for the system. Due to their design, a small level of pressure increase should be all that is required to fully open an SRV; this ensures that if they have to operate, they can quickly return the system to a safe working pressure. This rapid opening of the valve is often referred to as a snap or pop opening process. Therefore SRV's will operate closer to the maximum allowable working

pressure (MAWP), PRVs would be sized to open first, and if they were inadequate and the pressure increase continued, an SRV would operate.

SRVs come in two different forms, direct spring loaded and pilot operated, a spring-loaded device contains pressurised fluid through the use of a compressive force from an installed spring. A pilot operated SRV works by using the force of the system’s own fluid to control the valve opening and contain the pressure within the system it is attached to. The spring loaded SRV is the more common of the SRV’s used in practice and is the focus of this research study. Presented in figure 2.1 is a detailed drawing of a Broady Flow Control type 3500 direct spring-operated safety relief valve. This SRV is a typical American Petroleum Institute (API) compliant device that has applications on unfired vessels. This device will be



These Items are recommended spares.

Figure 2.1 – Typical API compliant SRV – this model is a Broady Flow Control type 3500.

used as the basis of this study as a representative safety valve, as such, when the term SRV is subsequently used it is a direct spring-operated device that is being referred to.

The type 3500 valve is shown with flanged connections for attaching to vessels and pipework. Other possible connections used in industry are screwed, welded or clamp joints, each for specific applications. The body [1] is used for housing all of the main pressure containing components, those being the nozzle [2] and disc [3], and these are used for containing the fluid within the pressurised system when the valve is closed. The force to counteract the disc is supplied from the spring [29] via the spindle [5] and disc holder [7]. In a normal closed position, the spring load on the disc is greater than the force experienced from the pressurised fluid; it is only when the fluid force becomes greater that the valve will begin to operate. The body dimensions are specified to follow API RP526, this document provides a recommendation for dimensions of flange connected spring operated pressure relief valves, ensures geometrical consistency throughout industry and greatly simplifies the design stage of any process plant that these devices will be a part of.

Flanged connections are compliant with the standard ASME B16.5 Pipe Flanges and Flanged Fittings. Similarly, with the API centre to face dimensions, the ASME B16.5 standard provides some geometrical consistency throughout industry, more importantly though, these dimensions ensure structural integrity of flanged components. As SRVs and other pressure equipment are required to operate at high pressures, it is essential to ensure that the components being used are structurally suitable for a given application. This guarantees that they have the necessary structural strength to operate at the required pressure. As such, the ASME B16.5 guidelines provide a range of flange sizes for different pipe diameters

at different pressure ratings. The end result is a specification of flanges that cover nearly all applications that should be encountered in industry. The benefit being that it ensures that all components are safe and suitable for use at a given pressure but also could be easily swapped out for different components as the pitch circle diameter of all holes on a flange will match that of an identical classed flange. Shown in figure 2.1 is an ANSI 150 class flange inlet and outlet, at higher pressures, the flange dimension requirements would result in a large diameter and thickness of flange. This also impacts on other valve components, the disc holder [7] would change dimensions to handle the increase load from a higher pressure. Also, the spring [29] and supporting components would also be larger in size to account for increased aerodynamic forces from the expanding fluid.

Some components are optional within this valve; for example, a bellows [21] can be fitted to help counteract the effects of back pressure on the set-point of the device. These operate by ensuring an area equal to the seat area is exposed to atmospheric pressure, without this component back pressure could result in a change to the valve set-point. For certain applications the valve can also be specified with a lifting device that can be used to manually open the valve. ASME specify that this device should be designed so that manual operation should be possible when the valve is sitting at 75% of set pressure.

Valve adjustment comes in two forms, firstly the set-point pressure that the valve will begin to open at is controlled by the adjusting screw [13], this is achieved by compressing the spring which produces a load holding the disc against the nozzle face. The opening and closing behaviour of the valve can be influenced by adjusting the blowdown ring [8], this component alters the flow path of the escaping fluid leaving the nozzle as the valve begins

to open. By adjusting the height of this ring, small changes in the flow path causes significant changes to the pressure distribution – and thus disc force - during opening. Consequently, this component can be used to fine tune the valve performance to meet any standards or specifications of governing bodies in industry. The blowdown ring is an important component within a SRV and will be a focal point when investigating the Broady Flow Control SRV. This component strongly influences the performance of a SRV thus it is essential to know its exact position. The ring is attached to the inlet nozzle via a thread, screwing the ring up or down the nozzle will adjust the behaviour of the gas as it escapes the nozzle. The ring has notches around its perimeter; a locating pin protrudes into one of these notches to fix it into position. The position of the ring is usually quoted as a number of notches, this refers to the number of notches that the ring has been rotated moving it away from the disc. A setting of 0 notches would refer to the ring being in contact with the disc, as the number of notches increases the ring would move further down the nozzle and away from the disc.

The operation of an SRV is controlled by the forces acting on the disc, an aerodynamic force experienced from the pressurised fluid and a counteracting force supplied by the spring. The movement of the disc is determined by the magnitude of net force acting upon it, in a normal closed position the spring load will be dominant and maintain the pressurised fluid within the inlet nozzle. It is only upon the pressurised fluid force overcoming the spring force that the valve will begin to open. In the event of a rise in pressure, the fluid force acting on the underside of the disc would increase, this would continue as the pressure continues to build. The result would be that the disc component would move off of the seat and begin to relieve fluid thus lowering the system pressure, this should continue until such

times that the system pressure returns to a safe level and the valve would close. The way in which the valve opens is determined by the design of the internal trim, primarily the disc, disc holder and blowdown ring. To achieve the snap action opening that is required of an SRV, the fluid forces acting on the disc must become dominant quickly after opening. The main principle behind SRV operation is that when opening occurs, the pressurised fluid is suddenly acting on a larger surface area thus resulting in a larger force transferred to the disc components thus overcoming the increasing spring force. This action continues as the valve opens until it reaches a fully open position. Once fully open, the valve lift would be restricted mechanically.

The primary purpose of an SRV is to relieve sufficient fluid to return the system to a safe working pressure. Thus, the quantity of fluid that it passes is of prime interest to manufacturers and customers. As the valve opens, the flow rate will increase with valve lift, this will continue to a stage where the cross-sectional area of the nozzle throat is the smallest cross-section in the whole flow path. At this point, an additional increase of valve lift has no effect on the flow rate, the point at which this occurs is termed full lift and it is at this height that a valve would be mechanically restricted to stop further opening. Once in a fully open position the flow rate is completely controlled by the nozzle throat area and following basic fluid mechanics principles the flow rate of a fully open valve can be calculated using the throat area and pressure upstream of the valve. This makes sizing for valves relatively straight forward.

The performance of an SRV is usually measured by three main criteria, these are, the flow coefficient (K_d), overpressure and blowdown. The K_d is a correction factor used to calculate

the actual flow rate from one that would be expected from a theoretical ideal nozzle flow rate equation. A low K_d would indicate that an SRV experienced large losses thus passes a low amount of fluid compared to an ideal nozzle. For a customer, this may mean having to opt for a larger sized valve than the ideal application, thus incurring more cost, therefore some valves may be more attractive than others due to a higher K_d value. The overpressure and blowdown are described relative to the valve set point, the set point being the term used for the pressure at which the valve begins to open. In industry and supported by the standards, each manufacturer is required to specify their interpretation of set point prior to starting product certification with ASME, possibly leading to ambiguity. For this research, the set point definition specified by Broady Flow Control shall be utilised and defined as the pressure at which the first audible stream of escaping gas can be heard leaving the nozzle. Therefore, the overpressure is determined by the difference between the pressure of the first audible stream and the pressure that the valve attains full lift, this is quoted as a percentage of the set point. The blowdown is calculated by the difference between the first audible stream and the pressure at which the valve fully closes, again this is quoted as a percentage. The value of overpressure and blowdown are two of the performance criteria that must be met when a product is being certified. ASME will specify a band in which the overpressure and blowdown must fall within for a valve to pass that specific standard. The Broady type 3500 SRV in figure 2.1 is certified for ASME Section VIII of the BPVC for unfired pressure vessel, this stipulates a maximum overpressure of 10% and maximum blowdown of 7%, whereas ASME Section I stipulates 3% and 4% respectively.

2.2.3 Working Fluid

This investigative study is using ASME BPVC Section I performance requirements as a target for SRV improvement, this particular code governs the design and operation of power boilers and super-heaters. Although this standard is based around a steam cycle system, the dominant flow physics are relevant to other fluids and applications. Pressure relief devices can be required to operate on different fluids therefore the effects of fluid properties must be taken into consideration when designing or specifying the device. Typically, a different valve trim is required to account for incompressible and compressible fluids, thus certification requirements differ for liquid and gases.

ASME BPVC Section I specifies the standards for equipment operating in a vapour power cycle - which is characterised by the working fluid existing in both the liquid and vapour phase throughout the full cycle. Water will exist as both a saturated liquid and superheated vapour at different points within the pressurised system. The SRVs specified within ASME Section I are for installation on the boiler and super-heater section of this system. Water will enter the boiler as a saturated liquid and through heat addition should exit as a superheated vapour. SRVs mounted on the boiler or super-heater may encounter fluid that is not superheated and may be partially condensed. When operating, the fluid flowing through an SRV will undergo a large pressure and temperature drop which could result in partial condensation occurring throughout the device. This situation could be intensified by the entrainment of droplets of water within the flow of steam exiting the boiler. Thus, it is possible that an SRV designed to work with steam under ASME Section I may operate under a two-phase fluid situation and this must be considered during the design and specification

phase. This situation could also be encountered in other operating fluids - under the right conditions any fluid could undergo partial phase change.

API 520 details the techniques used for sizing, selection and installation of PRVs and included in this document is the recommended practice for two-phase flow sizing. However, it is stated that there are currently no test methods for two-phase flow certification. The two main scenarios covered within the standard are a vapour producing liquid as a result of flashing and droplet production due to a condensing vapour. The standard addresses on the sizing of relief devices for flow rate capacity thus the main focus is on calculating the correct flow rate of a device. Although this is critical, it only accounts for part of the functionality required, since the disc forces are also likely to be altered under two phase conditions, resulting in the possibility of valve opening and closing diverging from design conditions thus altering the valve capacity. Consequently, a manufacturer must be aware of the variety of possible scenarios that their product could encounter; also, a customer purchasing valves must strive to provide an accurate specification of the conditions that the device will be operating under.

2.2.4 Pressure Scaling

Pressure relieving devices can be required to operate over a significant pressure range and it is common that they would be specified for applications outside what was testable in laboratory conditions. Typically, this would involve a device being specified to operate at pressures beyond what is available in a manufacturer's testing facility. It is possible to test the structural integrity of components (hydrostatic tests) and set valves at high pressure - as this can either be achieved on water or requires only a small volume of gas. However, to

properly test valve operation, a sustained upstream pressure is required necessitating a larger system volume to ensure that the opening and - most importantly – the closing process is captured properly. Without sufficient volume behind an SRV, the device could close without fully opening due to the pressure drop at the inlet side leading to false blowdown behaviour. Therefore a large enough vessel to sustain the SRV opening and closing is required. In any test facility this is only achievable to a certain valve size and pressure, after which the equipment costs become significant.

Manufacturing a pressure vessel for testing at higher pressures introduces certain challenges. The required wall thickness of larger pressure vessels for a high-pressure application begins to become a significant hurdle during fabrication. Pressure scaling is commonly used to circumvent this financial barrier when designing SRVs for high pressure operation. This technique is based on the assumption that the force acting on the SRV disc scales linearly with inlet pressure. The disc force is a result of pressure distribution on the disc face and it is presumed that the normalised pressure distribution stays constant as operating pressure increases. The disc force to operating pressure is thought to follow a relation such as

$$F = kPA \tag{2.1}$$

Where F represents the disc force, P represents the working pressure, A represents the area experiencing the pressure and k is a constant. The area A is usually not known exactly but is assumed to be a constant and is taken to be the orifice area when used in this study. This assumes that the gas dynamics within a device at low pressure is an accurate representation of the dynamics at higher pressures. A manufacturer would carry out tests at lower pressures and scale these results to the required higher pressure value; it is then assumed

that this gives an accurate representation of how the valve would behave under these conditions. Since the aim of this thesis is to develop design optimisation methods, the validity of pressure scaling will be revisited in this study using CFD methods which are believed to be fundamentally a more rigorous scaling approach.

2.2.5 Dynamics

Safety relief valves are self-actuating devices, thus knowledge of their behaviour during operation is of critical importance. It is essential to ensure that they will open and close as required for system protection but also achieve this in a controlled manner, i.e. no oscillations or other chaotic behaviour. SRVs are characterised by a rapid opening to a fully open position, this is to ensure that they quickly begin to relieve their design flow rate when required to operate. From a design standpoint, a manufacturer would want to ensure that their product exhibited this type of behaviour when functioning, and also had a similar closing characteristic. Poorly designed trim or wrongly sized springs could result in a multi-stage opening process to attain full lift. This would not be desirable for the system that it is protecting and would fail ASME certification.

During opening and closing, SRVs have been shown to encounter oscillations and vibrations, where the moving components oscillate in line with the axis of operation instead of exhibiting a smooth closure movement. These oscillations can range from small amplitude - that has little effect on the valve or system - to large amplitude that in some instances result in the sealing faces coming into contact with each other at a high frequency (chatter), invariably causing damage to these components. In cases where no sealing face contact is

caused, large amplitude vibrations (flutter) can still cause system damage as these vibrations are passed onto the system that the valve is meant to be protecting. Any vibrations are to be avoided when designing mechanical systems, so it is important to ensure that the SRV being installed does not introduce this type of behaviour. Vibrations, as a result of a poorly designed or sized SRV would not have been accounted for during the design phase of a mechanical system. Over a length of time, if unchecked these vibrations could lead to fatigue failure, with potentially catastrophic results. Furthermore, the final stages of the closure process are of interest to a manufacturer as the disc can bounce upon coming into contact with the nozzle sealing face. This is a result of the collision being slightly elastic in nature where some of the impact energy causes the disc to rebound off of the sealing face.

To summarise, a manufacturer is interested in the dynamics of their product to ensure correct operation under all conditions. The main processes that would be focused on are the movement from open to close position, this should be a smooth sharp process that is one complete movement. Secondly, they would be interested in the presence of any oscillations within the SRV caused by the moving components. Finally, a manufacturer would have to ensure that no significant bouncing was present within their device. These dynamics can be studied using both an experimental and numerical approach.

2.2.6 Design Methodology

Currently there is no documented design methodology in industry pertaining to the opening and closing of safety relief valves. Any design methods in use will be a product of individual

manufacturers and generally not made public. However, there are certain techniques that are common knowledge and are used throughout the design process. The opening and closing cycle is controlled by the net force acting on the moving components. The forces acting upon these parts come from the pressurised system fluid and a counteracting force from a spring. The spring force is easily calculated via spring data, if disc forces can be measured then the net force which operates a valve can be obtained. Disc forces are often obtained through experimental testing and plotted to produce a characteristic curve of the device, i.e. the valve force-lift characteristic. Comparing the disc force to the spring force, it becomes possible to understand how a given design will operate. Large differences within the force curve to spring line generally results in a poorly performing valve, thus minimising the net force will in general improve the performance of a valve. Fig 2.2 below is a typical force-lift curve produced by an SRV, this example is from a Broady type 3500 and includes measurements from various settings of the blowdown ring (component 8, fig 2.1). This data has been normalised as is common throughout industry to compare data from different operating conditions. The lift has been normalised to the maximum lift value used during testing this size of valve and the force data has been normalised against the force value at zero lift. It is worth mentioning here that a full lift height is thought of as $D/4$ where D represents the nozzle throat diameter. For this size of valve (E orifice) the throat diameter is 13mm, thus full lift should equal 3.25mm. However, it has been found that due to flow separation within the nozzle full lift does not occur until around 3.7mm height thus tests work up to a lift of 4mm.

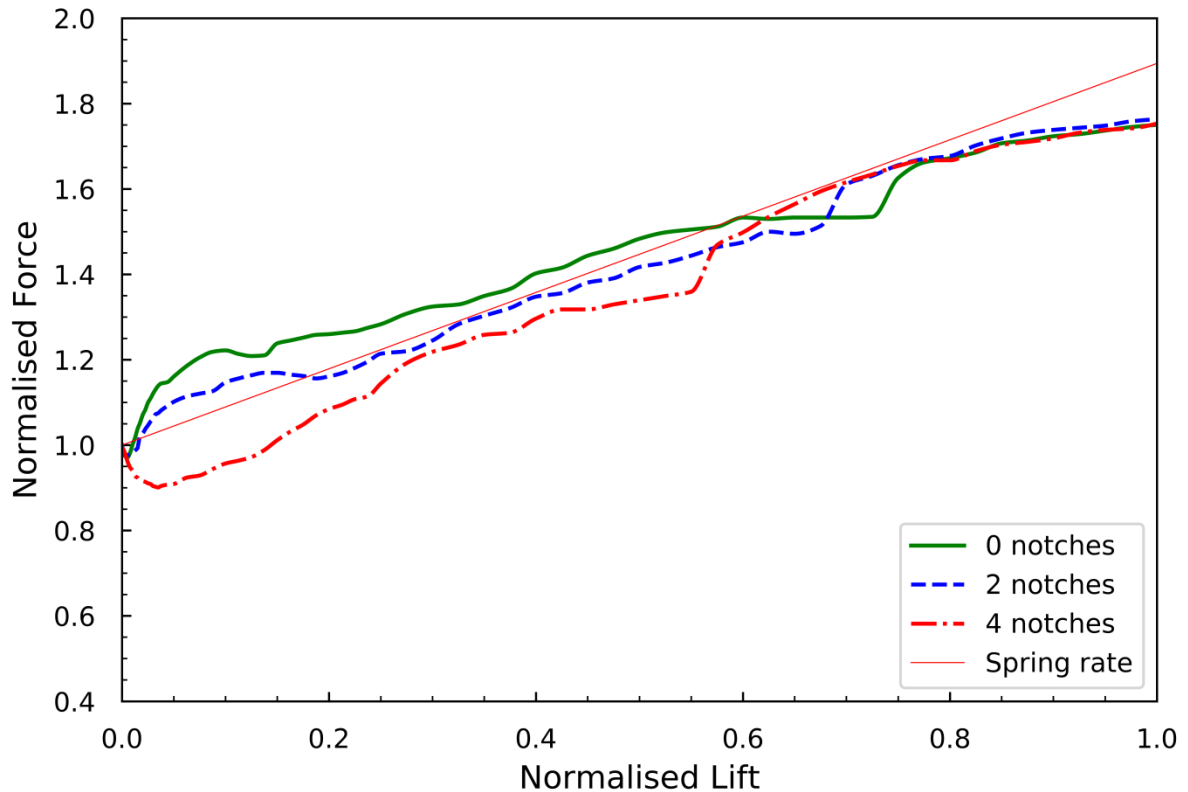


Figure 2.2 Force-lift plot - normalised data obtained from a Broady type 3500 on air at 3.3 barg.

The main assumption behind a force-lift curve as presented above is that a steady-state measurement provides an accurate representation of forces occurring during a transient event. To expand on this, an SRV operation is transient, the moving parts will change from a closed to open position throughout the operational cycle and during this the disc forces will change. As the disc moves off of the seat the fluid behaviour within the device will change - altering the pressure distribution on the disc face. In general, as the disc moves off of the seat the force will increase. When measuring the forces to produce a curve as in figure 2.2, the disc needs to be held at a discrete height at several points to produce a full curve. As the components are being held at a static height to obtain a measurement it is clearly not an exact representation to the quick snap-action that characterises an SRV. This commonly

used approach implies a quasi-steady state assumption is valid whereby the motion of the disc can be represented by a series of steady state conditions.

Force-lift curves, as shown on figure 2.2, are used to study the force change on the moving components throughout an operational cycle. This provides a manufacturer with data on how the pressurised fluid is behaving within the device. In general, as the disc moves off of the seat it is expected to experience an increase in fluid force as the fluid acts on a larger surface area and greater than the additional force required to compress the spring resulting in further movement away from the seat area. This shall continue until the valve becomes fully open, which in figure 2.2 is around a normalised lift value of 0.7-0.9. The fully open condition is considered to occur when the valve has opened sufficiently to move the controlling flow area from the disc seat region to the nozzle throat, which is a constant area.

A manufacturer can use the shape of the force-lift curve to determine the behaviour of the design being tested. Shown in figure 2.2 are 3 different curves, these correspond to different adjustment ring settings (fig 2.1, component 8). This ring is used to fine tune the shape of a force-lift curve to provide some adjustment when setting a valve. As SRVs are required to operate over a range of pressures this necessitates different spring rates thus one design would not suit all configurations for any specified spring. An SRV is limited in its operating pressure range and is required by ASME to be able to set at pressures of $\pm 5\%$ of the design pressure for a given spring, thus some level of adjustment is required. Shown in figure 2.2, the three curves vary in force in the lower opening lift regions; this will cause the valve to have different opening behaviour, thus different levels of overpressure.

The spring is a key component in an SRV and has to be correctly sized to ensure high performance from the device. To obtain the correct spring stiffness a manufacturer can use

the force-lift curve data. From this it is possible to determine the necessary deflection and spring rate required for each application. As stated above, ASME require a device to be able to function at pressures $\pm 5\%$ of the mid-point value for a given spring. So, when preliminary testing is being undertaken with ASME a range of springs will be specified to cover the operating pressures that that device is sold for. The midpoint pressure for each of these springs will then be specified then the valve should be able to be set at $\pm 5\%$ of this mid-point value.

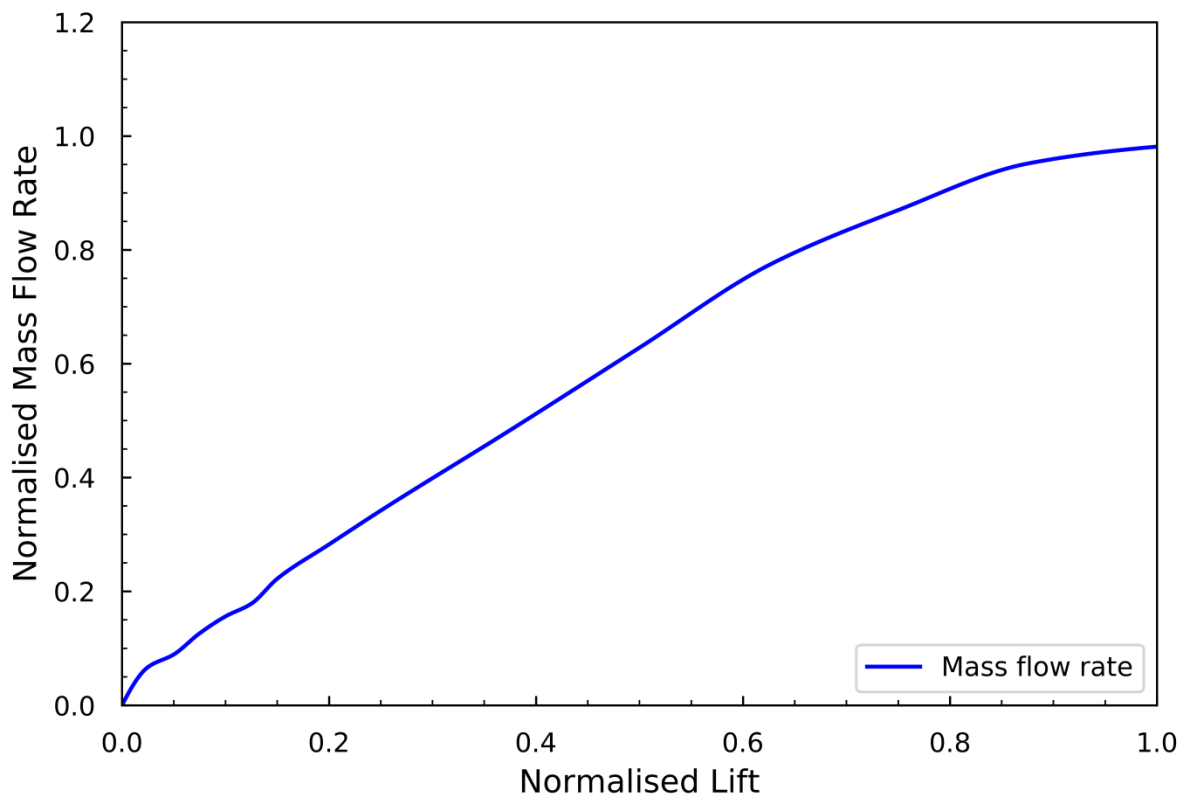


Figure 2.3 – Mass flow rate-lift plot – normalised data obtained from a Broady type 3500 on air at 3.3 barg.

In addition to the force-lift characteristics, a manufacturer is also interested in the flow rate behaviour of their device. For high pressure compressible gases, the flow rate is ultimately controlled by a compressible choking condition at the smallest cross-sectional area in the

flow path and determined primarily by the upstream pressure and the area. For a typical ASME/API safety valve the flow rate is restricted by the disc-seat geometry initially but ultimately by the throat diameter of the nozzle when in the fully open condition. Presented in figure 2.3 is a typical mass flow rate curve - the data has been normalised using the mass flow at maximum lift for the Broady type 3500 E orifice test valve.

Figure 2.3 presents the mass flow rate behaviour as the valve opens; this plot demonstrates the mass flow rate levelling off at a normalised lift value of approximately 0.9. This is a result of the nozzle throat area becoming the restrictive cross-section within the flow path of the device, thus any increase in valve lift doesn't equate to an increase in mass flow rate. This behaviour can be cross-referenced with the force lift characteristics in figure 2.2 which also displays similar behaviour, levelling off around a normalised lift of 0.9.

Obtaining force and mass flow rate measurements experimentally requires the construction of bespoke testing equipment. The measurements must be taken whilst holding the moving parts statically at discrete heights over the full operating range, thus a valve must be reconfigured to allow this to happen. This will involve the spring being removed and some supporting mechanism to hold the moving parts at a specific opening whilst taking a measurement. This mechanism would be required to provide fine adjustment to cover the full operating range of the test device. The force measurement would be obtained via a load cell installed where it could pick up any applied load to the disc holder assembly.

Using this test equipment, the moving parts would be held at a set height whilst the inlet pressure was held at a specific value and a force and mass flow measurement would be taken. The moving components would then be altered to a different height and the process would continue to obtain a full curve.

The remaining measurements are obtained through functional tests therefore the SRV would be configured as a completed product. The functional tests will allow for measurement of the dynamics of the device, the overpressure and blowdown, and also the flow coefficient. This final data will provide an indication to how the product will perform on-site. The dynamics of the valve would be measured by a displacement transducer from the movement of the spindle. The overpressure and blowdown figures are calculated from the figures obtained from functional tests.

The final measurement that a manufacturer would likely take during the design process would come from the flow rate throughout a device. This should be an easier performance criterion to achieve as the flowrate is controlled by the cross-sectional area of the inlet nozzle - ensuring this area is correct should result in a properly sized valve. However, during the flow throughout the device certain losses can be expected, thus the physically measured flow rate would always deviate somewhat from the theoretical value, the magnitude of this difference provides a measurement of the flow efficiency of the device, quoted as the valve K_d value.

The advancement of numerical modelling techniques has resulted in the development of new tools able to supplement traditional design methods in the development stage of new products. In the context of relief valves, these tools can be used to gain deeper insight into the behaviour of a valve under different operating conditions. Two main techniques are commonly used in studying relief valves, firstly, a low-order valve model (LVM), which is typically in the form of a set of ordinary differential equations to model the dynamics of a relief system operating. Secondly, CFD modelling can be used to model the fluid behaviour throughout a valve when operational, this provides significantly more detail than the LVM

approach but is also significantly more computationally expensive. Utilising these tools, it could be possible to make informed design decisions prior to manufacture.

An LVM, typically a 1 DOF approach, could be utilised to study the dynamics of the device under different operating conditions, this would give a manufacturer a tool for quickly and cheaply evaluating changes to their product. Conversely, undertaking a CFD analysis of a relief valve is significantly more time consuming but does provide much more detail in the solution. Once complete, it would deliver a representation of the fluid flow within the device. A representation of the pressure field within the device would be of particular interest to a manufacturer as this could be used to understand the reason for the forces acting on the disc at a particular lift. This then becomes extremely useful in the fine tuning of a design when the disc force needs to be adjusted at a certain point in the opening cycle to improve the valve performance. Inputting this data into the model would produce a fully digital stage to the design process that could make full design iterations by checking and altering geometry to improve an SRV performance.

To conclude, there is no specific design methodology currently in industry for SRVs, however there are commonly used techniques that have been introduced throughout this section. These are based around gaining knowledge of the net-force acting on the moving components within a valve. Classically this was achieved through experimental testing methods but in recent times numerical modelling has been found to complement these techniques during the design phase. From cross-examination of disc position and disc force via a force-lift curve a manufacturer can gain insight into the fluid behaviour within a device without any advanced modelling techniques. Using a force-lift curve it is possible to discover

points in the operational cycle that contains large net forces acting on the disc. This information can then be used to alter a design to try and improve valve performance. The force-lift curves are also useful for correctly sizing a spring for each application. Knowledge of the forces at closed and fully-open position can be used for calculating the necessary spring rate for a given pressure. However, including numerical methods such as CFD modelling can provide significantly more detail than a force-lift curve alone. This can aid a manufacturer in making informed design decisions in an attempt to alter the shape of the force-lift curve to something more desirable. One of the main objectives behind this research is to discover the impact that these techniques could make to the design phase of an SRV.

2.3 Literature Review

A review of the current literature in SRV design will now be presented. The review will be separated in a similar manner to that of the background studies and will address valve design aspects from the perspective of the fluid used, pressure scaling, dynamics and design methodology. This will allow addressing each aspect of SRV design individually and review the current progress found through published literature.

2.3.1 Working Fluid

As discussed, there are situations where an SRV configured for gas service can experience two-phase flow. The industry standards mostly focus on sizing of relief valves as their primary objective will be to ensure that an SRV is passing sufficient fluid thus ensuring the safety of a pressurised system. API 520 Part II specifies the methods to calculate reaction

forces from a relieving valve, this also covers two-phase flow situations. Although these are important factors to consider, from a design standpoint the disc force characteristics and fluid mechanics within the device will be of significant interest. As two-phase flow could alter the disc forces it would have a direct impact on the valve opening and closing characteristic thus could alter the flow rate through a device. When investigating two phase flow within SRVs Narabayashi (1986) found slight but not significant changes in disc forces under a two-phase condition. Similarly, Dempster et al. (2015), also found changes in disc forces within an SRV under two-phase flow conditions. However, on testing up to a liquid mass fraction of 79% a more pronounced disc force reduction of approximately 10% was experienced. It is important to note that it is a force *reduction* found under these conditions, this will consequently reduce the net force maintaining the disc in an open position thus could lead to partial closure of the device. This is an important point as it would directly lead to a reduction in flowing capacity of a device. The disc force variation effect is not covered within the standards. Schmidt et al. (2013) conducted a thorough study of different two-phase flow situations within relief valves. When discussing sizing for a condensing gas it was stated that ignoring the effects of condensation and sizing for vapour lead to a conservative figure for two-phase relief valve flow rate. This is contrary to the effects of two-phase disc force that could lead to a flow rate reduction through a partially closing device. Considering the possible consequences of a reduced flow rate the possibilities of two-phase flow within an SRV must be considered by individual manufacturers.

In the design stage of pressure relief devices, it is common to use pressurised air to represent the operation of the device for gas applications. The assumption is that air gives an accurate representation of the behaviour of all gasses that a valve could be used on.

However, Dossena et al. (2013) investigated the effects of different operating gasses in safety relief valves. Air, argon and ethylene were used for the study and both numerical and experimental methods were utilised. It was shown that fluids with γ (specific heat ratio) smaller than air produced a lower discharge coefficient. This was explained by the critical expansion ratio being lower but also the experienced disc force was also lower thus there would be less force to compress the spring with opening. This reduced compressive force on the disc components could lead to less valve lift and thus a lower K_d than expected. The outcome of this work clearly suggests some issues with industrial assumptions pertaining to operational fluids. The results suggest that manufacturers should strive to test their products on every fluid that it would operate on, or at least be aware of the possible behavioural changes from different operational fluids.

2.3.2 Pressure Scaling

Throughout industry it is commonly assumed that the aerodynamic forces caused by the expanding gas scale linearly with inlet pressure. However, Dempster et al. (2018) highlighted deviations from this assumption when investigating high pressure flows within SRVs. It was shown that at higher operating pressures, the valve body outlet can act as a second orifice and become choked. This resulted in a built-up back pressure within the valve body which would aid the spring in trying to close the valve. The outcome being that the disc would close by some amount until the aerodynamic forces and counteracting forces from the built-up back pressure and spring equalise. Consequently, the valve would be open less than expected and the flow rate would be reduced, leading to a lower K_d than expected. This

work was undertaken as part of this research and will be discussed more thoroughly in chapter 4.2.2.

In the PhD thesis of Beune (2009), the linear pressure scaling assumption was found to be inaccurate. However, this research focused on high pressure effects around the nozzle exit and disc face. It was found that the fluid escaping from an inlet nozzle behaved differently at elevated pressures, leading to an altered pressure distribution at higher pressures. Thus, even without the effects of back-pressure, the different pressure distribution would cause the valve to operate differently than originally assumed.

2.3.3 Dynamics

In addition to the aerodynamic forces within an SRV, OEMs will be particularly interested in how their device actually performs when operating. This dynamic behaviour is a direct consequence of the forces acting on the disc therefore this behaviour is directly linked to the disc force investigations taking place throughout the design process. When studying the dynamics of a relief valve, designers have to continually cross-examine the movement with the net-force on the disc as it is the force that controls the movement of the disc.

The operation of a pressure relief device can be modelled as a simple spring-mass-damper system to produce a low-order valve model. This technique is able to simulate the opening and closing behaviour of the device through a system of ordinary differential equations. This method makes it possible to analyse the dynamics of a pressure relief system numerically and with little computational costs. Unfortunately, the downside to using an LVM is that it

cannot capture the 3-dimensional fluid mechanics within the device. However, the data produced is still valuable and can be used to give insight into the dynamic behaviour of a system. Darby et al. (2014) used an LVM approach when studying the effects of inlet piping on an SRV dynamic response. The numerical model predicted valve chatter caused by increasing the inlet pipe length to a relief valve, this was subsequently validated against experiment. These instabilities are a common issue with pressure relief devices and the LVM was shown to accurately predict the onset of these vibrations. To avoid chatter, API recommends that inlet pressure loss be kept below 3% which is the reason that these devices should either be attached to a vessel or have orifice sizes much less than the pipeline diameter. The model by Darby was able to predict the inlet line pressure loss and the consequence of this on valve stability. Three different conditions were found under which valve chatter could occur, on opening, closing and also in a fully open position. The main conclusion drawn was that it was the pressure waves within the inlet line that were interacting with the disc holder components leading to instabilities. Hos, et al. (2017) studied the valve dynamics using a similar modelling approach to Darby. The research focused on the physics behind the instabilities previously predicted, which was explained as being as a result of the acoustic wave of this inlet line interacting with the SRV and the spring in the device was applying negative damping to the oscillations and causing chatter to initiate. The onset of chatter was categorised to five different causes; inlet pressure loss, over/undersized damping, valve jumps, Helmholtz instability and quarter-wave instabilities.

The LVM is driven by a force imbalance on the mass - or in the SRV context - the disc holder assembly. The force-lift curve used as an input for an LVM can be obtained experimentally or through CFD calculations, as used by Song, et al. (2014). This research obtained the force-

lift characteristics of the valve at constant heights throughout the opening cycle. This data was used to produce a curve that was the driving force behind an LVM such as described above. Using this method, the team were able to predict the blowdown performance of the SRV under study to a high degree of accuracy.

Another common method, such as that used by Hos et al. (2014), is to calculate the force from the operating pressure and disc face area - this preload value is generally calculated from manufacture drawings or a CAD model. After which, to account for the increase in force as the valve opens, a separation angle is used to account for the escaping fluid acting on a larger surface area as the disc moves further away. Parker (1985) used a similar technique to calculate the disc force via the working pressure and the surface area the fluid is acting upon. Using a slightly more complex geometry, this technique was still able to accurately predict the closure of the SRV. The model was validated against experimental data for a range of adjustment ring settings and was found to be accurate for all tested conditions.

The same LVM can be used for controlling the movement of mesh in a transient CFD simulation within a pressure relief device as used by Song et al. (2014). Here the disc forces are extracted directly from a CFD calculation as it is being calculated, this data is then used to calculate the loads acting on the moving parts. The numerical model is then used to calculate the movement of components and thus the degree of mesh deformation required within the simulation. This method has the benefit of being able to obtain the forces as the calculation is taking place, additionally, it is able to include any transients that may be present that would otherwise be missed when using a steady-state assumption. The

drawback of this technique is computational costs, a fully 3-dimensional transient SRV model could require 1000's core hours for solution, rendering this approach less attractive. A compromise could be made by using a 2-dimensional axisymmetric model such as used by Beune (2012), this research was still able to uncover the dynamics of the SRV being studied but with significantly less computational resources.

In summary, the literature on SRV dynamics covers both experimental and numerical approaches. Each method is being used to study how a device will operate when opening and closing. Two different numerical methods are commonly used, they differ in the way that the disc force is obtained. One, such as used by Hos et al. (2014) relies on the geometrical data of the valve internals and estimates the disc force from pressure distributions. The second technique, such as used by Song et al. (2014), obtained the disc forces via a CFD calculation thus should produce a more accurate representation but at a higher computational cost. This method also has the benefit of uncovering transient effects that may not appear in a quasi-steady state technique.

Throughout the literature there has been significant work published on oscillations found in SRV operation. These are undesirable and manufacturers must ensure that their device exhibits a steady sharp opening and closing characteristic that is oscillation free. A strong influence of the inlet line length on SRV oscillations is found throughout literature, this is not something that can be accounted for when designing a device and should be avoided by following the appropriate API guidelines for SRV installation.

2.3.4 CFD Literature Review

It has been shown that throughout industry and academia significant work has been carried out in applying CFD techniques to pressure relief valves. The two most important predictions to be made with CFD are the aerodynamic forces and the discharge coefficient. Both of these values are critical in design and specification of a pressure relief valve. The current literature available demonstrates the capabilities of CFD modelling within these devices. It may have been possible that industry assumes a discharge value if the valve is fully open, it could be thought that following compressible flow theory that the throat area in a compressible flow should control the flow rate. This may not be true when operating with a complex flow path as present within a relief valve. Aerodynamic forces responsible for compressing the spring are one of the main focal points in SRVs and being able to predict these accurately will greatly help in design and analysis. Considering the complex flow path present within an SRV and the high velocity and pressure gradients caused by the gas dynamics the capabilities of CFD are clearly demonstrated.

Due to the complexity of fluid mechanics and some of the necessary approximations required in CFD, much work has been carried out to build confidence in using these methods to study relief valves. Dempster et al. (2006), used CFD to predict the aerodynamic forces on the moving components of an in-line relief valve for the refrigeration industry. Prediction of these aerodynamic forces is essential to properly design a valve and size the correct spring. Throughout the research, CFD predicted forces had shown good agreement with experimental values, the work was able to predict the forces throughout the full opening cycle of the relief valve. For this type of in-line relief valve a 2D axisymmetric

approach was sufficient. Additionally, in the process of this research a strong geometrical dependency was uncovered. It was shown that small radii in critical positions could have a significant effect on the aerodynamic forces within a valve, particularly at low lift. This not only shows the necessity to produce an accurate geometrical representation for the CFD stage, but also the effect that small radii could have on a production valve. It is possible to unintentionally add a small radius or chamfer during the manufacturing stage when cleaning a sharp edge from a machining operation which could then result in the valve operating out with design specification.

CFD analysis provides a means of studying different configurations that may have been difficult to achieve experimentally. Dossena et al. (2013) utilised a discontinuous Galerkin solver as opposed to the more commonly used finite volume method for investigating a SRV response to the effects of different gasses. This approach was able to predict disc forces throughout the full operational cycle with different gasses generally within 1% accuracy. Further validation of this method was complete using water in the same valve (Bassi, et al., 2014), good disc force and discharge coefficient prediction was achieved. In the work of Follmer (2003), CFD modelling was used to predict the disc forces within API type SRVs, this was then used to optimise the flow path to gain improved performance

A discharge coefficient is generally used to describe how far off of ideal conditions a valve performs, and is used to correct the theoretically calculated flow rate. Obtaining the coefficient usually involves experimentally measuring the flow rate and comparing this value to that obtained theoretically. The same approach can be performed using CFD techniques to calculate the flow rate of a valve numerically and compare that with the theoretical

value. Given the conservative properties of the widely used FVM in CFD, this approach could be used with a good deal of confidence. This technique was validated in the work of Moncalvo (2009) when investigating the accuracy of CFD at predicting flow rates in API type SRVs, it was shown that given the correct turbulence model and a sufficiently fine numerical grid were chosen, the CFD codes could predict the flow rate with an error of <3%.

Numerical methods have the benefit of being able to study flows beyond testing conditions, high pressure or high flow tests could be dangerous and expensive to achieve experimentally. SRVs are assumed to operate as advertised at all pressure and flow conditions, however this could involve pressures over 1000 bar or flow rates exceeding 2000 kg/s, to achieve this experimentally would be challenging. Using CFD methods it is possible to study these conditions, and provided the configuration is correct, a high degree of accuracy could be expected. However, assuming the codes are applicable at all pressures could involve some risk, to address this concern research has been carried out to validate CFD codes at high pressure conditions. Beune (2008) created an SRV high pressure test rig which was used to validate flow rates and disc forces to a pressure of 600 bar. During this research a nozzle flow rate prediction was also validated up to a pressure of 3500 bar. As an example the work produced by Dempster et al. (2018) provides further confidence in the suitability of CFD codes. This work studied the effects of high pressure flows within relief valves and found the outlet flange becoming choked under certain conditions. Producing this work experimentally would have been difficult and expensive, but crucially, the ability to witness the flow velocities inside the valve was fundamental in explaining the gradual change in fluid behaviour within the valve.

Optimisation algorithms provide a means of altering parameters to improve the value of a function, these techniques can be used in a design process to improve the performance of a component. Different optimisation algorithms are available to meet the range of demands present in industry, gradient based methods are a common approach, where the algorithm uses the gradient of the objective function as a method of guiding the optimisation procedure. Following the steepest gradient towards the maximum or minimum objective function value would therefore steer the optimisation process towards the optimal inputs. Utilising this branch of mathematics greatly increases the speed and efficiency in undertaking a function optimisation. As the algorithm will make calculated change to a given parameter it should arrive at an ideal value quicker and with less iteration than doing such a method manually.

Optimisation within the design stage of a manufacturing process would provide a means of improving a product prior to prototype or manufacture. Coupling CFD modelling with optimisation methods is now a common approach which results in a completely digital design iteration stage and can lead to improvements in design before any manufacturing taking place. This coupled approach has been used extensively throughout the aerospace industry for aerofoil design. Unfortunately, CFD calculations are generally computationally expensive, driving geometry changes via an optimisation algorithm which requires hundreds of changes could result in long run times. Fortunately, this is a common problem when coupling these methods and several techniques to overcome this issue have been developed. Two main approaches can be used to reduce the computational time required during optimisation. Firstly, a simplified CFD model that still achieves an acceptable approximation of the physics could be used, such as a 2-dimensional model in place of a 3-

dimensional model or lower density numerical grids. Such an approach was used by Wu et al. (2018) for the optimisation of a steam ejector nozzle. The team utilised a 2-dimensional CFD model to analyse the performance of a steam ejector geometry, this simplified model was then used to evaluate the parameter optimisation of the nozzle design. Such an approach greatly reduces the computational effort in the evaluation stage whilst still capturing the physics to a satisfactory level.

An alternative approach uses a select number of CFD calculations throughout the design space and interpolates between points to give an approximation of the objective function value throughout the entire search space. These techniques may require some iteration as evaluation at intermediate values may uncover some discrepancies within the approximations - however a reduction in the overall solution time is still to be expected. This method was used by Li et al. (2015) where a safety relief valve geometry shape was optimised to achieve improved performance in opening and closing, the work focused around altering the shape of the force-lift curve produced by the SRV to improve the valve performance. It was recognised that the difference in flow force to spring load is what controls the required overpressure and blowdown in an SRV thus the optimisation was aimed at reducing the difference in area between the spring load and disc force. The researchers required a full 3-dimensional CFD calculation to accurately predict the flow forces within the SRV body, consequently a direct optimisation method could not be used. After an initial design space exploration, a surrogate model was constructed which would provide an approximation of the full design space via an interpolation between the initial points. A 48% reduction in the area between the disc forces and spring load was achieved using this approach. Similarly, Yang et al. (2017) used a CFD optimisation technique to

predict the blowdown of an SRV, the team recognised the efficiency of using a response surface approach for design space exploration. A CFD based dynamic model of the full operational cycle of an SRV was produced that could predict the blowdown of the device. The SRV under study had means of adjustment within its design, allowing for some fine tuning of the device. The target of the research was to optimise the performance by using the dynamic model to predict the optimal setting for each adjustment parameter. A response surface method was used to interpolate between measured points. The work was able to use the numerical methods to predict the optimal setting for the SRV being used.

In certain applications, the initial design space exploration phase requiring the construction of a surrogate model may still have a significant computational cost involved. A common solution is to combine both of the techniques previously introduced and explore the search space using a low fidelity approach and interpolate for objective function values between each evaluated points. The technique - frequently termed physics-based surrogate modelling - is common throughout aerodynamic optimisation studies where individual evaluation of designs can be computationally expensive. Leifsson et al. (2014) produced an application of this approach optimising the shape of an aerofoil is optimised utilising various low fidelity CFD calculations that still capture the required physical trends. This then provides the basis for a more efficient geometry optimisation.

2.4 Summary

This chapter began by providing a basic overview to the operation of pressure relieving devices - paying particular attention to safety relief valves. The focus then moved on to a summary of the industry standards that these devices are regulated by. This provided a clear

specification of the performance requirements used throughout industry. Emphasis shall be paid to the overpressure and blowdown requirements of ASME BPVC Section I, which are specified as a maximum of 3% and 4% respectively.

The second section of the chapter presented a critical review of the current literature on safety relief valve design. The review aimed to answer the questions raised during the background studies of SRV design and operation, presented in section 2.2. Some of the key findings from this review were as follows,

- Under certain conditions two-phase flow can occur, the effects of which have been presented in several research articles.
- Pressure scaling - often used throughout industry for specifying valves at elevated pressures – has been found to be inaccurate in many situations.
- No specific design methodology exists for SRVs however there are a few common techniques used, such as the use of force-lift curves.
- Low-order valve modelling has been used extensively to capture the dynamics of SRVs. This method has been found to accurately capture valve dynamics and was validated by Song et al. (2011) and also by Darby et al. (2014).
- There has been a small number of articles published featuring research using optimisation algorithms to fine-tune the performance of SRVs. Yang et al. (2018) was able predict the blowdown of an SRV to within 1% over a range of settings, thus the accuracy of this approach seems to be sufficient for design.
- Computational fluid dynamics has been used throughout academia and industry in an SRV context, there are several published articles on the capabilities of this technique. From the published literature it would suggest that CFD can be used

quantitatively in some SRV applications but there are some contradicting results thus further validation may be required.

These findings highlight the extensive work that has been published on safety relief valve research. The focus of the majority of this research however is on issues with existing SRVs and how they perform - there has been little work presented purely on design of SRVs. It seems that the prevailing techniques used in industry are still feature a test based iterative approach to design, this highlights an area for potential improvement in the design process. The proposed objectives of this research were focused on design optimisation within the context of safety relief valves and having reviewed the literature on the subject there have been some aspects that require further attention. For clarity the proposed key objectives are summarised below:

- Determine the accuracy of CFD for ASME type SRV.
- Prove the quasi-steady state assumption is valid and investigate the capabilities of low-order valve modelling in ASME type SRV.
- Develop an effective optimisation process.
- Undertake a geometrical optimisation of a SRV.

In the PhD thesis of Beune (2008) it was suggested that the accuracy of CFD in an SRV geometry is not sufficiently high enough for SRV design, however the paper published by Dempster et al. (2006) found CFD predicted forces to be in good agreement with experimental values. Also, certain papers have suggested using different turbulence models when undertaking a CFD analysis of an SRV such as Dempster et al. (2006) and in Moncalvo

et al. (2009). Thus, some level of clarification is necessary to discern the capabilities and required configuration of CFD in SRV analysis. Likewise, the quasi-steady state assumption was also found to be valid as in Dempster et al. (2006), but the PhD thesis of Beune (2008) found transient flow effects on disc force in compressible flows thus requiring further study.

Low-order valve modelling has been found to capture the dynamics of an SRV and has been validated in the literature however due to the sensitivity of relief valves a validation exercise is still necessary for each application. Therefore this method should be verified as accurate prior to using it throughout this research. It is possible to estimate the overpressure and blowdown using only the force-lift curves. However, using a low-order model it is possible to obtain these performance parameters whilst also uncovering any instabilities within the device. Thus, a low-order model can aid the design process in multiple ways.

A limited number of studies have examined design optimisation of SRV's. These mainly focused on altering the setting of the device to improve the performance and was found to be able to predict the blowdown accurately (Yang et al., 2018). Only one paper has been published on the design optimisation of internal components of an SRV (Li et al., 2015) and was able to alter the size of some internal dimensions to reduce the net force acting on the disc. However, this was not validated against experiment and the study did not investigate the effect on SRV performance. Thus this study will extend previous work by investigating alternative design optimisation methodologies to improve valve performance by optimising the valve trim geometries. It is also intended to manufacture the modified valve and verify the valves improved performance through physical testing. This exploration of the complete SRV design cycle using optimisation methods can be considered as one of the main contributions of this study.

3. Mathematical Models

This thesis will examine the use of well-established techniques for the modelling of the valve dynamics through the use of a one-degree of freedom low-order system approach and also the fluid flow using CFD methods. While well established, they should not be taken for granted as sufficiently accurate for the design optimisation studies. Hence the models will be discussed, followed by a verification and validation exercise to ensure the models are suitable to meet the requirements of this study.

3.1 Computational Fluid Dynamics

Fluid mechanics is a branch of physics concerned with the behaviour of deformable materials, generally focusing on liquids and gasses. The field is largely treated as continuum mechanics in that it accounts for a fluid as a continuous substance and not as individual molecules. This approach provides a significant reduction in resources required during analysis whilst still maintaining a high level of accuracy.

Fluid behaviour can be described by using the Navier-Stokes equations or one of their simplified variants. These equations are derived by applying Newton's second law to a deformable material, resulting in a system of highly non-linear partial differential equations. They are able to predict how the velocity, pressure, temperature and density of a fluid will change through time. In practice, obtaining a solution to these equations is extremely difficult, even with significant approximations only the simplest of boundary conditions can be solved directly. Consequently, techniques have had to be developed to allow these

equations to be used for the study of complex flows. The Navier-Stokes (NS) equation for a Newtonian fluid are defined as follows,

$$\frac{\partial \rho}{\partial t} + \frac{\partial}{\partial x_i} (\rho u_i) = 0 \quad (3.1)$$

$$\frac{\partial}{\partial t} (\rho u_i) + \frac{\partial}{\partial x_j} (\rho u_j u_i) = -\frac{\partial p}{\partial x_i} + \frac{\partial}{\partial x_j} [\tau_{ij} - \rho u_j'' u_i''] \quad (3.2)$$

$$\frac{\partial}{\partial t} \left(\rho \left(e + \frac{1}{2} v_j v_j \right) \right) + \frac{\partial}{\partial x_i} \left(\rho v_i \left(e + \frac{1}{2} v_j v_j \right) \right) = -\frac{\partial q_i}{\partial x_i} - \frac{\partial p v_i}{\partial x_i} + \frac{\partial \tau_{ij} v_j}{\partial x_i} + \rho v_i f_i \quad (3.3)$$

Where ρ is the density, u is the velocity, p is the pressure term, τ is the deviatoric stress tensor, e is the energy and q is the heat flux. The stress tensor consists of 9 components that define the stresses acting on a fluid parcel, both the principle and shear stresses are present. Inclusion of this stress tensor within the Navier-Stokes equations is what gives rise to turbulence and consequently, a significant increase in complexity in obtaining a solution. Employing an inviscid assumption on a fluid system would result in this stress tensor dropping out of the Navier-Stokes equations leaving the system called the Euler equations. Unfortunately, an inviscid assumption is only able to be used under certain conditions thus treatment of the stress tensor is generally required.

To be able to use the Navier-Stokes equations for practical applications additional approximation and simplifications are required. Osborne Reynolds first proposed a decomposition of turbulence into a mean and fluctuating component. This approach introduces extra stress terms, called the Reynolds Stresses, and these need to be modelled separately. The new system of equations is called the Reynolds Averaged Navier-Stokes

(RANS) equations and provides a significant reduction in computational resources required to achieve a solution.

Calculation of the Reynolds stresses is obtained by turbulence models, these extra equations are able to close the RANS equations to produce a fully defined system. Many different turbulence models are available, they are usually classed by how many additional transport equations they introduce and range from 0 to 5 equation turbulence models.

If the RANS approach introduces too much approximation, a different technique is to filter out the smallest length scales and fully resolve the larger turbulent vortices. This method is termed a Large Eddy Simulation and is commonly found in combustion, acoustics and atmospheric flows, however, RANS modelling still forms the basis for most industrial flows. A popular two-equation RANS turbulence model is the shear stress transport (SST) model of Menter (1993), this model builds upon the strengths of earlier turbulence models to produce formulation that is more suitable to a wide variety of flow conditions. This model is given below where kinematic eddy viscosity is defined as

$$\nu_T = \frac{\alpha_1 \kappa}{\max(\alpha_1 \omega, SF_2)} \quad (3.4)$$

the transport equation for the turbulence kinetic energy k is defined as

$$\frac{\partial(k)}{\partial t} + U_j \frac{\partial k}{\partial x_j} = P_k - \beta^* k \omega + \frac{\partial}{\partial x_j} \left[(\nu + \sigma_k \nu_T) \frac{\partial k}{\partial x_j} \right] \quad (3.5)$$

and the transport equation for the specific dissipation rate ω is defined as

$$\frac{\partial \omega}{\partial t} + U_j \frac{\partial \omega}{\partial x_j} = \alpha S^2 - \beta \omega^2 + \frac{\partial}{\partial x_j} \left[(\nu + \sigma_\omega \nu) \frac{\partial \omega}{\partial x_j} \right] + 2(1 - F_1) \sigma_\omega \frac{1}{\omega} \frac{\partial k}{\partial x_i} \frac{\partial \omega}{\partial x_i} \quad (3.6)$$

and some additional relations and closure coefficients defined as

$$F_2 = \tanh \left[\left[\max \left(\frac{2\sqrt{\kappa}}{\beta^* \omega y}, \frac{500\nu}{y^2 \omega} \right) \right]^2 \right] \quad (3.7)$$

$$P_\kappa = \min \left(\tau_{ij} \frac{\partial U_i}{\partial x_j}, 10\beta^* \kappa \omega \right) \quad (3.8)$$

$$F_1 = \tanh \left\{ \left\{ \min \left[\max \left(\frac{\sqrt{\kappa}}{\beta^* \omega y}, \frac{500\nu}{y^2 \omega} \right), \frac{4\sigma_{\omega 2} \kappa}{CD_{\kappa \omega} y^2} \right] \right\}^4 \right\} \quad (3.9)$$

$$CD_{\kappa \omega} = \max \left(2\rho \sigma_{\omega 2} \frac{1}{\omega} \frac{\partial \kappa}{\partial x_i} \frac{\partial \omega}{\partial x_i}, 10^{-10} \right) \quad (3.10)$$

$$\phi = \phi_1 F_1 + \phi_2 (1 - F_1) \quad (3.11)$$

$$\alpha_1 = \frac{5}{9} \quad (3.12)$$

$$\alpha_2 = 0.44 \quad (3.13)$$

$$\beta_1 = \frac{3}{40} \quad (3.14)$$

$$\beta_2 = 0.0828 \quad (3.15)$$

$$\beta^* = \frac{9}{100} \quad (3.16)$$

$$\sigma_{\kappa 1} = 0.85 \quad (3.17)$$

$$\sigma_{\kappa 2} = 1 \quad (3.18)$$

$$\sigma_{\omega 1} = 0.5 \quad (3.19)$$

$$\sigma_{\omega 2} = 0.856 \quad (3.20)$$

RANS models have been shown to produce satisfactory accuracy over different conditions (Versteeg et al., 2007) and although they can produce a detailed view of the flow, they are still only modelling the behaviour.

In practice it is common to use an ideal gas assumption, however this is only valid for air above a temperature and pressure of around 140K and 40 bar respectively. Given that SRVs can be required to operate out with these conditions, real gas effects require to be modelled. Real gases account for compressibility, variable specific heats, van der Waals forces and non-equilibrium effects, which become significant under the above-mentioned conditions and will have to be accounted for. Thus, when working out-with the ideal gas limits a real gas model has to be used in place of the ideal gas equation of state. Several real gas models are available, Beune (2009) carried out an extensive validation of the Redlich-Kwong model and found acceptable accuracy up to pressures of 2000 bar. Therefore, when necessary, his work shall be used to guide the selection of a suitable real-gas EoS for this research.

3.1.1 CFD Configuration

Presented in figure 3.1 is an image of a CAD assembly of the test valve being used, this is a type 3500 SRV from Broady Flow Control Ltd. It is a 1x2" E orifice relief valve designed for gas service that has been certified for ASME Section VIII and could typically be found on unfired pressure vessels. Throughout industry when designing relief valves air is commonly used as the reference gas upon which the valve is designed. This approach will be used in this research for the initial validation exercise and any subsequent design work.

In figure 3.2 below the internal fluid domain extracted from the CAD geometry is shown, on the left is the 3-dimensional domain and on the right is the 2-dimensional equivalent. To obtain greater control of the mesh a domain decomposition method (DDM) was utilised to split up the geometry into individual sections. Having the domain split up as shown below will allow for fine control of the mesh sizing at critical points in the flow path.

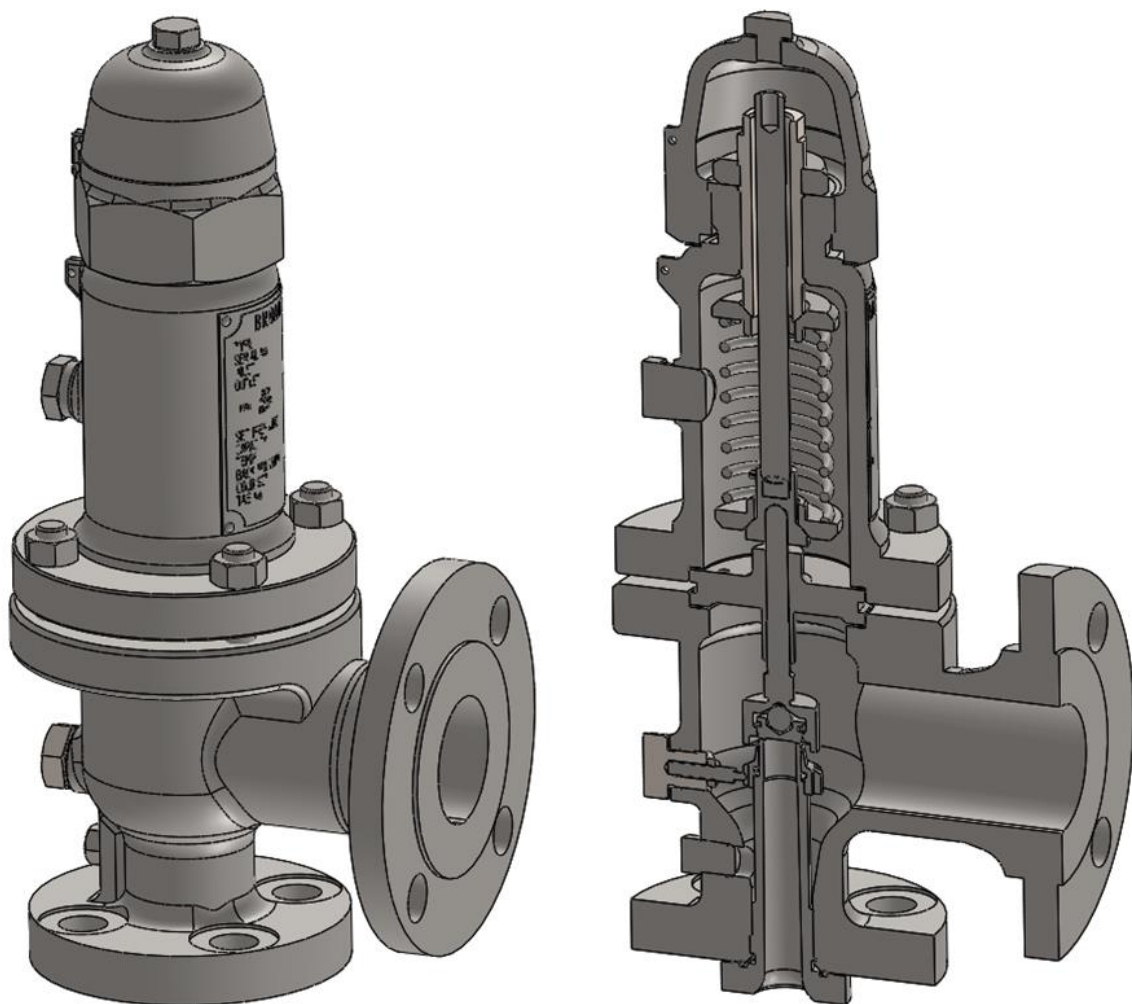


Figure 3.1 – CAD Image of Broady type 3500 1x2" E SRV

Modelling the full operational cycle of the SRV will require starting from an opening height of 0.01mm lift, it is postulated that at this height, a 2-dimensional axisymmetric simulation should be sufficient to capture the disc forces. As the valve opens further it will be necessary to switch to a 3-dimensional simulation. The validity of this hypothesis and the height that this change should take place will be investigated further in the following section.

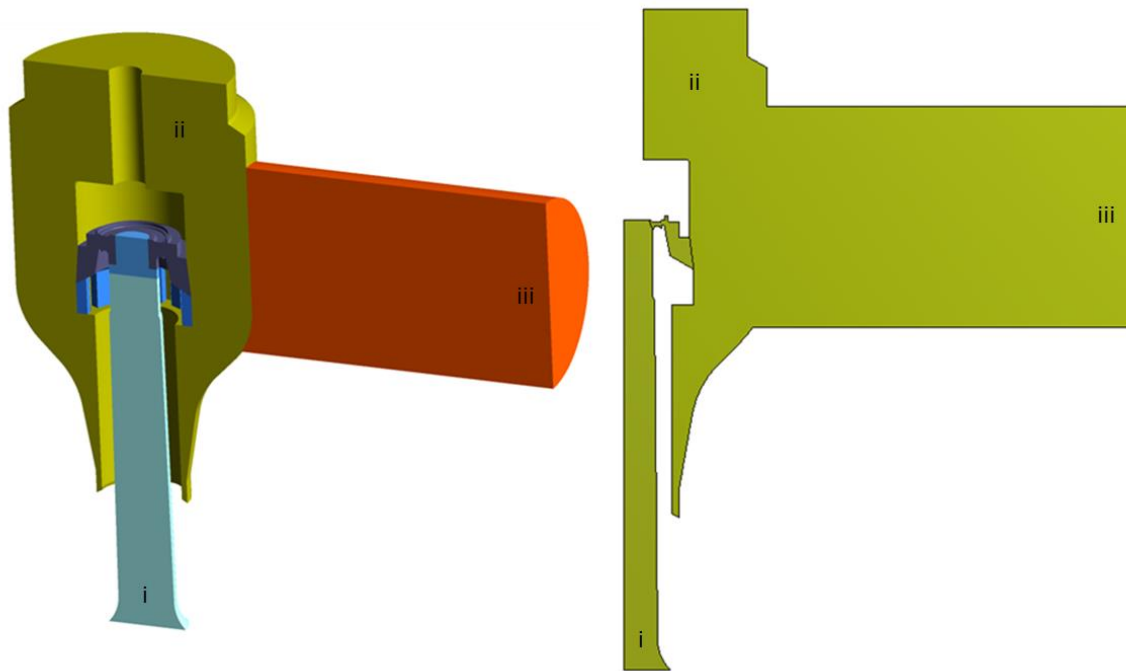


Figure 3.2 – 3-D & 2-D axisymmetric – fluid domain used for CFD analysis – (i) inlet – (ii) body
(iii) outlet

The tables below present the setup used in the CFD calculation, a justification for this configuration shall be discussed throughout the following section. Particular interest should be drawn to the choice of turbulence model - this research utilised the $k-\omega$ SST model. From the literature review some ambiguity was found in the required turbulence model, thus an

investigation into the correct method was undertaken, this is presented in section 3.1.2 below.

Table 3.1 presents the general settings used in the initial CFD setup, the pressure-based solver in the commercial code ANSYS Fluent was used for this research. Pressure-velocity coupling is usually achieved through either the SIMPLE algorithm or one of its variants, however, the coupled algorithm was found to be most stable for the highly compressible internal flows found in relief valves. This SIMPLE-like method is more akin to a density-based solver in that the momentum and continuity equation are solved together rather than in a segregated manner typical of pressure-based schemes (ANSYS, 2018). In a SIMPLE algorithm the momentum equation is solved followed by a pressure correction equation. A coupled algorithm solves the momentum and a pressure-based continuity equation together.

Valve	Broady 3500
Orifice	E
Working Fluid	Air-Ideal Gas
Solver	Pressure-based
Steady/unsteady	Steady state
Energy equation	On
P-V Coupling	Coupled

Table 3.1 – General settings.

An investigation in to the available discretisation schemes available in Ansys Fluent was undertaken. Initially focusing on the second order upwind differencing scheme, this provided reasonable accuracy but had some stability issues. When the first order scheme was studied it provided greater stability but the level of accuracy is generally lower. The QUICK scheme provides third order accuracy for the face values and second order accuracy

for cell values on hexahedral grids, however on non-hexahedral grids Fluent will switch to second order discretisation. This scheme should provide accuracy equal to or slightly better than second order upwind but has improved stability and rate of convergence. It was found to perform better and more stable than the first or second order schemes. The third-order MUSCL scheme is a combination of central and upwind differencing and is suitable for arbitrary meshes - an improvement over the QUICK schemes hexahedral limitation. Unfortunately the MUSCL implementation in Fluent does not contain a flux-limiter which can result in under and overshoots in the presence of shocks. This made it an unsuitable choice for an SRV application which regularly experience strong shocks. Thus, the QUICK scheme was found to be the most suitable for SRV CFD analysis, the resultant discretisation used is presented in table 3.2 below.

Gradient	Least squares
Pressure	Second order
Density	QUICK
Momentum	QUICK
Turbulence kinetic energy	QUICK
Turbulence dissipation rate	QUICK
Specific dissipation rate	QUICK
Energy	QUICK

Table 3.2 – Discretisation.

Table 3.3 presents the boundary conditions used for the validation exercise, the set pressure was set at 3.3 barg, this pressure was used for all investigations in this chapter.

Inlet type	Pressure
Inlet value	3.3 (barg)
Outlet	Pressure
Outlet value	0 (barg)

Table 3.3 – Boundary conditions.

Table 3.4 presents the turbulence model settings; these will be covered in more detail in the following section as it involved a dedicated investigation to obtain the necessary configuration.

Turbulence model	SST
Turbulence wall treatment	Scalable wall function
Inlet turbulence intensity	5%
Outlet turbulence intensity	5%

Table 3.4 – Turbulence boundary conditions.

3.1.2 CFD Verification and Validation

Verification and validation is an important stage of any computational physics analysis. The aim of the process is to build up confidence in a model by ensuring the correct techniques have been employed and in the correct manner. Mathematical models are generally complex in nature thus it is essential to have in place a system of rigorous checks and tests to minimise any errors and uncertainty.

Verification and validation is a two-step process, the verification procedure is purely a mathematical process which could essentially be performed without any interaction with the physics being modelled. The validation process is the point at which the mathematical models will be compared to experimental results. This section shall follow the procedures outlined in the ASME Standard for Verification and Validation in Computational Fluid Dynamics and Heat Transfer (ASME, 2016). This standard provides a method of quantifying an accuracy threshold that a model should meet to be classed as validated, it is based on the premise that should the error between simulation and experiment be less than the sum of all uncertainties in the modelling process, that model can be classed as validated. Therefore it is required that all the uncertainties be defined and their influence on the model quantified.

The comparison error (E) between experimental (D) and simulated (S) results is defined as

$$E = S - D \quad (3.21)$$

The total validation uncertainty u_{val} , comprises of uncertainties from numerical solution methods used u_{num} , uncertainties arising from the measurement of physical data u_D , and input uncertainties in each of the prescribed boundary conditions u_{input} . Using an RMS addition, the total validation uncertainty becomes

$$u_{val} = \sqrt{u_{num}^2 + u_D^2 + u_{input}^2} \quad (3.22)$$

provided $E < u_{val}$ the calculation can be classed as validated. The allowable magnitude of u_{val} is problem specific, with an appropriate u_{val} being specified to ensure a relevant validation has been conducted. The consequence of this is that each problem requires the user to decide what level of uncertainty is acceptable in each application. Throughout the following chapter the magnitude of errors and uncertainties will be calculated and in doing so the model setup presented in section 3.1.1 will be justified. Although the full opening cycle of an SRV is under study, the validation process will focus on a 4mm lift position.

Verification – calculation of u_{num}

Solution verification is primarily associated with ensuring the model design and boundary conditions match that of the real-world physics under analysis. Factors to consider include geometry, boundary conditions, parameters of interest, numerical grid quality and solution methods. Small geometry features have been found to play an important role in SRV CFD studies, the work by Dempster et al. (2006) found that small radii in the flow path can have an effect on the aerodynamic forces experienced by an SRV. These effects will be amplified in the low lift region as the valve is beginning to open. At this stage in operation the disc and spring forces are nearly balanced thus small changes would affect the performance of the

valve. Boundary conditions are set to match those of the experimental value, there is a degree of uncertainty in the exact value but that shall be accounted for in the validation procedure. One parameter that has become apparent when studying ASME type SRVs is the turbulence model utilised. Moncalvo et al. (2009) initially showed inadequacies in the once industry standard κ - ϵ model, which was found to over predict flow separation within the nozzle seat area, which in turn under predicts flow forces on the SRV disc.

Representing the solution of the governing equations via a discretised space invariably introduced some degree of error to the solution. The degree of error can be controlled by decreasing the size of control volumes resulting in a more accurate solution of the continuous function. The consequence of this is an increase in computation costs for the solution process - resulting in a trade-off between an accurate representation of the real world physics and a quick solution time. An ideal situation would be to use an infinitely fine grid upon which to solve the governing PDEs, unfortunately the required computational power is out of reach, and thus it is necessary to find a balance between a dense grid and a shorter solution time. Part of the CFD analysis process involves the user undertaking a grid convergence study in which the numerical grid is refined and the effects of this refinement on the numerical solution are closely monitored. Although an acceptable quality of mesh is required over the full domain, grid refinement may only take place in areas of interest - certain parts of the solution that experiences high gradients or areas close to surfaces being monitored. SRV analyses will tend to involve a finer grid around the nozzle exit and seat area, this region experiences both high gradients and shocks and significantly influences the disc forces. The grid refinement process involves the CFD user reducing the grid node

spacing whilst monitoring the effects on parameters of interest. This will continue until a point when the changes drop below an acceptable level. The main issue with this process is that the user generally does not know the grid requirements prior to undertaking some initial analyses. The user will generally have to undertake some initial calculations to discern the behaviour of the model before moving onto denser grids. It is essential for the user to know the error introduced by the discretisation process - methods first introduced by Richardson (1920) allow the user to quantify this. Richardson Extrapolation, taking its name from the primary author provides the user a means of quantifying the level of error from their numerical grid. It is based on the premise that upon refinement, spatial and temporal errors should asymptotically approach zero (Slater, 2008). To undertake an extrapolation, it is generally advised to use 3 grids of increasing refinement, these should be of sufficient density that the parameter of interest should be in the asymptotic region. It is not necessary to half the grid spacing each time, as this may result in unmanageable grid sizes but a sufficient difference in grid spacing is required and failure to do so may result in false predictions. Roache (1998) extended the Richardson Extrapolation to include a Grid Convergence Index (GCI) which is used to provide a measure of the difference between the computed value and that of the asymptotic one. It will give a clear indication to how the solution would behave upon further refinement. A sample solution verification process has been included below which is used to calculate the numerical uncertainty for the validation uncertainty equation (u_{num}).

Firstly, the true order of convergence should be calculated, CFD code algorithms use a theoretical value of 2 however the true value would be lower (Slater, 2008), p is the true order of convergence,

$$p = \ln \left(\frac{f_3 - f_2}{f_2 - f_1} \right) / \ln(r) \quad (3.23)$$

where f is the parameter of interest (in this study either disc forces or mass flow rate) and r is the grid refinement ratio. Traditionally Richardson Extrapolation uses a value of 2 however utilising a non-integer level of refinement r can be calculated using the following formula,

$$r = \frac{h_2}{h_1} \quad (3.24)$$

h being the grid node spacing. To ensure that p does not become undefined sufficient difference between h_1 & h_2 is required since r could approach a value of 1.

The Grid Convergence Index can now be calculated using the following formula

$$GCI = \frac{F_s |\varepsilon|}{(r^p - 1)} \quad (3.25)$$

F_s being a factor of safety, which is recommended to be 3 when using 2 grids or 1.25 when using 3 grids, ε is the relative error calculated by

$$\varepsilon = \frac{f_2 - f_1}{f_1} \quad (3.26)$$

The extrapolation can now take place using the following method and indicates the grid independent approximation for a solution parameter of interest.

$$f_{h=0} \simeq f_1 + \frac{f_1 - f_2}{r^p - 1} \quad (3.27)$$

A sample of a full solution verification process is included in table 3.5 below,

Grid number	Elements (x10 ⁶)	Force (N)	Discretisation error (%)	Mass flow rate (kg/s)
1	0.025	71.065	17.627	0.08135652
2	0.040	72.646	15.795	0.08147521
3	0.076	73.539	14.760	0.07927049
4	0.098	83.414	3.313	0.08529766
5	0.125	83.221	3.537	0.08039441
6	0.145	83.859	2.797	0.07906506
7	0.253	87.915	-1.904	0.07985669
8	0.547	89.742	-4.022	0.07868908
9	1.096	87.189	-1.062	0.07900364
10	3.263	86.514	-0.280	0.07921158

Table 3.5 Grid refinement study – 3511E 1x2" 3.3barg 2mm lift.

The results of a Richardson Extrapolation are included in table 3.6 below, where the subscripts 10-9 and 9-8 refer to grid levels 10 & 9 and 9 & 8 respectively.

Richardson Extrapolation & GCI	
h10 (fine grid)	0.10
h9	0.15
refinement ratio	1.50
Order of solution	3.28
Force 10 (N) (fine grid)	86.51
Force 9 (N)	87.19
Force 8 (N)	89.74
Extrapolated force (N)	86.27
FOS	1.25
GCI ₁₀₋₉ (%)	-0.35
GCI ₉₋₈ (%)	-1.31
Asymptotic range check	0.99
Extrapolated value	86.27
Error (%)	-0.35

Table 3.6 Richardson Extrapolation and GCI check.

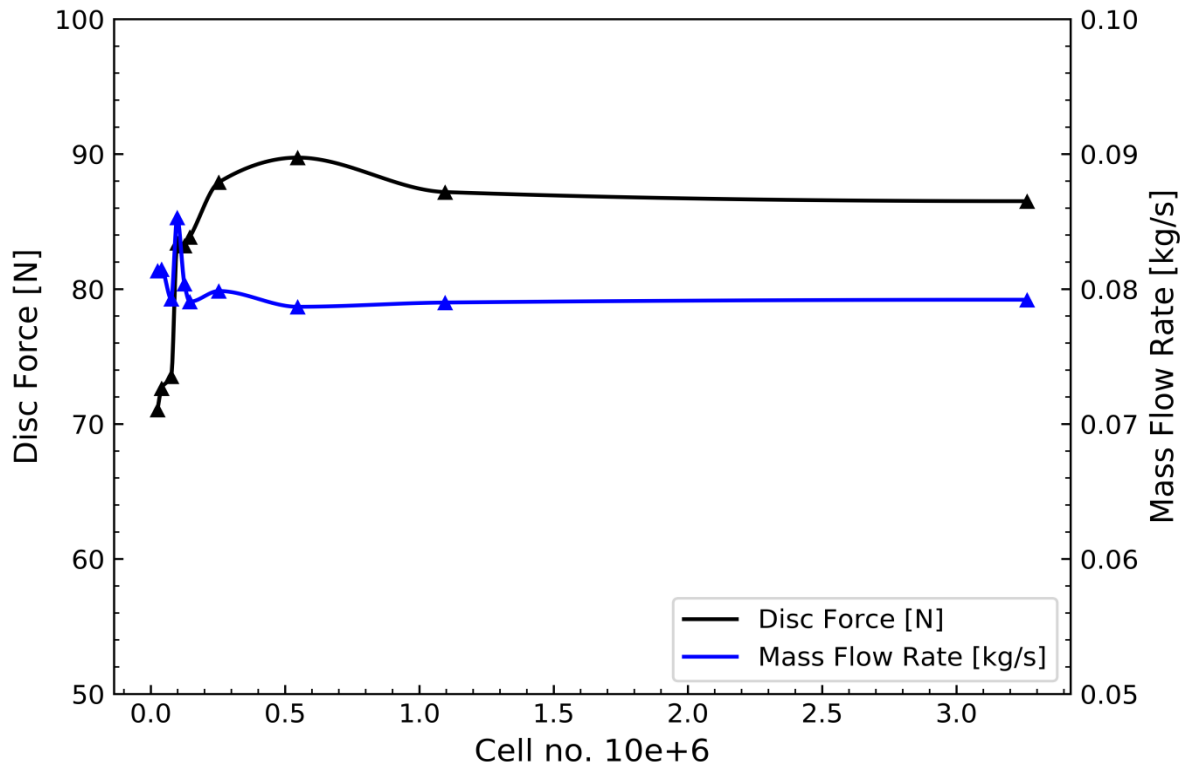


Figure 3.3 – Grid refinement study.

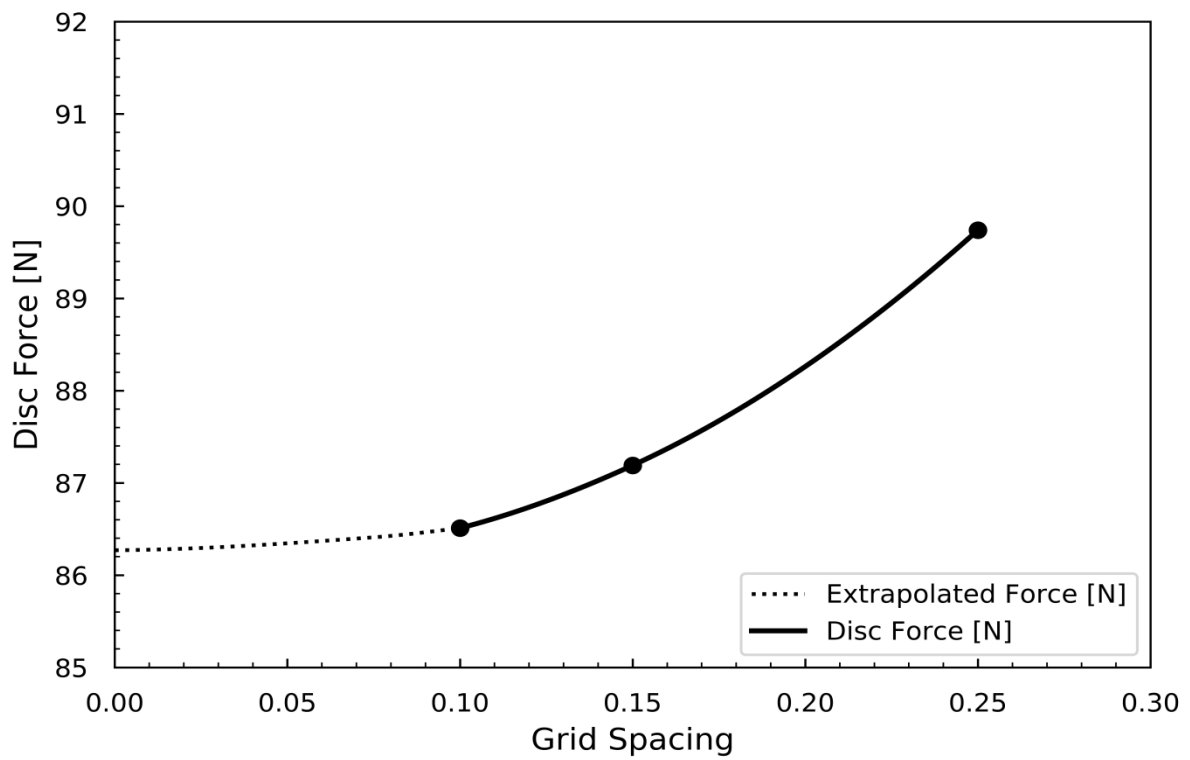


Figure 3.4 – Richardson Extrapolation.

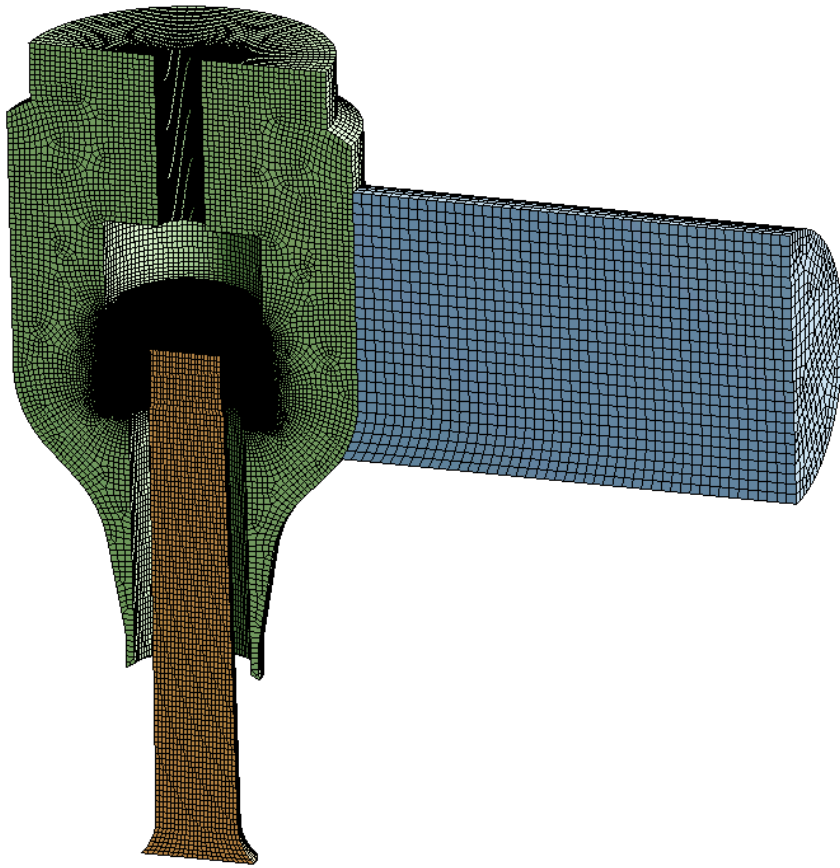
Figure 3.3 clearly shows the significant variation of the results on a low-quality grid, confirming the need for a full grid independence study; the results can be seen to enter the asymptotic region from 0.5M elements. Figure 3.4 displays the extrapolated force using the Richardson extrapolation technique. This figure can be quoted with the GCI value to give a final solution of

$$f_{h=0} = 86.27 \pm 0.35\% \quad (3.28)$$

The discretisation error presented here is one part of the numerical uncertainty, the other part comprises the iteration error during the solution process. This however is much less than the discretisation error. Assuming the numerical uncertainty is being treated as comprising fully of the discretisation error thus

$$\begin{aligned} u_{num} &= \frac{GCI_{10-9}}{2} f \\ &= \frac{0.35 \times 10^{-3}}{2} 106.06 \\ &= 0.02N \end{aligned} \quad (3.29)$$

where f is a scaling parameter (in this study the disc force at 4mm lift), used to dimensionalise the non-dimensional GCI value resulting in a numerical uncertainty of 0.02N. Figures 3.5-3.7 display the final mesh configuration used throughout this initial validation. Figures 3.6 and 3.7 focus on the nozzle exit and disc area - this is the region that will experience highest gradients.



Figures 3.5 – Final computational grid.

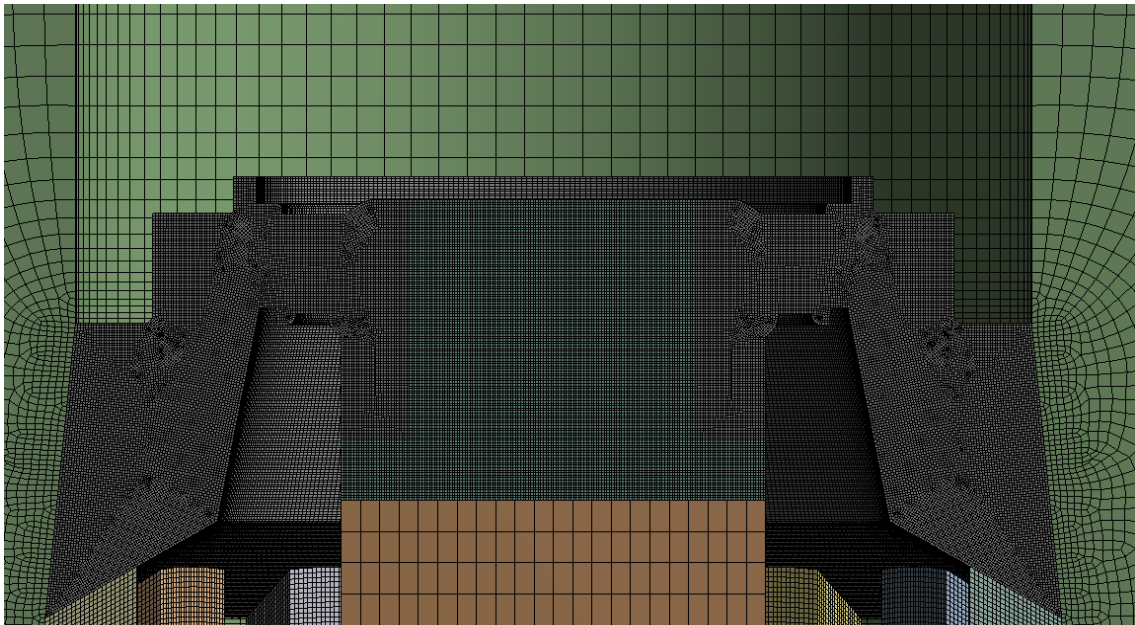


Figure 3.6 – Final mesh configuration – nozzle exit region.

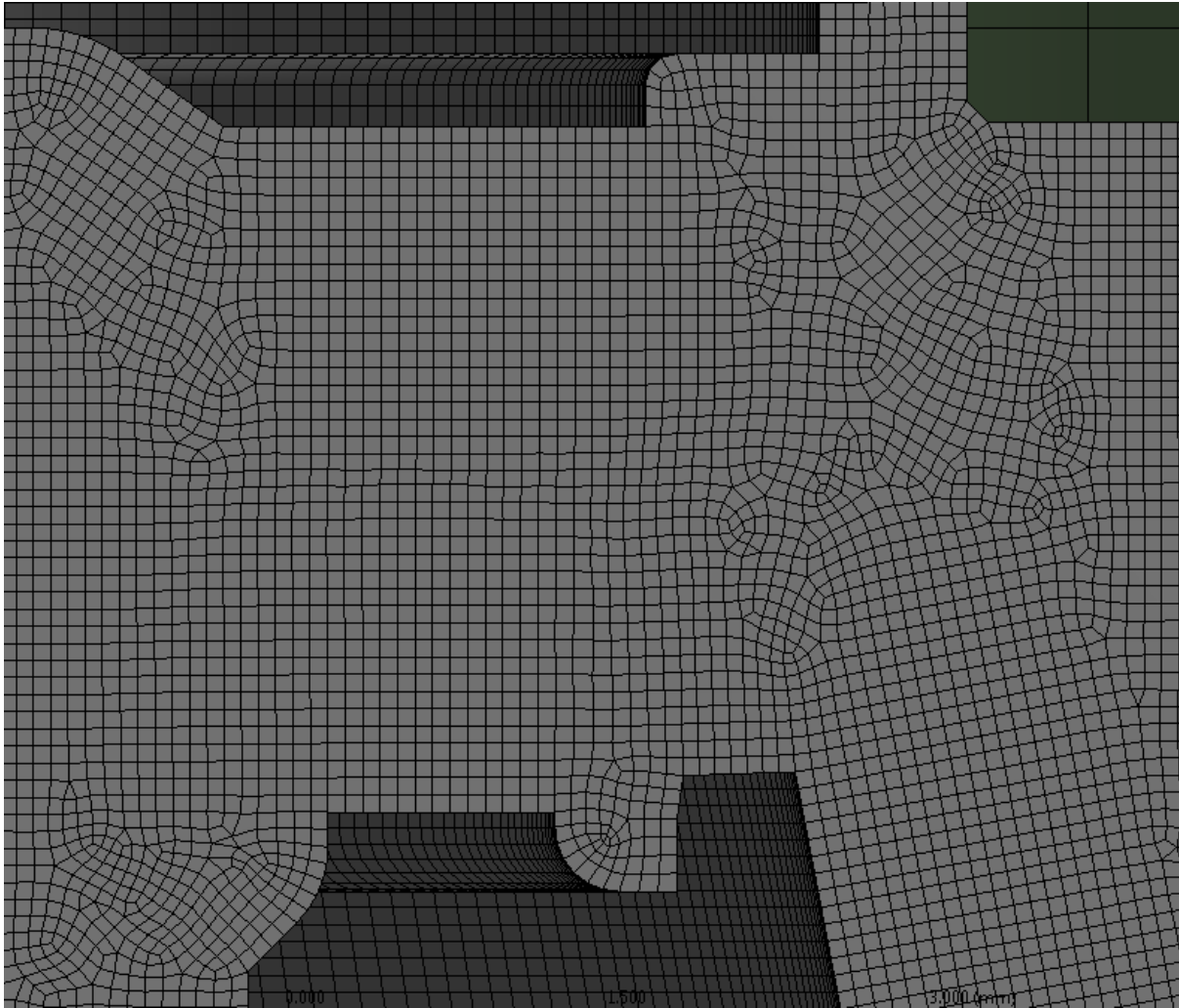


Figure 3.7 – Final mesh setup – focusing in the seat area which will experience the strongest gradients – approximately 2100 cells per mm³ in this region.

Validation – calculation of u_D

The experimental results were obtained from the test facility provided by Broady Flow Control, which were configured following the guidelines by the ASME PTC 25 Performance Test Code pertaining to Pressure Relief Devices (ASME, 2014). This standard designates the setup that should be used for capacity testing of pressure relief valves. The facility also included PRV flow force measurement equipment - essential for the development of PRVs.

A P&ID of the test facility at Broady Flow Control presented in figure 3.8, the main components have been numbered for clarity. The test rig operates by using a small feed compressor (1) to build up a large supply of compressed air, this is opposed to having a large compressor to continually provide the pressurised fluid necessary for the test. This approach makes achieving the required flow rates possible with a smaller compressor, which has obvious financial benefits. The working medium is air compressed at 14 barg and held in 4 large storage vessels (3) with a total capacity of 10000l. The storage vessels are connected to a buffer vessel (8) on which the test valve (9) is mounted. Test measurement is achieved by various transducers located throughout the test rig in accordance with ASME PTC 25.

The test facilities are supplied with air from an Ingersoll Rand screw type compressor (1) with a capacity of 1.61m³/min and discharge pressure of 14 barg. The output from this compressor is fed through an Ingersoll Rand condensing air dryer (2) with a capacity of 2.4m³/min - this is used to remove any moisture from the system as this can cause problems. As a consequence of the Joule-Thomson effect, significant temperature drops at the SRV nozzle are present so any moisture in the expanding fluid can solidify and cause an ice build-up on the disc face. The main system is fed through a 1" line from the air dryer to the 4 storage vessels (3) - this line has 2 ball valves situated just after the air dryer and just before entering the main storage vessels.

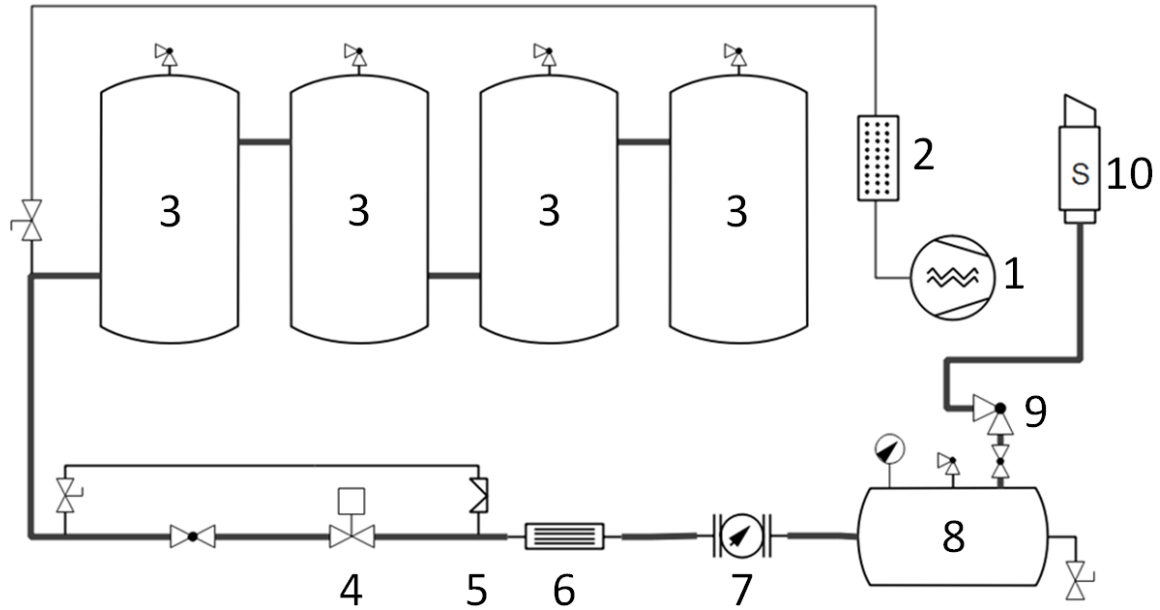


Figure 3.8 – P&ID of the test facilities at Broady Flow Control.

The test rig uses 4 storage vessels that have a working pressure of 14 barg and a capacity of 2m³ each, they are all connected using DN100 pipework and are each protected by a Niezgodka SRV. From the storage vessels the system consists mainly of DN100 pipework, reducing to DN80 when passing through the control valve and the flow meter. Situated between the control valve and the storage vessels is a ball valve that can be used to manually stop any flow. The control valve (4) is produced by Valvitalia, it is a 3" line size model and is controlled pneumatically by a Valvitalia diaphragm rotary actuator.

Downstream of the control valve the system has straightening vanes (6) to reduce turbulence, as requested by PTC 25. These straightening vanes are essential when either of the upstream ball valves is in a partially open condition. The control valve is only suitable for higher flow rates (>0.2kg/s), at lower flow rates it is not possible to get a stable balanced

flow. To maintain constant pressure in the buffer vessel, a bypass line has been installed that uses a Broady C6 diaphragm valve (5) to control the inlet flow. This valve is able to control the flow into the buffer vessel up to around 0.25 kg/s.

Downstream of the flow straightening section, an Emerson Coriolis meter (7) is used to measure the flow rate of the system. This uses a DN80 nominal line size so the flow cross section is reduced at this point, this flow meter can operate on gas to 10 kg/s. This meter is rated to 0.1% accuracy and a repeatability of 0.02% of the reading. The last stage in the flow test rig is a buffer vessel (8) on which the test valve is mounted. This tank is rated at 10 barg and has a 1500l capacity. This is protected by a Niezgodka safety relief valve set at 10 barg which vents to atmosphere. The buffer vessel is fed from the Coriolis meter via DN100 pipework which enters at the lower section on one end of the vessel, the test valve is mounted on top of the vessel at the opposite end. The test valve can vent into the atmospheric conditions of the testing facility or it can be attached to a silencer section (10) to reduce the level of noise of the discharge. The inlet pressure of the test valve is determined by taking a reading within the buffer vessel. A Druck PTX 1400 pressure transducer is used for this measurement, it has an accuracy of 0.25% and a maximum operating pressure of 10 barg. The pressure and flow rate measurement are transmitted to a data acquisition device connected to a PC within the laboratory. Data processing is achieved using the QuickDAQ software.

The aerodynamic force experienced by the SRV disc is of primary importance with the measurement of this force achieved by a load cell mounted within a specially designed mounting. The force is recorded at several different opening heights to produce an array of forces covering the full opening cycle of the SRV. These results are used as a measure to

validate the mathematical models against. The aerodynamic force experienced by the disc is measured by an Omega Engineering Ltd. load cell, this has a range of 0-200N and an accuracy of $\pm 0.5\%$. This is connected to the data acquisition hardware via an RDP transducer amplifier. The test rig has been designed to give the operator a high degree of control over the position of the disc in relation to the seat. The force measurement procedure starts with setting the valve in contact with the seat, i.e. a fully closed position. This is used as the datum point on which the test will proceed. The preload value - which is the required force to ensure fluid containment within the nozzle - is measured by compressing the disc on the valve seat and slowly reducing the load until the set point is reached. As Broady Flow Control utilise the 'first audible' definition of set point, the disc is compressed against the nozzle seat and the applied load is slowly reduced until the compressed air is heard escaping from the nozzle. The load at this point is recorded and this height is used as a datum. It is worth noting at this stage that although the fluid is heard escaping from the nozzle the disc and nozzle sealing faces are still in contact, although they are polished to a lapped finish they are not completely smooth. Upon bringing the sealing faces into contact any microscopic roughness on the surfaces is elastically deformed to produce a seal. On setting the preload value of the SRV the first audible point will still be in contact but the elastic deformation will have relaxed sufficiently to allow for working fluid to escape. This set point is then used as the datum from which the experiment shall proceed, the set point is taken as 0mm lift, the disc is then moved off the seat by a discrete amount to allow a force measurement to take place. During this whole process the buffer vessel pressure is maintained at the test pressure. Force measurements are then taken across the full opening range (0-4mm) of the valve to obtain a set of measurements which when plotted against the lift value produce what is termed a force-lift curve. This curve gives an indication of the fluid

behaviour inside the PRV and can allow the user to approximate the performance of the test valve. The lift measurement is achieved using a dial gauge which has a resolution of 10µm and an accuracy of 0.5%. The spindle/disc position is adjusted by a M32×1mm pitch thread giving the operator a high degree of fine adjustment over the full opening cycle.

In addition to the flow force experiments, functional tests are also carried out using the same facility. Functional tests determine the over pressure, blowdown and displacement of the specimen valve. During these tests the operator will also be able to determine how the PRV behaves and whether stable performance was achieved. The overpressure and blowdown are simply calculated from recording the pressure at which the valve fully opens and the pressure when it recloses. The displacement is measured by using a linearly variable displacement transducer (LVDT). As with the load cell, the LVDT is connected to the data acquisition system via an RDP transducer amplifier.

The validation process requires both the displacement and force measurement from the test facilities. When quoting the measured results an estimation of uncertainty must be included. This was calculated following the guidelines set out in ASME PTC 19.1 Test Uncertainty and ASME Verification & Validation 2009 (ASME, 2009), these codes provide a clear statement to measurement uncertainty and how it should be estimated. Table 3.7 below, summarises the measurement equipment used in this part of the research.

Property	Transducer	Accuracy (total range)	Range
Pressure	Druck PTX 1400	0.25%	10bar
Pressure	Druck PTX	0.15%	10bar
Flow rate	Emerson Coriolis meter	0.1% (of reading)	10kg/s
Disc force	Omega load cell	0.5%	200N
Displacement	LVDT	0.5%	0-10mm
Data acquisition	DT9813	0.1%	100kHz
Data acquisition	QuickDAQ	N/A	N/A

Table 3.7 – Test equipment.

Experimental errors fall into two categories, statistical errors arising from the random differences apparent from multiple measurements and systematic errors as a result of inaccuracies in the equipment used to obtain the results. Statistical errors are random differences between each time a measurement is taken, individual values cannot be predicted but an average is calculable from numerous results. Increasing the amount of data available will increase the accuracy of the calculated average result. More data will help to dampen the effects of any individual outlying data points. Systematic errors are a result of the experimental design and equipment; these errors are not random and will affect the results in a quantifiable manner (Cartwright, 2003). Equipment manufacturers will provide an estimate of their equipment accuracy, using this figure the total systematic error of all the equipment can be calculated. Once each error is quantified the total experimental error can be calculated and used when quoting results.

With the aim to quantify a statistical error of an experiment it is beneficial to obtain many data points for the same measurement condition and this will allow for the Gaussian distribution to be extracted from the data which will be centred at the true average value.

An estimate of the true value of x can be obtained by the following formula

$$x_0 = \frac{1}{N} \sum_i x_i = \bar{x} \quad (3.30)$$

Where N is the number of measurements in the sample, the error on each measurement can be calculated as follows

$$s^2 = \frac{1}{N-1} \sum_i (x_i - \bar{x})^2 \quad (3.31)$$

Combining these equations to obtain an estimate of error on the average result \bar{x} produces the following standard error

$$s_{\bar{x}} = \frac{\sigma}{\sqrt{N}} = \left[\frac{1}{N(N-1)} \sum_i (x_i - \bar{x})^2 \right]^{\frac{1}{2}} \quad (3.32)$$

This now provides an estimate of the error on the average result in the experiment, following this procedure the statistical error was obtained from a series of repeated tests. An average statistical error of 0.64N was calculated for the total measurement, the results are presented in the table 3.8 below. The error estimation was evaluated for a fully open valve at 4mm lift, experiencing a force of 106.6N the statistical error becomes 0.6%.

The systematic uncertainty is calculated using the accuracy figure provided by the manufacturer for each measurement device. The true value of systematic uncertainty is unknown but its standard deviation can be calculated using an RMS addition from the following formula

$$b_{\bar{x}} = \left[\sum_{i=1}^i \left(\frac{\partial F}{\partial X_i} b_i \right)^2 \right]^{\frac{1}{2}} \quad (3.33)$$

Where $\frac{\partial F}{\partial X_i}$ accounts for the sensitivity of the force measurement to each instrument and b_i is an estimation of the uncertainty of each instrument. The flow force measurement systematic uncertainty will be quantified by the sum of uncertainties of the load cell, pressure transducer and the data acquisition device.

$$b_{\bar{x}} = \sqrt{0.1064^2 + 0.0532^2 + 0.2128^2} = 0.24$$

Lift (mm)	Test 1 Force (N)	Test 2 Force (N)	Test 3 Force (N)	Test 4 Force (N)	Test 5 Force (N)	Test 6 Force (N)	x_0 Force (N)	$\sigma_{\bar{x}}$
0.000	62.10	61.90	61.90	61.00	61.30	61.00	61.53	0.49
0.010	61.38	59.28	59.98	59.98	59.98	60.18	60.13	0.69
0.020	60.16	58.66	58.86	59.26	59.06	59.36	59.23	0.52
0.030	59.05	58.05	58.05	58.25	57.85	58.15	58.23	0.42
0.040	58.31	57.71	57.51	57.21	57.31	57.71	57.63	0.39
0.050	58.53	57.93	57.53	57.73	57.33	57.93	57.83	0.41
0.060	57.93	58.03	57.33	58.13	57.23	58.33	57.83	0.45
0.070	58.06	58.26	58.06	59.26	57.26	59.66	58.43	0.88
0.080	58.50	58.70	58.60	60.20	58.00	60.80	59.13	1.10
0.090	59.95	60.25	60.15	61.95	59.55	60.75	60.43	0.84
0.100	60.98	60.98	60.68	63.08	60.08	61.58	61.23	1.03
0.110	61.76	62.06	61.36	64.16	60.86	62.56	62.13	1.15
0.120	62.33	62.73	62.13	64.53	61.33	63.33	62.73	1.10
0.130	62.91	63.31	62.41	64.71	62.01	64.01	63.23	1.01
0.140	63.83	64.33	63.13	65.43	62.73	64.73	64.03	1.01
0.150	64.80	64.90	63.70	66.10	63.40	65.50	64.73	1.03
0.175	66.36	66.26	65.16	67.16	64.96	66.86	66.13	0.89
0.200	67.78	66.48	66.58	67.38	66.38	68.18	67.13	0.76
0.250	67.93	67.43	67.33	66.53	67.13	68.23	67.43	0.60
0.300	68.41	67.61	67.41	66.61	67.51	68.21	67.63	0.64
0.350	67.51	66.71	67.21	66.41	67.71	67.81	67.23	0.56
0.400	67.01	66.51	66.91	67.01	67.91	68.01	67.23	0.60
0.450	67.98	68.68	69.68	69.88	69.78	70.58	69.43	0.94
0.500	69.93	70.33	70.13	70.23	70.03	70.73	70.23	0.28
0.550	71.18	70.28	70.38	70.28	70.18	70.88	70.53	0.40
0.600	71.31	70.81	70.41	70.51	70.31	71.01	70.73	0.39
0.650	71.41	70.91	70.41	70.11	70.61	70.91	70.73	0.45
0.700	71.55	70.95	70.35	70.75	70.75	71.25	70.93	0.42
0.750	71.46	70.56	70.56	70.66	70.46	71.26	70.83	0.42
0.800	71.21	70.41	70.91	71.11	71.21	71.91	71.13	0.49
0.850	70.36	70.86	71.46	71.26	71.36	72.66	71.33	0.77
0.900	70.01	70.61	71.11	71.01	71.91	72.11	71.13	0.79
0.950	71.81	71.71	72.61	72.11	72.51	73.21	72.33	0.56
1.000	72.70	72.40	72.90	73.00	73.00	73.60	72.93	0.40
1.100	72.56	72.26	72.76	72.36	72.76	73.66	72.73	0.50
1.200	74.38	73.48	74.38	74.98	74.58	75.38	74.53	0.64
1.300	76.93	76.03	76.23	77.13	76.13	77.33	76.63	0.57
1.400	78.41	78.11	77.41	77.81	77.21	78.01	77.83	0.45
1.500	79.61	79.21	78.91	79.21	78.61	79.21	79.13	0.34
1.600	80.76	80.76	80.16	79.96	79.66	80.66	80.33	0.47
1.700	82.41	82.21	82.31	82.11	82.01	82.31	82.23	0.15
1.800	83.28	83.68	83.08	83.18	82.48	83.68	83.23	0.45
1.900	82.81	82.81	83.11	83.51	82.91	84.21	83.23	0.55
2.000	84.16	84.06	83.46	83.96	83.46	84.46	83.93	0.40
2.100	85.43	85.73	84.83	85.43	84.83	85.73	85.33	0.41
2.200	87.01	87.21	85.71	85.91	84.91	86.61	86.23	0.88
2.300	88.53	88.43	86.93	87.53	86.33	87.43	87.53	0.85
2.400	90.80	90.40	88.50	88.80	88.00	89.50	89.33	1.10
2.500	91.76	91.26	92.36	92.66	91.86	92.86	92.13	0.61
2.600	95.13	94.93	96.23	96.83	94.93	96.33	95.73	0.83
2.700	97.78	97.08	98.18	98.18	96.88	98.28	97.73	0.61
2.800	99.01	98.71	99.41	100.01	98.81	100.01	99.33	0.58
2.900	97.65	97.65	98.55	100.25	98.75	100.15	98.83	1.15
3.000	99.55	99.75	100.25	101.15	100.45	100.85	100.33	0.62
3.100	101.05	101.25	101.55	102.45	101.45	102.05	101.63	0.52
3.200	101.91	102.31	102.51	103.31	102.21	102.91	102.53	0.51
3.300	103.91	103.61	103.91	104.81	103.51	104.41	104.03	0.50
3.400	105.13	104.43	104.83	105.73	103.73	105.13	104.83	0.69
3.500	105.51	105.51	105.31	106.21	104.71	105.91	105.53	0.52
3.600	107.33	106.83	106.83	107.43	105.83	106.73	106.83	0.57
3.700	107.53	106.83	106.93	107.43	105.83	107.03	106.93	0.61
3.800	107.06	107.16	107.36	108.16	106.66	107.56	107.33	0.51
3.900	104.56	104.76	105.66	106.46	105.96	106.36	105.63	0.80
4.000	105.53	105.93	106.23	107.23	106.93	107.33	106.53	0.74

Table 3.8 – Random uncertainty calculation data.

To provide a confidence level around this result it is common to include a coverage factor to account for a distribution (ASME, 2009), using a coverage factor of 2 for a Gaussian distribution the systematic uncertainty for a 95% confidence level becomes

$$b_{\bar{x}} = 0.48$$

The total experimental uncertainty is obtained using an RMS addition of the statistical and systematic uncertainty given below

$$u_{\bar{x}} = \sqrt{(b_{\bar{x}})^2 + (s_{\bar{x}})^2} = 0.77\% \quad (3.34)$$

To obtain the data uncertainty u_D from this equation it needs to be scaled to the validation point being used in this study - 106.6N disc force at 4mm lift - thus the data uncertainty value becomes

$$\begin{aligned} u_D &= 0.77 \times 10^{-2} \times 106.6 \\ &= 0.82N \end{aligned} \quad (3.35)$$

Turbulence model comparison

For many years after its introduction, the κ - ϵ model was at the centre of industrial CFD analysis and was once the industry standard turbulence model (Tu et al., 2013). It still remains one of the most widely used and validated turbulence models in use - performing notably well in confined flows. However, the model has been shown to produce less accurate results in unconfined and recirculating flows. Many variants of the κ - ϵ model have been published to address some of these shortcomings. A popular alternative to the κ - ϵ was published by Wilcox (1988) termed the κ - ω model. This model produces better results in the boundary layer but the free stream is sensitive to the assumed value of ω (Menter, 1992).

To address the free stream dependency of the κ - ω model Menter (1993) produced 2 new variations of the κ - ω model, the Baseline model (BSL) which removes the dependency on free stream values, and the Shear Stress Transport (SST) model which is the same as the BSL model but accounts for transport of turbulent shear stresses in adverse pressure gradient boundary layers. The BSL works by blending from the κ - ω in the inner boundary layer to the κ - ϵ in the outer boundary layer region providing a model with the strengths of each individual model. The SST model operates in the same manner as the BSL model but also allows for the transport of turbulent shear stresses, which has been shown to provide better agreement with adverse pressure gradient flows (Menter, 1993).

Research undertaken by Moncalvo (2009) investigated the sensitivity of discretisation and turbulence model on the ability of ANSYS CFX to predict flow rates through 2 ASME type SRVs. The κ - ϵ model was found to be least accurate when compared to the κ - ω and SST, with the SST generally producing the best results with an error of <3%. In his PhD thesis Beune (2009) performed a comparison into the effects of different RANS based turbulence models in a compressible flow application prior to his investigation into high-pressure SRVs. Using the 2D supersonic ramp study of NASA (Settles, 1991) it was shown that the SST model provides the best results, the κ - ω and κ - ϵ were not able to converge on this application. In a 2D SRV style geometry he found that the κ - ϵ and SST both predicted density variations well when compared to experiment however only the SST was stable enough on finer grids which were required to resolve the shocks correctly. In a sensitivity study of a 3D SRV model Beune found that variation in the turbulence model effected the predicted mass flow rates by up to 4%. Beune and Moncalvo's studies did not investigate flow forces, however Dempster et al. (2006), were able to validate an SRV CFD study using the κ - ϵ model

showing that it is able to predict the disc forces adequately over a range of valve openings. However, this was for a through-flow type valve with axisymmetric flow, not a right-angled ASME style device thus a comparison may not be applicable. Due to the uncertainty in the appropriate turbulence models for an SRV analysis and also the well documented separated flow sensitivity of the κ - ϵ model in what will be a separated flow, a turbulence model sensitivity analysis was undertaken. A set of calculations were performed using an identical configuration presented in section 3.1.1, the κ - ϵ and SST models were utilised to compare their ability in calculating the SRV disc forces. As before a range of openings were checked in the study of the Broady SRV, up to 4mm lift, the results are tabulated in table 3.9.

Lift (mm)	Experimental Force (N)	SST Force (N)	SST Δ Force (%)	KE Force (N)	KE Δ Force (%)
0.80	70.13	70.86	-1.04	68.85	1.83
1.00	73.33	74.28	-1.29	69.71	4.94
1.20	75.20	77.13	-2.56	73.24	2.61
1.40	78.70	78.84	-0.17	75.06	4.63
1.60	81.40	80.54	1.06	76.97	5.45
1.80	83.40	82.34	1.27	79.00	5.28
2.00	85.60	83.90	1.98	80.90	5.49
2.20	87.20	85.65	1.78	82.59	5.29
2.40	89.10	87.79	1.48	84.12	5.59
2.60	90.30	90.97	-0.74	86.56	4.14
2.80	97.30	95.48	1.87	87.95	9.61
3.00	100.00	99.96	0.04	88.83	11.17
3.20	101.30	102.00	-0.69	90.16	11.00
3.40	103.80	103.00	0.77	90.91	12.41
3.60	105.00	103.50	1.43	91.75	12.62
3.80	105.60	105.10	0.47	92.69	12.23
4.00	106.50	106.06	0.41	93.02	12.66

Table 3.9 - CFD Force validation against SST and $\kappa\epsilon$ turbulence models.

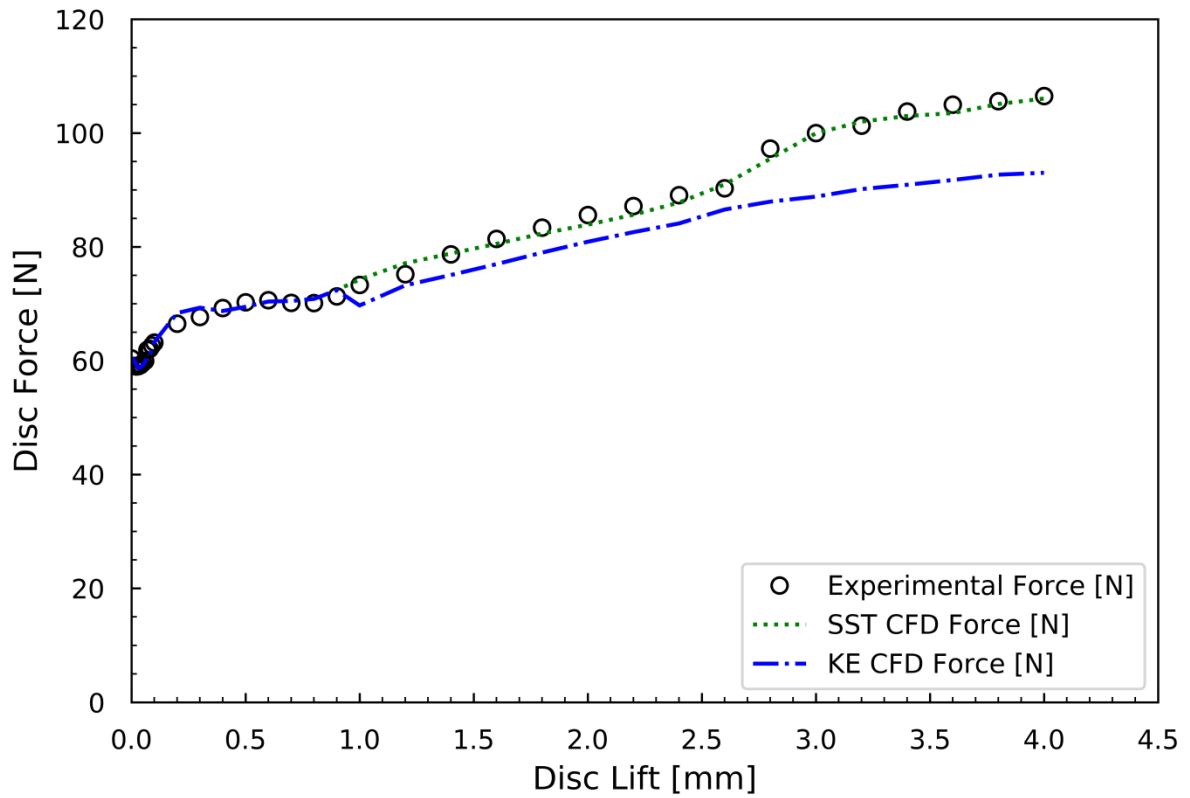


Figure 3.9 – Broady 3511E Force-lift plot using κ - ϵ and SST turbulence models – air at 3.3 barg.

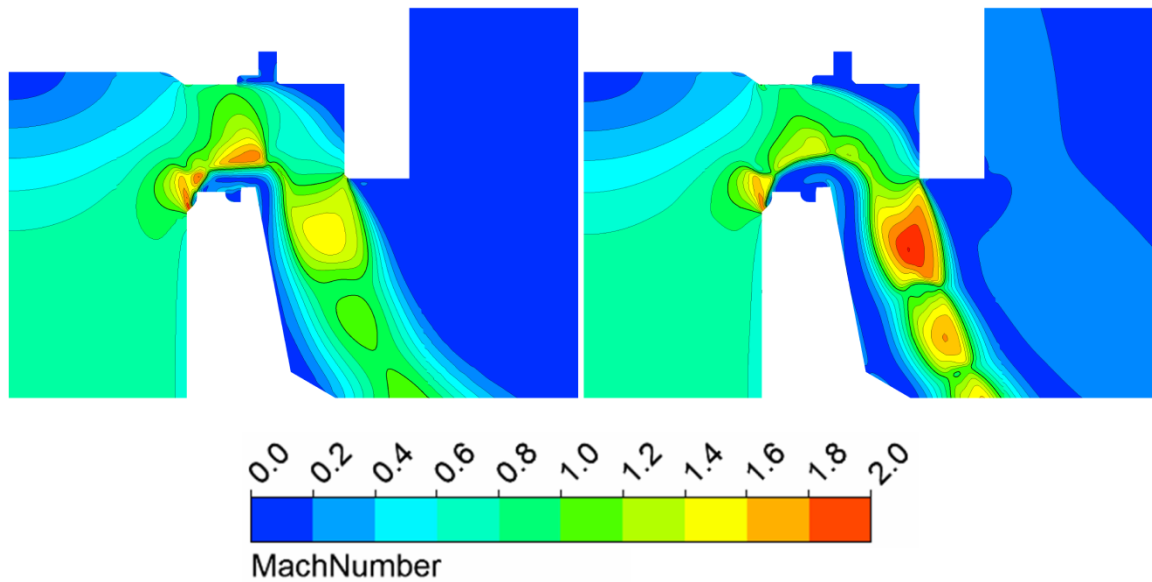


Figure 3.10 – 3-D – Mach number contour plot of KE (left) and SST (right). Ma = 1 marked in black – air at 3.3 barg at 4mm lift.

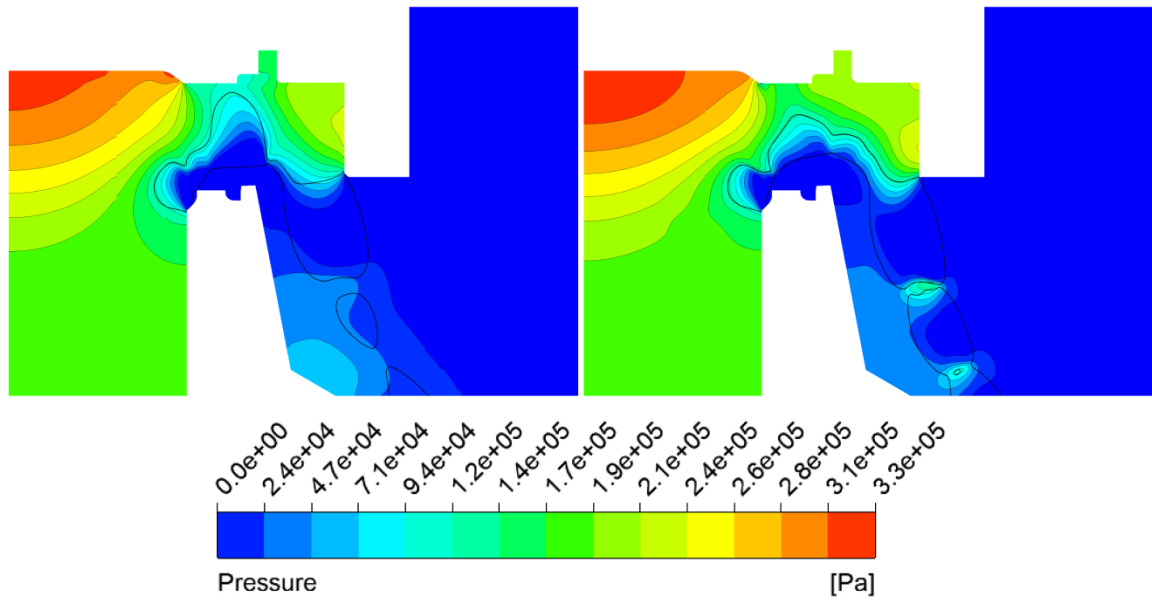


Figure 3.11 – 3-D – Pressure contour plot of KE (left) and SST (right). Ma = 1 marked in black – air at 3.3 barg at 4mm lift.

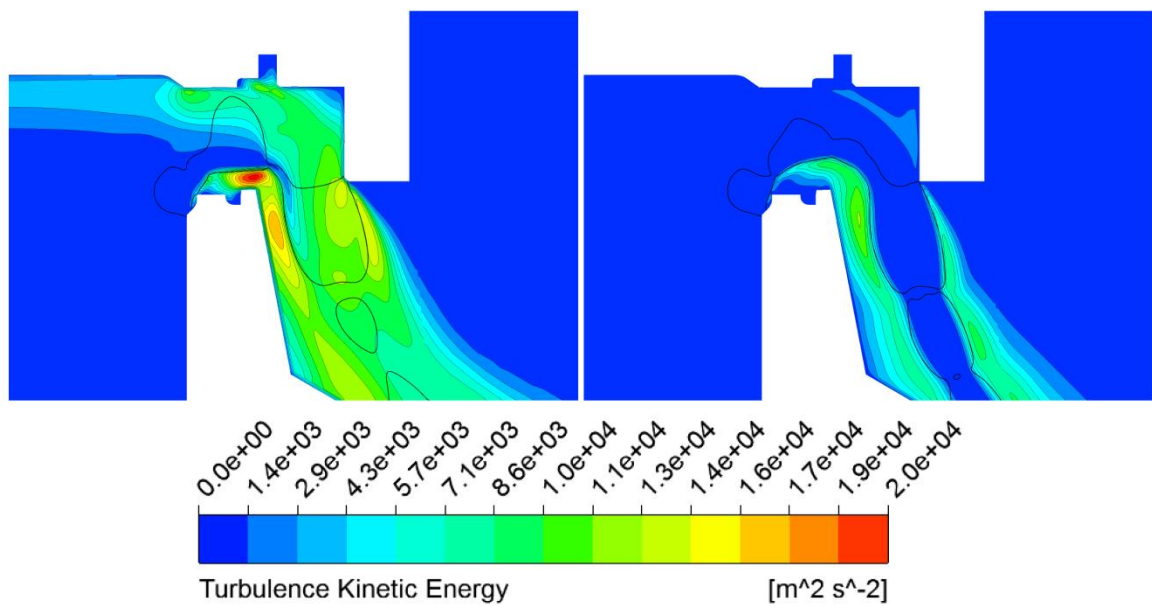


Figure 3.12 – 3-D – turbulent Kinetic Energy contour plot of KE (left) and SST (right). Ma = 1 marked in black – air at 3.3 barg at 4mm lift.

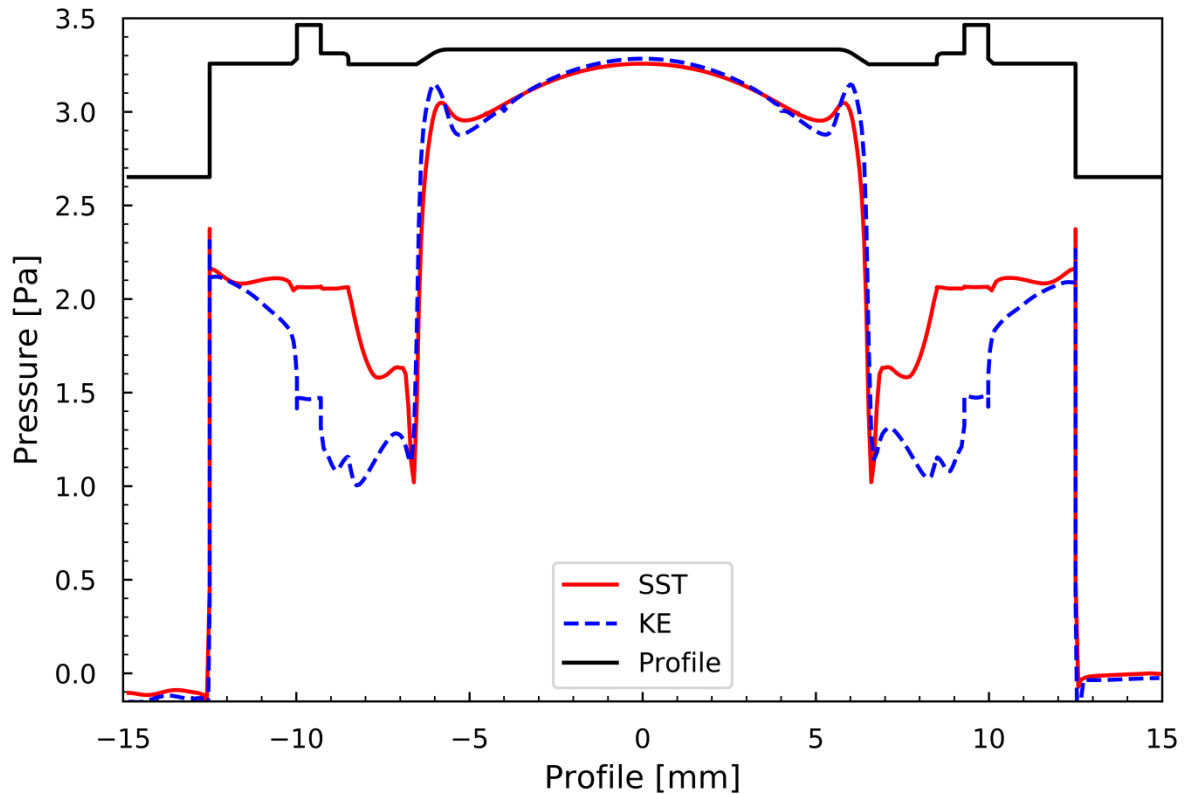


Figure 3.13 – 3-D - pressure distribution comparison between κ - ϵ and SST turbulence models at 4mm lift.

The force-lift data presented in figure 3.9 clearly shows the differences between calculated disc forces from both of the investigated turbulence models. The discrepancy starts from around 0.8mm lift as some flow separation begins to occur. The under prediction of force by the κ - ϵ model continues to grow up to maximum opening at 4mm lift. In comparison, the SST model agrees well with experiment frequently predicting forces to within 1% difference. The Mach number contours in figure 3.10 show the κ - ϵ model predicting choking to occur more upstream compared to the SST model and to a greater extent; this corresponds with a lower pressure in the same region in plot 3.11. The pressure distribution in figure 3.13 is able to quantify the pressure distribution more clearly. The region of force under prediction

becomes evident when analysing the curves in figure 3.13, as the flow is leaving the nozzle, the κ - ϵ force is much less. This is the region that sees flow separation as displayed in figure 3.10, the iso-line at $Ma=1$ highlights the differences in choking prediction of each of the models. The κ - ϵ model is showing a much wider region in the choking plane at the nozzle seat region, clearly having an effect on the pressure distribution.

As the fluid is leaving the nozzle the gas displays an expansion fan attached the inside edge of the nozzle sealing face, this expansion follows the flow downstream of the nozzle to the disc holder shroud region. At this stage a second expansion fan can be see attached to the inside edge of the disc holder shroud. This then leads to successive expansion and shock waves to bring the fluid to equilibrium with the conditions in the valve body. This complex expansion process is happening in a confined region around the nozzle exit disc holder shroud. The κ - ϵ model is known to be insensitive to adverse pressure gradients and to poorly predict separated flows which would agree with the results presented in this section. The sensitivity of disc force prediction to flow separation can be appreciated from this investigation. The level of separation has a direct impact on the pressure distribution on the disc face. The SST turbulence model is known to predict separated flow behaviour more accurately and this would agree with the finding of this investigation. The SST model is capable of predicting the disc forces accurately over the full operating cycle of the SRV including the region with high levels of separation. The force-lift plot in figure 3.9 clearly shows the improved accuracy of the SST model and the pressure distribution plot in figure 3.13 is able to show the differences in pressure distribution of each model at 4mm lift.

Axisymmetric comparison

Under certain conditions, the flows within an SRV may be treated as axisymmetric. In particular, flows contained within the nozzle should be able to be calculated using a 2-dimensional approach. As with most CFD calculations, any opportunity to reduce the computational costs are greatly valued thus it was necessary to investigate the validity of an axisymmetric assumption within the Broady 3500 series test valve. The mesh requirements below 1mm lift start to become quite demanding, when modelling the huddling height (<0.1mm) the cell height necessary to capture the gradients begins to approach 1μ . As a result, it is necessary to model the lower lift as 2-D regardless, a 3-D simulation at this height would result in a numerical grid of considerable magnitude, thus low lift 3D simulations were avoided.

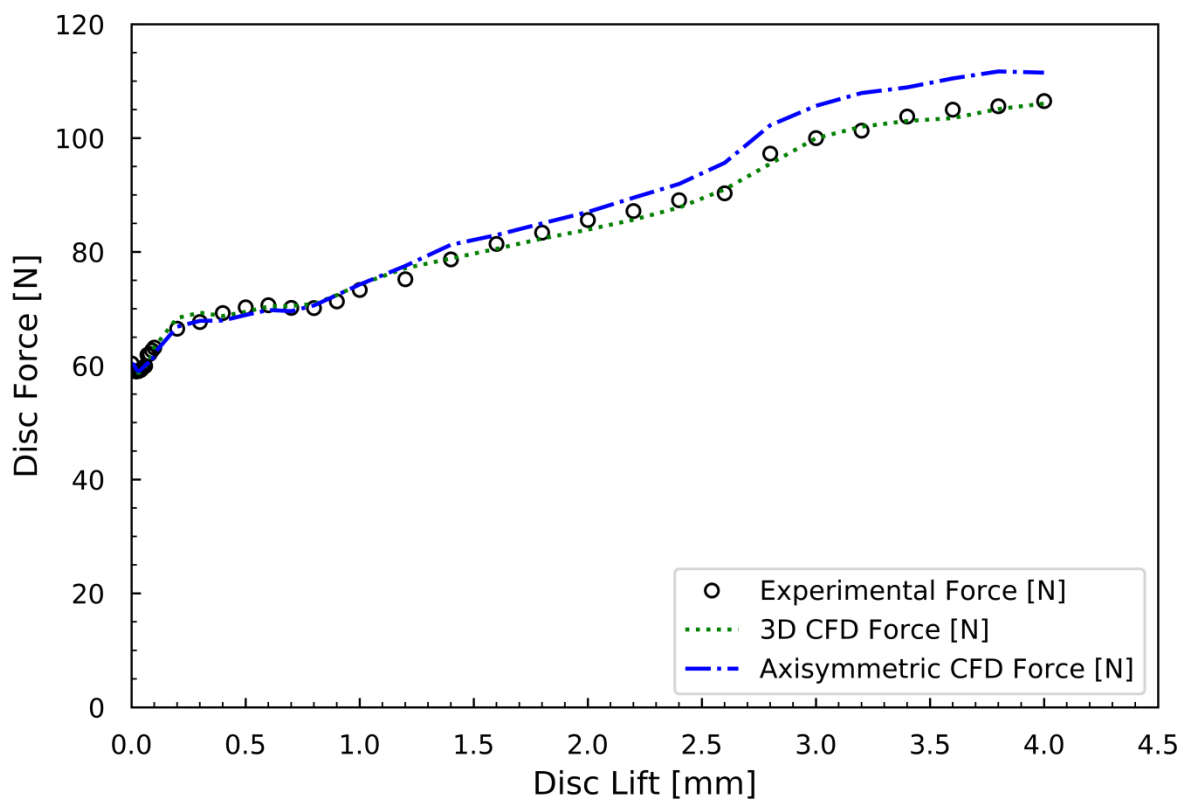


Figure 3.14 – 2-D axisymmetric CFD validation, force-lift plot – air at 3.3 barg.

Lift (mm)	Experimental force (N)	3D CFD Force (N)	3D CFD error (%)	2D CFD Force (N)	2D CFD error (%)
0.00	60.40			60.40	0.00
0.01	59.10			60.21	-1.87
0.02	59.00			59.41	-0.70
0.03	59.08			59.04	0.06
0.04	59.28			59.24	0.07
0.05	59.63			59.63	-0.01
0.06	59.98			60.05	-0.12
0.07	61.93			60.47	2.36
0.08	62.08			60.12	3.15
0.09	62.68			60.78	3.03
0.10	63.18			62.16	1.61
0.20	66.53			66.85	-0.48
0.30	67.68			67.88	-0.30
0.40	69.28			67.94	1.93
0.50	70.28			68.91	1.96
0.60	70.63			69.79	1.19
0.70	70.18			69.59	0.84
0.80	70.13			70.59	-0.65
0.90	71.33			72.41	-1.51
1.00	73.33	74.28	-1.29	74.26	-1.27
1.20	75.20	77.13	-2.56	77.53	-3.10
1.40	78.70	78.84	-0.17	81.25	-3.24
1.60	81.40	80.54	1.06	82.96	-1.91
1.80	83.40	82.34	1.27	85.01	-1.93
2.00	85.60	83.90	1.98	87.01	-1.64
2.20	87.20	85.65	1.78	89.51	-2.65
2.40	89.10	87.79	1.48	91.93	-3.18
2.60	90.30	90.97	-0.74	95.64	-5.91
2.80	97.30	95.48	1.87	102.25	-5.08
3.00	100.00	99.96	0.04	105.66	-5.66
3.20	101.30	102.00	-0.69	107.91	-6.52
3.40	103.80	103.00	0.77	108.90	-4.92
3.60	105.00	103.50	1.43	110.48	-5.22
3.80	105.60	105.10	0.47	111.70	-5.78
4.00	106.50	106.06	0.41	111.50	-4.69

Table 3.10 – Axisymmetric CFD validation, force data – air at 3.3 barg at 4mm lift.

It was presumed that 3-dimensional effects would only become apparent as the choking point in the flow path moved away from the seat area. Therefore the region from 0-1mm lift could be modelled using an axisymmetric approach, an investigation into its validity at higher lifts was carried out and the results are shown in table 3.10 and plotted in figure 3.14.

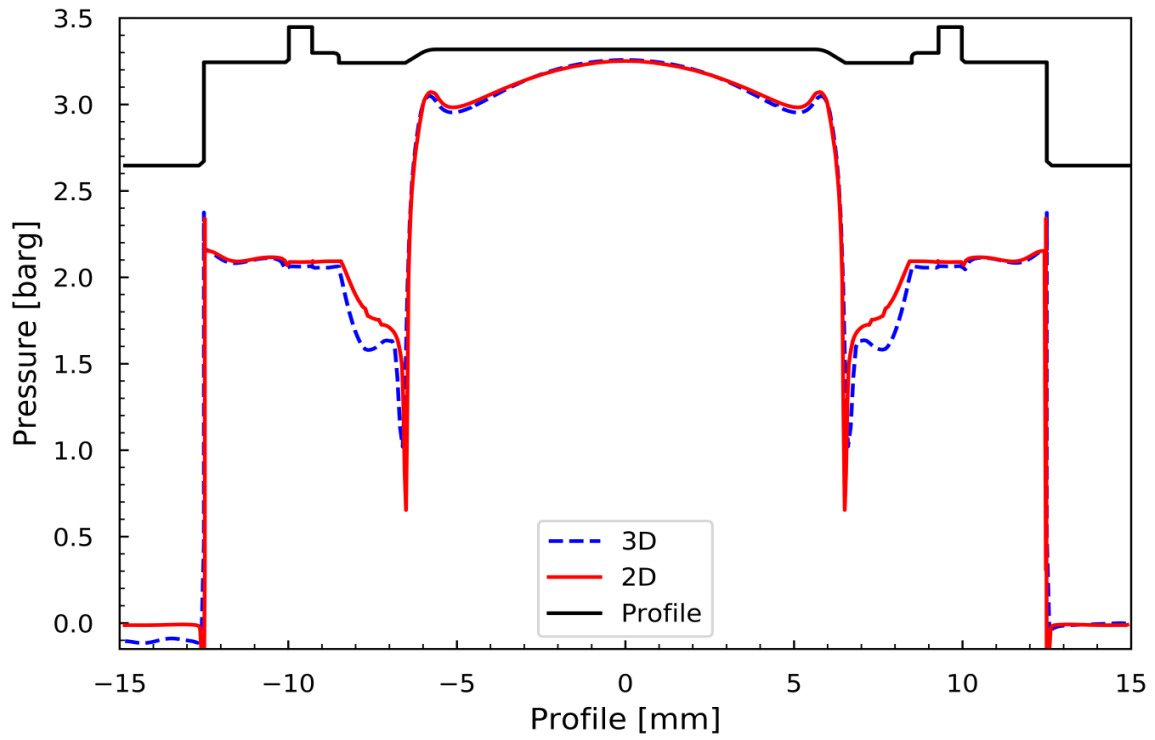


Figure 3.15 – Pressure distribution comparison of 2-D axisymmetric and 3-D CFD calculations – 4mm lift.

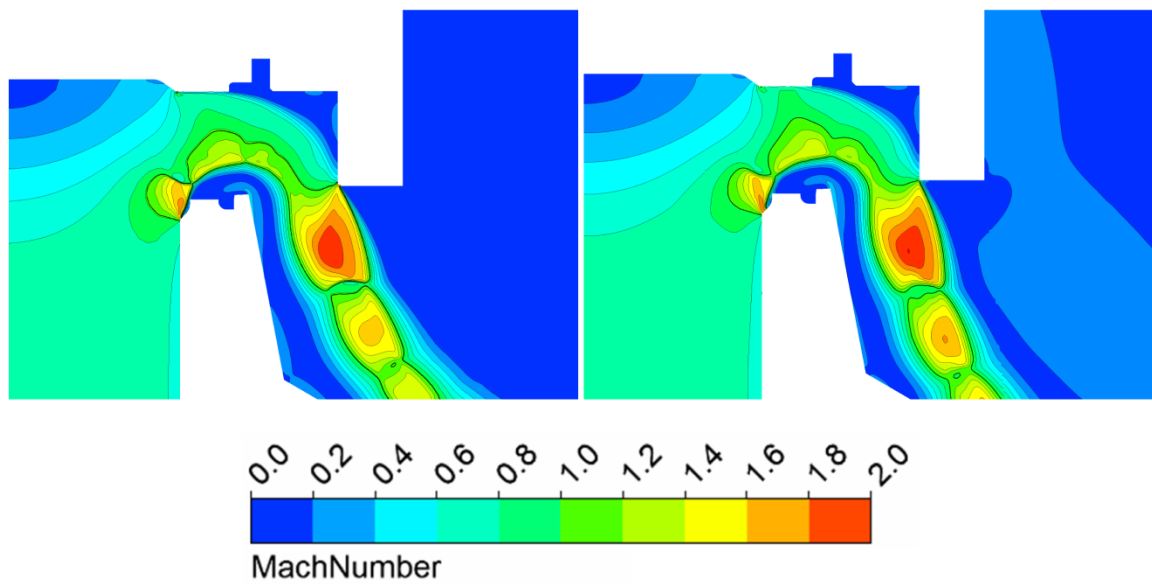


Figure 3.16 – 2-D axisymmetric – (left) and 3-D (right) Mach number contour plots at 4mm lift. $Ma = 1$ marked in black – air at 3.3 barg at 4mm lift.

In figure 3.14 it can be seen that the 2-D axisymmetric assumption is valid to around 1mm lift, after this height the disc force begins to be over predicted, with a maximum error occurring at 3.8mm lift. The pressure distribution plot in figure 3.15 shows the data for 4mm lift 2-D & 3-D CFD. From the plot, the differences in pressure distribution can be realised. The pressure around the seat area is slightly higher for the 2-D calculation, this is the region where the primary choking point is located. This suggests that the 2-D calculation is under predicting separation resulting in a lower pressure drop. The Mach number plot in figure 3.16 shows the slight differences in choking behaviour, the 2-D plot on the left shows a smaller choking plane at the seat area, this is the high-pressure region of the disc face so it is sensitive to small differences. Also, to note is the pressure difference around a radial position of -12mm, this is due to the valve body influencing the pressure distribution at full lift. In the axisymmetric model the 2-D slice is taken to include the outlet thus will not be affected by the valve body in this region. Due to the 3-D nature of a turbulent flow, an axisymmetric approach will struggle to capture flow physics accurately. This will begin to have a pronounced effect as the valve opens further and the flow begins to separate at the tip of the inlet nozzle.

The data within table 3.10 and figure 3.14 clearly show that an axisymmetric assumption is valid to around 1 mm lift. The outlet area for a 3-D calculation is $1.9364 \times 10^{-3} \text{ m}^2$, the 2-D outlet area is $1.806 \times 10^{-2} \text{ m}^2$, clearly showing a large difference in the outlet areas in each configuration. Having a larger outlet affects the pressure within the valve body, as the valve opens past 1 mm lift the pressure within the valve body begins to increase thus it is at this stage where the 3 dimensional effects of the outlet must be accounted for. A separate axisymmetric calculation was carried out, this time using a reduced outlet size appropriate

for an axisymmetric approach. To achieve a 2-D axisymmetric representation of the 3-D outlet, the outlet of the valve had to be reduced in height from 50mm down to 2.717mm, to produce an outlet area of $1.9635 \times 10^{-3} m^2$. A plot of the data is included in figure 3.17 below, it clearly shows that the reduced outlet area axisymmetric calculation still over predicts disc force, a slight improvement is found above 2.6mm lift but not sufficient enough to switch to a fully axisymmetric approach.

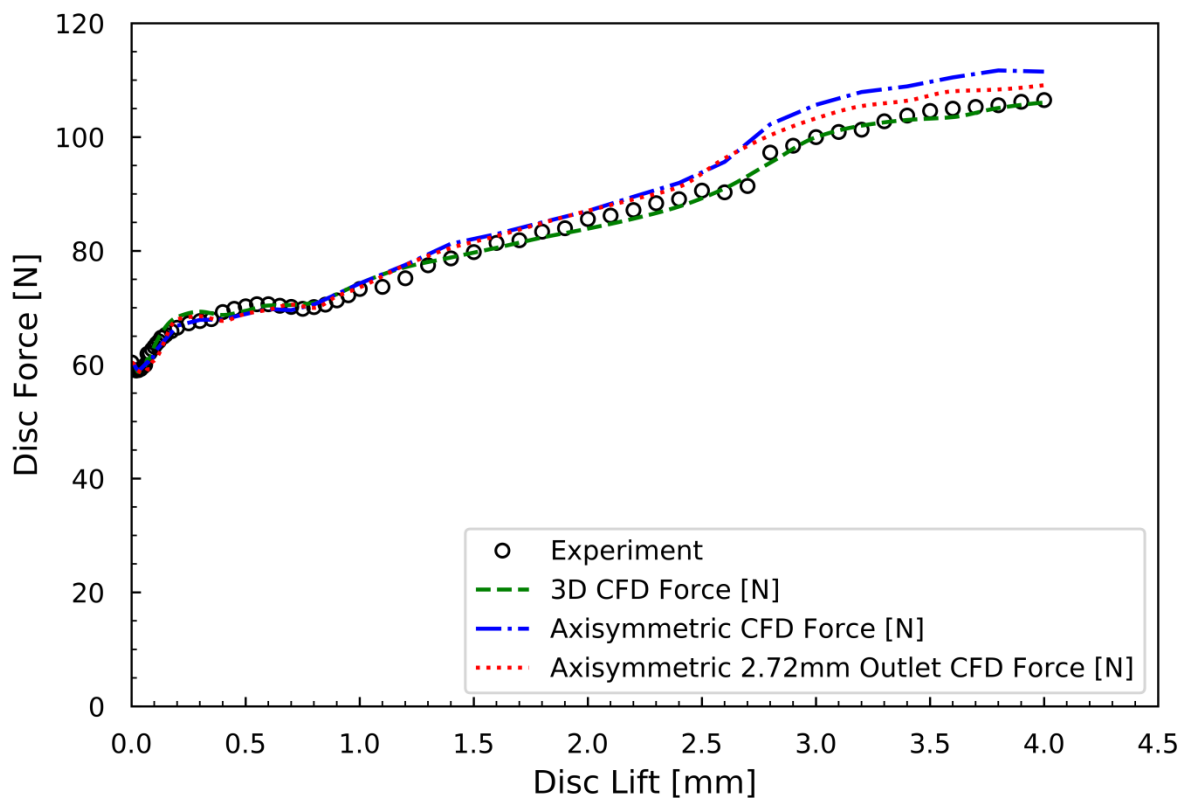


Figure 3.17 – 2-D axisymmetric CFD validation, force-lift plot – air at 3.3 barg at 4mm lift.

Therefore to capture the full opening cycle a combination of 2-D and 3-D models should be utilised. 0-1.0 mm should be modelled as axisymmetric and >1 mm should use a 3-D model. Building on this information, the region from 0-1.0 mm will now be referred to as low-lift and the region from 1.0-4.0 mm will be referred to as high-lift. It is worth noting that this will

only be valid for this size of orifice as the full-lift and change over values would differ with a change in throat area.

Input sensitivity – calculation of u_{input}

The following section presents the sensitivity analysis of the CFD model to input variations, a requirement in quantifying the input uncertainty u_{input} for the validation process. The sensitivity to input variations is obtained by perturbing selected boundary conditions and recording the effects on the observed disc force. The chosen boundary conditions are presented in tables 3.11, 3.12 and 3.13 below, each was varied by $\pm 5\%$ and the gradient was calculated by a central differencing method.

Temperature (K)	Disc Force (N)	Force Change (N)
315	105.84	-0.22
300	106.06	N/A
285	105.92	-0.14

Table 3.11 – Temperature sensitivity.

Pressure (barg)	Disc Force (N)	Force Change (N)
3.135	100.12	-5.94
3.300	106.06	N/A
3.465	110.93	+4.87

Table 3.12 – Pressure sensitivity.

Lift (mm)	Disc Force (N)	Force Change (N)
3.80	104.32	1.74
4.00	106.06	N/A
4.20	106.18	0.12

Table 3.13 – Disc position sensitivity.

The sensitivity coefficient for each input parameter is equal to the partial derivative of the simulated disc force (S) with respect to the input parameter (X_i) $\partial S / \partial X_i$. This is evaluated using a second order finite difference approach

$$\frac{\partial S}{\partial X_i} = \frac{S(X_i + \Delta X_i) - S(X_i - \Delta X_i)}{2\Delta X_i} \quad (3.36)$$

The input uncertainty is given by the following

$$u_{\text{input}}^2 = \sum_{i=1}^n \left(\frac{\partial S}{\partial X_i} u_{X_i} \right)^2 \quad (3.37)$$

where u_{x_i} is the standard uncertainty of input parameter X_i as used in the experimental uncertainty. Of the parameters investigated only the pressure and disc lift had any noticeable effect. Temperature variations only resulted in a small change in disc force and even this is thought to be from the iteration error as the central value is the minimum of those calculated. Thus, only the input pressure and disc position will be used in the input uncertainty calculation. As before, this value will be dimensionalised using a scaling parameter of 106.06N to comply with the other derived uncertainty values resulting in the following

$$u_{\text{input}} = 0.1N$$

Final validation – calculation of u_{val}

Compiling all of the calculated uncertainties - u_{num} (3.29), u_D (3.35) and u_{input} (3.37) – the total validation uncertainty u_{val} (3.22), can now be evaluated,

$$u_{val} = \sqrt{u_{num}^2 + u_D^2 + u_{input}^2} \quad (3.22)$$

$$= 0.83N$$

Presented below in tables 3.14 & 3.15 are the results from a set of CFD calculations at 2 different lower ring settings, this process was used to evaluate the comparison error E. Figures 3.18 and 3.19 presents the validation of CFD data against experiment, this data was obtained with the lower ring set at 2 notches, figure 3.19 focuses on the low lift region. From these plots the CFD data can mostly be found to fall within the error bars throughout the full force-lift curve. The same tests carried out at a lower ring setting of 3 notches is presented in figures 3.20 and 3.21. Similar levels of accuracy can be found however a slight over prediction on disc force at 0.4mm from the CFD calculation is shown. As with all other calculations in this section, the following results were obtained at a working pressure of 3.3 barg. As before, figure 3.21 focuses on the low-lift region of the data in 3.20. Figures 3.19 and 3.21 have been included to highlight the accuracy of the CFD in the low-lift region as this is crucial in predicting the opening process of an SRV.

Lift (mm)	Experiment Force (N)	CFD Force (N)	Comparison Error E (N)	Difference %
0.00	60.40	60.40	0.00	0.00
0.01	59.10	60.19	-1.09	-1.84
0.02	59.00	59.35	-0.35	-0.59
0.03	59.08	58.72	0.36	0.60
0.04	59.28	58.87	0.41	0.69
0.05	59.63	59.25	0.38	0.64
0.06	59.98	59.79	0.19	0.32
0.07	61.93	61.01	0.92	1.48
0.08	62.08	61.06	1.02	1.64
0.09	62.68	61.96	0.72	1.15
0.10	63.18	63.27	-0.09	-0.14
0.20	66.53	68.37	-1.84	-2.77
0.30	67.68	69.32	-1.64	-2.43
0.40	69.28	68.74	0.54	0.79
0.50	70.28	69.47	0.81	1.16
0.60	70.63	70.40	0.23	0.32
0.70	70.18	70.50	-0.32	-0.46
0.80	70.13	70.86	-0.73	-1.04
0.90	71.33	72.39	-1.06	-1.49
1.00	73.33	74.28	-0.95	-1.29
1.20	75.20	77.13	-1.93	-2.56
1.40	78.70	78.84	-0.14	-0.17
1.60	81.40	80.54	0.86	1.06
1.80	83.40	82.34	1.06	1.27
2.00	85.60	83.90	1.70	1.98
2.20	87.20	85.65	1.56	1.78
2.40	89.10	87.79	1.32	1.48
2.60	90.30	90.97	-0.67	-0.74
2.80	97.30	95.48	1.82	1.87
3.00	100.00	99.96	0.04	0.04
3.20	101.30	102.00	-0.70	-0.69
3.40	103.80	103.00	0.80	0.77
3.60	105.00	103.50	1.50	1.43
3.80	105.60	105.10	0.50	0.47
4.00	106.50	106.06	0.44	0.41

Table 3.14 – 2 notches CFD validation.

Lift (mm)	Experiment Force (N)	CFD Force (N)	Comparison Error E (N)	Difference %
0.00	60.00	60.40	-0.40	-0.67
0.01	59.13	60.20	-1.07	-1.81
0.02	58.03	59.42	-1.39	-2.40
0.03	57.83	58.98	-1.15	-1.98
0.04	57.93	59.04	-1.11	-1.92
0.05	57.93	58.91	-0.98	-1.69
0.06	57.73	58.81	-1.08	-1.86
0.07	57.63	58.63	-1.00	-1.74
0.08	57.73	57.43	0.30	0.52
0.09	57.73	57.39	0.34	0.58
0.10	57.83	58.28	-0.45	-0.78
0.20	59.83	60.40	-0.57	-0.96
0.30	60.50	61.65	-1.15	-1.89
0.40	60.93	63.85	-2.92	-4.80
0.50	59.63	61.76	-2.13	-3.58
0.60	62.53	63.83	-1.30	-2.08
0.70	66.03	65.65	0.38	0.58
0.80	67.63	67.97	-0.34	-0.50
0.90	69.63	70.31	-0.68	-0.97
1.00	70.93	72.75	-1.82	-2.56
1.20	73.50	75.61	-2.11	-2.87
1.40	77.10	78.12	-1.02	-1.33
1.60	79.10	79.99	-0.89	-1.12
1.80	81.40	81.64	-0.24	-0.29
2.00	83.50	83.75	-0.25	-0.30
2.20	85.30	86.75	-1.45	-1.70
2.40	87.90	87.60	0.30	0.34
2.60	94.30	94.77	-0.47	-0.50
2.80	97.40	97.89	-0.49	-0.50
3.00	99.70	100.04	-0.34	-0.34
3.20	101.30	101.20	0.10	0.10
3.40	103.70	102.40	1.30	1.25
3.60	104.80	103.01	1.79	1.71
3.80	105.20	104.32	0.88	0.84
4.00	105.90	106.00	-0.10	-0.09

Table 3.15 – 3 notches CFD validation.

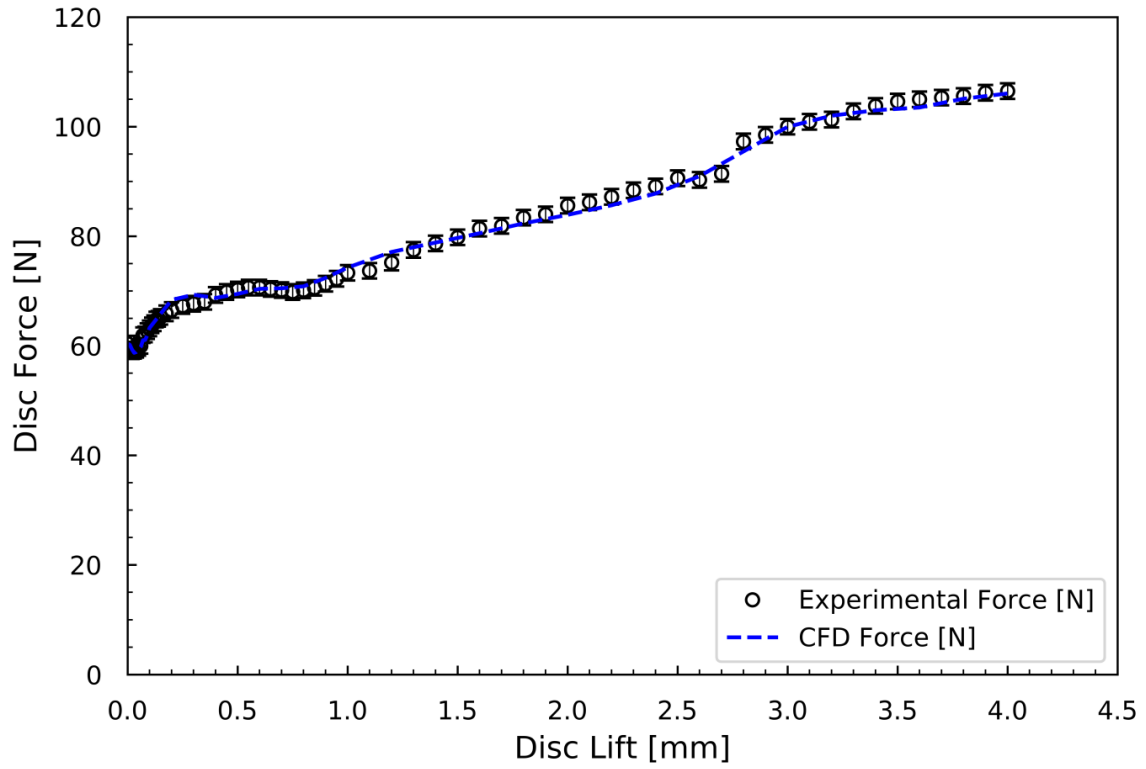


Figure 3.18 – 2 notches full lift force-lift curve – CFD validation.

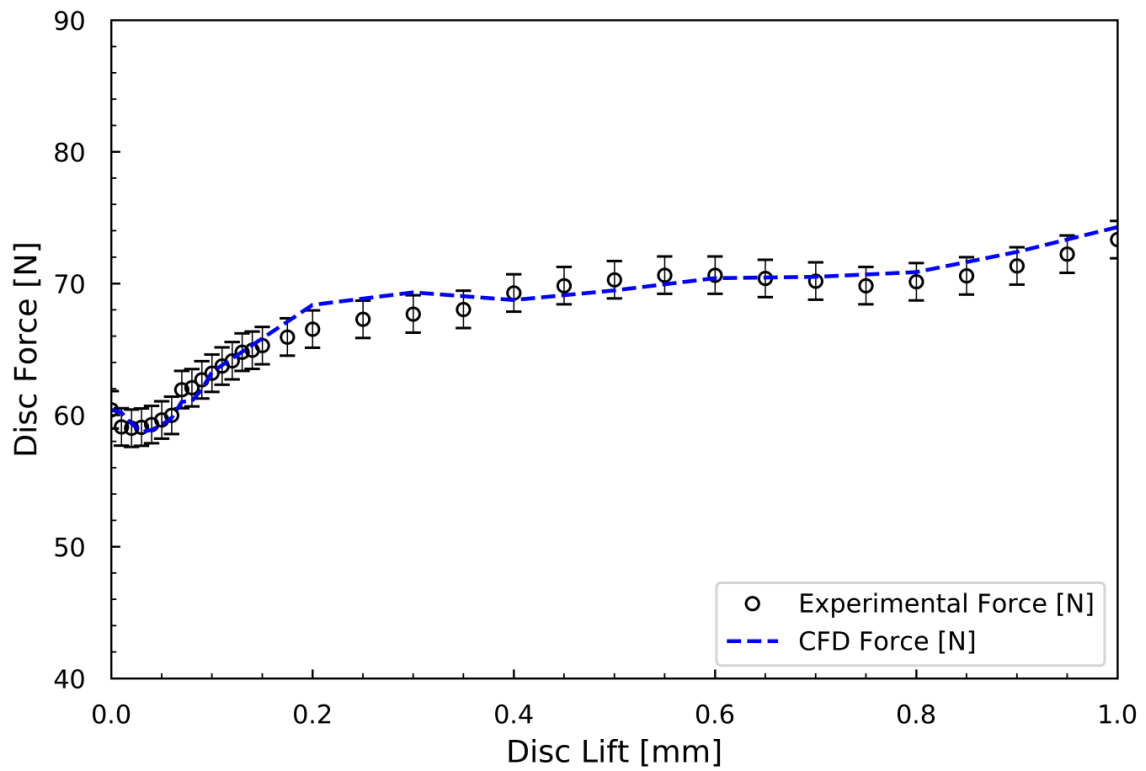


Figure 3.19 – 2 notches – low lift force-lift curve – CFD validation.

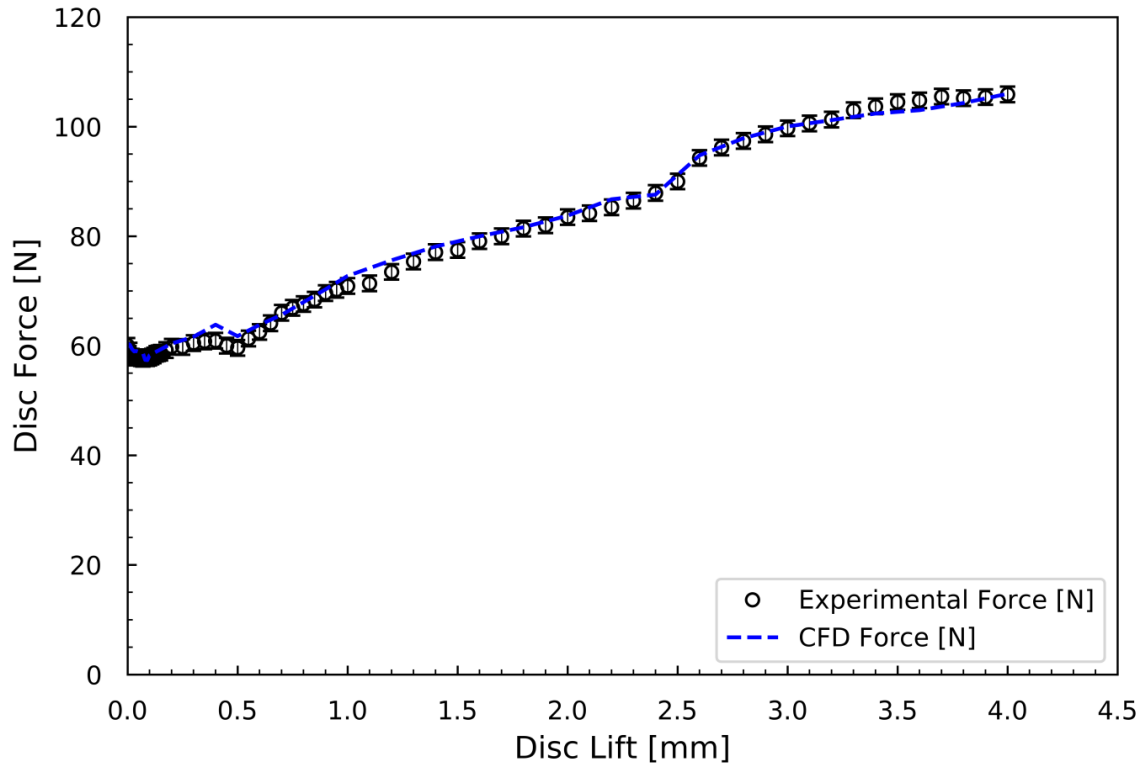


Figure 3.20 – 3 notches full lift force-lift curve – CFD validation.

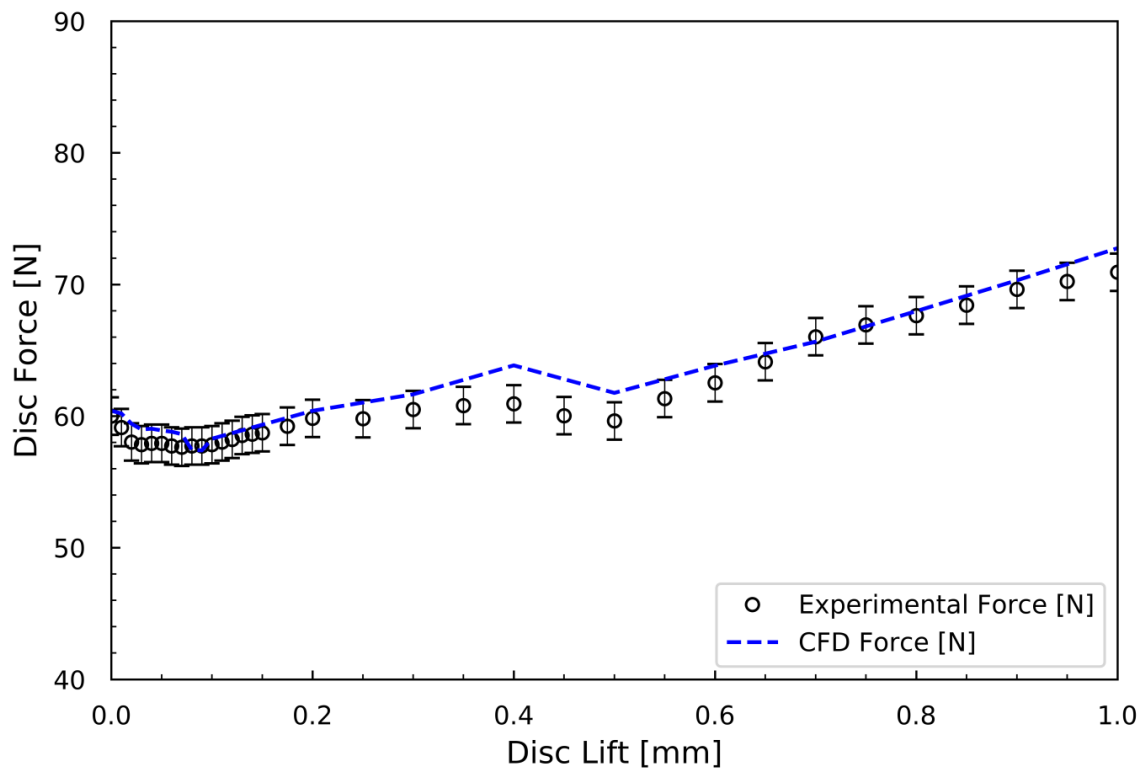


Figure 3.21 – 3 notches – low lift force-lift curve – CFD validation.

It becomes apparent that at the 4 mm position chosen for the validation process the magnitude of E falls below the uncertainty threshold u_{val} thus, the simulation would be regarded as validated. At points over the span of the force-lift curve the error exceeds the uncertainty but overall it is generally within the uncertainty threshold.

3.2 Description of Low-order Valve Model

3.2.1 Low-order Valve Model Governing Equations

It has been established that the movement of the disc in an SRV is the result of a force imbalance acting on the moving parts. Although there is some damping and friction present, the main driving force in the system is supplied by the aerodynamic forces from the expanding fluid and the compressive spring force. It is when one of these forces becomes dominant that the force balance is lost and the system can change state (open/close). If this configuration is modelled as a spring-mass-damper system with one degree of freedom, the following equation derived from Newton's second law of motion can be used,

$$m\ddot{x} + b\dot{x} + kx = F(x) \quad (3.38)$$

where m is the mass of the moving parts, \ddot{x} is the acceleration of the disc, b is the damping coefficient (neglected for this application), \dot{x} is the velocity of the moving parts, k is the spring stiffness, x is the spring compression and F the disc forces. F contains forces from two sources, firstly the aerodynamic forces from the escaping pressurised fluid and secondly the force required to create a seal between the disc and nozzle. This sealing force is termed the preload and is responsible for maintaining a seal between the nozzle and disc in a normally closed position. The sealing faces have a lapped finish but are not completely smooth,

therefor, a load is required to elastically deform the small surface imperfections to create a seal. This preload value has a strong influence on the opening characteristics of an SRV so an accurate measurement of this load is essential to represent it in a mathematical model. The load from the aerodynamic force from the expanding fluid can be obtained using 2 methods. If the model is being used to replicate the dynamics of an already existing valve, the forces would be recorded through experimental methods by measuring the disc force over the full opening cycle of the SRV. In the event of the LVM being utilised for research purposes, the aerodynamic forces can be purely theoretical, however experimental results would still usually be the starting point for this technique. Essentially, the disc force is present in the model as an equation fitted to the 2D force-curve, representing how the disc force changes at different opening heights. This curve can be altered to change the valve behaviour and improve its performance - this is the basis for one part of the optimisation process that will be presented in the following chapters.

For the purposes of the verification and validation process the force data required in equation 3.38 is obtained from experimental data. The disc force is recorded over the full operational cycle of the test valve (Broady Flow Control 1x2" 3511E) these forces are then used as the force within the LVM. This data is discrete points but is interpolated using a Piecewise Cubic Hermite Interpolating Polynomial (PCHIP) method. To account for a force change as the pressure builds and falls the force data is firstly normalised with respect to inlet pressure. This then allows for the force-lift curve to be scaled as the pressure increases which would allow the valve to open. As the valve in the LVM opens and allows the system pressure to drop the force-lift curve will be scaled down accordingly, this will then allow the

valve to reclose. The pressure scaling discrepancies will be minimal at such a small pressure change, the system pressure is typically scaled by around $\pm 7\%$.

To give an accurate representation of the SRV dynamics, the full pressurised system needs to be modelled, in essence, the volume of pipework and vessels making up the system have to be accounted for. To operate the LVM a mass flow inlet is specified to cause the system pressure to increase, this will cause the valve to open, at this point the mass flow inlet is closed off and the system pressure will decrease and the valve will close.

During a vessel blowdown event, all fluid properties within the system can change and must be accounted for within the calculation. Equations to account for the change in pressure, temperature, and mass flow rate are added to equation 3.38 to complete the set of equations required to model the SRV dynamics. The following set of equations are used for this purpose,

$$\frac{dp}{dt} = \frac{Cp(\gamma-1)(m_i T_o - m_e T)}{v} \quad (3.39)$$

$$\frac{dT}{dt} = \frac{T}{P} \times \frac{dp}{dt} - \left(\frac{R \times T^2}{P \times V} \right) \frac{dm_v}{dt} \quad (3.40)$$

$$m_e = A C_d \frac{p_t}{\sqrt{T_t}} \sqrt{\frac{\gamma}{R}} \left(\frac{\gamma+1}{2} \right)^{-\frac{\gamma+1}{2(\gamma-1)}} \quad (3.41)$$

$$\frac{dm_v}{dt} = m_i - m_e \quad (3.42)$$

equation 3.39 accounts for the change in pressure, equation 3.40 calculates the change in temperature, equation 3.41 calculates the mass flow rate leaving the vessel and equation 3.42 calculated the mass rate of change in the vessel, which is obtained from the difference in the user specified mass flow inlet m_i , and the mass flow leaving the vessel (equation 3.41). To allow for the valve to close the mass flow inlet will be changed to zero once the valve has attained full lift. The model was constructed in Matlab and solved using the Runge-Kutta method with the ODE45 solver. A derivation of these equations is provided in appendix A.4.

This LVM is able to calculate the overpressure, blowdown, mass flow rate, temperature and dynamic behaviour over the full operating cycle. Using this information, it is possible to gain insight to how a valve will perform in the current configuration but also discover any undesirable vibrations that may be present within the system. This data also provides a means to validate the performance of the model and will be the subject of the remainder of this chapter.

3.2.2 Low-order Valve Model Verification and Validation

Verification

A numerical model has been produced that can predict the opening and closing process of a direct spring operated SRV. This tool will be used throughout this research project as a method of predicting the opening and closing behaviour of the SRV under study. This model is able to calculate both the overpressure and blowdown of an SRV in addition to providing the dynamic response of the system. As such, this model should be subject to the same verification and validation procedure as the CFD element of this research.

The safety relief valve dynamics are modelled using equations 3.38-42, these equations were solved using a Runge-Kutta RK45 solver in the commercial package Matlab. Verification of an ODE solver is a simpler process as ODEs can have an analytical solution. The second order ODE 3.38 was solved using RK45 in Matlab it has been repeated again below for reference

$$F(t) = m\ddot{x} - b\dot{x} - kx \tag{3.38}$$

this can be compared to an analytical solution

$$f(t) = Ae^{-\beta t} \cos(\omega t + \varphi) \tag{3.43}$$

The results are presented in figure 3.22 below

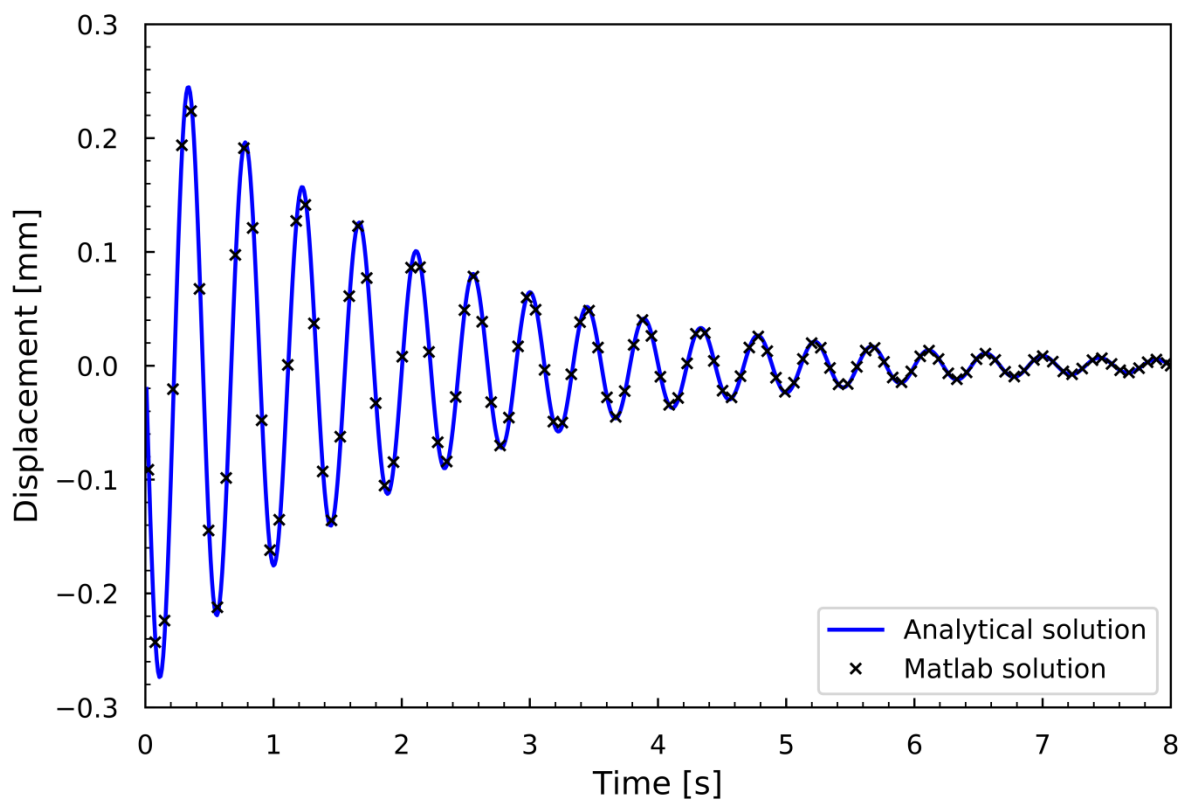


Figure 3.22 – Validation of the RK45 ODE solver in Matlab.

Figure 3.22 clearly shows the Runge-Kutta method is capable of solving the ODE to closely match the analytical solution. The RK45 solver has an error level set prior to implementation. If this error level is not met the solver reduces the time-step to meet the error requirements. It will initially attempt a 4th order solution before switching to 5th order if necessary. The maximum error between the numerical and analytical solution was found to be 1×10^{-4} .

Validation

Validation of the LVM shall follow the same guidelines as the CFD element of this study, however the level of detail in the description will not be necessary.

Calculation of u_D

The standard uncertainty u_D , comprises of the systematic and random uncertainty in the experimental data, as the LVM predicts the overpressure and blowdown of the test valve these were the parameters of interest. The systematic uncertainty only consisted of one pressure gauge and the random uncertainty was obtained by repeatedly running a functional test to uncover the variability in the test results. These are included in table 3.16 below

Test	Overpressure	Overpressure (%)	Blowdown	Blowdown (%)
1	3.48	5.45	3.19	3.33
2	3.48	5.45	3.20	3.03
3	3.47	5.15	3.21	2.73
4	3.49	5.76	3.21	2.73
5	3.48	5.45	3.19	3.33
6	3.46	4.85	3.19	3.33
7	3.49	5.76	3.20	3.03
8	3.50	6.06	3.20	3.03
9	3.48	5.45	3.21	2.73
10	3.46	4.85	3.21	2.73

Table 3.16 – Experimental results to determine u_d

For clarity the equation for calculating u_D will be repeated here.

$$u_D = \sqrt{(b_{\bar{x}})^2 + (s_{\bar{x}})^2} \quad (3.35)$$

Where $b_{\bar{x}}$ is defined as

$$b_{\bar{x}} = \left[\sum_{i=1}^i (b_{\bar{x}_i})^2 \right]^{\frac{1}{2}} \quad (3.33)$$

For this study with only one pressure gauge with an accuracy of 0.25%

$$b_{\bar{x}} = 0.25$$

As with the CFD validation exercise a coverage factor of 2 for a Gaussian distribution with a systematic uncertainty for a 95% confidence level becomes

$$b_{\bar{x}} = 0.50$$

And $s_{\bar{x}}$ is defined as

$$s_{\bar{x}} = \frac{\sigma}{\sqrt{N}} = \left[\frac{1}{N(N-1)} \sum_i (x_i - \bar{x})^2 \right]^{\frac{1}{2}} \quad (3.32)$$

Which was calculated on the overpressure as this had the highest variance,

$$s_{\bar{x}} = 0.000052 \text{ barg}$$

Finally, to obtain the data uncertainty u_D from this equation it needs to be scaled to the validation point being used in this study – 3.48 was the average overpressure in this study and will be used as the validation point - thus the data uncertainty value becomes

$$u_{\bar{x}} = 0.50 \%$$

$$u_D = 0.0005 \times 3.48$$

$$= 1.74 \times 10^{-3} \text{ barg}$$

Calculation of u_{num}

Fortunately the numerical error level can be specified for ODE45 solver that was used in Matlab, this greatly simplifies the evaluation of u_{num} as it is specified by the user. This study specified a level of $1e-11$, as before, this must be scaled to a validation point and for consistency the average overpressure value shall be used

$$U_{\text{num}} = 1 \times 10^{-11} \times 3.48$$

$$= 3.48 \times 10^{-11} \text{ barg}$$

Calculation of u_{input}

The sensitivity coefficient for each input parameter is equal to the partial derivative of the overpressure (S) with respect to the input parameter (X_i) $\partial S / \partial X_i$. This is evaluated using a second order finite difference approach

$$\frac{\partial S}{\partial X_i} = \frac{S(X_i + \Delta X_i) - S(X_i - \Delta X_i)}{2\Delta X_i} \quad (3.36)$$

The input uncertainty is given by the following

$$u_{\text{input}}^2 = \sum_{i=1}^n \left(\frac{\partial S}{\partial X_i} u_{X_i} \right)^2 \quad (3.37)$$

where u_{x_i} is the standard uncertainty of input parameter X_i as used in the experimental uncertainty. For the LVM the input parameters that could affect the result are the mass of the moving parts (m) and the spring constant (k). These were perturbed $\pm 5\%$ to discern their impact on the LVM overpressure and blowdown prediction, the results are included in tables 3.17 and 3.18 below.

	Mass	Overpressure	Blowdown
+5%	0.684	8.966	3.528
Standard	0.951	8.965	3.528
-5%	0.618	8.964	3.528

Table 3.17 – Mass input sensitivity

	Spring	Overpressure	Blowdown
+5%	16994	9.013	3.289
Standard	16185	8.966	3.528
-5%	15376	7.871	23.449

Table 3.18 – Spring input sensitivity

For consistency with the data uncertainty u_D , the input uncertainty will be evaluated on the overpressure prediction. The value of u_{input} is given below

$$u_{\text{input}} = 7.88 \times 10^{-3} \text{ barg}$$

It is worth noting that the blowdown was more sensitive to the spring constant thus using the blowdown to evaluate u_{input} may have been more conservative. To compare results the input uncertainty calculated on blowdown is given below

$$u_{input} = 2.4 \times 10^{-2} \text{ barg}$$

It can be appreciated that this is still a relatively small value thus to ensure consistency throughout this validation process the input uncertainty will be evaluated on the overpressure. If the blowdown figure was used, this would have resulted in a larger u_{input} value leading to a much easier to achieve validation.

Final validation – calculation of u_{val}

Finally the total validation uncertainty can be calculated using equation 3.22 which is repeated below

$$u_{val} = \sqrt{u_{num}^2 + u_D^2 + u_{input}^2} \quad (3.22)$$

Giving an answer of

$$u_{val} = 8.07 \times 10^{-3}$$

Low order valve model configuration

The LVM was configured to match the experiment, the main criteria being, set pressure, spring rate, mass of moving parts, temperature, mass flow inlet and vessel volume. These are summarised in table 3.18 below

Parameter	Value
Set pressure (barg)	3.3
Spring rate (N/mm)	16.185
Mass of moving parts (kg)	0.651
Temperature (K)	288
Mass flow inlet (kg/s)	0.055
Vessel volume (m ³)	1.5

Table 3.18 – LVM & Experiment configuration.

The performance results of the LVM for a range of notch settings are included in table 3.19, table 3.20 presents the same results in barg rather than percentage, this was necessary to complete the validation as the total validation uncertainty is in barg.

Presented in tables 3.19 and 3.20 is the LVM experimental data comparison, clearly showing the accuracy of the LVM at predicting the overpressure and blowdown performance. The difference between experiment and LVM was quoted in table 3.20, this is the E figure used in equation 3.21 repeated below.

$$E = S - D \tag{3.21}$$

Notches	Overpressure Experiment (%)	Overpressure LVM (%)	Difference	Blowdown Experiment (%)	Blowdown LVM (%)	Difference
0	2.73	3.00	-0.27	11.21	10.95	0.26
1	4.55	5.41	-0.86	8.48	7.45	1.03
2	4.85	6.12	-1.27	2.12	2.90	-0.78
3	11.21	9.75	1.46	-7.58	-5.98	-1.60
4	16.36	15.82	0.54	-7.58	-7.62	0.04
5	17.27	17.24	0.03	-7.58	-7.71	0.13
6	20.00	20.29	-0.29	-7.58	-7.46	-0.12
7	21.82	22.11	-0.29	-8.18	-7.74	-0.44
8	21.82	22.09	-0.27	-8.48	-8.69	0.21

Table 3.19 – LVM validation results.

Notches	Overpressure Experiment (barg)	Overpressure LVM (barg)	Difference (barg)	Blowdown Experiment (barg)	Blowdown LVM (barg)	Difference (barg)
0	3.3090	3.3099	-0.0009	3.2630	3.2639	-0.0009
1	3.3150	3.3179	-0.0028	3.2720	3.2754	-0.0034
2	3.3160	3.3202	-0.0042	3.2930	3.2904	0.0026
3	3.3370	3.3322	0.0048	3.3250	3.3197	0.0053
4	3.3540	3.3522	0.0018	3.3250	3.3251	-0.0001
5	3.3570	3.3569	0.0001	3.3250	3.3254	-0.0004
6	3.3660	3.3670	-0.0010	3.3250	3.3246	0.0004
7	3.3720	3.3730	-0.0010	3.3270	3.3255	0.0015
8	3.3720	3.3729	-0.0009	3.3280	3.3287	-0.0007

Table 3.20 – Final LVM validation results, cells coloured with green for pass and red for fail.

Where the E value in table 3.20 was less than the total validation uncertainty ($u_{val} = 8.07 \times 10^{-3}$) the cell colour was changed to green. As displayed in table 3.20, all simulation error has fallen below the validation uncertainty thus the LVM can be classed as validated. The data in table 3.19 was plotted in figure 3.23, further demonstrating the capabilities of this model.

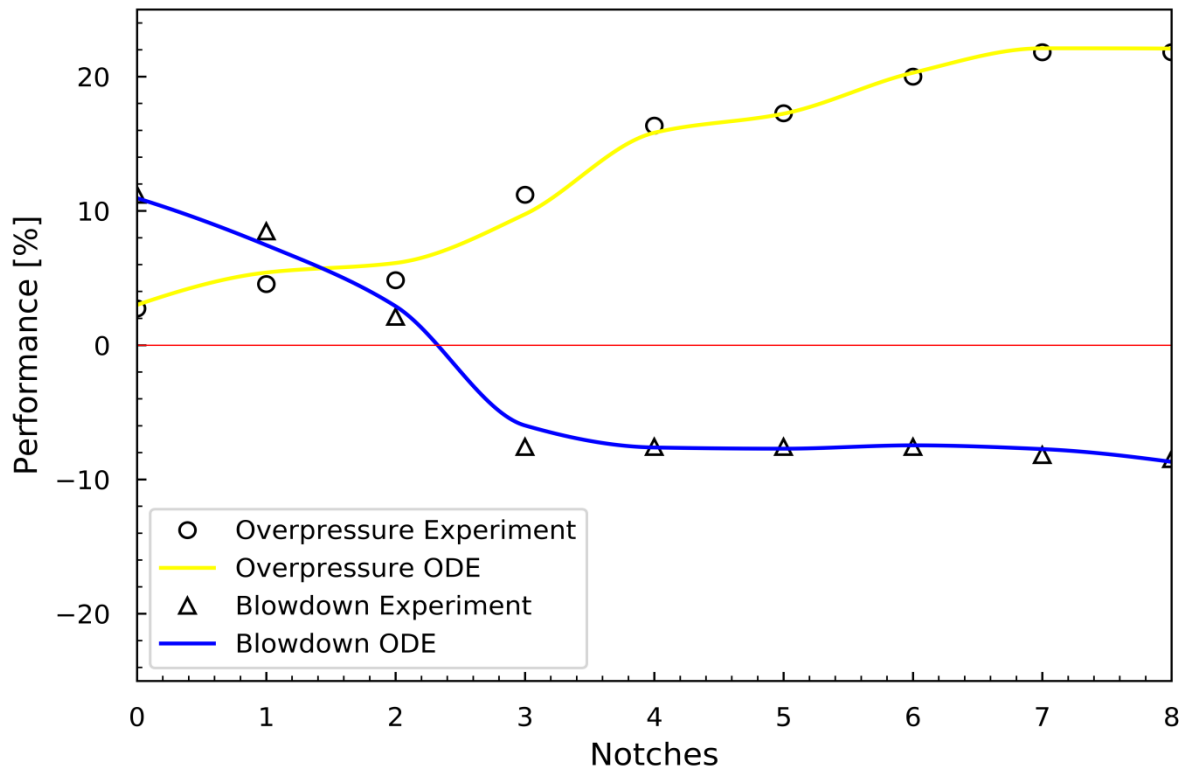


Figure 3.23– LVM overpressure & blowdown validation.

The LVM also produces a displacement output of the valve as it operates; this data was compared with LVDT data obtained through experiment. This is only used as a visual check on valve behaviour and will not be part of the optimisation process therefore it was not subject to the same verification and validation procedure. The comparison of the LVM displacement and LVDT data at 2 and 4 notches is included in figures 3.24 and 3.25 respectively. From these plots it can be appreciated that the LVM can accurately predict displacement over at different settings. It is worth noting that at 2 notches (figure 3.24) the SRV did not fully open, this is not a setting that the valve would be configured at for production, this was used purely for validation purposes.

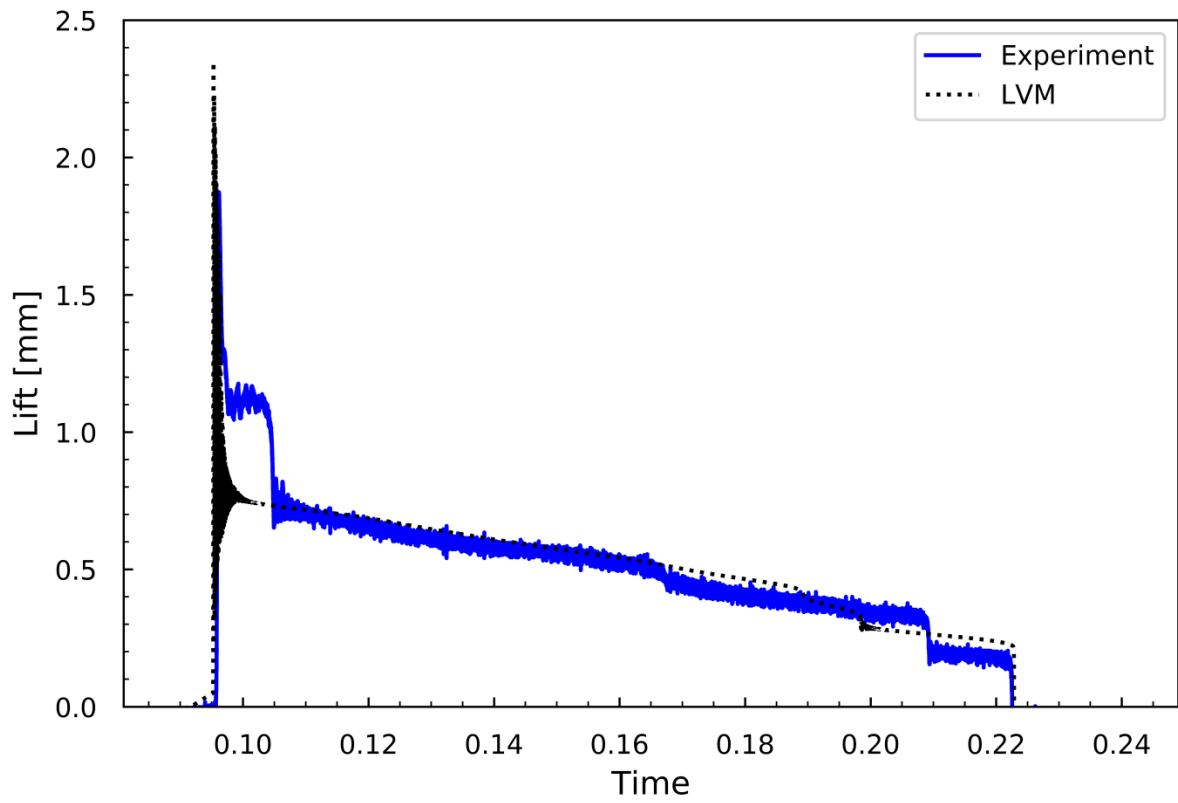


Figure 3.24– LVM displacement validation, 2 notches.

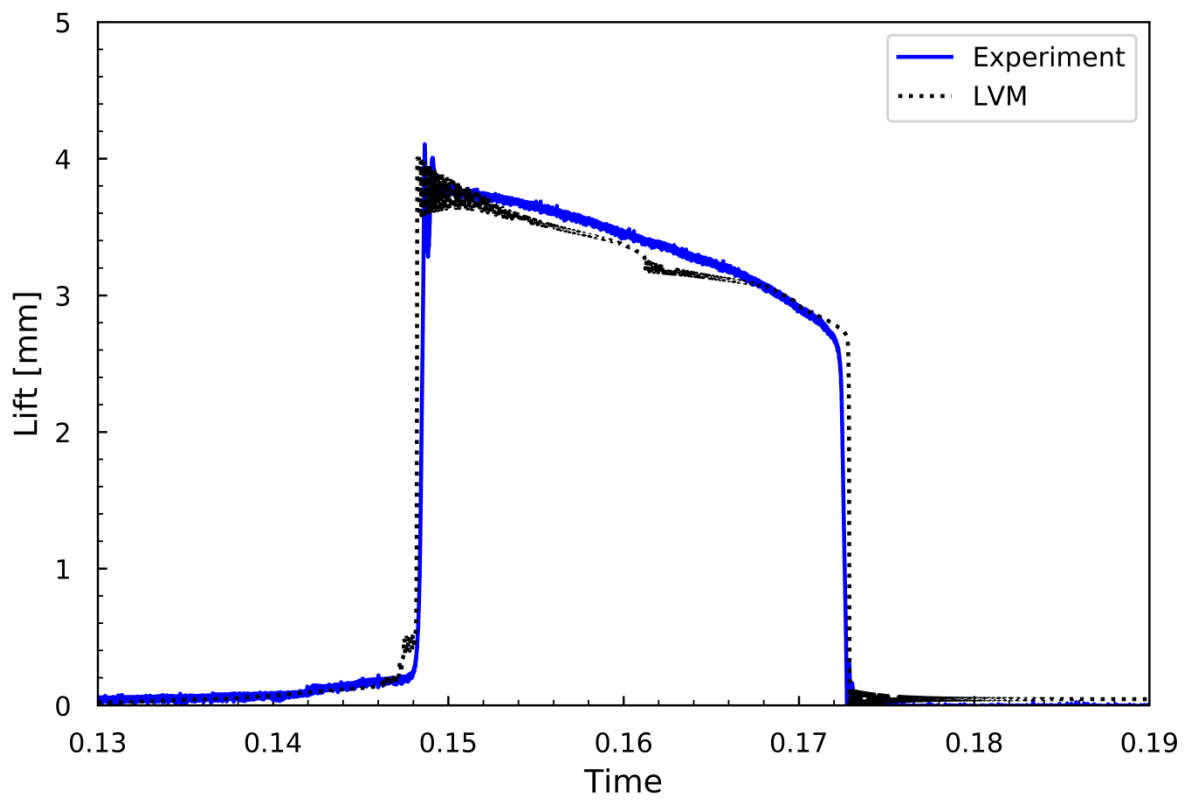


Figure 3.25 – LVM displacement validation – 4 notches.

3.3 Discussion

In this chapter the mathematical models used in this study have been presented, followed by a verification and validation exercise. Verification of the CFD solution setup was undertaken using grid refinement and Richardson extrapolation techniques. These techniques are complementary in that they are used to discover the mesh requirements of the numerical solution whilst also quantifying the error due to discretisation of the governing PDEs. A discretisation error of 0.35% was found when utilising a typical grid value of 0.08mm in the area of interest (nozzle exit), at this stage the changes to the monitored parameter with grid refinement became insignificant.

In contrast to the PDE solution methods utilised in the CFD code, the Runge-Kutta ODE solver employed in the SRV dynamics model can be compared to an analytical solution. In doing so it was shown to closely match the analytical solution, the adaptive time-step control utilised in the Runge-Kutta 45 method ensures a predefined level of accuracy is achieved during each time-step a maximum error of 1×10^{-4} was found.

The verification and validation process has resulted in the derivation of the required CFD configuration for an ASME type SRV. It has been shown that a 2D axisymmetric assumption is valid from 0-1mm valve lift, above this point 3-dimensional effects become apparent and a 3D half model should be used whilst utilising a symmetry plane in the centre of the SRV model.

LVM validation was achieved using nine separate valve settings from 0-8 notches. The significantly less computational costs from an ODE model allows for a greater number of tests to be undertaken. The validation exercise carried out on the LVM was able to show

that the accuracy of the model was satisfactory as the comparison error fell below the validation uncertainty for all configurations of the model. LVM displacement prediction was compared to LVDT data obtained through experiment for two different notch settings. These were generally found to be in good agreement throughout the operating cycle.

4. Safety Relief Valve Operation

The valve behaviour is essentially dynamic in operation, however the use of steady-state force-lift curves can be used to explain the gross opening and closing behaviour. In this section the experimental and CFD methods discussed in chapter 3 will be used to explain the overall valve behaviour and allow the key design variables to be identified.

4.1 Experimental and CFD Analysis

This section will explain the valve behaviour using the experimental and CFD data obtained during the validation and verification exercise, an explanation of the valve behaviour will be produced by cross-referencing the CFD data with disc force measurement.

Presented in figure 4.1 is a force-lift curve of the Broady 3500 tests valve at 3.3 barg at a lower ring setting of 2 notches. Also shown is the spring line and the maximum over-pressure and blowdown conditions, which for an ASME Section VIII certified valve are 10% and 7% respectively. A small force decrease is evident in the low lift region of the force-lift curve (0-0.20mm), this dip is responsible for controlling the opening performance of the SRV. With a pressure increase, the magnitude of the force curve would increase but requires that dip crosses the spring line before the valve can quickly open. Conversely, as the system pressure decreases the force curve needs to drop below the spring line before the valve can close. Therefore, it is the shape of the curve at low and high lifts that controls the opening and closing behaviour of the SRV. Section 4.1.1 will focus on the initial dip in the force-lift curve, following this the high lift behaviour will be explained in section 4.1.2.

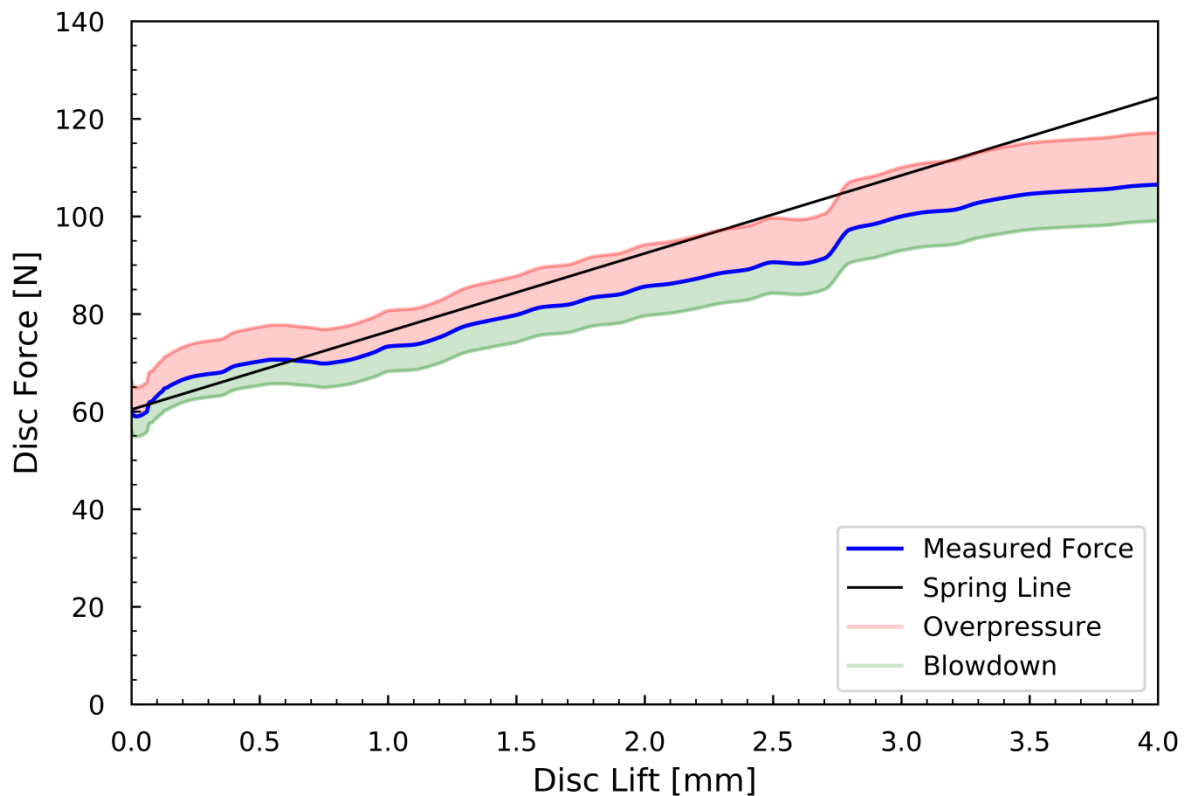


Figure 4.1 – 3511E – 2 notches – 3.3 barg set pressure - force-lift plot.

4.1.1 Opening Process

Figure 4.2 presents the force-lift data from the Broady test valve from 0-1.0mm lift. Again included in this plot are the maximum overpressure and blowdown. Using linear pressure scaling, an additional force-lift curve has been included to highlight how a pressure increase would continue until the disc forces overcome the spring force. The magnitude of the initial force dip will determine the required pressure increase to allow the valve to open, controlling the shape of the curve in this region would enable overpressure adjustment. The scaled curve used to represent a pressure increase was scaled by 3.4% showing that at its current setting this valve should produce an overpressure of 3.4% which is well within the

allowable 10% overpressure. The magnitude of overpressure required can be associated with the difference between the dip in force lift curve and the spring line. Consequently, control of this dip is fundamental to producing a high-performance valve.

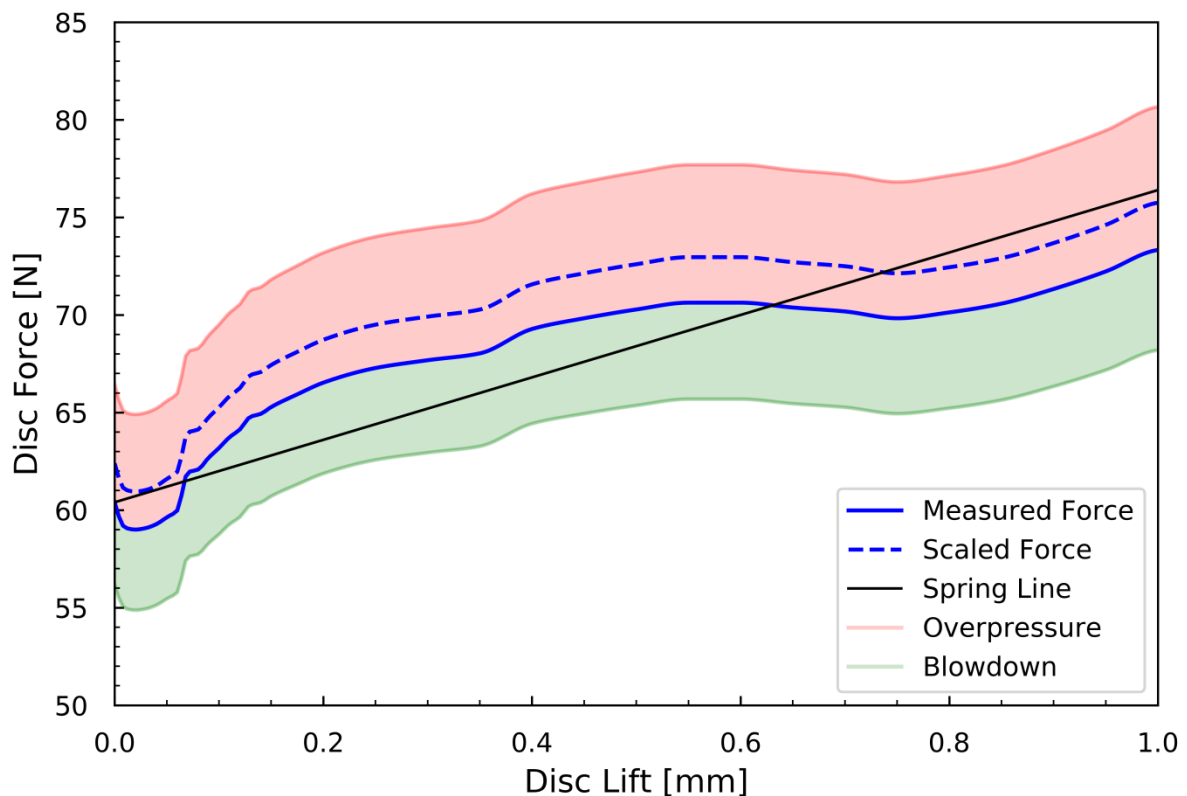


Figure 4.2 - 3511E – 2 notches – 3.3 barg set pressure - force-lift plot – low-lift.

The initial force dip is a consequence of a pressure reduction on the disc face as the valve moves off of the seat. The pressure reduction is due to the acceleration of the gas escaping from the inlet nozzle and can simply be explained by the Bernoulli principle. The pressure reduction in this region continues as the valve further opens. Figure 4.3 below presents the internals of the test valve, figure 4.4 focuses on the disc and disc holder of the reference

valve used in the study. This is taken from a CAD file and the small radii present in the actual geometry are not present here. The surface exposed to the inlet pressure during operation has been divided into 4 areas to make it easier when discussing what surfaces the pressure is acting on. These areas will be referenced when giving an explanation of the gas flows within the reference valve.

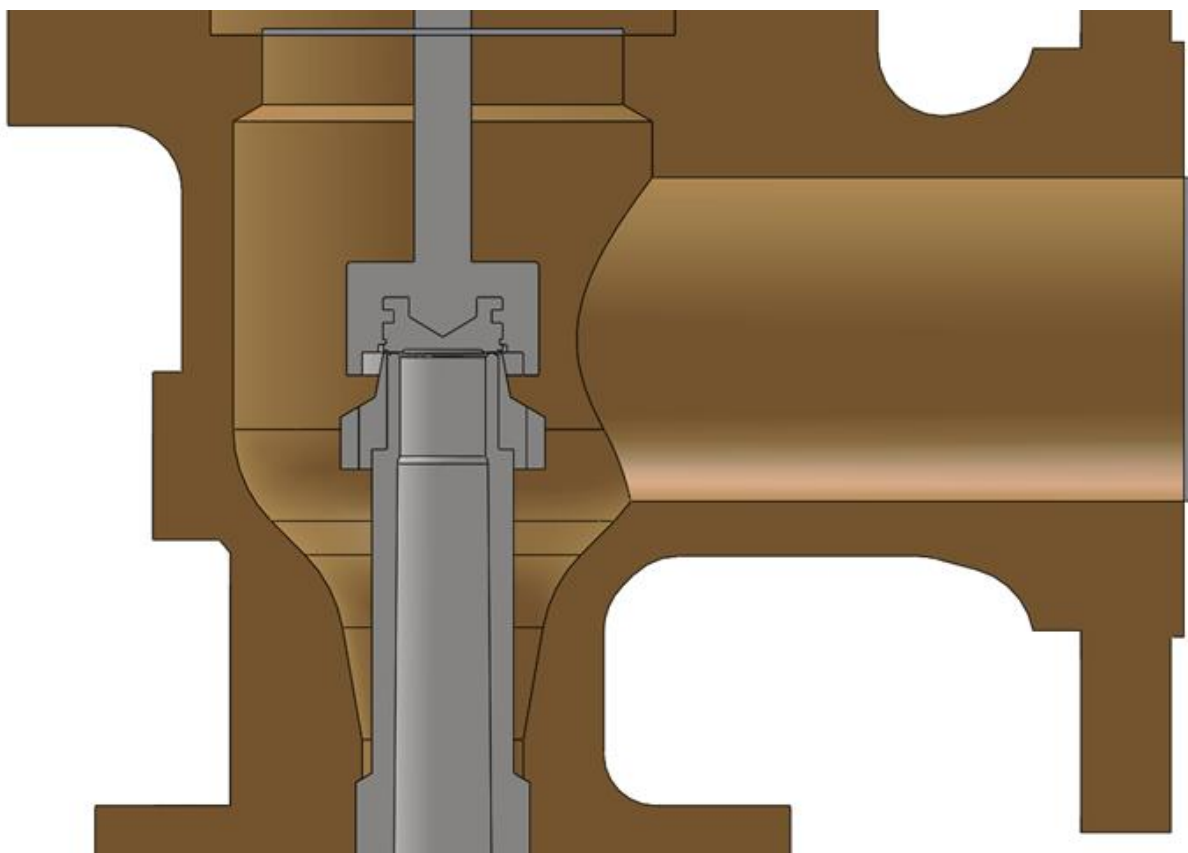


Figure 4.3 Test valve internals.

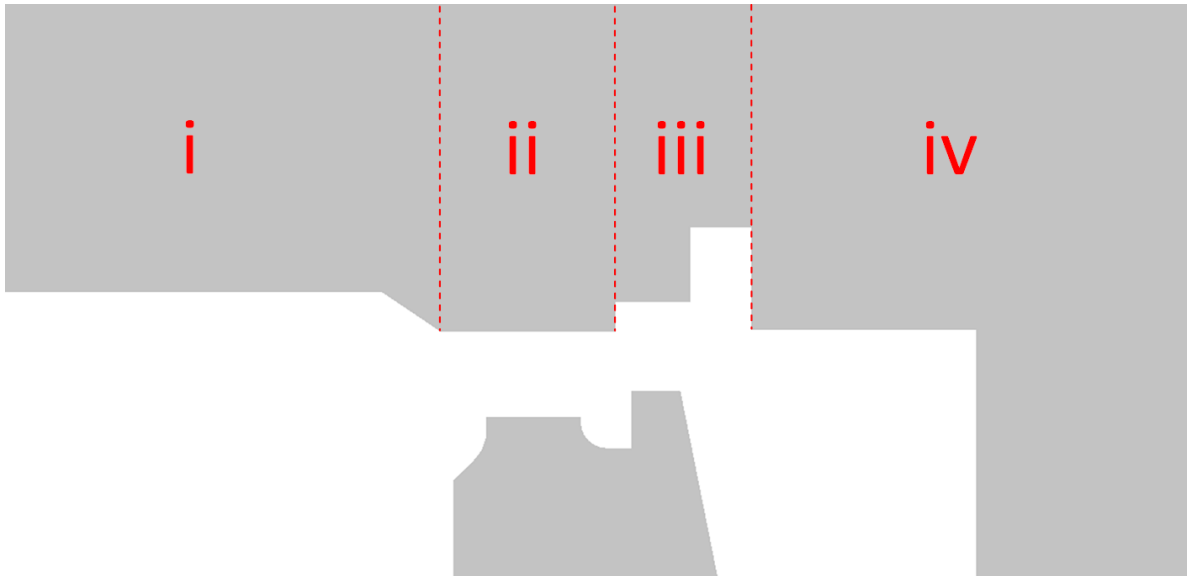


Figure 4.4 – Disc holder assembly surface area segregation.

Figure 4.5 displays the pressure distribution on the disc face from 0.01-0.1mm lift, a sharp pressure decrease between lifts of 0.01-0.03 mm is evident. It is after this stage that the pressure increases radially further out from the axis in region iv and compensates for the pressure reduction in the seat area. After a lift of 0.06mm the rate of pressure reduction in the seat area (region ii) reduces whilst the pressure increase in region iii continues to rise, this explains the quicker increase in force in figure 4.2 after 0.06mm lift.

The benefit of the lower adjustment ring can be appreciated from this behaviour. The ring is positioned radially at approximately 8mm and is used to restrict the escaping gas as the valve is beginning to open. This restriction helps to control the pressure reduction at low lift, minimising the magnitude of the initial dip in the force-lift curve. Altering the height of this ring in relation to the disc face alters the range over which the ring will influence the escaping gas upon opening. Figure 4.6 presents contour plots at a selection of heights between 0.01-0.1mm lift. The gas acceleration and pressure reduction upon opening

becomes clear from these plots. The pressure contours show the area between the disc and adjustment ring (region ii) increasing in pressure as the valve opens further. This behaviour demonstrates the benefits of the adjustment ring, without the ring in position to minimise the gas acceleration, the pressure reduction would continue at lifts beyond 0.03mm. Both plots in figure 4.6 have an iso-surface of Mach number = 1, the inclusion of this highlights the area where the gas is choking throughout the opening cycle.

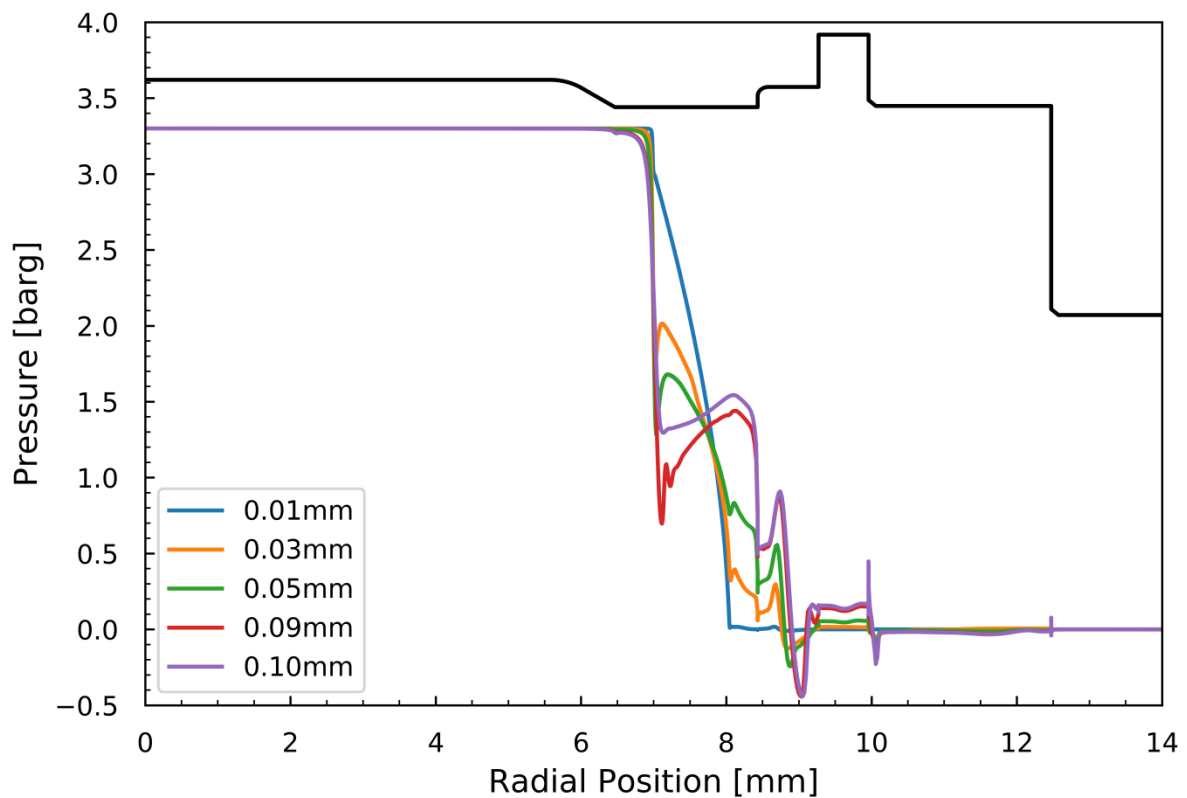


Figure 4.5 – 2d axisymmetric – 3511E – 2 notches – 3.3 barg set pressure – pressure distribution
0.01-0.1mm.

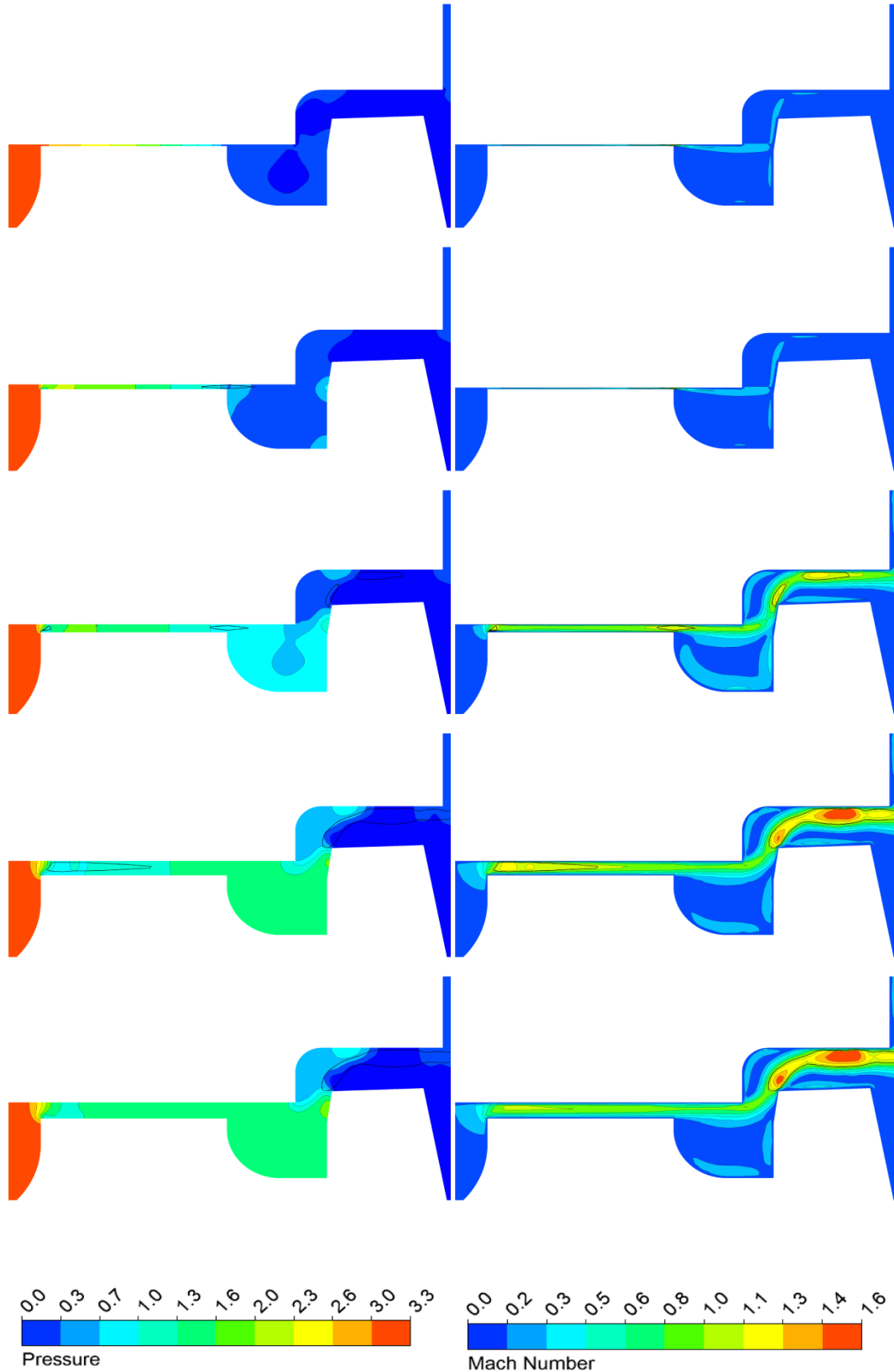


Figure 4.6 – 2- D axisymmetric – contour plots showing pressure (left) and Mach number (right) at 0.01mm, 0.03mm, 0.05mm, , 0.09mm and 0.10mm lift, iso-surface of Ma=1 has been included in both plots, (region I, ii & iii in figure 4.3)

Continuing on from 0.1mm lift, the force-lift curve experiences a steady increase as the valve opens, upon passing the height of the adjustment ring (0.19mm) the pressure begins to increase in the disc holder shroud area (region iv). Figure 4.7 presents the pressure distribution from 0.1-1.0 mm, from this plot the change in pressure distribution as the valve opens becomes apparent. As the valve passes 0.3 mm lift the force in region iv increases, it is also around this height that the force in the disc face region (region ii) starts to decrease. This behaviour can be explained by the disc moving past the height of the adjustment ring, and thus the ring is losing its influence on the expanding fluid. This facilitates greater acceleration and pressure drop around the sealing face region but also allows for the pressure to build up in the disc holder shroud. A gradual increase in pressure can also be found in region iii as the valve opens. At 0.6 mm lift the gas is beginning to move from choking at the tip of the adjustment ring to choking at the seat area, the transition can be seen as several choking points between nozzle exit and ring tip, it is only after the valve passes 0.6mm that the gas becomes fully choked at the nozzle exit. The pressure distribution plot in Figure 4.7 gives a clearer indication to what areas of the disc holder assembly experience the greatest force, after 0.7 mm lift the force is moving further out to the disc holder shroud region. The fluid behaviour at 0.6 mm can be further examined in the contour plots in Figure 4.8. In the Mach number plot of 0.6 mm several choking points across the sealing face region can be witnessed as the fluid begins to choke at the nozzle exit. The iso-lines at Mach 1 clearly highlight this behaviour.

Comparing this flow pattern to the data presented in the force lift curve in Figure 4.2, a plateau in force – even a slight decrease - can be observed at 0.6 mm. Showing that the accelerating gas in the disc sealing face region is causing a pressure reduction but is being

offset by a pressure increase in the disc holder shroud area. As the valve opens further, this pressure increase in the shroud over compensates for the disc sealing face pressure reduction and allows the flow force to increase, this is evidenced in the force-lift curve by the force beginning to increase again. The disc force now steadily increases as the disc moves further away from the seat.

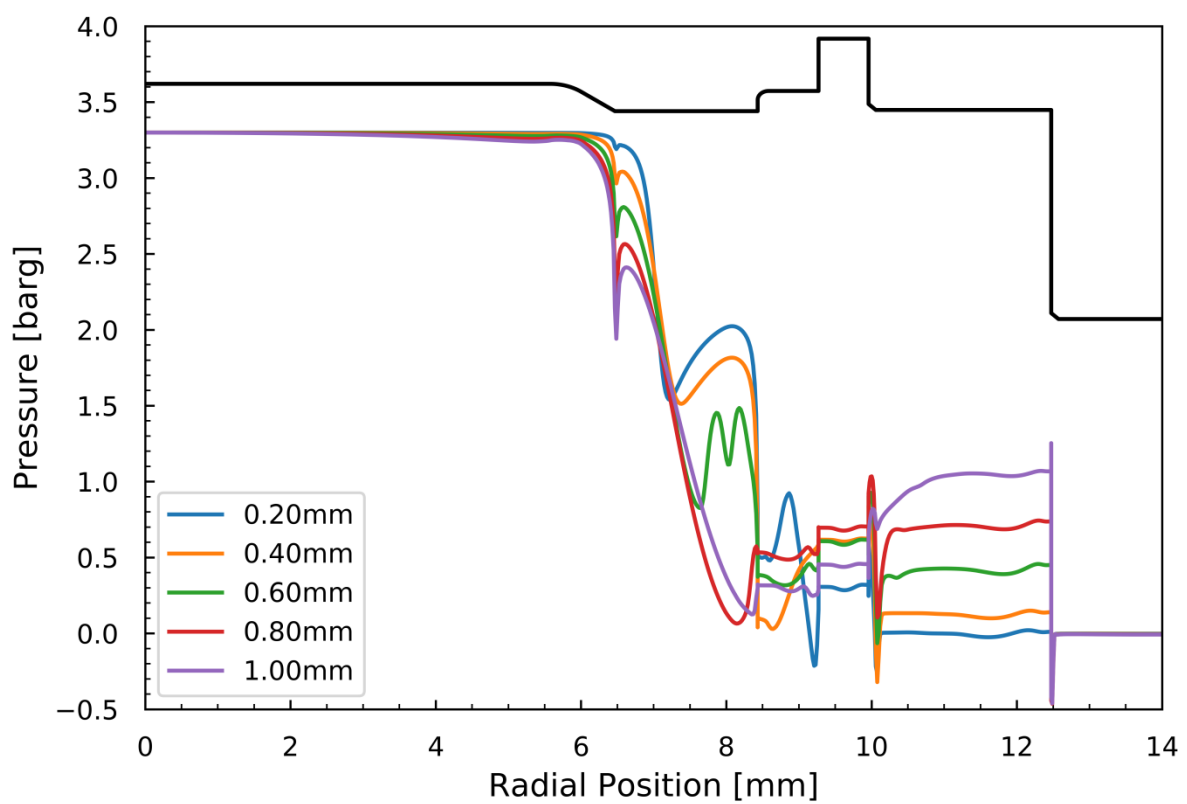


Figure 4.7 – 2-D axisymmetric – 3511E – 2 notches – 3.3 barg set pressure – pressure distribution
0.1-1.0mm.

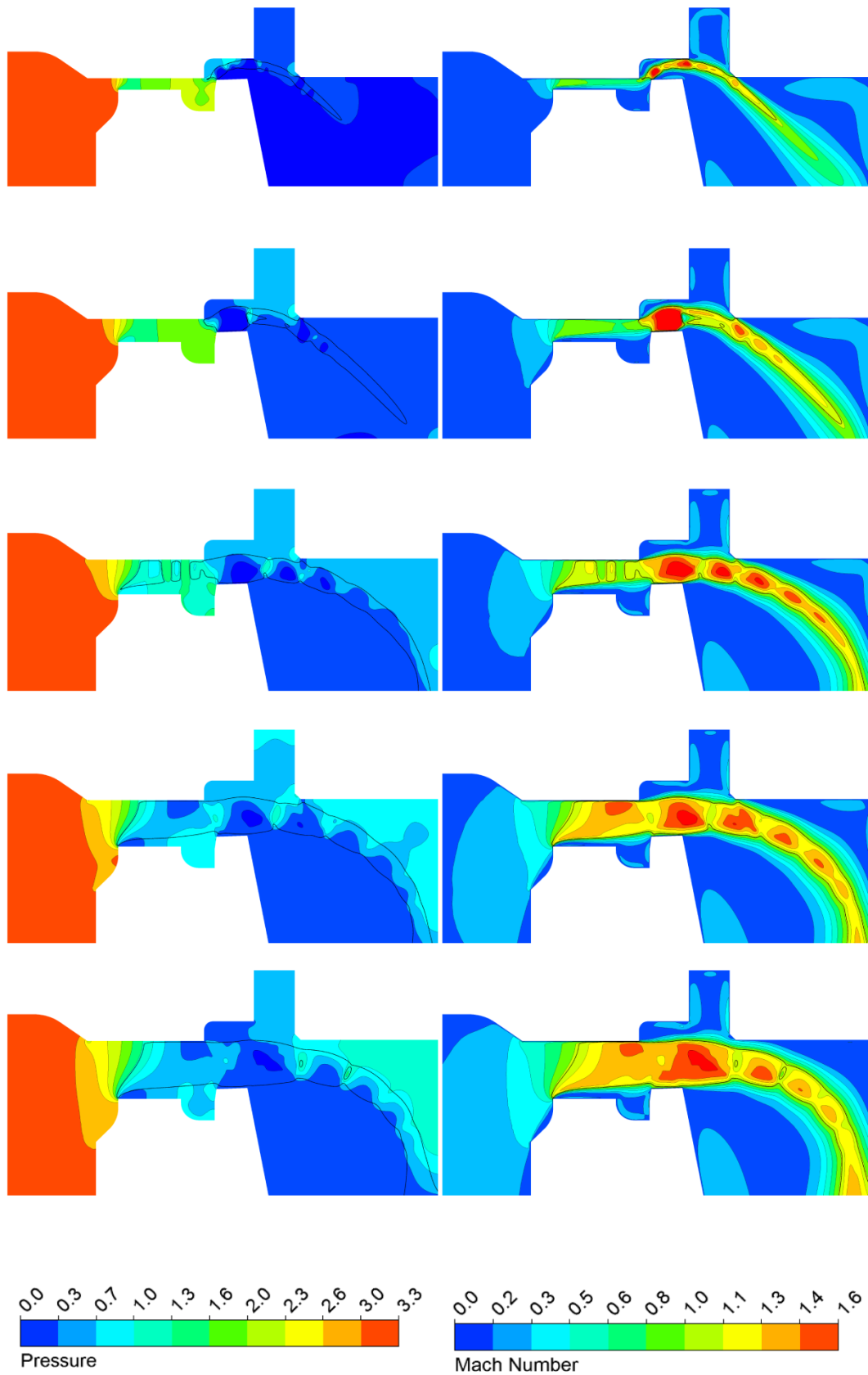


Figure 4.8 – 2-D axisymmetric – contour plots showing pressure (left) and Mach number (right) at 0.20mm, 0.40mm, 0.60mm, 0.80mm and 1.00mm, iso-surface of $Ma = 1$ has been included in both plots. (region i, ii, iii, iv in figure 4.3)

4.1.2 Closing Process

The closing process of a snap-action pressure relief valve is controlled by the forces in the higher lift region, primarily the area of the force-lift curve (figure 4.1) from 2.6-4.0 mm. A steady increase in force from 1.0 mm is experienced by the valve as it opens further, this continues to around 2.8 mm lift where a sharp increase in force can be observed.

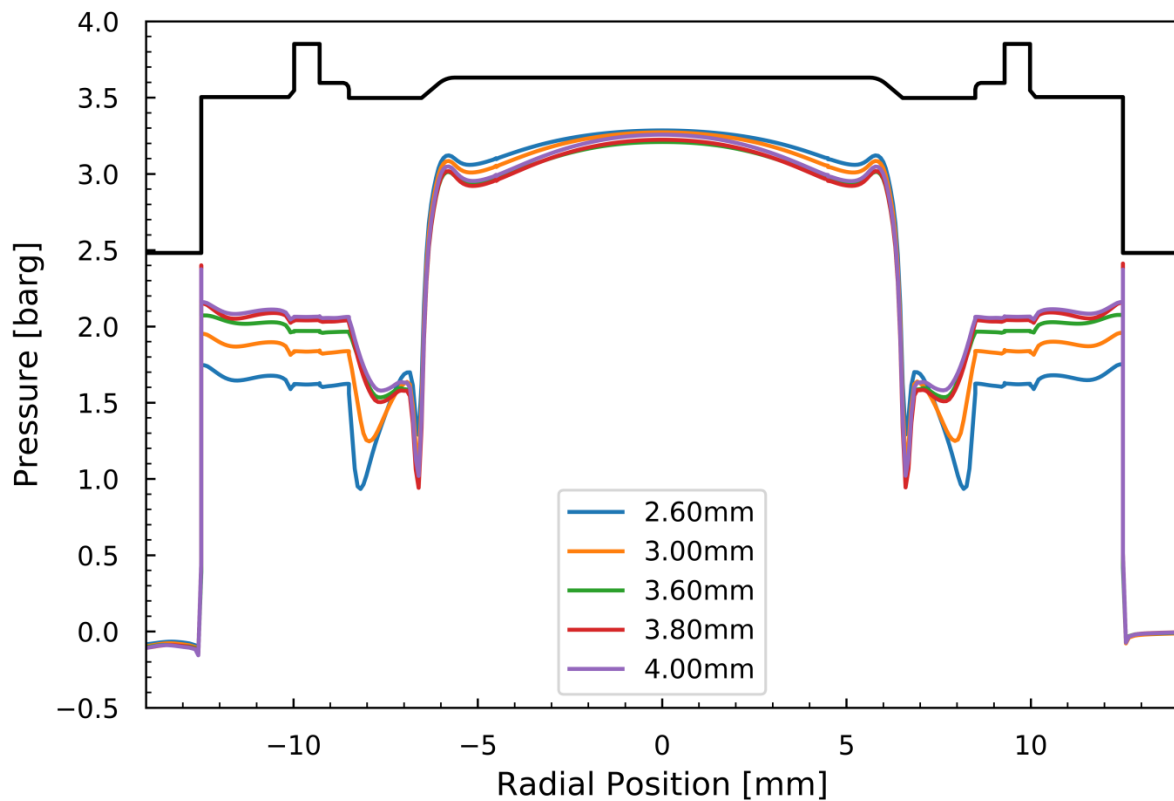


Figure 4.9 – 3-D - 3511E – 2 notches – 3.3 barg set pressure – pressure distribution 2.6-4.0mm.

The relatively sudden change in disc-force at 2.8 mm lift can be studied in more detail using the pressure distribution plot presented in figure 4.9. Focusing on the disc holder shroud region at a radial position of ± 8 -12 mm (region iv), an increase on surface pressure can be

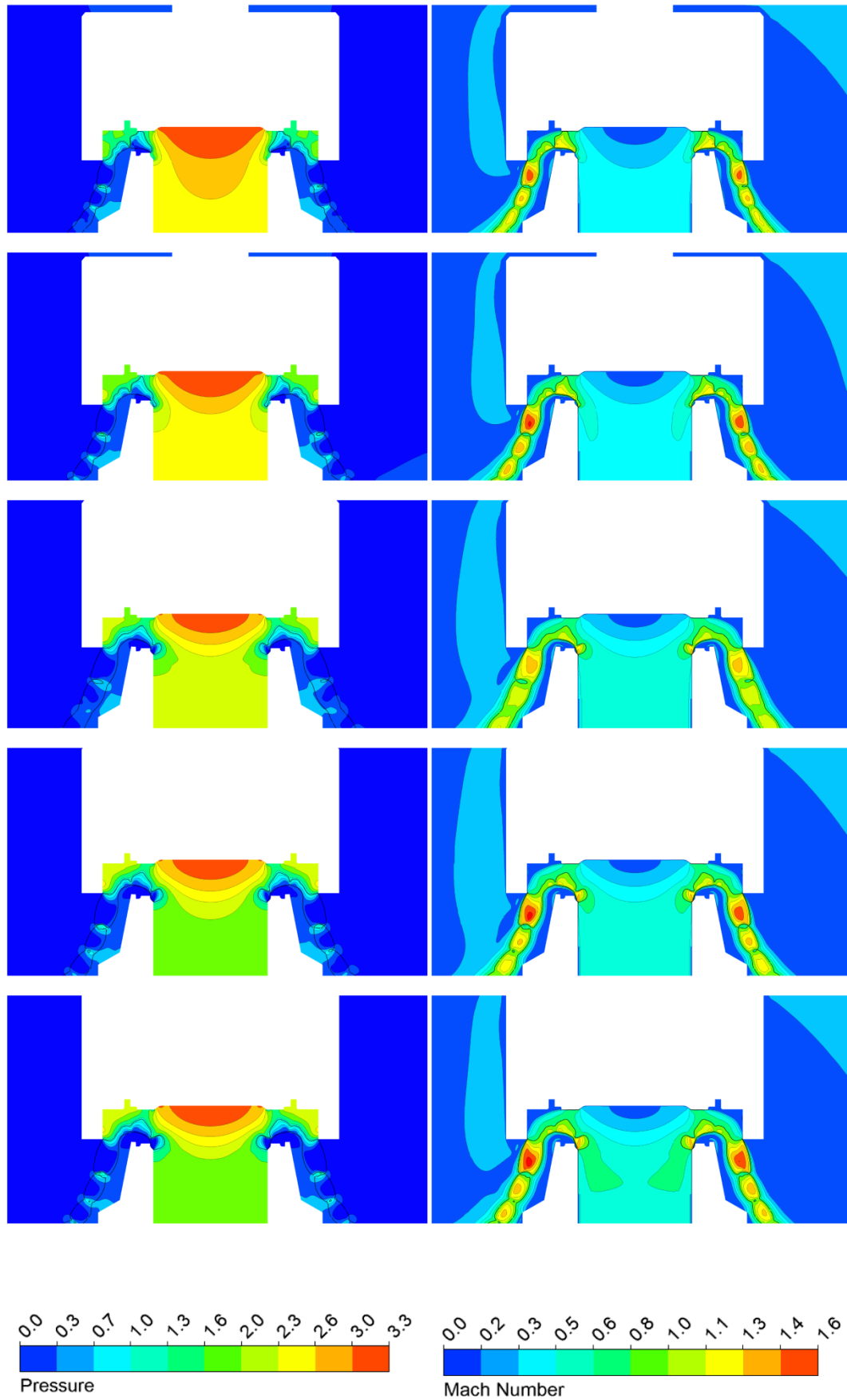


Figure 4.10 – 3-D – contour plots showing pressure (left) and Mach number (right) at 2.6mm, 3.0mm, 3.6mm, 3.8mm and 4.0mm, iso-surface of Ma=1 has been included in both plots.

witnessed as the valve moves from 2.6-3.0 mm lift, after this point the disc force resumes a more gradual increase to the full opening height of 4 mm lift. Inspecting the contour plots in figure 4.10, the choking behaviour of the gas becomes clearer. At 2.6mm lift the fluid is choking across the full opening between the sealing faces, resulting in a low-pressure region around the sealing face of the disc. This low-pressure region can be cross referenced with the pressure distribution plot in figure 4.9, at 2.6-2.8 mm where a dip in the pressure distribution is clear.

As the valve opens further and the fluid becomes less attached to the disc face, the pressure builds up in this region. As stated, the main force increase is experienced from the change in pressure distribution at the disc holder shroud area. From inspecting the contour plots this change in distribution can be explained by the high velocity region becoming less attached to the disc surface restricting the available flow area and introducing a pressure increase in the shroud area.

The disc force continues to increase as the valve opens, when the valve is fully open a force plateau is attained and further increase in lift does not affect the valve. In the full lift position, the nozzle throat area should become the restrictive point in the flow path and the fluid should move to choking at this point, however at 4mm lift it is apparent from inspecting the contour plots in figure 4.10 that the gas is still choking around the nozzle exit and shroud region. It is postulated that the gas would move to choking in the nozzle throat if the valve was further opened. This however is not necessary as it has been proven to pass the required amount of fluid in the current setup, evidently, the different choking position is not causing a detrimental effect on the valve performance.

4.2 Pressure Scaling

One of the main components within a relief valve is the spring; this is responsible for counteracting the system pressure and maintaining the valve in a closed position. To ensure correct operation of a relief valve the spring rate must be carefully selected to match the conditions at which the valve will operate. Although knowledge of the disc forces across the full operating cycle would be ideal, the spring rate could essentially be determined by the closed and fully open disc force measurement. The closed disc force can be estimated from the valve geometry at any fixed pressure, whereas the fully open disc force is generally obtained via experiment. This data may be easily measured at low pressures, however at higher pressures obtaining this disc force becomes extremely difficult. As valves could be required to operate at 100s of bar pressure, the equipment to carry out tests at these conditions would be expensive and involve serious safety issues when in use. To circumvent this requirement, manufacturers generally rely on pressure scaling; this industry standard technique assumes that disc forces are linearly proportional to operating pressures. Thus, a relief valve manufacturer will obtain a disc force via experiment at a low pressure then scale this value to the desired operating pressure which will then be used to specify the required spring rate.

There have been potential shortcomings with this technique reported in the literature (Dosenka, 2013), where it has been found that under certain flow conditions this technique is not accurate. This could result in poorly sized springs which would lead to a relief valve that does not operate as intended. Therefore an investigation into the suitability of pressure scaling was undertaken using a 3500 series valve from Broady Flow Control. It is intended to

investigate both low and high lift conditions as each of these phases in the valve operating cycle control the opening and closing process respectively.

4.2.1 Low Lift Pressure Scaling

The requirements of ASME Section I certification are strict and to maintain performance a precise knowledge of the force-lift curve under all conditions is essential. Small changes in the force-lift curve at this height could lead to the over-pressure falling outside of the allowable tolerances. To compare data at different pressures it is common to normalise the disc force with respect to inlet pressure. If an SRV were truly independent of operating pressure the normalised disc force line should be the same for all operating conditions. Essentially, a normalised force-lift curve should give an accurate representation of an SRV under all conditions and therefore could be used for studying a valve over a range of pressures.

Due to the elevated pressures involved, CFD calculations were utilised for this investigation. This initial section is focused on low-lift pressure scaling using the 1x2" E orifice 3500 from Broady Flow Control. Low-lift conditions for this valve are regarded as 0-1.0 mm - this is the region that will control the opening process - particularly 0-0.2 mm lift. Incremental pressure changes up to a value of 40 barg were used for this investigation and the geometry was consistent to that used in the validation exercise in chapter 3.

Figure 4.11 presents the force-lift curves up to a pressure of 40 barg and figure 4.12 presents the same data normalised with respect to inlet pressure and orifice area, the normalised data displays a noticeable variation between the curves - this should be a single

curve if the fluid mechanics were truly independent of operating pressure. The variation in curves suggests that scaling is not accurate.

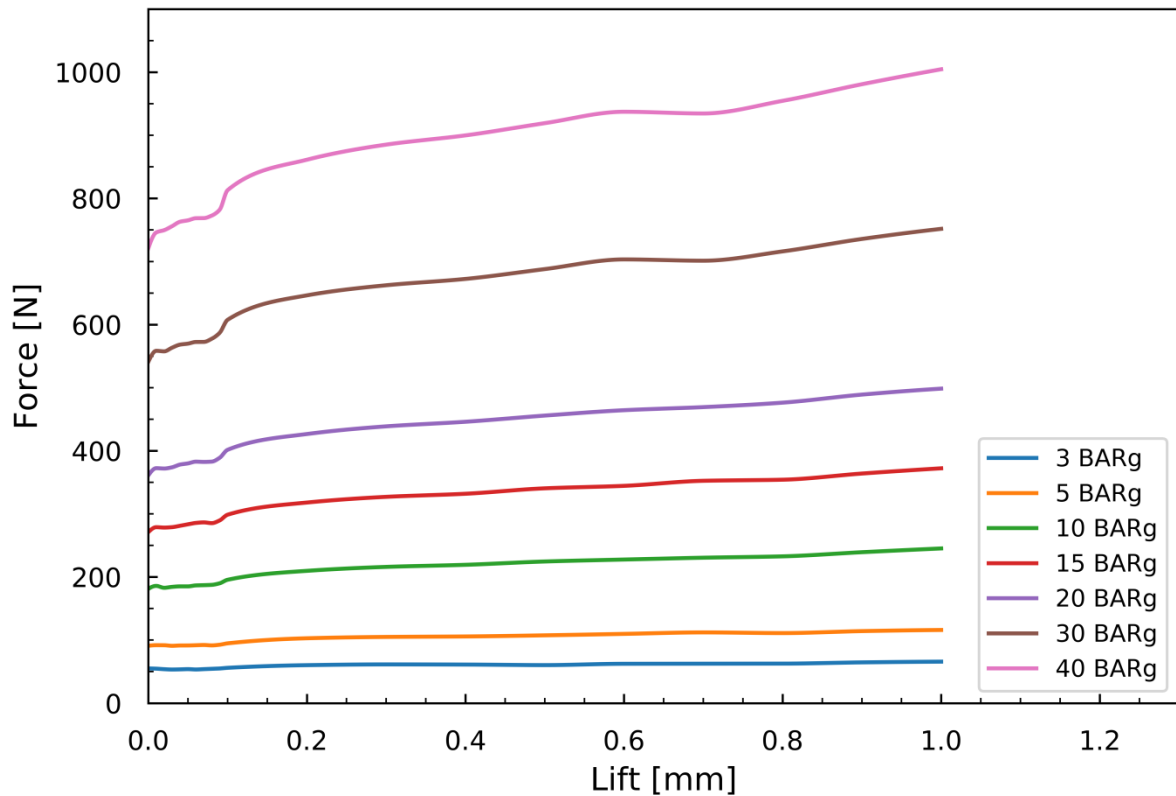


Figure 4.11 – 3511E – 2 notches – force-lift curves – 3-40 barg set pressure.

Figure 4.13 presents the normalised force at a fixed lift for 3 different values of lift, 0.1mm, 0.5mm, and 1.0mm. This data demonstrates that as the inlet pressure approaches 40 barg the normalised disc force tends towards a constant value. The disc force is a consequence of the pressure distribution on the disc face thus this information is showing that the pressure distribution changes with respect to inlet pressure.

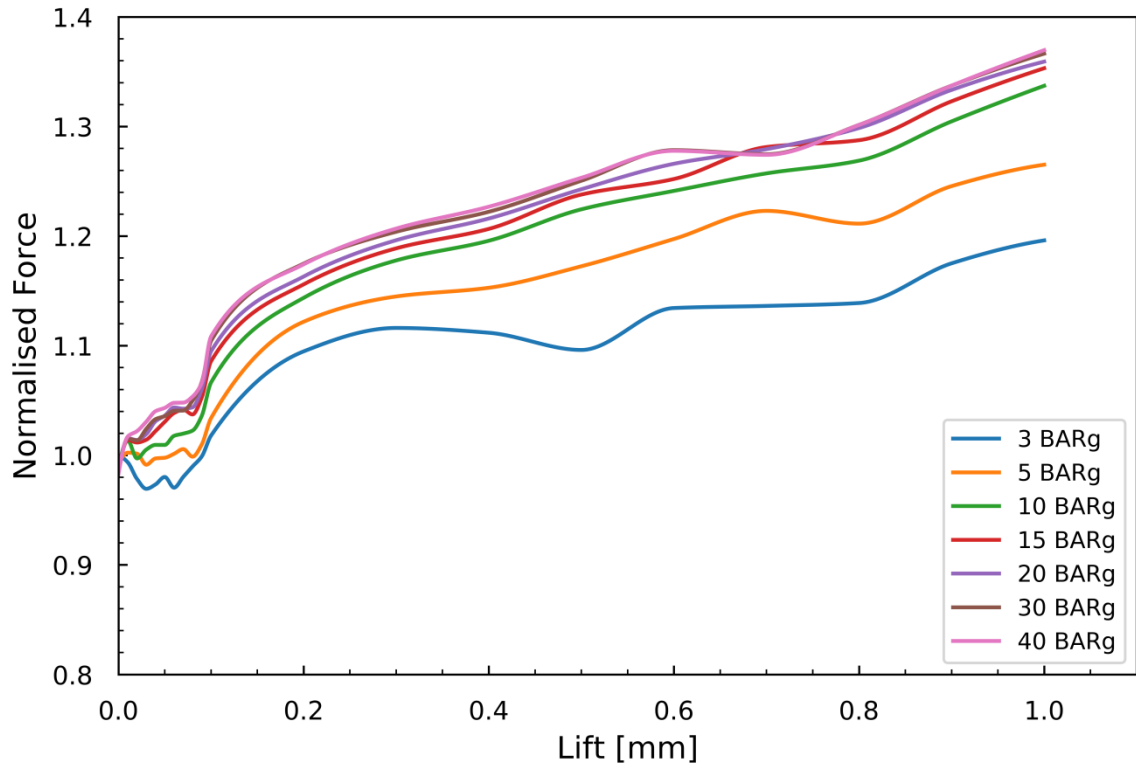


Figure 4.12 – 3511E – 2 notches – normalised force-lift curves – 3-40 barg set pressure.

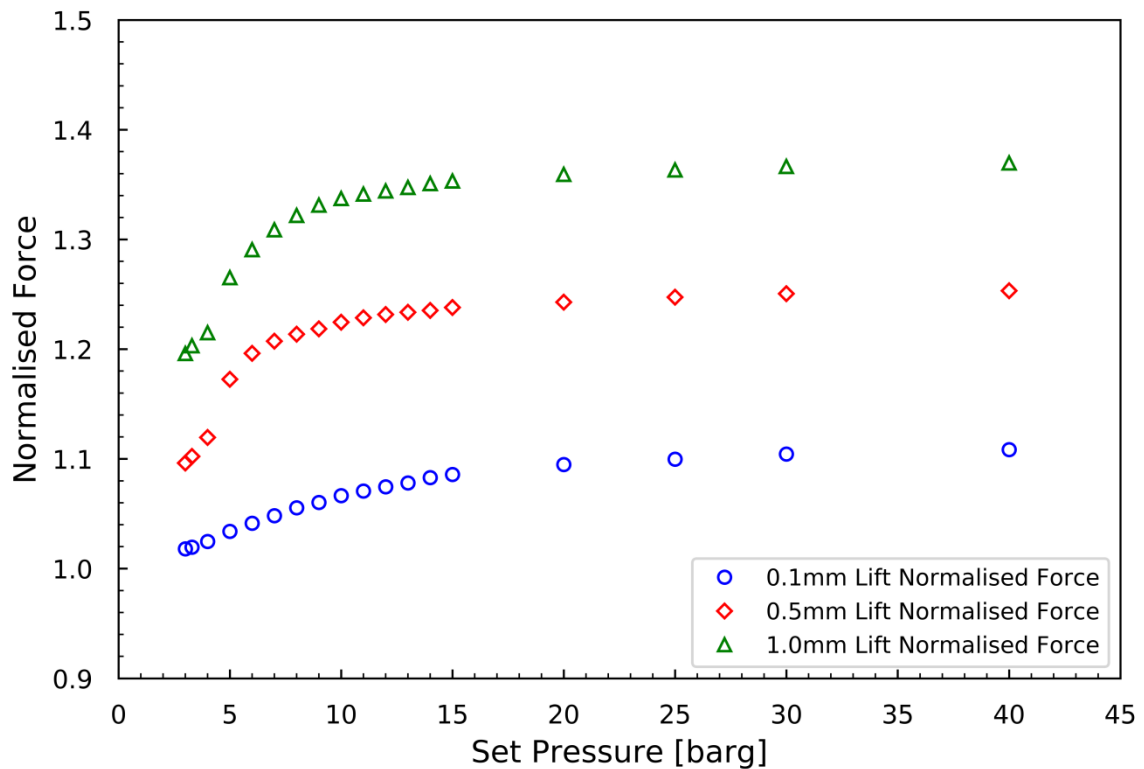


Figure 4.13 – Plot of normalised disc forces at a constant lift over a range of pressures.

Additional evidence exhibiting this behaviour can be found from figures 4.14-4.16, where the normalised pressure distribution on the disc face is plotted at 3 different lifts again, 0.1mm, 0.5mm, and 1.0mm. It is shown that the majority of force variation is in the region between the sealing face and disc notch. The main stagnant region in the centre of the disc and the lifting aid shroud in the outer regions of the disc holder stay fairly consistent throughout the pressure range. The behaviour shows that it is the variation in the high velocity expansion region located around the nozzle exit that is responsible for the normalised force variation across the pressure range.

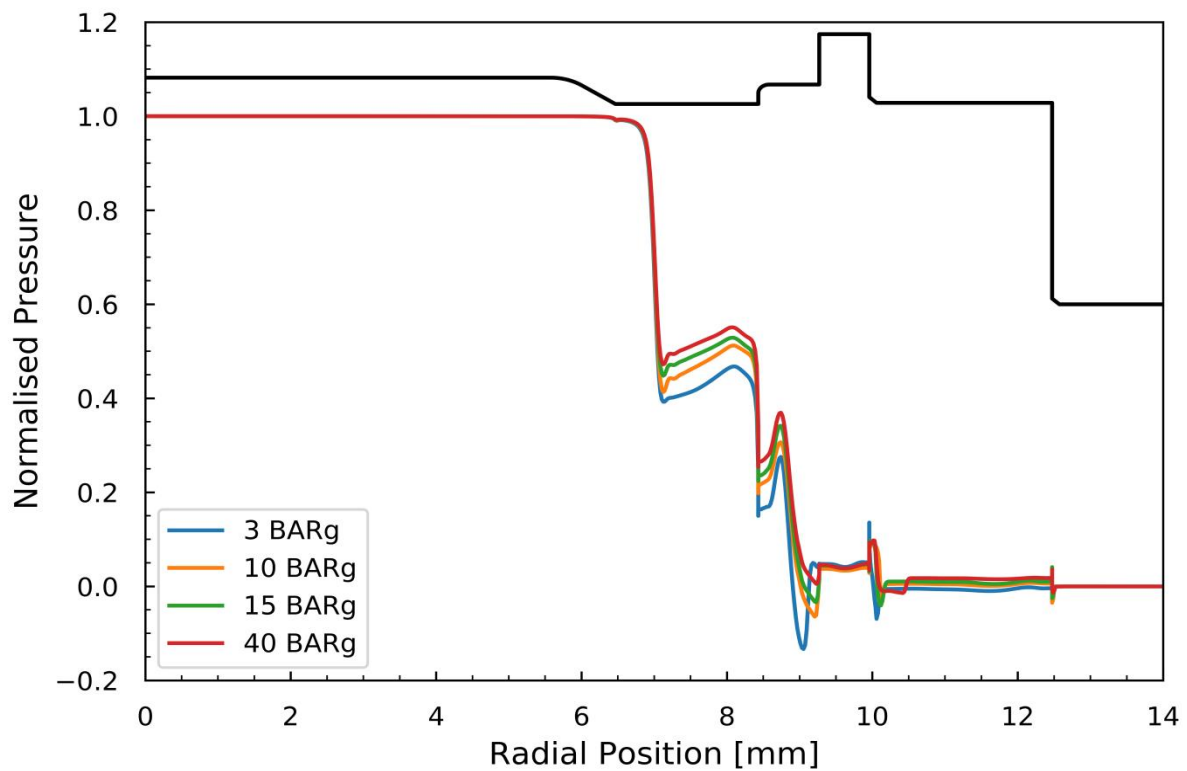


Figure 4.14 – 2d axisymmetric – 0.1mm lift pressure distribution.

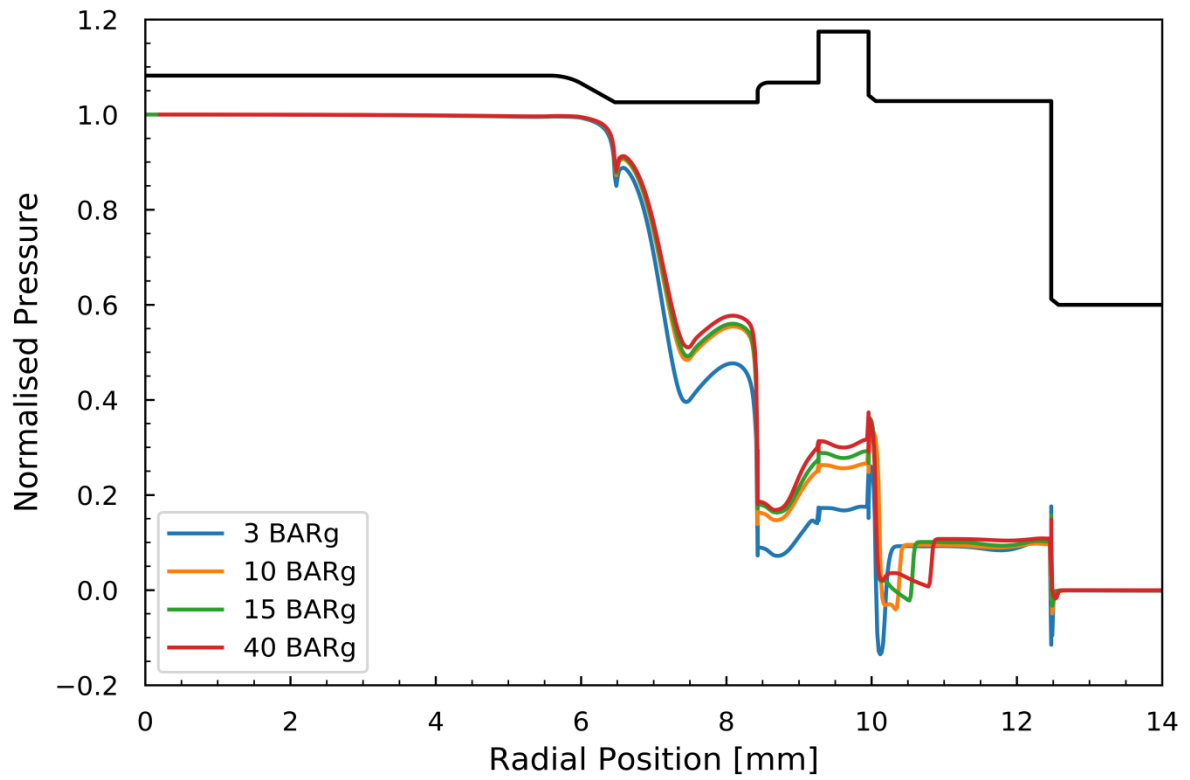


Figure 4.15 – 2-D axisymmetric – 0.5mm pressure distribution.

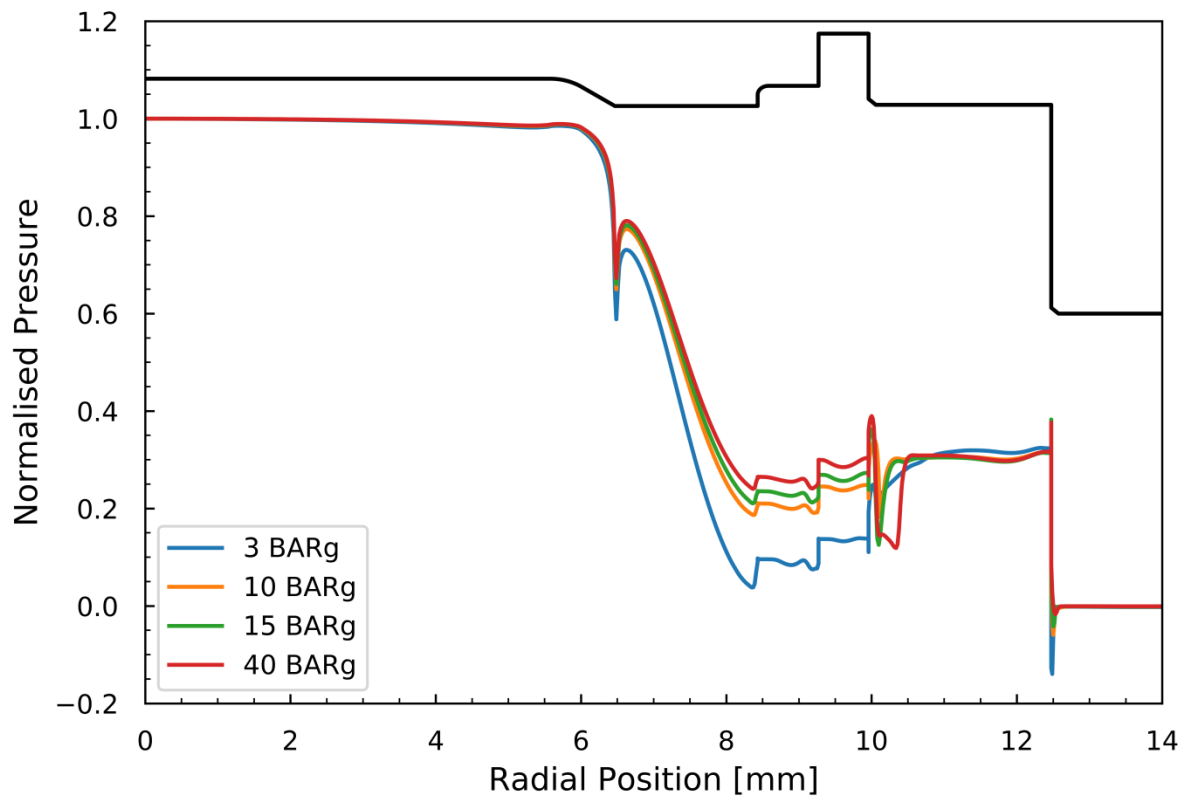


Figure 4.16 – 2-D axisymmetric – 1.0mm pressure distribution.

Figure 4.17 presents the Mach number contours at the disc face and variation in the fluid velocity can be found when comparing 3 barg and 40 barg data. Levels seen in the 40 barg plots are clearly more significant and strong shocks are present there that are not found in the 3 barg plot.

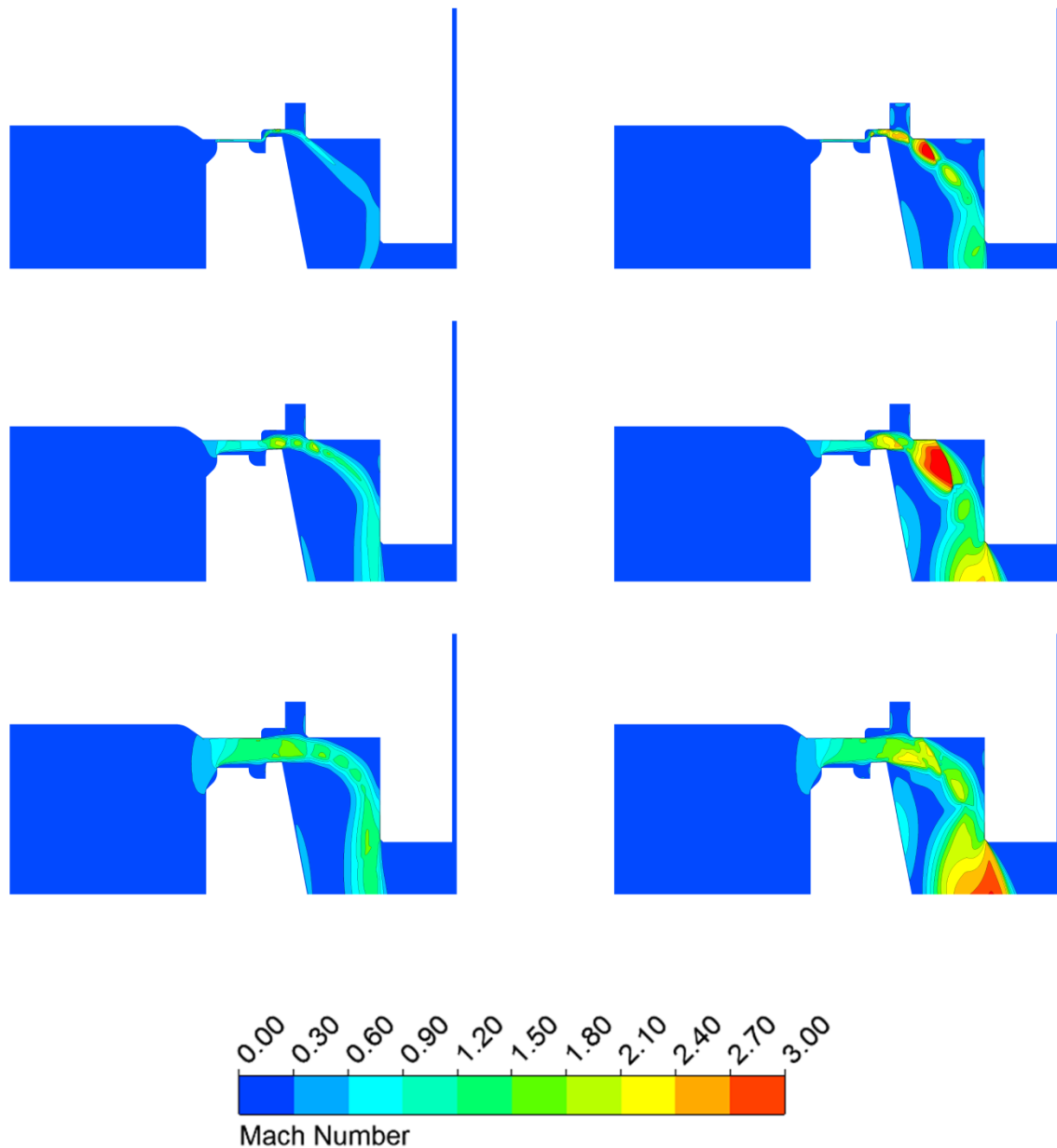


Figure 4.18 – 2D axisymmetric – Mach number contour plots of 3 barg (left) and 40 barg (right) at lifts of 0.1mm, 0.5mm and 1.0mm. (Region i, ii, iii, iv, figure 4.3)

The pressure contour plots presented in figure 4.18 demonstrate the variance in pressure distribution between the different pressure conditions, however a more quantifiable depiction is found in the pressure distribution plots of 4.14-16.

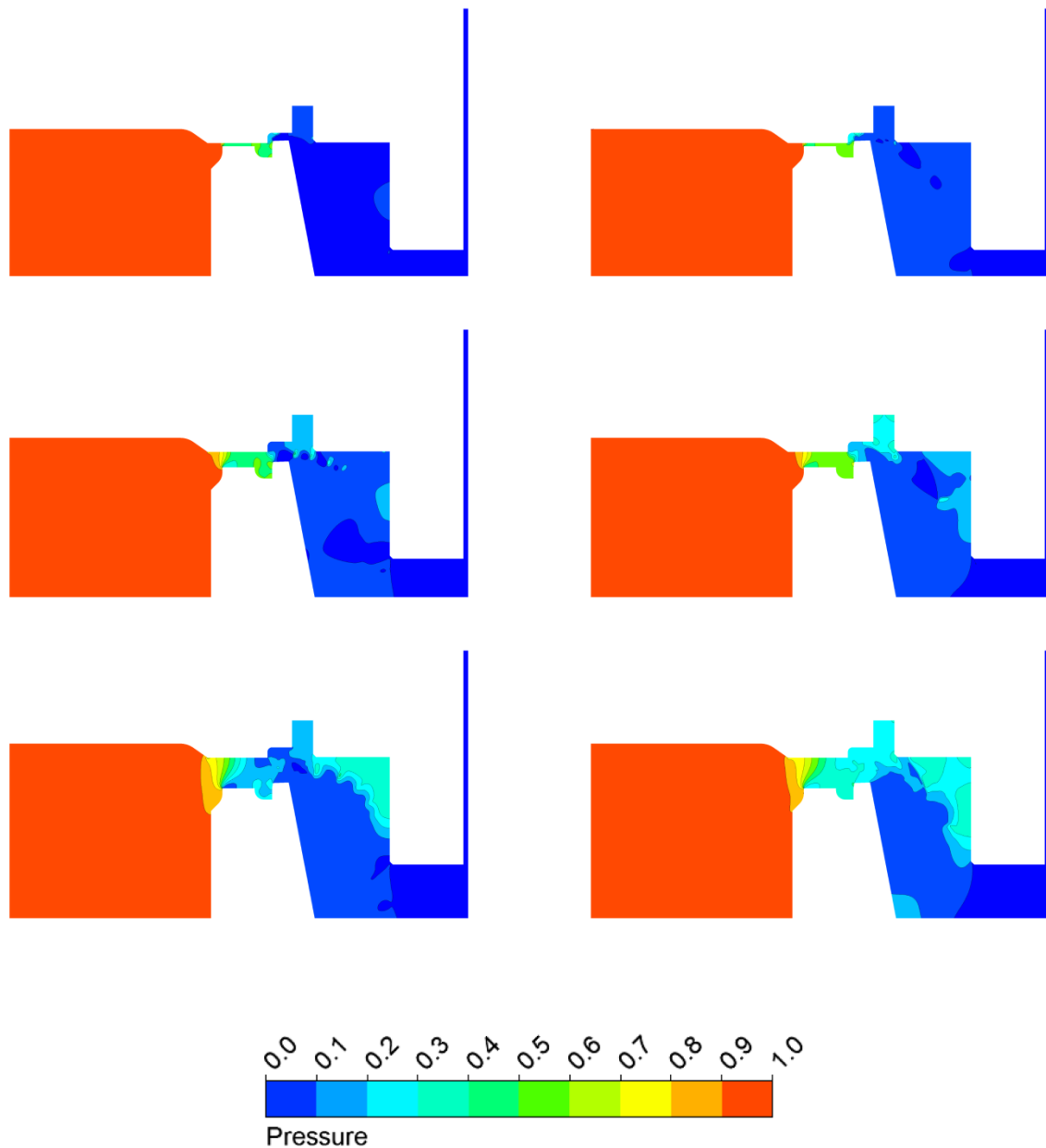


Figure 4.18 – 2D axisymmetric – normalised pressure contour plots of 3 barg (left) and 40 barg (right) at lifts of 0.1mm, 0.5mm and 1.0mm. (Region i, ii, iii, iv, figure 4.3)

Analysis of a Simplified Geometry.

To gain deeper insight into the underlying physics present in the current investigation a geometry simplification was undertaken. The presence of the lower adjustment ring and other geometrical features would interfere with the behaviour of the gas and could affect the results. Therefore, the lower adjustment ring was not included, secondly the disc notch was removed as it introduces unnecessary flow complexity and finally the disc recess (region i) was adjusted to be in line with the nozzle sealing face. The simplified configuration is presented in figure 4.19 below.

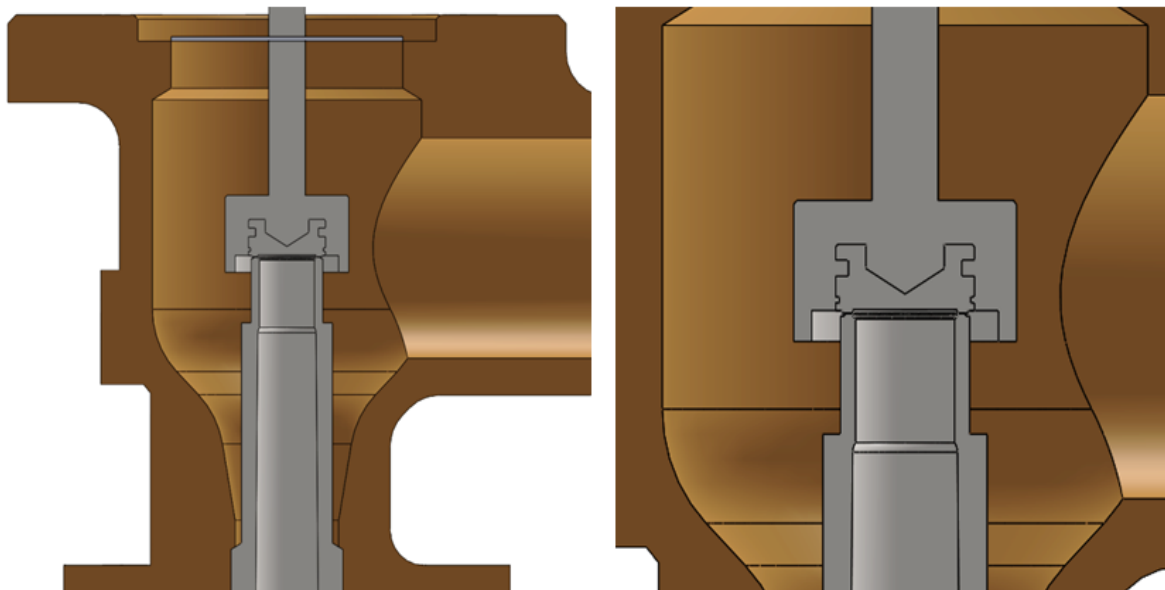


Figure 4.19 – Simplified valve internals.

The disc recess alteration would result in the inside diameter of the raised face on both the nozzle and disc being equal diameter, leading to a symmetrical entrance to the gap between the sealing faces. The disc face recess change was carried out after examining the pressure contour plots at low lifts, it was realized that the fluid expansion and acceleration starts from the inner edge of the nozzle and disc sealing face. As the disc sealing face inside diameter was smaller than that of the inlet nozzle, the gas was accelerating from further into the inlet nozzle than necessary; this can clearly be seen in the 0.50mm pressure contour plot in figure 4.18. As the disc force is a result of the pressure distribution on the disc face, allowing the fluid to accelerate from its original position resulted in an unnecessary force reduction. Also, it was postulated that at higher pressures flow separation in this region could become significant and having a symmetrical entrance to the sealing faces should help reduce any variation with pressure increase.

Figures 4.20-22 present the pressure distribution data for 0.1mm, 0.5mm, and 1.0mm lift at 3 barg and 40 barg set pressure. These plots show that there still exists disc force variation over a range of pressures with a simplified geometry. This indicates that the force variation over a pressure range is primarily a consequence of the fluid mechanics and not a geometrical issue. This deduction is further strengthened by the Mach number contours of figure 4.23 and the pressure distribution of figure 4.24, variation present in these plots illustrates that the pressure scaling inconsistency is a result of the fluid behaviour. Strong shocks are again present in the 40 barg contour plots of 4.23 and 4.24 that are not found in the lower pressure counterparts. From this data it is clear that the change in fluid behaviour over a pressure range cannot be removed via a change in valve design. The change in

expansion and presence of shocks clearly shows that it is a fluid mechanical problem and not one with the valve internal geometry. Therefore to gain control of the fluid behaviour over a range in pressures an adjustment ring will be required. This component is a common feature in SRVs and the ASME BPVC stipulates that one must be present in a SRV to pass certification.

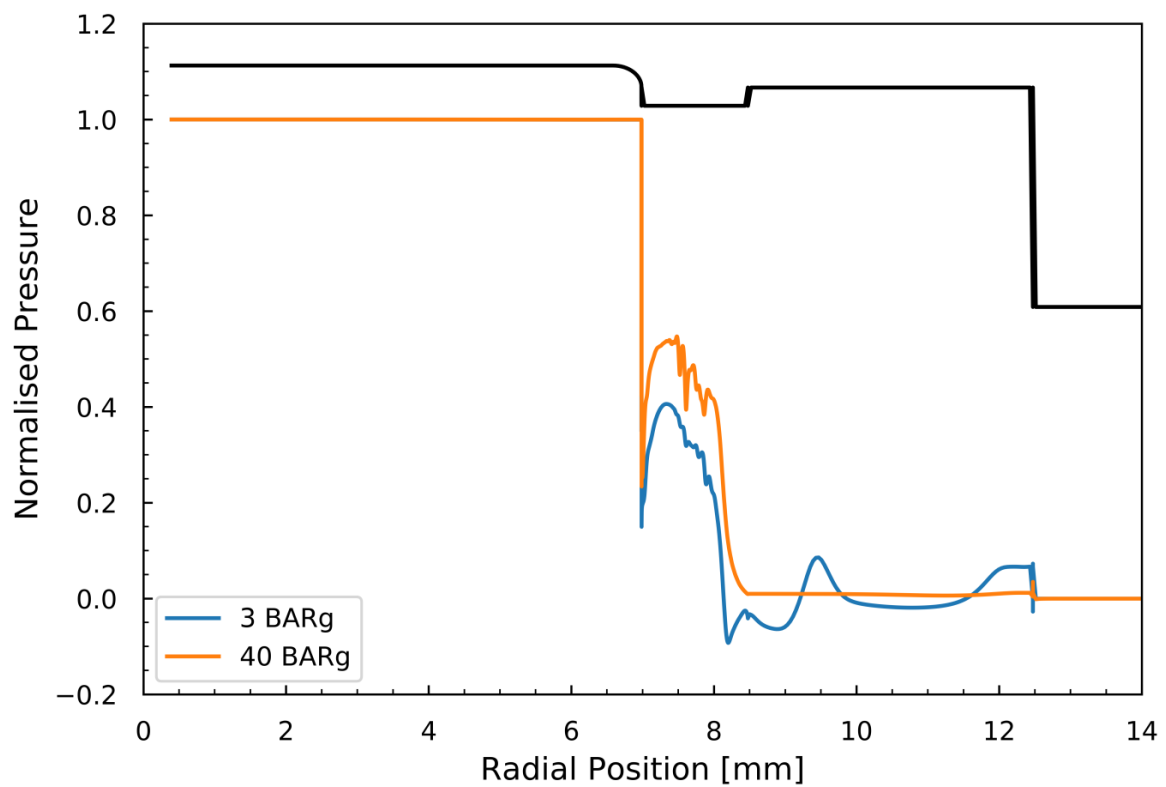


Figure 4.20 – 2D axisymmetric – 0.1mm lift pressure distribution, simplified geometry.

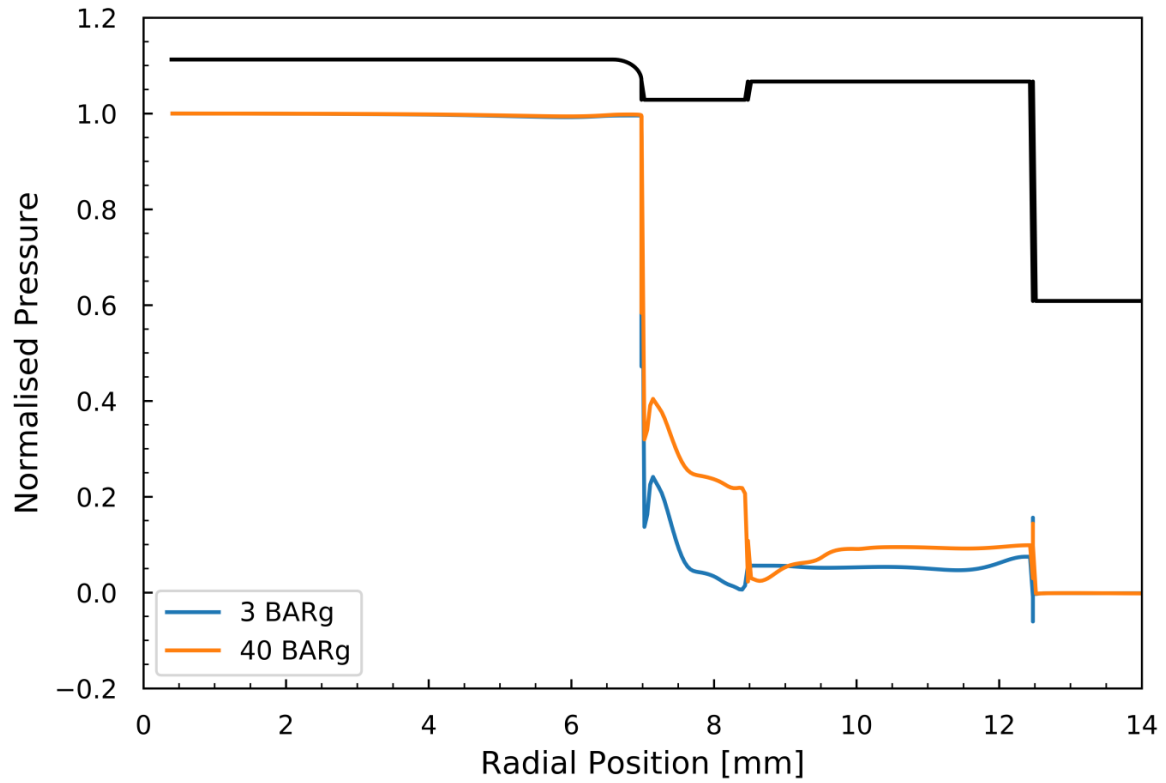


Figure 4.21 – 2D axisymmetric – 0.5mm lift pressure distribution, simplified geometry.

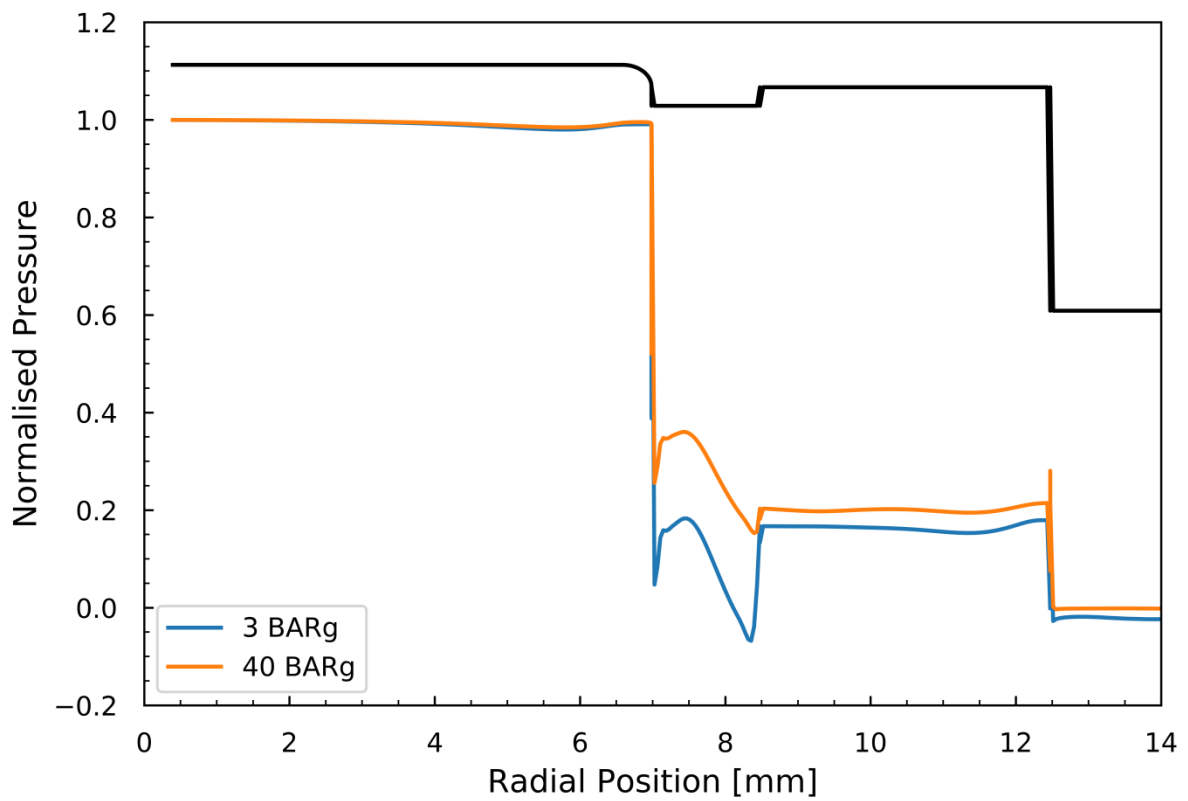


Figure 4.22 – 2D axisymmetric – 1.0mm lift pressure distribution, simplified geometry.

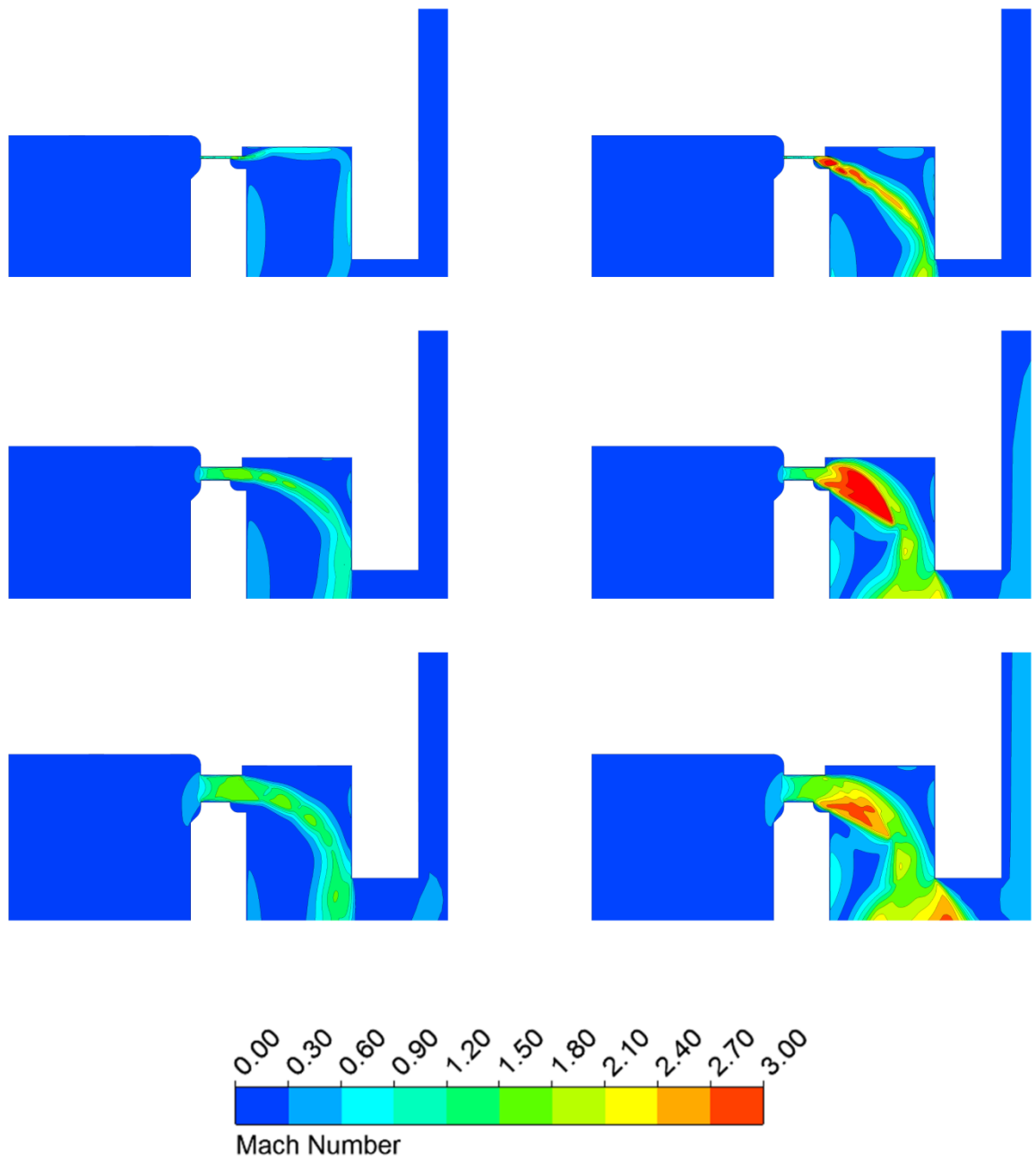


Figure 4.23 – 2D axisymmetric – Mach number contour plots of 3 barg (left) and 40 barg (right) at lifts of 0.1mm, 0.5mm and 1.0mm.

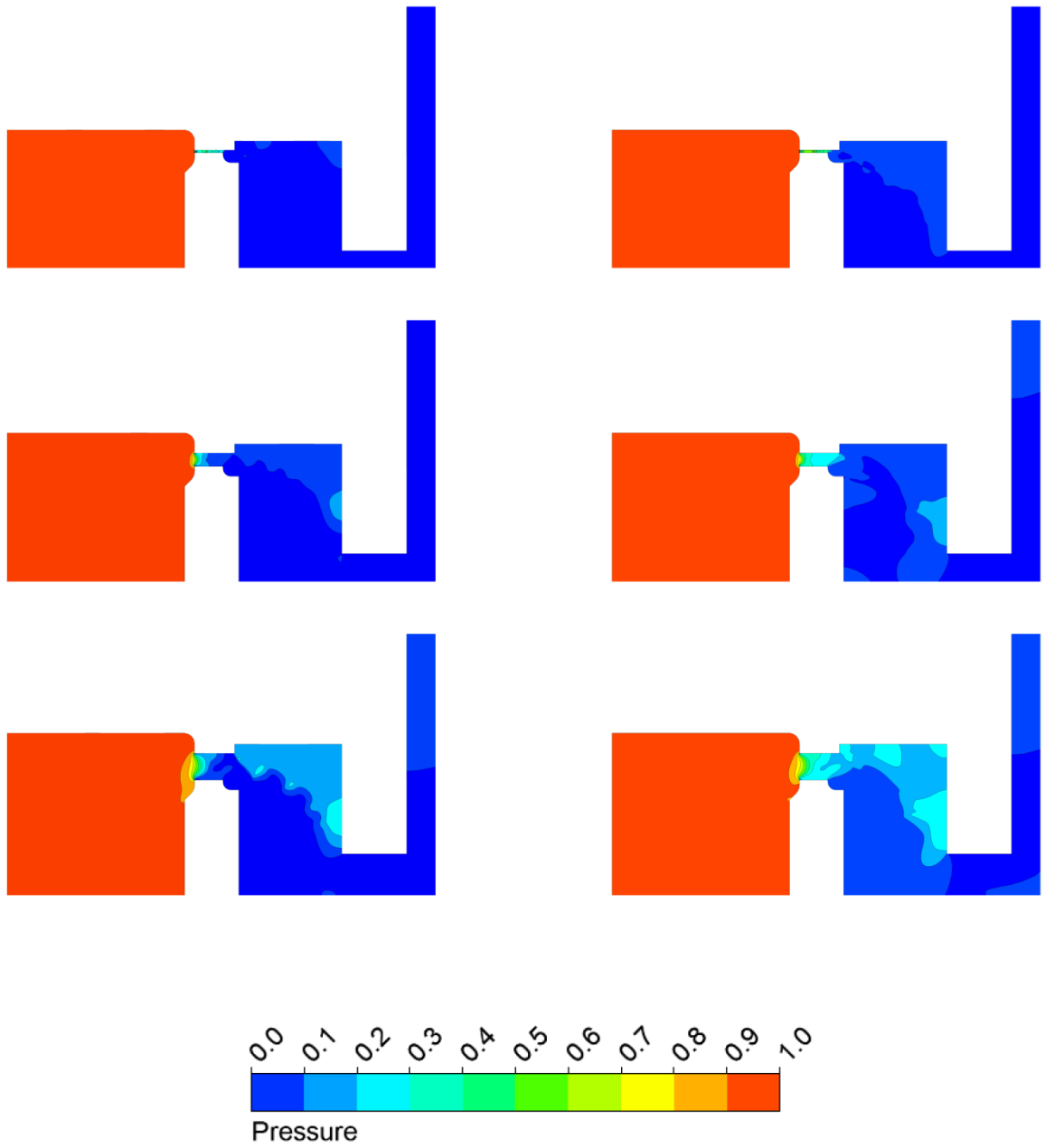


Figure 4.24 – 2D axisymmetric – normalised pressure contour plots of 3 barg (left) and 40 barg (right) at lifts of 0.1mm, 0.5mm and 1.0mm.

4.2.2 High Lift Pressure Scaling

Recent work has highlighted potential shortcomings in the industry standard pressure scaling techniques (Dempster et al., 2018), (Dossena, 2013). The work has shown that under certain conditions an SRV outlet can become choked and act as a second orifice, leading to a pressure build up within the valve body.

In nearly all applications a relief valve will operate under a choked flow condition where the flow rate through the device is set by the nozzle throat area. Under such conditions the behaviour of the device is solely dependent on the upstream pressure that the inlet is exposed to - the valve is independent of downstream conditions. The movement of the operational parts is driven by a force imbalance on the disc, this force imbalance is a consequence of a pressure difference between the front and rear face of the disc holder. When operating in choked flow conditions it is assumed that the front face is exposed to the inlet pressure whilst the rear face experiences atmospheric pressure. However, under certain applications the flow rate through the valve can cause the outlet flange to begin to choke in addition to the nozzle throat. This action results in the outlet acting like a second orifice area. The consequence of this is a build-up of pressure within the valve body which will affect the pressure difference – and therefore the driving force – on the disc and disc holder components. This could lead to the valve closing prematurely and a reduction in relieving capacity, which ultimately could have dire consequences for the pressurised system, (Dossena, 2013).

Back pressure in relief valves is not a new phenomenon, it is well documented and can be split into 2 different categories, superimposed and built-up, the former is due to pressure already present at the outlet of the valve, the latter is due to downstream pipework, flow

restrictions or the valve's own geometry influence on the fluid mechanics - and it is the focus of this current investigation. The difference between each type of back pressure is that superimposed back pressure is generally known of and accounted for when sizing a valve, whilst built-up back pressure is inherent and can occur even when operating under atmospheric conditions.

In a pressure relief valve the spring is one of the main components and its properties has a significant effect on the performance of the device. To specify the correct stiffness of spring requires knowledge of the disc forces at the desired working pressure - in particular the closed and fully open position. The closed position can be obtained from the geometry of the valve, the disc force at a fully open position must be obtained through experiment. While this may be easily achievable at low pressures, obtaining this figure at high pressures becomes problematic. To circumvent the need for high pressure measurements, a common approach in industry is to use pressure scaling. This technique assumes that the disc forces are linearly proportional to operating pressure. As it has been shown in literature (Dossena, 2013) that a built-up back pressure can occur at higher pressures and flow rates the validity of pressure scaling is thrown into question.

As pressure relief valves are required to operate on a range of flow rates, different orifice sizes are available, these are standardised by API and given a letter designation of D-T for the 14 sizes of orifices. To accommodate larger inlet nozzles, relief valve bodies must also increase in size, the API standard covers from 1x2" up to 10x16" bodies. Dossena (2013) has shown that the ratio of orifice area to outlet area is not constant over the range of valves. For example, a D orifice has an orifice to outlet area ratio of 29, while a T orifice reduces to 3. The result of this is the introduction of an outlet choking effect currently under

examination will be more prevalent in larger valves due to the reduced area ratio. The area ratios for the full API range are presented in table 4.1. Consequently, for this study a mid-sized valve was chosen as this should be more susceptible to outlet choking.

Orifice	Throat Area (mm ²)	Outlet Area (mm ²)	Area ratio
D	71.00	2027.09	28.55
E	126.00	2027.09	16.09
F	198.00	2027.09	10.24
G	324.00	4560.96	14.08
H	506.00	4560.96	9.01
J	830.00	4560.96	5.50
K	1185.00	8108.37	6.84
L	1840.00	8108.37	4.41
M	2323.00	18243.83	7.85
N	2800.00	18243.83	6.52
P	4116.00	18243.83	4.43
Q	7129.00	32433.48	4.55
R	10322.00	32433.48	3.14
T	16774.00	50677.32	3.02

Table 4.1 – Area ratio data covering a range of API orifice sizes.

Pressure Scaling Analysis and Applicability.

Presented in equation 4.1 is a definition of the driving force within an SRV arrangement, demonstrating the pressure difference that drives the movement of an SRV working components.

$$F = P_1 A_1 - P_2 A_2 \tag{4.1}$$

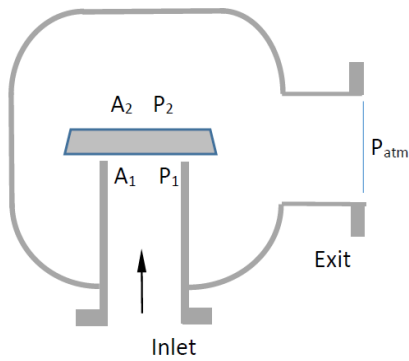


Figure 4.25 – SRV geometry.

From figure 4.25 it can be understood that the disc force is a result of the pressure difference between the front and back face, P_1 being the inlet pressure within the nozzle, P_2 being the pressure within the valve body itself. Under normal operating conditions P_2 is regarded as atmospheric pressure, this may hold true under certain flows but in the event of a build-

up of pressure within the valve body itself this assumption does not hold. The area ratios in table 4.1 clearly show that larger valves will suffer more from a build-up of body pressure than smaller sized valves. The smallest to largest area ratio varies by a factor of 10 thus there is a clear geometrical variation across the valve range. Using equation 4.1 as a starting point, linear pressure scaling will be analysed to determine its applicability over a wide pressure range.

Under these conditions, there are three different flow cases that could occur within a SRV, case (i) normal operating conditions where the outlet is not choked and P_2 is atmospheric, case (ii) onset of a back pressure build-up but outlet is still sub-critical, and case (iii) a fully choked outlet and a built-up back pressure within the valve body. Each of these cases will be considered separately.

Case (i) $P_2 = P_{atm}$

Under these conditions equation 4.1 becomes

$$F = P_1 A_1 - P_{atm} A_2 \tag{4.2}$$

Normalising with the orifice area and system pressure 4.2 becomes

$$\frac{F}{A_0 P_1} = \frac{A_1}{A_0} - \frac{P_{atm} A_2}{P_1 A_0} \quad (4.3)$$

For pressure scaling to be accurate it requires that the force normalised with pressure equals a constant $\frac{F}{A_0 P_0} = C$ however, it can be appreciated from equation 4.3 that this will only become true as $\frac{P_{atm}}{P_1} \rightarrow 0$, P_1 increases and the second term on the LHS becomes insignificant.

Case (ii) $P_{atm} < P_2 < P_{2 \text{ exit choking}}$

Under these conditions the body pressure is above atmospheric pressure but the exit is still sub-critical, the degree of pressure build-up will depend on the mass flow rate through the device. For subsonic compressible flow through the outlet, assuming stagnation conditions in the valve bowl, the mass flow rate can be expressed as

$$\dot{m} = C_{d \text{ exit}} A_{\text{exit}} P_2 \left[\frac{2\gamma}{(\gamma+1)RT_2} \left\{ \left(\frac{P_{atm}}{P_2} \right)^{\frac{2}{\gamma}} - \left(\frac{P_{atm}}{P_2} \right)^{\frac{\gamma+1}{\gamma}} \right\} \right]^{0.5} \quad (4.4)$$

Where $C_{d \text{ exit}}$, A_{exit} are the valve exit flange valve flow coefficient and area respectively. R , T_2 and γ are the gas constant, upstream temperature and ratio of specific heats, respectively. To progress the analysis, it is desirable to explicitly express P_2 in terms of the other parameters. However, since this is not feasible analytically an alternative approach is taken. If equation 4.4 is examined for the dependency of P_2 on \dot{m} , as shown on figure 4.26 below it can be seen that the trend is quadratically dominated.

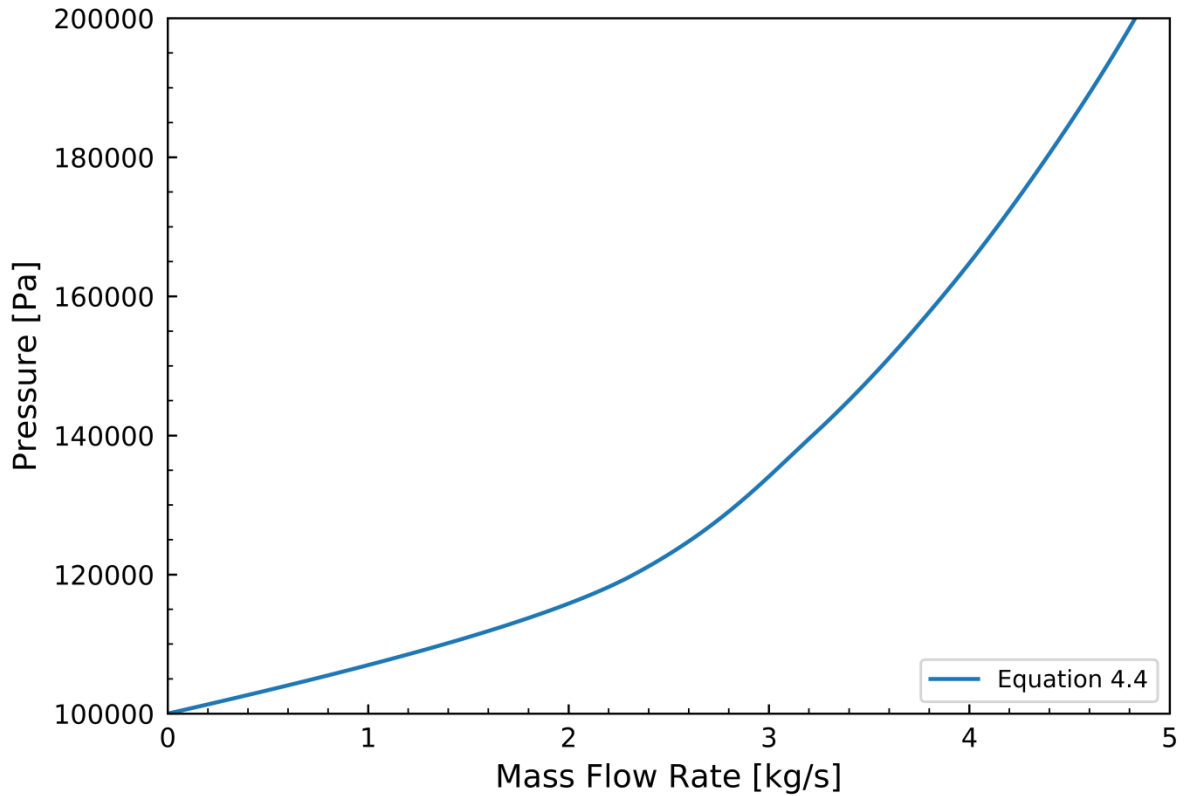


Figure 4.26 – P_2 dependency on mass flow rate.

Therefore, in general a relationship between P_2 and \dot{m} can be expressed as follows

$$P_2 = P_{atm} + \frac{\dot{m}^2}{k_1^2} \quad (4.5)$$

Where k_1^2 is a function of the remaining variables in equation 4.4 and can be taken to be constant.

$$k_1^2 = f(C_{d\ exit}, A_{exit}, R, T_2, \gamma) \quad (4.6)$$

Equation 4.5 can be taken advantage of by noting that safety relief valves normally operate under choked flow conditions determined by the orifice area upstream of the exit flange, the mass flow rate is calculated as follows

$$\dot{m} = C_o A_o \sqrt{\frac{\gamma}{R}} \left(\frac{\gamma+1}{2}\right)^{-\frac{\gamma+1}{2(\gamma-1)}} \frac{P_1}{\sqrt{T_1}} \quad (4.7)$$

Where C_o , A_o and γ are the flow coefficient, orifice area and specific heat ratio respectively.

Taking T_1 as the total temperature and fixed throughout the process, the mass flow rate equation can be written as

$$\dot{m} = k_2 P_1 \quad (4.8)$$

Where k_2 is defined as

$$k_2 = \frac{A_o C_o}{\sqrt{T_1}} \sqrt{\frac{\gamma}{R}} \left(\frac{\gamma+1}{2}\right)^{-\frac{\gamma+1}{2(\gamma-1)}} \quad (4.9)$$

Thus, noting continuity of mass flow between the nozzle exit and valve exit we can substitute equation 4.8 into equation 4.5, resulting in equation 4.1 becoming

$$F = P_1 A_1 - P_{atm} A_2 - \frac{k_2}{k_1^2} P_1^2 A_2 \quad (4.10)$$

Normalising in terms of $P_1 A_0$

$$\frac{F}{P_1 A_0} = \frac{A_1}{A_0} - \frac{A_2}{A_0} \left[\frac{P_{atm}}{P_1} + \frac{k_2}{k_1^2} P_1 \right] \quad (4.11)$$

Which is similar to case (i) but with additional terms on the right-hand side, indicating further dependence on the upstream pressure.

Case (iii) $P_2 \geq P_{2 \text{ exit choking}}$

If the exit plane is choked then equation 4.8 becomes

$$\dot{m} = k_3 P_2 \quad (4.12)$$

Where k_3 is defined as follows

$$k_3 = \frac{A_3 C_3}{\sqrt{T_1}} \sqrt{\frac{\gamma}{R} \left(\frac{\gamma+1}{2} \right)^{-\frac{\gamma+1}{2(\gamma-1)}}} \quad (4.13)$$

The SRV will still be operating under choked conditions thus equation 4.8 still holds and P_2 can be determined, again assuming continuity of mass flow.

$$P_2 = \frac{k_2}{k_3} P_1 \quad (4.14)$$

Substituting this into equation 4.1 leads to

$$F = P_1 A_1 - \frac{k_2}{k_3} P_1 A_2 \quad (4.15)$$

Normalising with respect to $P_1 A_0$

$$\frac{F}{P_1 A_0} = \frac{A_1}{A_0} - \frac{k_2}{k_3} \frac{A_2}{A_0} \quad (4.16)$$

Where the RHS has no pressure terms therefor showing that when the exit flange is fully choked the scaled force is exclusively dependent on geometry. For this condition the disc force is linearly dependent on pressure and linear pressure scaling is valid.

To investigate this phenomenon further, CFD calculations were utilised as the pressure and flow rate requirements render an experimental investigation impractical. A CFD configuration similar to what has been established was used for this investigation, the only change being a larger sized valve, for which a 4x6" P (figure 4.27) orifice from Broady Flow Control was chosen. An inlet pressure range from 1-100 barg investigated to ensure the

inclusion of the outlet choking process. As this effect is dominant at high lift that valve was held in a fully open position (24mm lift) for each calculation.

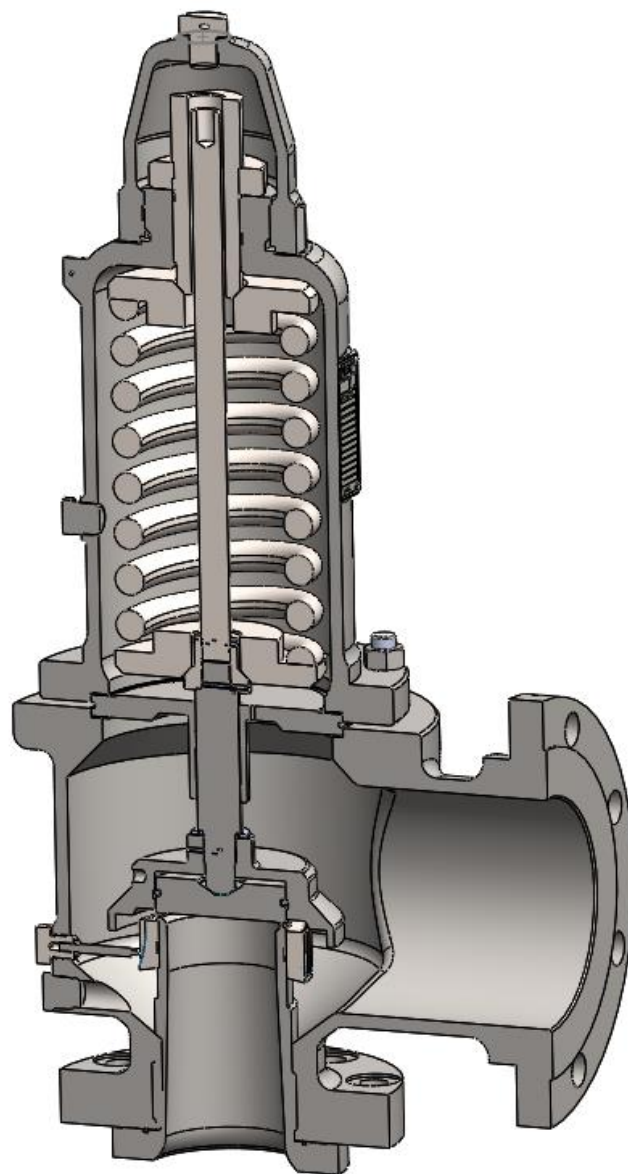


Figure 4.27 – CAD image of a Broady Flow Control 4x6" 3511P

The Mach number contour plot of this investigation at 30 barg working pressure is shown in figure 4.28, this plot displays choked flow across the outlet of the SRV. Figure 4.29 presents the normalised force over the pressure range and clearly demonstrates the change in disc force as the pressure ratio increases, if the disc force was truly independent of pressure conditions this plot would be a constant value across the full range. A steady decrease in normalised force to a final constant value is shown in figure 4.29. The decrease in normalised force is a result of the build-up in back pressure, when it finally reaches a steady point the outlet is fully choked, after this condition the normalised force is then a constant value. Similar behaviour can be found in Plot 4.30 which displays the rear disc force as a percentage of the total force; this is found to increase to a constant value once the outlet of the valve reaches a choked condition.

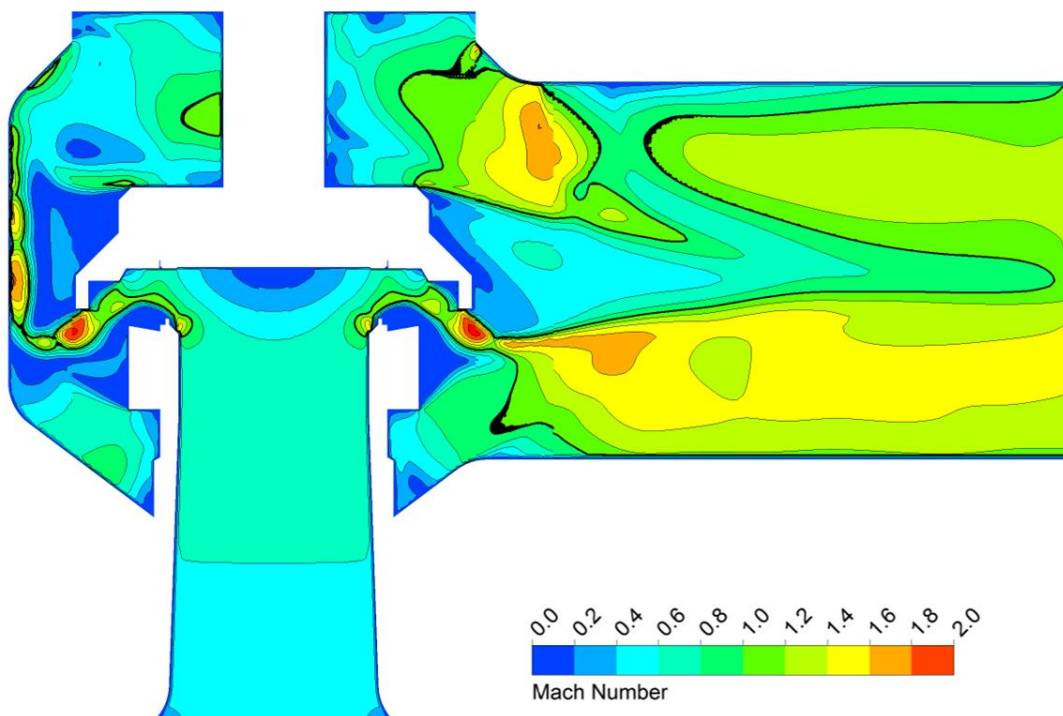


Figure 4.28 – 3D Mach number contour of a 4x6" Broady 3500 series SRV – inlet pressure of 30 barg and a lift of 24mm - displaying a fully choked outlet – iso-surface showing Mach number of 1.

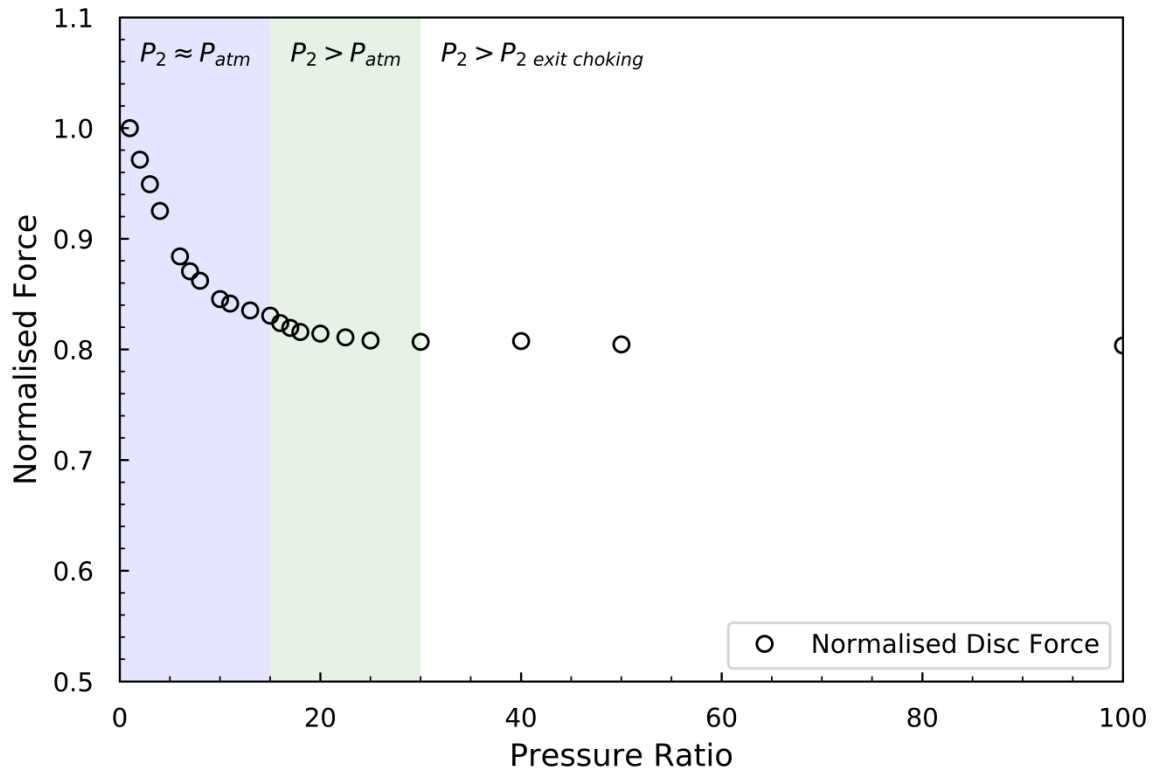


Figure 4.29 – Normalised disc force over pressure range for test valve.

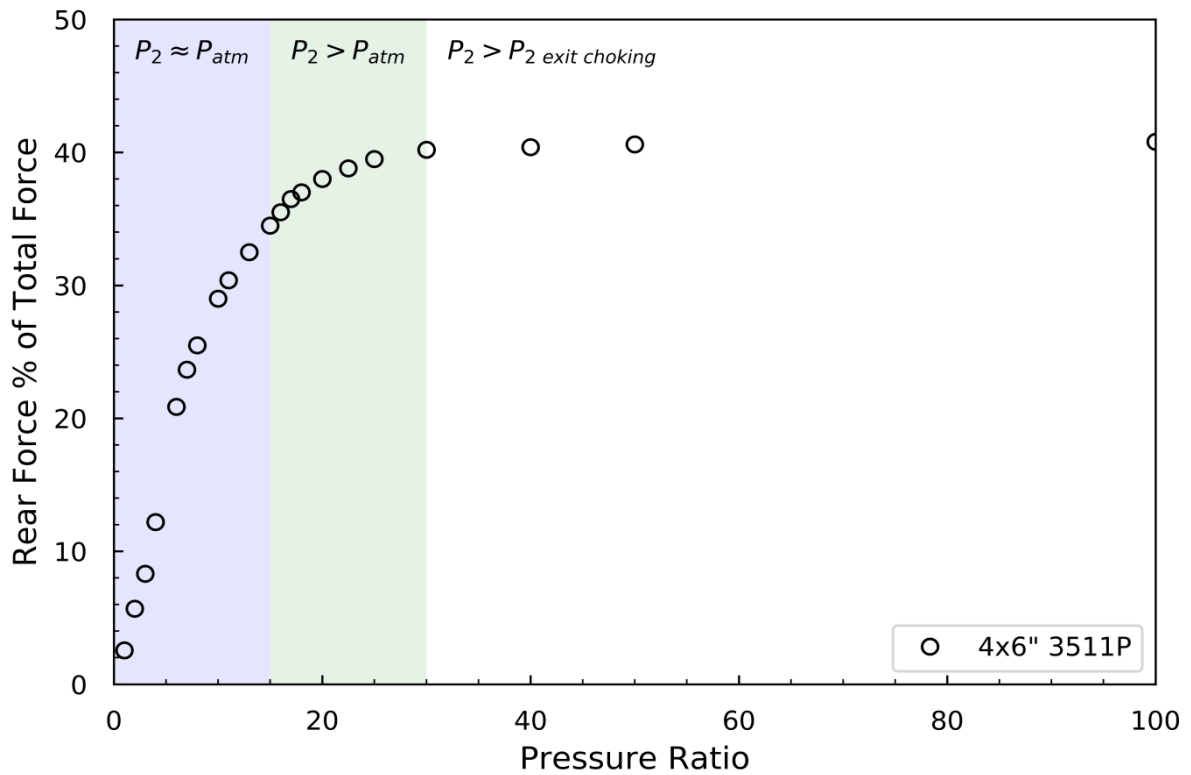


Figure 4.30 – Rear disc force as a percentage of total disc force over pressure range for test valve.

The data displays a gradual choking of the outlet flange as the pressure ratio is increased, this can be explained by examination of the plot in figure 4.28, here the Mach number contours show that the velocity distribution across the outlet is non-uniform where a stratified flow pattern exists. This is due to the shape of the valve body redirecting the gas escaping from the nozzle to the outlet flange, causing stratification to develop. Simplified gas dynamics theory would suggest that the outlet would choke as the body pressure to atmospheric pressure - i.e. exit pressure ratio - was above the critical pressure ratio, which equates to around 2. However, it can be seen that due to the flow stratification this pressure ratio is over 10 times what would be expected.

Through the process of this investigation three distinct flow conditions were found at the valve outlet. An atmospheric, sub-critical and a fully choked condition were shown to exist under different flow rates for this size of valve. The pressure scaling analysis presented an explanation for each condition and was able to explain the behaviour of the normalised disc force over a range of pressures. Case i and case ii were both dependent on the inlet pressure to some degree, it was only upon the fully choked condition of case iii that the normalised disc force became fully independent of upstream pressure, this is clearly shown in equation 4.16. This analysis was cross referenced with the CFD data produced when undertaking an investigation into the Broady Flow Control 4x6" P orifice SRV up to a pressure of 100 barg. Identical behaviour to that predicted in the pressure scaling analysis can be found in figure 4.29 and 4.30. The normalised disc force becomes fully independent of inlet pressure once the outlet is fully choked - this was found above an inlet pressure of 30 barg. Consequently the industry standard linear pressure scaling technique only becomes valid under a fully choked outlet condition. Unfortunately due to the high flow rates

required to fully choke an outlet of an SRV this technique would be unsuitable for many manufacturers. Given the accuracy, a solution is to use CFD calculations to determine the disc forces as the codes have been shown to be valid over a wide range of pressures.

4.3 Discussion

This chapter began with an examination of the data attained from the CFD investigation in the Broady Flow Control 1x2" 3511E SRV. Through this investigation a thorough understanding of its behaviour has been achieved. The data produced by CFD calculations has provided another method to study the force-lift behaviour of the valve - having to rely on purely experimental methods could limit the information available. Some important points on the force-lift curve have been highlighted throughout this study. The small inflection in the curve at low lifts is what controls the degree of overpressure required to open the valve. Reducing the magnitude of this would result in lowering the overpressure requirements. The aim of this investigation was to determine the mechanisms behind this small force dip, this was achieved through the CFD and experimental analysis coupled with an understanding of gas dynamics. The force reduction was explained as the result of the gas accelerating through the opening between the sealing faces at low lift, this acceleration causes a reduction in pressure which is experienced as a disc force drop.

This behaviour can be controlled by geometry changes, in practice the adjustment ring is used to alter the flow path to provide different fluid behaviour in a fixed geometry. This ring provides the manufacturer with some level of control in the valve operation. The tip of the ring, seen protruding above the nozzle sealing face in figure 4.4, is used to reduce the degree of acceleration as the valve begins to open. Applying some degree of resistance to

the expansion of the contained fluid results in a reduction in pressure loss or force dip. Increasing the height of the ring relative to the nozzle seat will result in the ring controlling the expansion over more of the opening cycle. Setting the ring in a lower position will only reduce the pressure loss to a smaller opening height. Consequently, the position of the ring relative to the nozzle sealing face gives an indication of how the force-lift curve will appear. Experimental work presented in figure 4.31 clearly illustrates how the ring height alters the flow force on the valve disc.

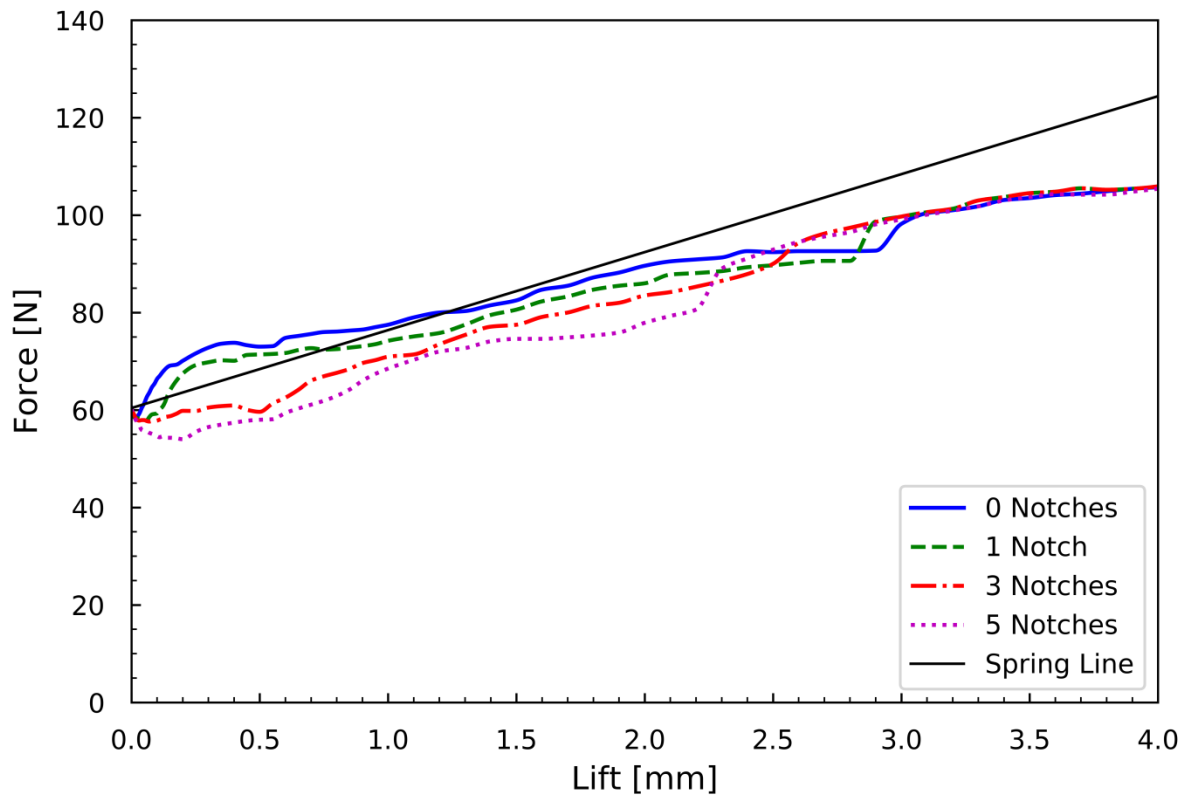


Figure 4.31 – Broady 1x2” 3511E Experimental work over a range of lower ring settings at 3.3barg set pressure.

With the ring in an elevated position it can be seen that the disc force increases as the valve opens, this is due to the ring controlling the expansion of the gas which results in less of a pressure loss upon opening, at 3 notches it can be seen from the results that the disc force decreases more considerably as the valve opens, this is more apparent at 5 notches.

For reference, a table presenting the lower ring heights at different settings has been included (table 4.2). This data is able to express how sensitive the disc force is to ring position, changes in height of the sub-millimetre level have a significant effect on the valve behaviour. Figure 4.32 provides a depiction of the measurement used to determine the ring position, it is taken as the difference in height from the tip of the ring and the nozzle sealing face.

Notches	Ring height relative to nozzle sealing face(mm)(α)
0	+0.35
1	+0.28
2	+0.19
3	+0.11
4	+0.02
5	-0.05
6	-0.13
7	-0.22
8	-0.32

Table 4.2 – Adjustment ring positioning.

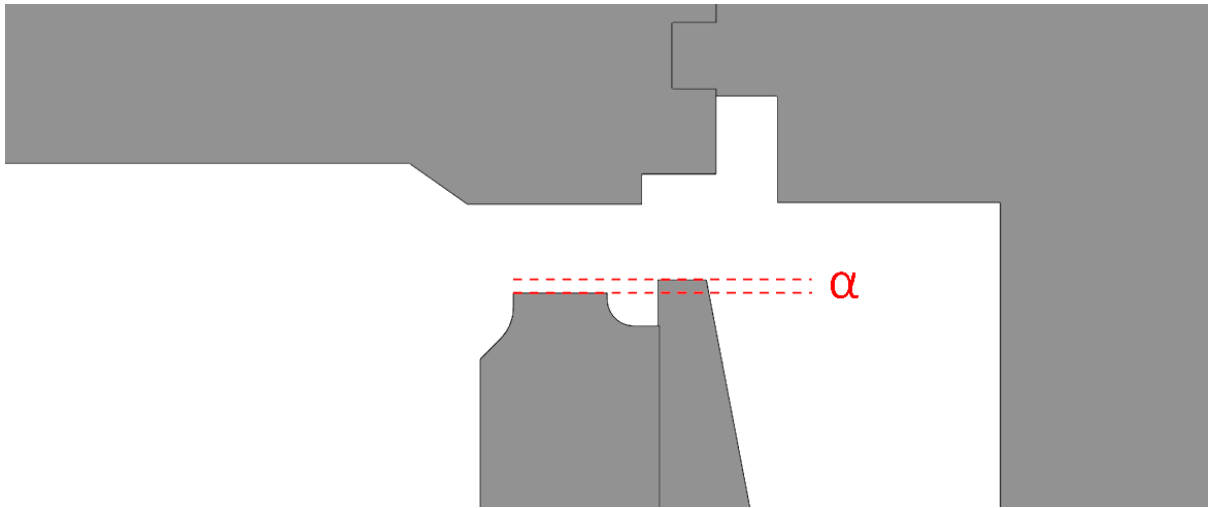


Figure 4.32 – Lower ring height relative to valve seat.

The difference between 1 and 3 notches is 0.17mm, comparing this to the curves presented in figure 4.31, the significance of this ring becomes apparent. Also, from this data it can be seen that to have a minimal dip in the force curve at lower lifts requires the ring to be in an elevated position from the nozzle sealing face. Therefore, to control the disc force at low lifts - which will control the overpressure requirements of the SRV - requires altering the position of this ring above the nozzle face.

At higher lifts (>2.5mm) the disc force is controlled solely by the design of the disc & disc holder, the force-lift curves in figure 4.31 show that all different force curves converge after the valve moves nearer the fully open position. As the valve fully opens, the flow becomes detached from the tip of the ring thus its position should not affect the disc force. It can be appreciated from figure 4.31 that having the ring in a lower position results in the fluid detaching at a lower opening height. The force curve of 5 notches – which is below the nozzle seat height – can be seen to become independent of the lower ring from around 2.3mm, however the adjustment ring can be seen to affect the 0-notch curve to an opening of nearly 3mm lift. This demonstrates that although the adjustment ring is used for

controlling the forces at lower lifts, it is found to affect the disc forces up to nearly 3mm lift in some cases. This could result in the ring having an effect on the closing or blowdown value, but it would be minimal. On the closing cycle the valve will begin to close as the force curve drops below the spring line and the spring becomes the dominant force. Inspecting the curves, it can be seen that there will come a point where a large drop in forces is experienced, e.g. 3mm at the 0-notch position. As the force drops away suddenly, the valve should begin to rapidly close. Consequently, it could be argued that as the lower ring position controls the point at which the sharp change in disc force is experienced, it could control the closing cycle of the valve. However, it is expected to have a minimal influence on the closing procedure due to the following. On closing, the valve will initially be positioned at a lift where the disc force and spring force are equal. Inspecting the gradient of the spring line in figure 4.31 it can be seen that the disc forces at high lift are of a similar gradient. As the pressure reduced in the valve inlet, causing the disc forces to reduce, the valve will close following the spring line as the pressure reduces. As the forces and spring line are of a similar gradient a small reduction in pressure will have a large impact on the position of the disc. Therefore, although the lower ring may control the point at which the sharp increase/decrease in disc forces occurs, the closing procedure will be greater influenced by the reduction in inlet pressure than the location of the force decrease.

Pressure scaling is used for estimating valve behaviour outside of testable conditions, this technique is used for calculating the required spring load at elevated pressures. The whole opening cycle is controlled by the initial dip in force lift curves as the valve begins to open – as presented in section 4.1.1. From the investigation carried out the normalised force distribution at low lifts was not constant, the behaviour of the expanding fluid changed as

the set pressure increased. An additional investigation was undertaken using a simplified geometry and this also found similar effects. Therefore, if a valve cannot be made to be independent of operating pressure, a degree of control is required and for this an adjustment ring can be used. This component provides a means of adjusting the force-lift curve at low lifts to control the opening process.

Further shortcomings with pressure scaling techniques were shown under a fully open position. The outlet of a relief valve was found to become choked as the pressure ratio increases, the transition to fully choked was found to be gradual thus it would be difficult to predict when the outlet would choke without some investigation. Therefore it would be recommended that CFD simulations be used to check the body pressure conditions prior to selecting springs.

The work presented within this chapter is able to show the value that can be added by utilising CFD simulations within the design stage of a relief valve. Fluid mechanics were uncovered that would have been difficult to explain using any other method, and in the case of the fully open pressure scaling investigation, it would have had a significant financial barrier to achieve the level of data produced using the present CFD methods.

5. Design methodology

The valve shown in figure 5.1 is a modified Broady 1x2" 3500 E orifice SRV, the 3500 model that this was based on was discussed in length in chapter 4. The Broady 3500 series valve meets the ASME BPVC Section VIII performance criteria, the objective of this study is to develop an optimisation process to design SRV internals to meet the ASME BPVC Section I. Noting that a certain degree of adjustment is required to account for pressure effects (as discussed in chapter 4) it was decided that control of the forces would benefit from an additional adjustment ring. This upper ring would complement the lower ring in providing additional control over the forces. The lower adjustment ring would be used to control the low lift forces and the upper adjustment ring would be able to control the high lift forces. Thus the baseline valve is established from a Broady 3500 E orifice valve and the trim has been modified by including an upper ring to provide additional control. The design challenge then becomes what geometry dimension one should allocate to achieve the desired performance.

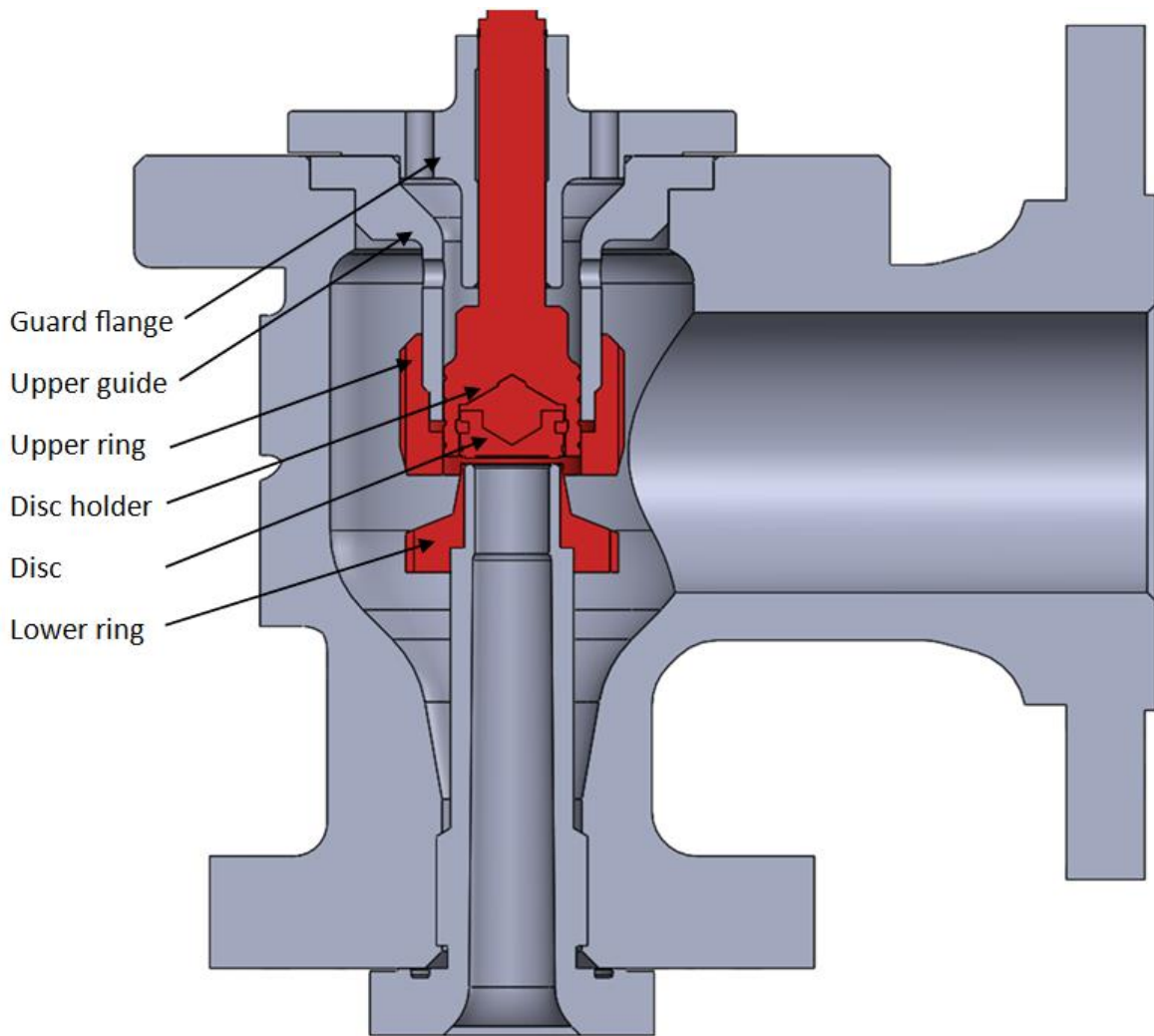


Figure 5.1 – Reference valve for optimisation.

The flow path within a relief valve – particularly around the nozzle exit area – is directly responsible for the performance and behaviour of the device. The significant impact of small geometry changes on valve performance was the essence of the previous chapter. Sub-millimetre movement of the adjustment ring is all that is required to control the performance of an SRV. The impact of small radii and chamfers on valve performance has also been established. These are often added unintentionally during the manufacturing process and can result in behaviour that is extremely different to the initial design. From this

evidence it can be appreciated that to optimise the design of a pressure relief valve the changes in geometry will not be significant. It is also now clear that the geometry changes required to influence performance will be in the region of the nozzle exit - the components in question are the disc, disc holder and adjustment rings (highlighted in 5.1). Modification of these components should achieve the desired force-lift characteristic.

The information presented in the previous chapter distinguishes the surfaces that are most influential throughout the force-lift curve. The disc face centre always experiences a stagnation region with maximum pressure, therefore this area is treated as a constant over the full operational cycle. The surface area around the edge of the disc where the lower adjustment ring is located has most influence during the early opening stages (outlined in figure 5.2). It is this region where the escaping gas is most present when the valve begins to open and the behaviour can be controlled by the shape and position of the adjustment ring. Thus, all geometrical changes to control the opening process will occur in this region. Alterations to the disc shape (parameter A) and the lower ring height and shape (parameter B & C) will be sufficient to control the opening process of the relief valve - these parameters are highlighted in figure 5.3.

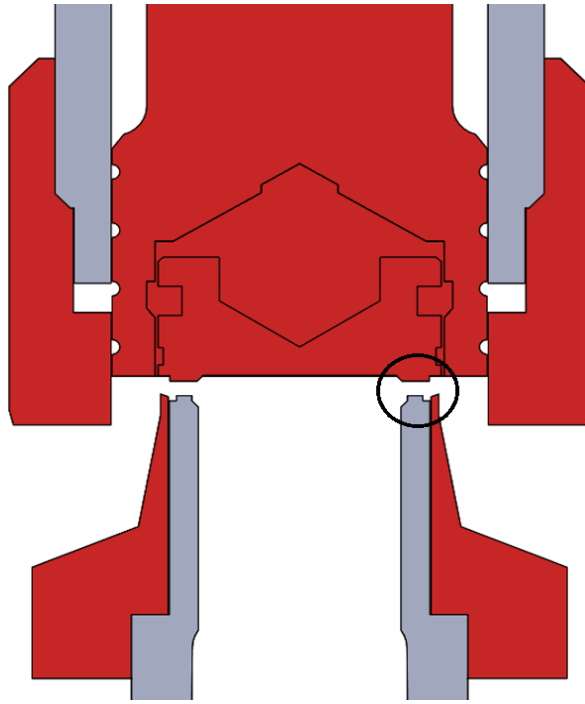


Figure 5.2 – Area of focus for low lift optimisation.

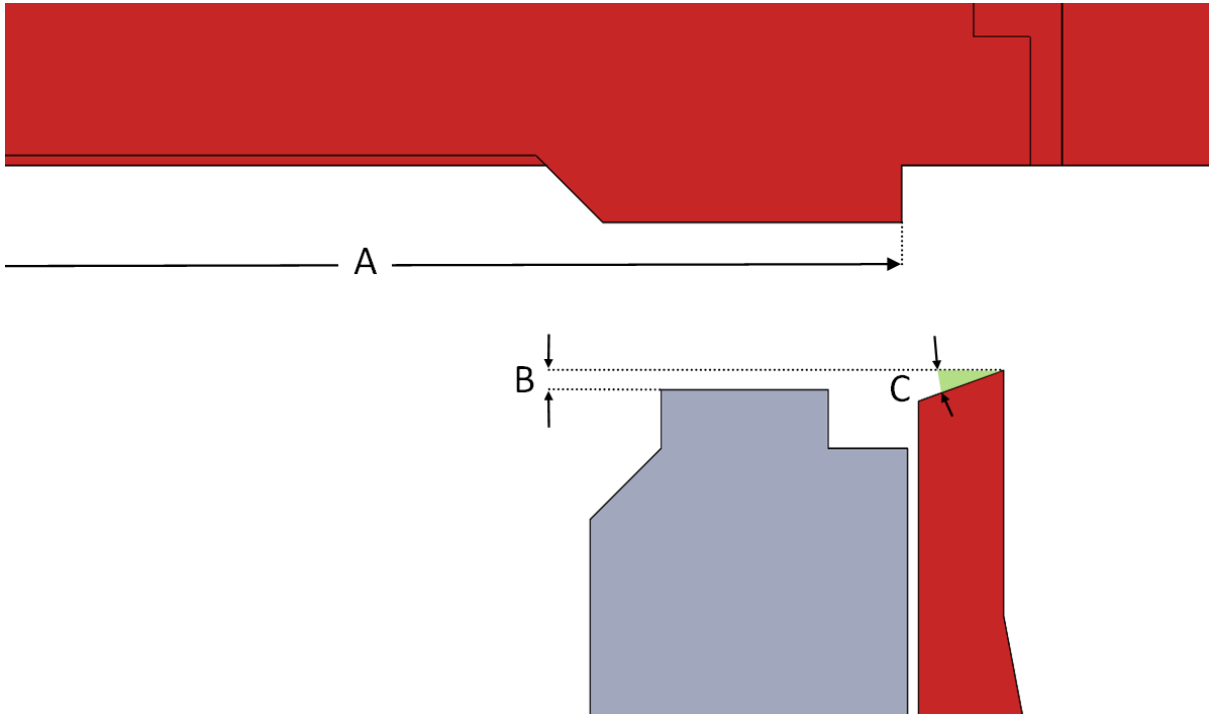


Figure 5.3 – 3 parameters required for low lift optimisation.

As the disc moves further off of the seat, the outer disc holder region becomes the surface experiencing most change in the pressure distribution. The lower adjustment ring begins to lose influence on the shape of the force-lift curve above 1mm, the main surface force change is experienced in this outer disc holder region. Thus, the section of force-lift curve above 1mm is essentially controlled by the pressure distribution in this outer region. Adjusting the pressure distribution should meet the force lift-curve requirements. Altering the diameter of this outer shroud (figure 5.4, parameter D) would give sufficient control during the optimisation process.

The impact of a lower adjustment ring is now understood, not only is this component useful for modifying the behaviour of a valve, it is also a requirement in the ASME certification process. From the work already presented, the physics that cause the lower adjustment ring to function is now clear, it has also been shown that it has most effect on the lower regions of the force-lift curve. To gain a higher degree of control over the valve performance it is necessary to influence the upper section of the force-lift curve. This is generally achieved by a second upper adjustment ring that acts similar to the shroud in the Broady type 3500 disc holder. This second ring can be used to finely tune the level of pressure distribution on the disc holder face as the valve moves to a higher open position. Inclusion of an upper adjustment ring provides control of the force-lift curve over the full height that it operates. Therefor utilising two adjustment rings, a manufacturer can fine tune both the opening and closing process of an SRV. Figure 5.4 presents the two geometrical parameters to be used for the high lift optimisation process. The vertical dimension (parameter E) will be used as a design parameter for optimisation but in the completed valve this dimension will be adjustable. This component is threaded to an upper guide flange to hold it in position and

both of these components form a cylinder in which the disc holder assembly can move as the valve opens. Figure 5.1 shows this arrangement, the guide flange on which the upper ring is screwed on to can be seen.

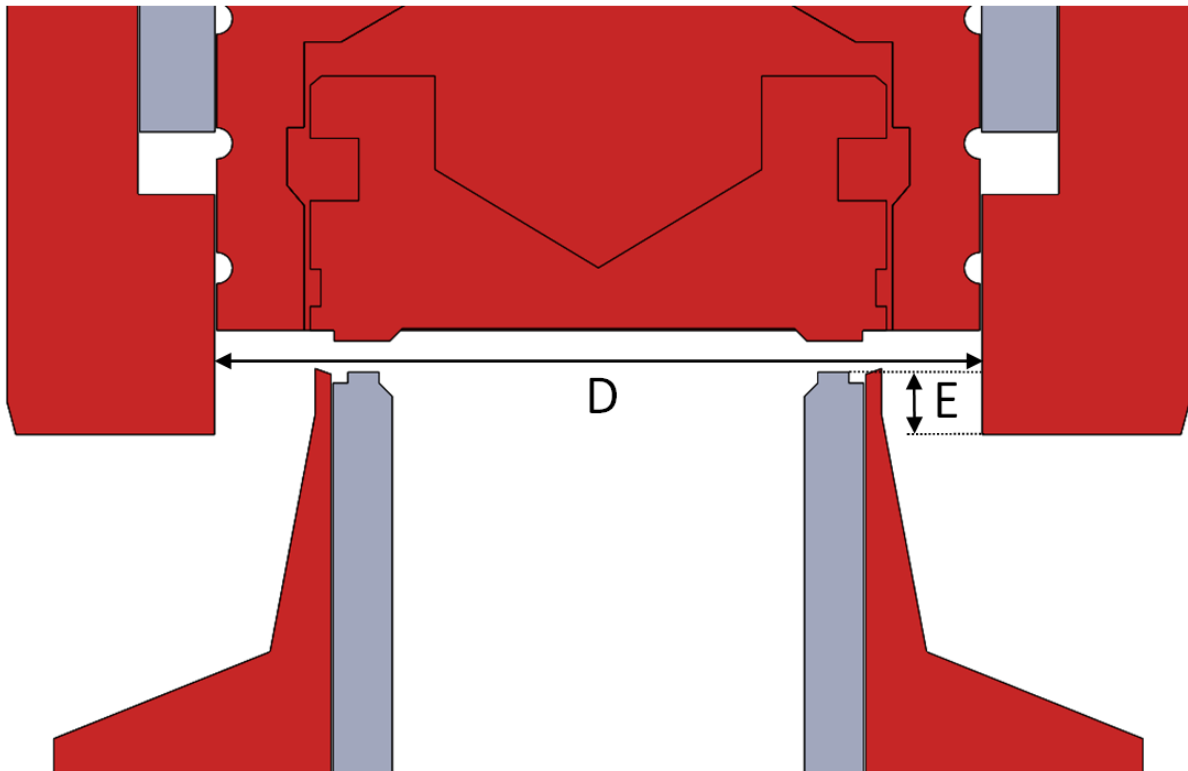


Figure 5.4 – 2 parameters required for high lift optimisation.

The upper adjustment ring works by acting as a shroud to contain the escaping pressurised fluid leaving the inlet nozzle. Altering the height of the shroud will change the path that the escaping jet takes as it leaves the nozzle, this will alter the magnitude of pressure distribution on the disc face. Without a shroud the escaping jet would exit the nozzle and spread across the disc face at a high velocity and thus a low pressure. Having a shroud in place redirects the jet downwards outside of the nozzle and creates a stagnation region in

the corner between the disc face and shroud itself. This stagnation region is what is responsible for the increase in pressure. Adjusting the level of the shroud can thus give a level of control over the force characteristics at higher lifts. By lowering the height of the upper adjustment ring the stagnation area increases, thus, the level of disc force experienced increases. In summary, the opening process can be controlled by adjusting the geometry around the nozzle exit region, in particular the lower adjustment ring and the disc face. The upper regions of the force-lift curve can be controlled by the disc holder diameter and the level of the upper adjustment ring.

One of the key components that control the operation of a relief valve is the spring, correctly chosen, it should ensure the device operates as intended. Due to the importance of this component, a brief discussion on spring design and selection will now be given.

It has been well established that the disc movement and valve behaviour is controlled by the net forces acting on the disc holder assembly. The net force is a consequence of the aerodynamic fluid force and the spring load, so far little attention has been given to the spring load. A correctly chosen spring rate is critical in achieving high performance from a relief valve. As valves are required to operate at a range of pressures, different spring rates will be needed to maintain performance over all conditions.

A spring is characterised by the spring rate, this is calculated by the magnitude of force to compress a spring by a given length. For a relief valve this will be calculated from the difference between the full lift disc force and the initial preload, and the height of the disc at full lift. Figure 5.5 below displays a typical spring drawing used at Broady Flow Control. The values C1 and C2 are the preload and full lift disc force respectively. F2 is the height of the disc at full lift – in the case of a 1x2" E orifice this value is 4mm. These figures can then be

used to obtain the spring rate which then allows for the precompression (F1) necessary to produce the preload value.

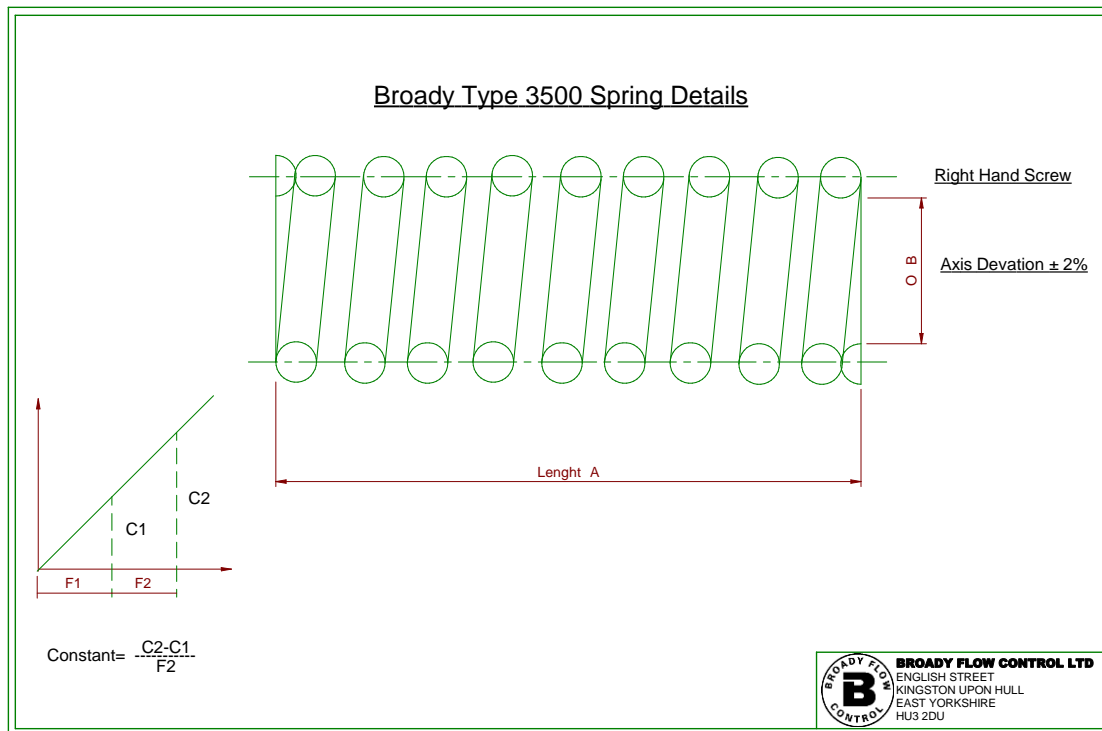


Figure 5.5 – Spring design drawing – property of Broady Flow Control Ltd.

The length of the spring must be sufficient to allow for the required full compression ($F_1 + F_2$) for a given application. In the ASME BPVC PG-73-2-3 states that

“The spring shall be designed so that the full lift spring compression shall be no greater than 80% of the nominal solid deflection”.

This will need to be taken into account when designing the spring for a given application and will ultimately provide the overall length of the spring. The outside diameter of a spring will be chosen such that it should fit inside the valve bonnet. However, at elevated pressures the material to meet the required spring rate and compression may make it impossible to

produce a spring to meet the initial outside diameter. This can lead to the condition where a spring will be unable to fit inside a standard bonnet. In such a case a valve manufacturer is required to increase the dimensions of the bonnet to accommodate the larger spring. Most likely the stud specifications that attach the bonnet to the body - and maintains the spring compression - will also have to be adjusted. Therefore relief valve manufacturers have a range of bodies and bonnets to accommodate the components needed for operating at elevated pressures.

To summarise, this chapter presented the baseline valve to be used during the geometrical optimisation process. The valve was based on a Broady 1x2" 3500 E orifice, to gain more control over the flow force characteristics an additional upper adjustment ring was added to the valve trim. This additional component will be able to provide adjustment to the force-lift curve at high lift, the lower ring will be able to provide adjustment at low lift. The design parameters that will be used in the optimisation process were introduced. These parameters were selected as they each impact the force-lift curve at a certain point. By adjusting these dimensions it will be possible to improve the force-lift characteristics of the baseline valve to one that will meet the performance criteria specified in ASME BPCV Section I.

6. Optimisation

6.1 Optimisation Methods

Mathematical optimisation is a branch of techniques used to obtain the best input to a function from a set of suitable candidates. Generally, the process would be to minimise or maximise a function by systematic adjustment of the inputs directed by observation of the function behaviour. A typical minimisation formulation is presented below

$$\text{minimise } F = f(x_1, x_2, \dots, x_n) \quad (6.1)$$

Where F is a function typically termed the objective function and depends on the variables x_1, x_2, \dots, x_n . The optimisation problem will then aim to minimise F by adjusting the input variables. Each optimisation algorithm uses different methods to adjust the function input to progress towards an improved output. This study uses a two-stage optimisation process; firstly, the low-order valve model presented in chapter 3 was optimised to improve the overpressure and blowdown performance of the model. Secondly the geometry of a reference valve was optimised to produce the force-lift characteristics obtained during the first optimisation stage.

6.1.1 Low-Order Valve Model Optimisation

The initial optimisation step required a constrained minimisation technique that could alter the force-lift curve to achieve superior SRV performance. Essentially, this is a process that will adjust x-y data (force-lift curve coordinates) to minimise the overpressure and blowdown of the SRV model whilst still achieving a fully open position. The Interior Point

Algorithm was chosen for this step, this is a convex optimisation process that utilises the interior of the solution space and not just the hypersurface. The problem was constructed into the typical optimisation form shown in equation 6.1, where the x-y coordinates that specify the force-lift curve are inputs. Thus the objective function is established from the overpressure value OP and the blowdown value BD. The OP and BD are evaluated using the Low-order Valve Model (LVM) and are dependent on the force lift curve $f(x,y)$ which is constructed from a finite number of x-y coordinates, $x_1, y_1, x_2, y_2, \dots, x_n, y_n$.

To obtain a scalar value necessary for the objective function, the overpressure and blowdown were summed using an RMS addition, this was essential to safeguard against the situation where a negative OP cancels out the BD or vice versa. Therefore the optimisation algorithm will adjust the x-y coordinates of the force-lift curve to obtain an improved overpressure and blowdown value. Presented in the form of equation 6.1 the first stage of the optimisation takes the following form,

$$F = \sqrt{OP^2 + BD^2} = LVM(x_1, y_1, \dots, x_n, y_n)$$

$$\text{minimise } [F] \tag{6.2}$$

Subject to the inequality constraints of performance (ASME Section I requirements)

$$OP < 2\%$$

$$BD < 4\%$$

And further subject to the following constraints on the search domain, established by the coordinates of $f(x)$.

$$\begin{array}{ll}
 x_1 = 0.0 \text{ mm} & f(x_1) = F_{preload} \\
 a_2 < x_2 < b_2 & c_2 < f(x_2) < d_2 \\
 a_3 < x_3 < b_3 & c_3 < f(x_3) < d_3 \\
 a_4 < x_4 < b_4 & c_4 < f(x_4) < d_4 \\
 a_5 < x_5 < b_5 & c_5 < f(x_5) < d_5 \\
 x_6 = 4.0 \text{ mm} & f(x_6) = F_{spring}(x_6)
 \end{array}$$

Where a_i , b_i , c_i and d_i $i=2..5$ are constraints to limit the computational search region to a practical range, and usually limited to $\pm 10\%$ of the spring force, $F_{spring}(x_i)$. To further elaborate on the above formulation, the force-lift curve represents the force of the expanding gas within the SRV, the shape of this curve is directly responsible for the performance of the valve. Thus, altering the shape of the curve will affect the behaviour of the SRV, using the overpressure and blowdown value as an objective, the curve shape can be adjusted to optimise the performance.

During the validation process in chapter 3, the force-lift curve was represented by 64 experimental measurement points throughout the full operation cycle of the valve. This number of points was necessary to produce an accurate representation of the valve under examination. During that exercise, the force-lift curve was shown to have non-smooth behaviour, i.e. large changes in the force characteristics could be seen and these would require a high resolution of sample points to provide an accurate representation via discrete values. Thus, if the experimental valve behaviour were to be reproduced by the low-order

model this number of sample points were again required to represent the force-lift curve. It is known that these discontinuities can cause undesirable behaviour within an SRV, therefore the design phase should strive to remove them and produce a smooth continuous force-lift curve.

The goal of the force-lift curve optimisation process is to produce a curve that will simulate an SRV operating to within specified overpressure and blowdown requirements – ASME Section I for this case. The curve will then be used as a target for the second stage of the optimisation process which will adjust the internal trim geometry of the reference valve (discussed in chapter 5) using CFD modelling. As the shape of the curve should ideally be smooth and free of discontinuities the curve could be produced by an interpolation between only a few points. The coordinates of these points could then be adjusted, altering the shape of the curve and ultimately the performance of the valve. Through the use of optimisation methods, the optimal coordinates to meet the required performance could be obtained.

To understand the requirements of producing a force-lift curve for the LVM the number of points specifying it were initially set at a value of 10, this was then reduced to ascertain the minimum number of points that could be used to produce a force-lift curve whilst still maintaining the shape required to operate the LVM. The number of points was reduced to 6 and this was found to still produce a feasible shape of curve. These points could now be adjusted by an optimisation algorithm to direct the LVM towards the target performance. To further reduce the number of optimisation parameters, the first and last points were fixed. These values were obtained as follows: The initial force value (the preload) was calculated from the nozzle and disc geometry, requiring only the total area of the

components exposed to pressure in the closed position – easily obtained from any CAD package. The final force-lift curve value could be chosen to be any value, however, an initial CFD exploration of the chosen base geometry produced a small range of values that could be used. These were all within a small percentage of each other, thus the average value was chosen. Therefore the final force-lift curve optimisation could be realised using only 4 variable coordinates (figure 6.1) and 2 fixed points at the extremities of the curve.

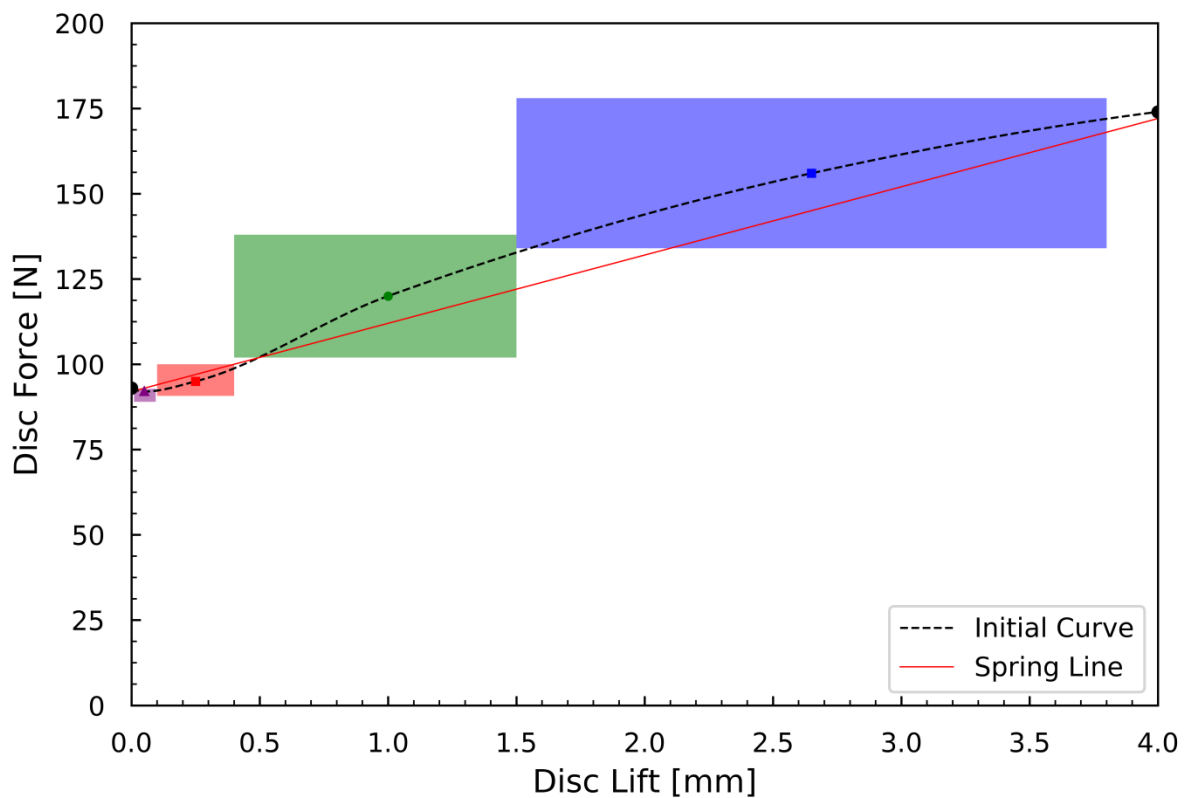


Figure 6.1 – Force-lift curve parameters plotted with upper and lower bounds.

To provide some stability within the optimisation process these coordinates were provided with bounds so the optimisation did not produce any unrealistic curves. It was found that without bounds the algorithm produced curves that met the criteria but had large force variations which would be completely unsuitable for a SRV.

The overpressure and blowdown values obtained from the LVM simulation were used as an objective function output during the optimisation process. These were also given constraints prior to starting the calculation. The blowdown has a minimum value required by ASME of 2%, the overpressure should also have a minimum as there should be a level of pressure build up to ensure the valve achieves a pop-action required by this type of device. Therefore, the overpressure and blowdown were constrained to a minimum value of 1.5% and 2% respectively. The maximum values were also in line with ASME requirements at 3% for overpressure and 4% for blowdown. Although the maximum allowable blowdown figure varies with pressure, the smallest figure is 4% of set pressure; the full requirements were given in table 2.1. These optimisation constraints are summarised in the table 6.1 below.

	Maximum	Minimum
Overpressure	3%	1.5%
Blowdown	4%	2%

Table 6.1 – ASME Section I safety relief valve performance requirements.

Table 6.2 displays the parameters used in the LVM during optimisation.

Parameter	Value
Set pressure (barg)	5.00
Spring rate (N/mm)	20.012
Mass of moving parts (kg)	0.651
Temperature (K)	288
Mass flow inlet (kg/s)	0.03
Vessel volume (m ³)	1.5

Table 6.2 – LVM optimisation configuration.

6.1.2 Geometrical Optimisation

Computational fluid dynamics simulations were used during the geometrical optimisation as it is much cheaper than physical testing. Although CFD calculations may be a quick and easy check to a design change they are still computationally expensive. To assess one full force-lift curve for one design change would require over 30 steady state calculations - half of which are 3D - resulting in a solution time of over 2 weeks on a mid-range desktop PC. To undertake a direct optimisation using a gradient based method this approach becomes extremely prohibitive. Fortunately, this is a common issue in industry and techniques have been developed to alleviate some of the solution time by introducing some approximations in the model configuration.

Surrogate modelling can be used to approximate the objective function throughout the solution space circumventing the need to evaluate the function at every single point. The search space can be sparsely populated with data points obtained from an initial exploration phase, a surrogate model would then be used to interpolate between the points and avoid the need to check the intermediate values. This does introduce some approximation to the solution space but when areas of interest have been located, further exploration can take place to increase the density of data in this region.

The initial exploration phase is achieved by constructing a database of CFD force-lift curves over a range of design parameter values. Each design parameter is then adjusted incrementally and the force-lift curve was then recorded, resulting in a database of force-lift curves that could be used for surrogate model construction.

The initial solution space exploration utilises a combination of 2D and 3D CFD calculations for low-lift and high-lift respectively, with the justification discussed in chapter 4. The data produced during this exploration phase is included in the appendix 1 & 2. The design parameter rationalisation was presented in the previous chapter. The infill points evaluated between the boundaries are selected by many different strategies. Some popular techniques include, factorial design (star distribution), random distribution, uniform grid sampling or Latin hypercube sampling (LHS). Each of these methods prescribes a way of dividing up the solution space for each parameter between the boundary values. This research utilised a uniform distribution as the number of design parameters was relatively small.

The data obtained during the solution space exploration phase consists of force-lift curves at different values of each design parameter. By perturbing a design parameter the produced force-lift curve indicates how this parameter will influence the force-lift curve. The aim of this second stage of the optimisation process is to obtain a value of each design parameter that produces a force-lift curve identical to the target force-lift curve obtained in the first optimisation stage (6.1.1). Thus the suitability of a produced curve against the target curve must be evaluated. This could be done during the optimisation process, however it was possible to do this step prior to the optimisation. When exploring the solution space, several force-lift curves are produced, one for each variation of a design parameter. Instead of storing the force-lift curve in a database for the surrogate model it is possible to store the difference between that curve and the target curve. In doing so and constructing the database from the force-differences removes the need to evaluate a force-lift curve during the optimisation process.

To evaluate the fitness of a given force-lift curve the difference between that curve and the target curve was measured. i.e. close matching curve would have minimal force-difference between that and the target curve. This is depicted in figure 6.2 (left) below, a force-lift curve is evaluated against the target force lift curve at several points along the length of the curve - these force-differences are plotted in figure 6.2 (right). An RMS addition of these sample points then provides a scalar value for each objective function evaluation - leading to a perfect fitting curve having a force-difference value of zero.

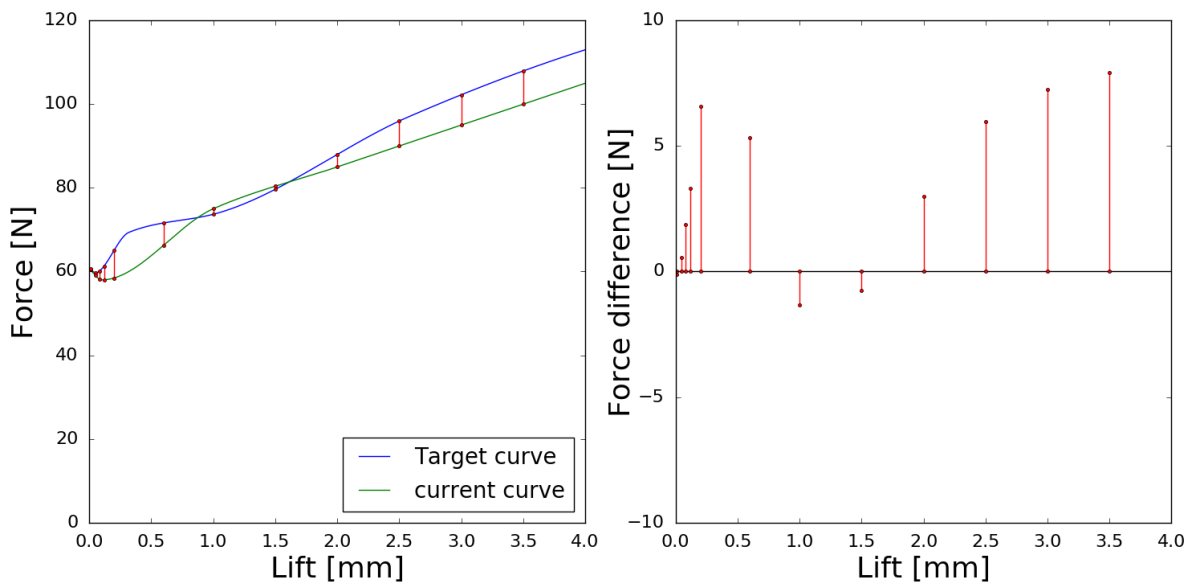


Figure 6.2 – Force lift curve comparison (left), force difference data (right).

For this second optimisation problem, the surrogate model takes place of the objective function, the variables are the design parameters, and the output of the objective function is the value indicating the magnitude of force difference between the current evaluation and the target curve. Inputting a value for each design parameter into the surrogate model will output a value indicating the fitness of the input values. Presented in the form of equation 6.1, the second stage of the optimisation process takes the following form

$$F = \sqrt{d_1^2 + \dots + d_n^2} = \text{surrogate model}(A, B, C, D, E)$$

$$\text{minimise } [F] \tag{6.3}$$

Subject to the following constraints

$$a_1 < A < b_1$$

$$a_2 < B < b_2$$

$$a_3 < C < b_3$$

$$a_4 < D < b_4$$

$$a_5 < E < b_5$$

Where A-E are the design parameters presented in chapter 5 and a_i and b_i $i=1..5$ are constraints to limit the search space. $d_1 \dots d_n$ represent the force differences sampled along the length of the force lift curve. The optimisation problem now has to utilise an algorithm to adjust the variables to minimise the force difference vector.

The surrogate model is constructed to allow for a computationally efficient evaluation of the objective function at points between those previously calculated during the exploration phase. As such, the surrogate model is produced by an interpolation algorithm estimating the value between data points. The Surrogate Modelling Lab (SUMO) from Ghent University (Gorissen, et al., 2010) was utilised, this operates within the Matlab package. The surrogate model produced from this package is in the form of a Matlab object, when provided with a set of input values for each parameter the surrogate model object will output the predicted objective function value for those given values. Thus giving an efficient evaluation of the objective function throughout the solution space.

Different algorithms were available for producing the model such as, polynomial regression, radial basis function, kriging, artificial neural networks and rational approximation. Kriging is a popular approach – and the one utilised in this research - which can be described as a Gaussian process interpolation that is used to approximate deterministic noise-free data (Couckuyt, et al., 2013). It is a two-step technique consisting of a regression function $f(x)$ and a Gaussian process Z , to account for variation.

$$Y(x) = f(x) + Z(x), \quad (6.4)$$

The Gaussian process has a normal distribution and a variance given as σ^2 . Different forms of Kriging exist and have different treatments of the regression function $f(x)$, ordinary kriging treats this as a multivariable polynomial, given as,

$$f(x) = \sum_{i=1}^p \alpha_i b_i(x), \quad (6.5)$$

Where $b_i(x)$ are the (polynomial) basis functions, and α denotes the coefficients, p is the total number of basis functions. The regression function should produce the general trend of the data and the Gaussian process treats the variance in the data.

Constructing the surrogate model is the primary stage of the geometry optimisation process, the second stage requires the selection of a suitable optimisation algorithm to utilise the surrogate model. The way in which the optimisation problem has been configured means that a constrained minimisation method as used in the initial optimisation problem can be utilised. The interior point algorithm was used again, this will alter the input parameters A-E to minimise the output of the surrogate model. Constraints were required on the input parameters to set the limits of the search space, this was not only necessary to limit the computational costs but the parameters would be limited physically by the internal

valve geometry. For select parameters it was not obvious what the required upper and lower limits were. Some parameters are limited physically such as the lower ring height upper limit, however others had to be gauged as the solution space was being explored. This led to the solution space being explored incrementally, CFD data was post-processed as it became available and this provided the effects of parameter variation on the force-lift curve.

The disc holder diameter lower limit was such that shroud area could not reduce lower than the nozzle throat area as this would cause a downstream restriction leading to a reduced valve capacity. The upper limit was found by increasing the dimension and plotting the data as it became available - an upper limit of 27mm was found to be sufficient for the variation. Similarly, the upper ring height produced enough variation in 0-4mm. One of the benefits found in using a surrogate model technique was that the bounds could be adjusted as the solution space was being explored. The 2D and 3D CFD calculations that were used to populate the solution space were configured as was presented in tables 3.1, 3.2, 3.3 and 3.4, the only difference being that the working pressure 5 barg instead of 3.3 barg. The final limits used during the exploration phase are included in table 6.3 below.

Parameter	Limits	2D/3D
Disc notch diameter (A)	16.60-17.00 (mm)	2D
Lower ring height (B)	0-0.30 (mm)	2D
Lower ring chamfer (C)	0-20 (deg)	2D
Disc holder diameter (D)	24.0-27.0 (mm)	3D
Upper ring height (E)	0-4.0 (mm)	3D

Table 6.3 Optimisation parameters.

The CFD calculations were undertaken through a combination of 2D and 3D configurations. Throughout the validation exercise (chapter 3) a 2D assumption held true up to 1mm lift, thereafter 3-dimensional effects began to become noticeable thus it was necessary to move to a 3D CFD calculation. Previous work utilised steady state calculations at 0.2mm increments, this provided a high-resolution representation of the force-lift curve. For the design space exploration stage of the optimisation exercise this level of resolution would not be necessary, it was decided to use 0.5mm increments to reduce some of the computational expense.

If sampling 3 points within the range of a specific parameter, i.e. the maximum, minimum and mid-point value, the total number of required force-lift curves required is calculated as 3^n , with 3 representing the evaluation of the low, mid and high parameter value and n representing the number of parameters.

Total number of parameters (n)	Required force-lift curve
2	9
3	27
5	243

Table 6.4 – Calculation requirements for each number of parameters.

Table 6.4 clearly show the number of required force-lift curves for an optimisation quickly increases with an increase in parameters being explored. Thus as the low-lift region and high-lift are relatively independent it was decided to optimise each part of the force-lift curve separately. The saving of using two separate optimisations (i.e. 2D and 3D) on the

relief valve geometry can be appreciated. It is important to note that optimising 5 parameters at once would require a full force-lift curve evaluation 243 times, as each curve contains seven 3D calculations and nineteen 2D calculations - the computational savings become clear. Therefore equation 6.3 that represents the second optimisation problem can now be split into two separate optimisation problems, where low-lift 2D problem can be written as follows

$$\text{minimise } [F] = \text{surrogate model } (A, B, C) \quad 0 < \text{lift} < 1\text{mm} \quad (6.7)$$

And the high-lift 3D problem is represented by

$$\text{minimise } [F] = \text{surrogate model } (D, E) \quad 1\text{mm} < \text{lift} < 4\text{mm} \quad (6.8)$$

Thus a surrogate model was constructed for 6.7 and 6.8 as explained previously, the only difference is that the low-lift surrogate model data spans from 0-1.00 mm and the full lift surrogate model data spans from 1.00-4.00 mm and the variables for each model are A-C and D-E respectively.

6.2 Optimisation Results

6.2.1 Force-lift Curve Optimisation

The results of both optimisation processes – LVM and geometry – will now be presented. Figure 6.3 below displays the initial input force-lift curve prior to optimisation and the curve after being optimised using the interior point algorithm. The initial curve was created using a random number generator function. The difference between both curves is clear; the optimised curve follows the spring line much more closely.

Figure 6.4 displays the difference in dynamic performance of both the initial and optimised force-lift curves. It can be seen from figure 6.4 (b) that the optimised curve clearly requiring much less overpressure to fully open the valve. Table 6.5 presents the opening and closing performance of the initial and optimised force-lift curves. At first it may seem that the initial blowdown was promising, however this is due to the shape of the curve at high lift which requires a large overpressure to attain full lift. Once optimised, both the opening and closing performance is much more acceptable, as can be seen in figure 6.4 (left).

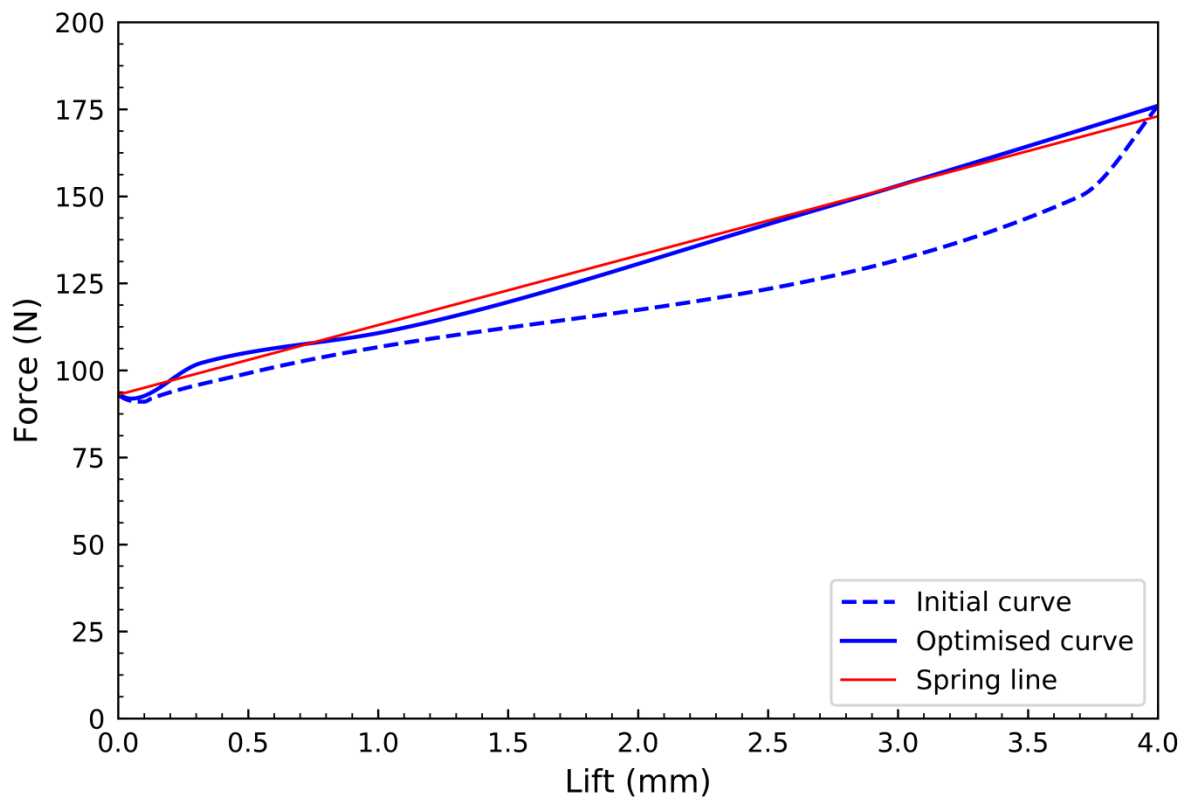


Figure 6.3 – Initial and optimised force-lift curve for use in LVM.

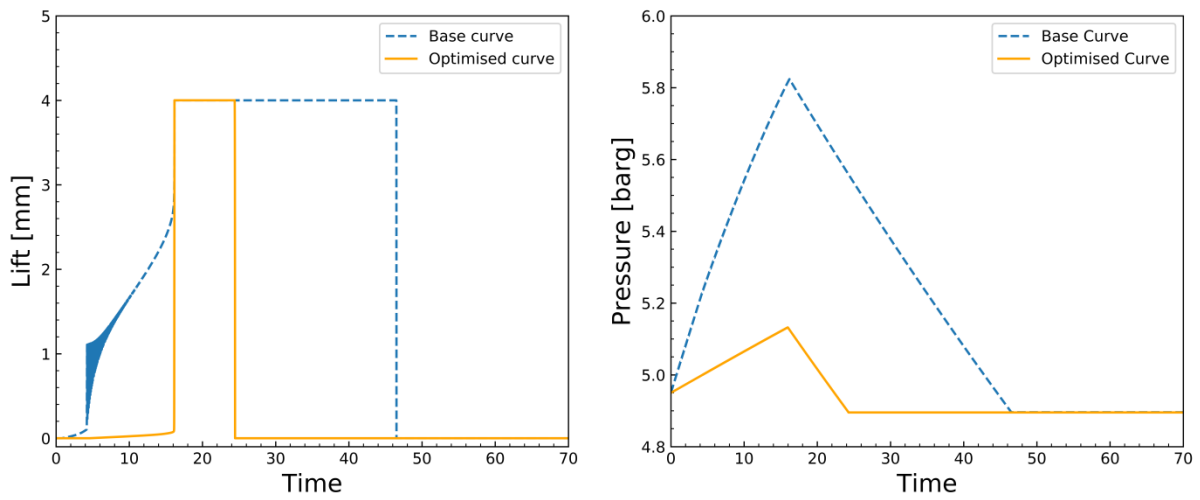


Figure 6.4 – Dynamic performance of initial and optimised force-lift curve – displacement (left) and pressure (right).

	Blowdown (barg)	Blowdown (%)	Set (barg)	Overpressure (barg)	Overpressure (%)
Initial	4.89	2.20	5.00	5.82	16.48
Optimised	4.90	2.00	5.00	5.13	2.64

Table 6.5 – LVM performance of initial and optimised curve.

6.2.2 Geometrical Optimisation

Table 6.6 contains the geometrical parameters results obtained through the geometry optimisation process, included are the upper and lower bounds for each parameter.

Parameter	Bounds	Optimised Size
A	16.6-17.0 (mm)	16.9 (mm)
B	0.0-0.3 (mm)	0.15 (mm)
C	0-20 (deg)	4 (deg)
D	24.0-27.0 (mm)	25.4 (mm)
E	0.0-4.0 (mm)	1.00 (mm)

Table 6.6 – Parameters used in geometrical optimisation.

Figure 6.5 displays the force-lift curve produced through CFD calculations on the optimised geometry. Included within this plot is the target curve obtained in the initial optimisation process. Worth noting is the small inflection point around 0.05mm, this is what controls the opening performance and from this plot it is clear that the CFD model closely matches the target force.

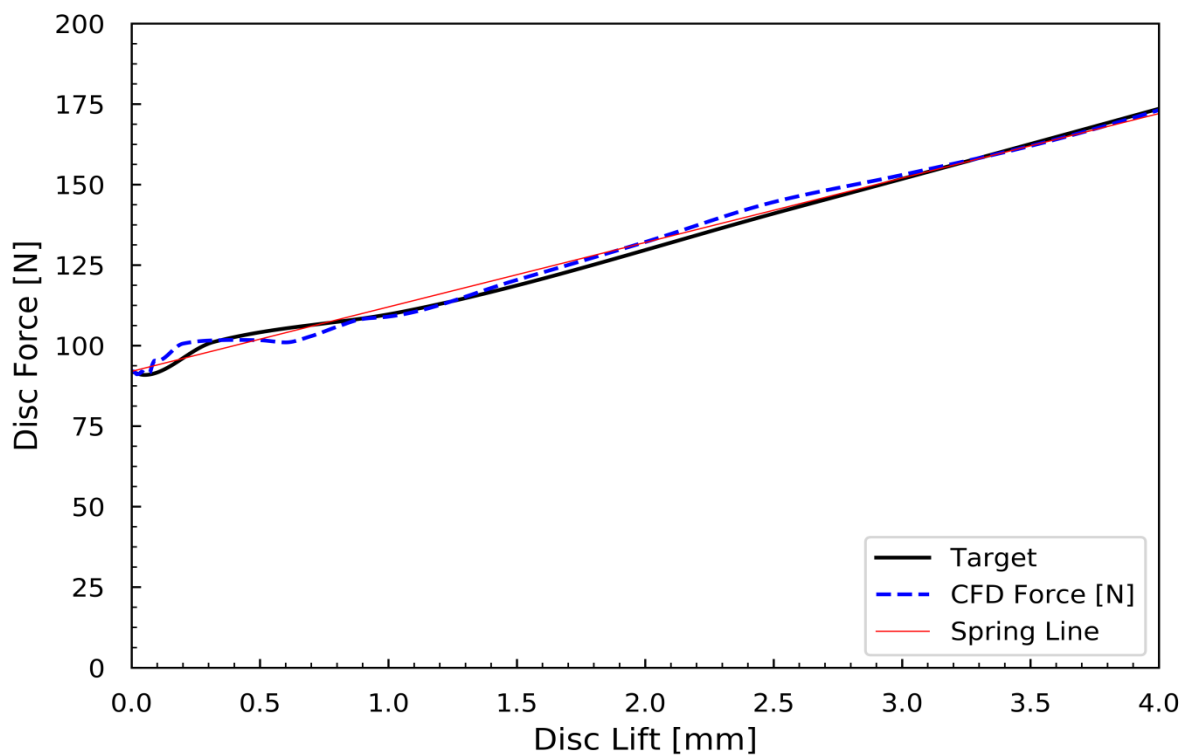


Figure 6.5 – Force-lift curve produced by optimised geometry.

In table 6.7 below the opening and closing performance of the CFD produced data is compared to the target performance. Here the CFD data can be found to produce an improved figure, due to the sensitivity of the LVM to force-lift curve shape, small changes in the curve can produce a large difference in the overpressure and blowdown.

	Blowdown (barg)	Blowdown (%)	Set (barg)	Overpressure (barg)	Overpressure (%)
Target	4.90	2.00	5.00	5.13	2.64
Optimised	4.93	1.06	5.00	5.14	1.59

Table 6.7 – Dynamic performance of CFD data compared to optimised curve performance.

Figure 6.6 displays the dynamic behaviour of the optimised geometry obtained using the CFD data in the LVM.

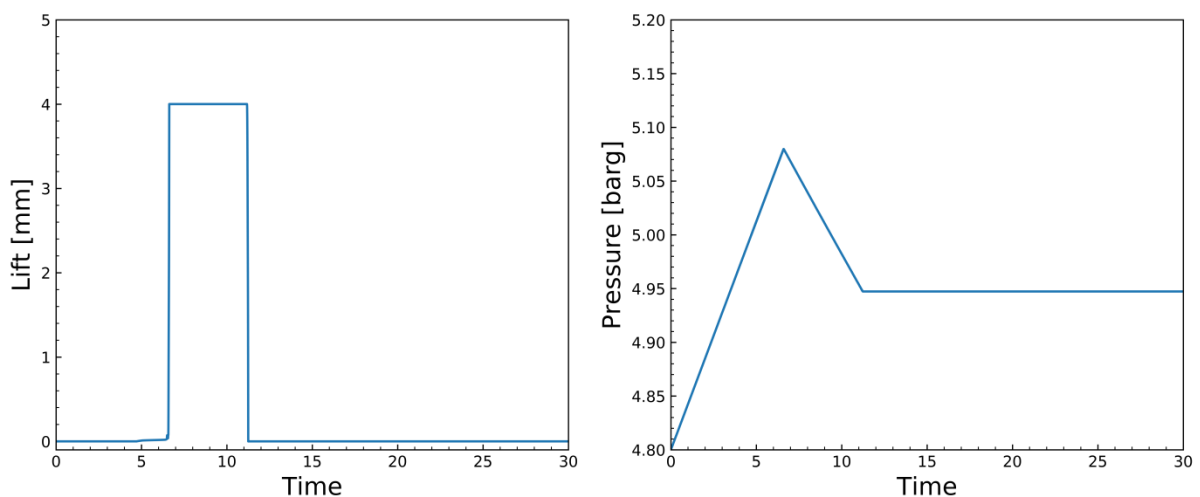


Figure 6.6 – Dynamic performance of optimised geometry CFD data.

Figure 6.7 contains the pressure distribution on the disc face in the optimised geometry, this data is in the huddling height region of 0.01-0.10mm. This height is predominantly responsible for the opening process.

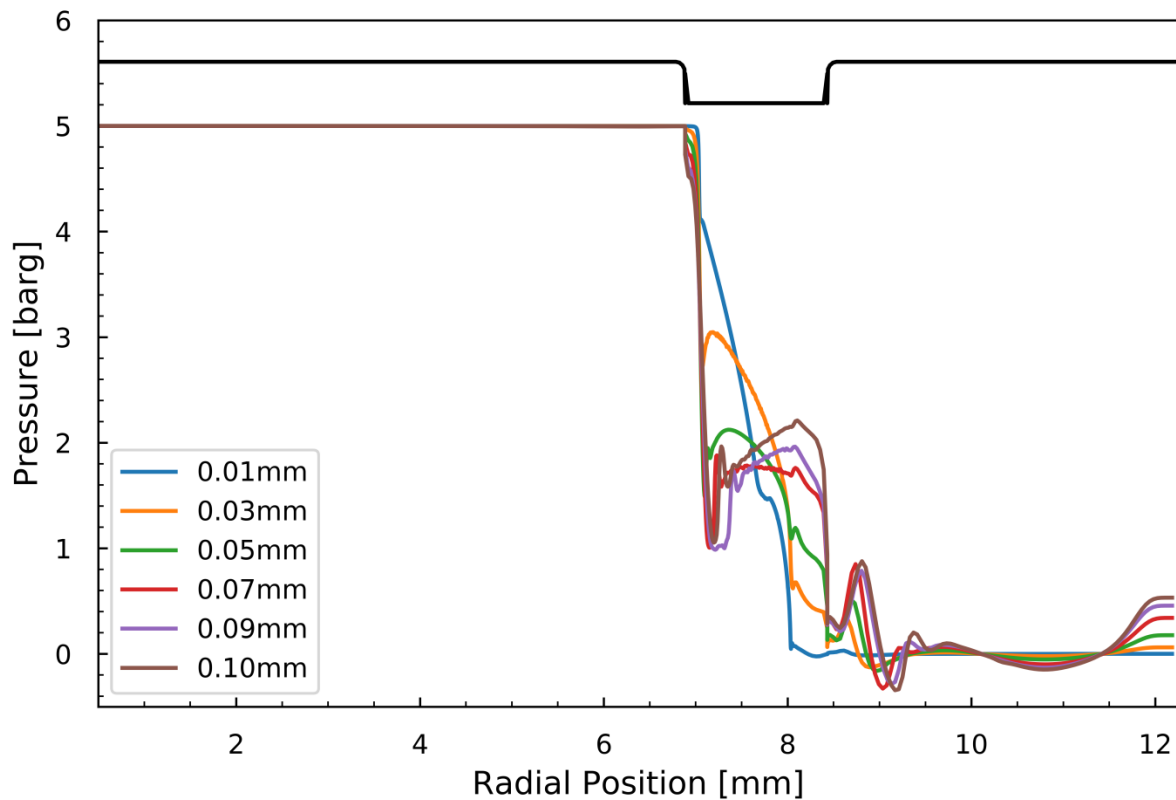


Figure 6.7 – 2D axisymmetric – optimised geometry pressure distribution 0.01 – 0.10mm lift.

Figure 6.8 below presents the contour plots from the optimised geometry CFD data, this is in the region of 0.01-0.10mm, included is both the pressure and Mach number plots. Figure 6.9 presents the pressure distribution data from 0.10-1.00mm lift, the corresponding contour plots for this data is in figure 6.10. In all plots an iso-surface at Mach number of 1 is included to give an indication of the choking behaviour as the valve opens.

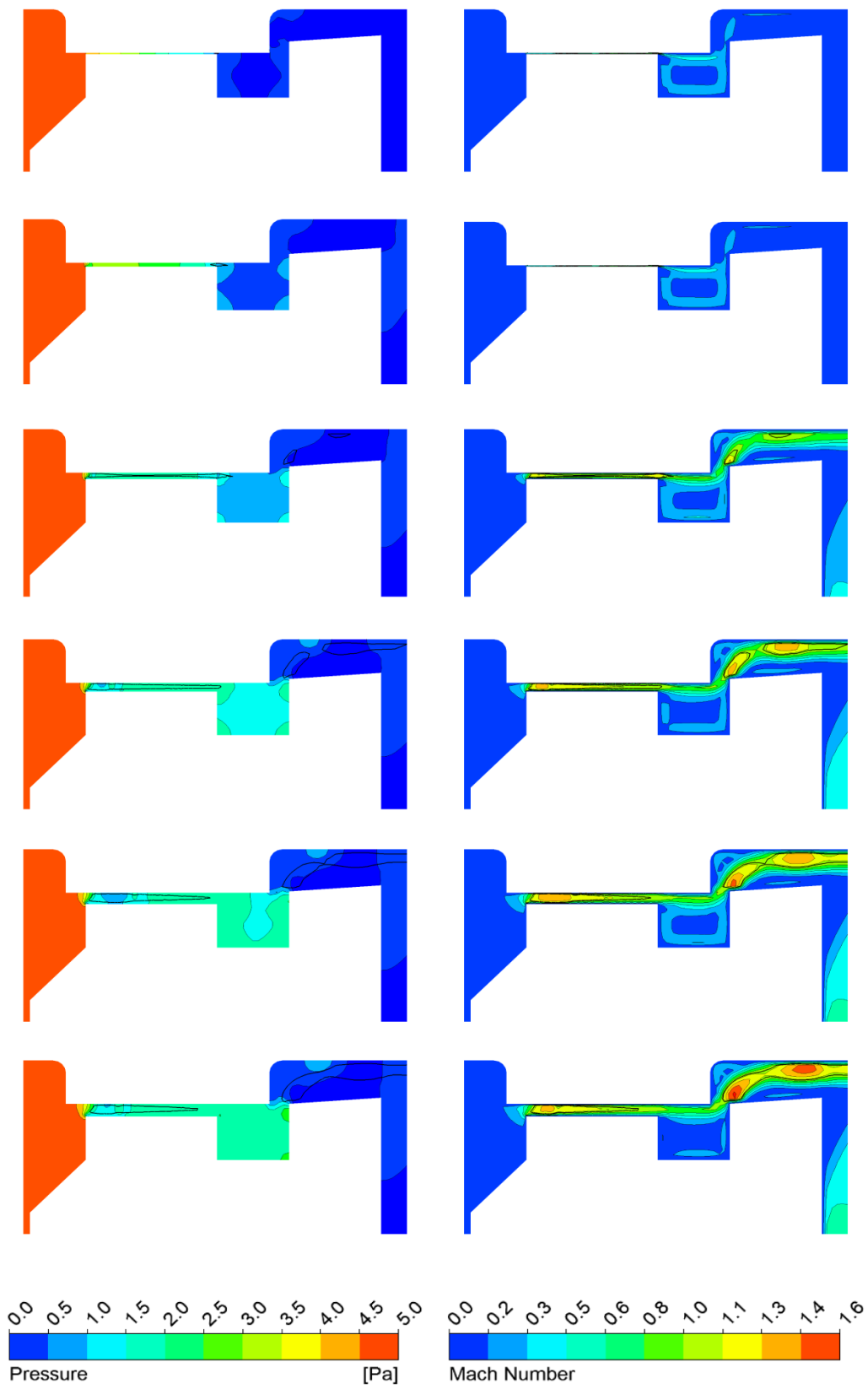


Figure 6.8 – 2D axisymmetric – optimised geometry contour plots, pressure (left) and Mach number (right) – 0.01mm, 0.03mm, 0.05mm, 0.07mm, 0.09mm & 0.10mm.

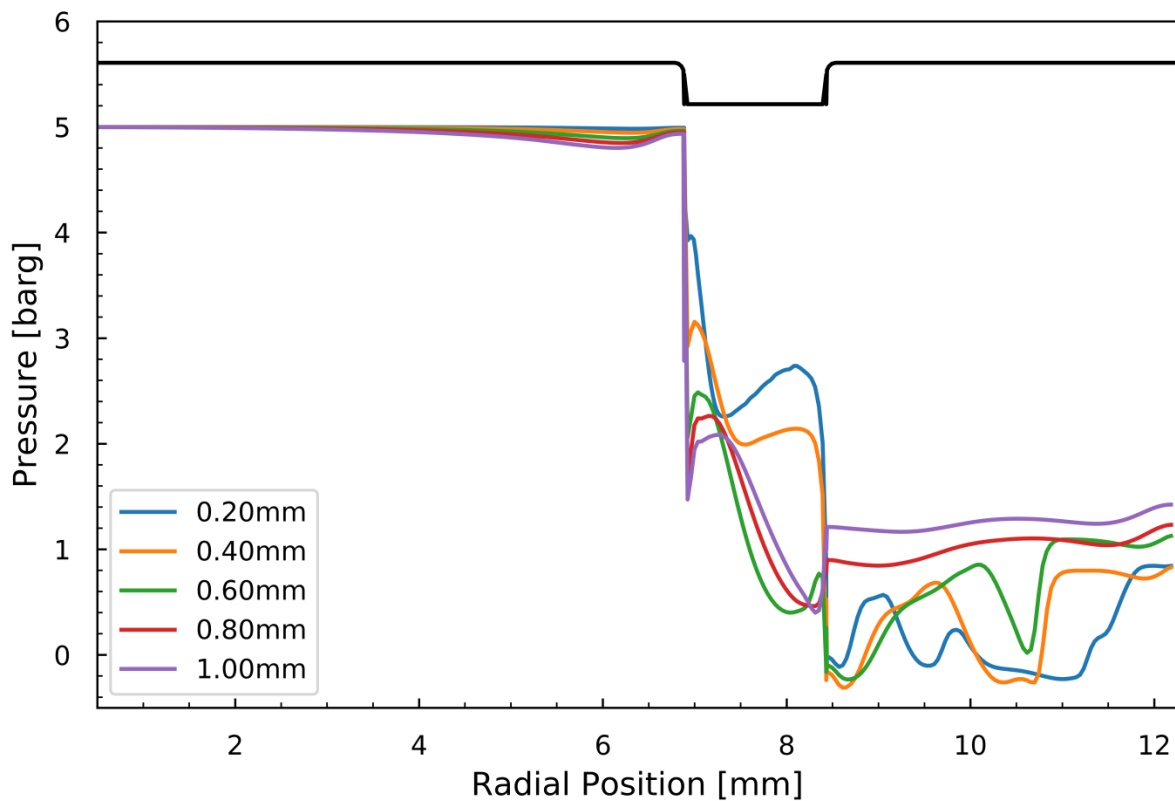


Figure 6.9 – 2D axisymmetric – optimised geometry pressure distribution 0.10 – 1.00mm lift.

As explained similar behaviour is found in this geometry to that of the Broady 3500 test valve, the build-up of pressure in the outer regions of the disc holder as the valve lifts counteracts the pressure drop in the sealing face region. The pressure contours presented in figure 6.8 clearly show the lower adjustment ring maintaining a level of pressure within the sealing face as the valve begins to open, this ensures a small level of force reduction which results in a sharp opening process. Without this ring in position the pressure drop at the sealing face would be significant, even with the pressure build-up in the outer disc holder region to counteract this it would still result in a large overpressure.

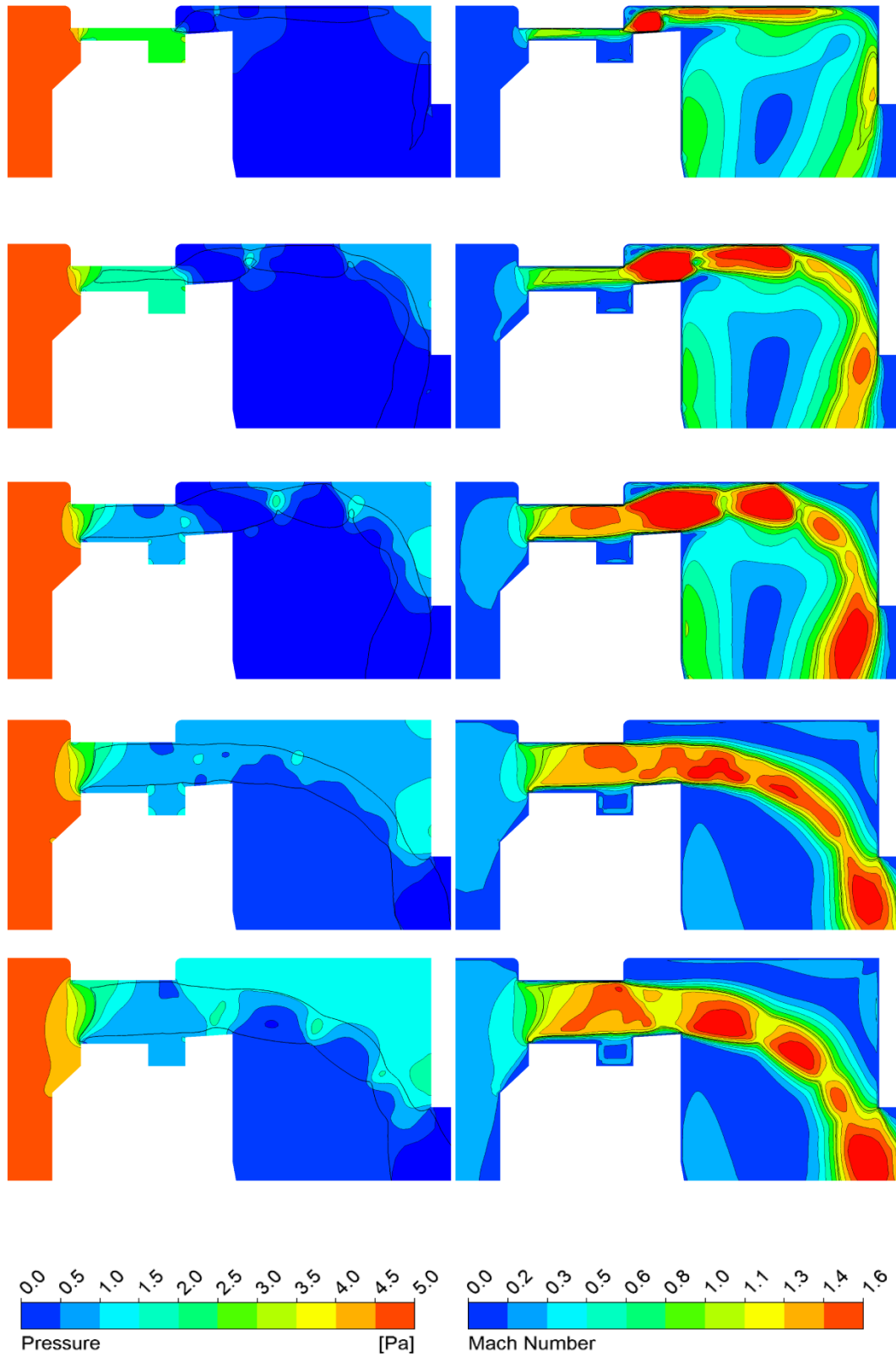


Figure 6.10 – 2D axisymmetric – optimised geometry contour plots, pressure (left) and Mach number (right) – 0.20mm, 0.40mm, 0.60mm, 0.80mm & 1.00mm.

Figure 6.11 displays the pressure distribution in the optimised geometry from 1.00-4.00mm, a gradual increase in pressure in the outer disc holder region can be witnessed as the valve opens. The corresponding contour plots are given in figure 6.12.

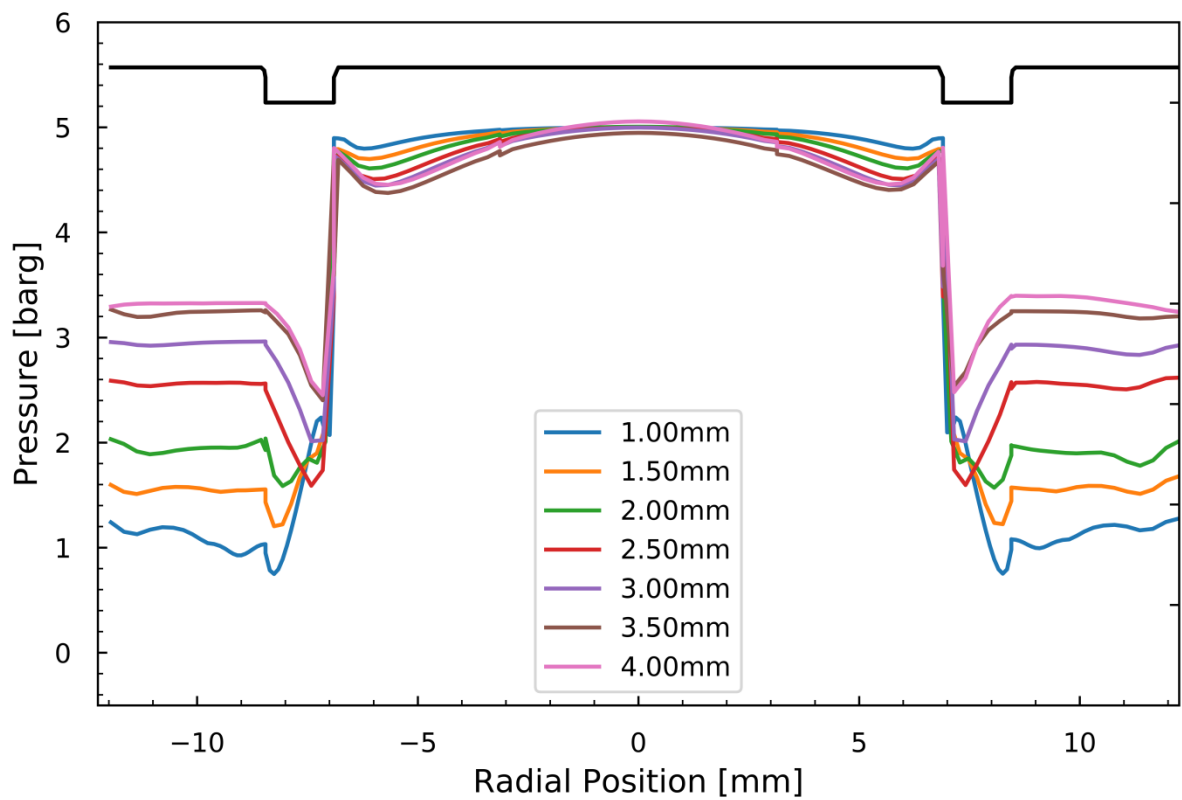


Figure 6.11 – 3D – optimised geometry pressure distribution 1.00 – 4.00mm lift.

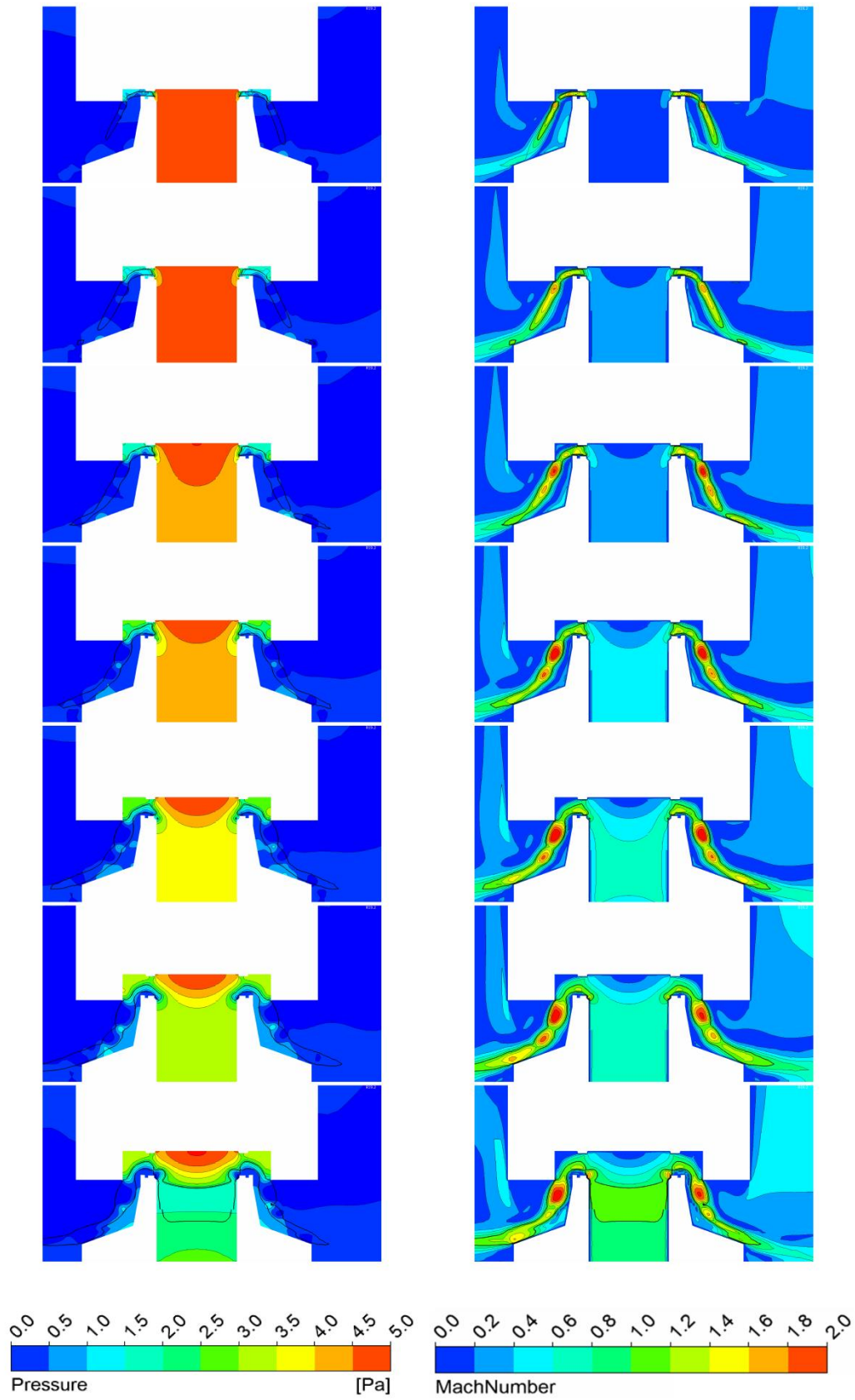


Figure 6.12 – 3D – optimised geometry contour plots, pressure (left) and Mach number (right) – 1.00mm, 1.50mm, 2.00mm, 2.50mm, 3.00mm, 3.50mm & 4.00mm.

7. Optimisation Validation

The previous chapter shows promising results for the optimisation methods and have resulted in a theoretically improved valve performance. It is worth noting that the improvements are only valid within the validity of the models used. Given that the models don't fully represent reality it is important to experimentally prove the improved performance.

Initially, the optimised geometry presented in the previous section shall be validated against experimental data at 5 barg. This was achieved by manufacturing the optimised components and installing them within a suitable relief valve assembly. The testing equipment of Broady Flow Control that was previously introduced was again used to obtain the data. This data consists of force measurements across the full opening cycle of the valve, LVDT data from a functional test and also the overpressure and blowdown figures - these can be calculated from the functional test data. To further investigate the capabilities of this design approach a range of pressures shall be tested.

The first section of this chapter will focus on the data obtained at 5 barg, this is the pressure used for the validation exercise and has been the main focus of the thesis thus far. Firstly, the force-lift curve produced via CFD calculations will be compared to that measured via experiment. This will give an indication to the capabilities of the CFD modelling of this type of SRV geometry. Secondly, the CFD data will be used in the LVM to obtain the dynamic behaviour of the optimised geometry and also the overpressure and blowdown figures. These will be compared to LVDT data and the overpressure and blowdown measured through experiment. This section will conclude with an adjustment of the lower and upper

rings, the position of these components will be altered in both the numerical and experimental setups and the figures will again be compared.

The second section shall focus on a slightly higher pressure of 9 barg, the maximum allowable working pressure of the flow test rig at Broady Flow Control is 10 barg thus 9 barg shall be used to allow for overpressure. This pressure will be validated against LVDT data and the overpressure and blowdown figures.

Finally, this chapter will undertake CFD calculations at 50 barg and use this data to obtain the dynamic behaviour and overpressure and blowdown figures. These 3 settings should provide a clear indication to the effectiveness of the optimisation design approach.

7.1 Validation at 5 barg set pressure.

This section will present the validation results obtained at 5 barg working pressure, below in figure 7.1 is the comparison of force-lift curves produced through CFD calculation and experiment. Good agreement can be found over most of the curve, a slight discrepancy can be found around 1.0mm, however the overall accuracy is acceptable and generally within the uncertainty discussed in chapter 3.

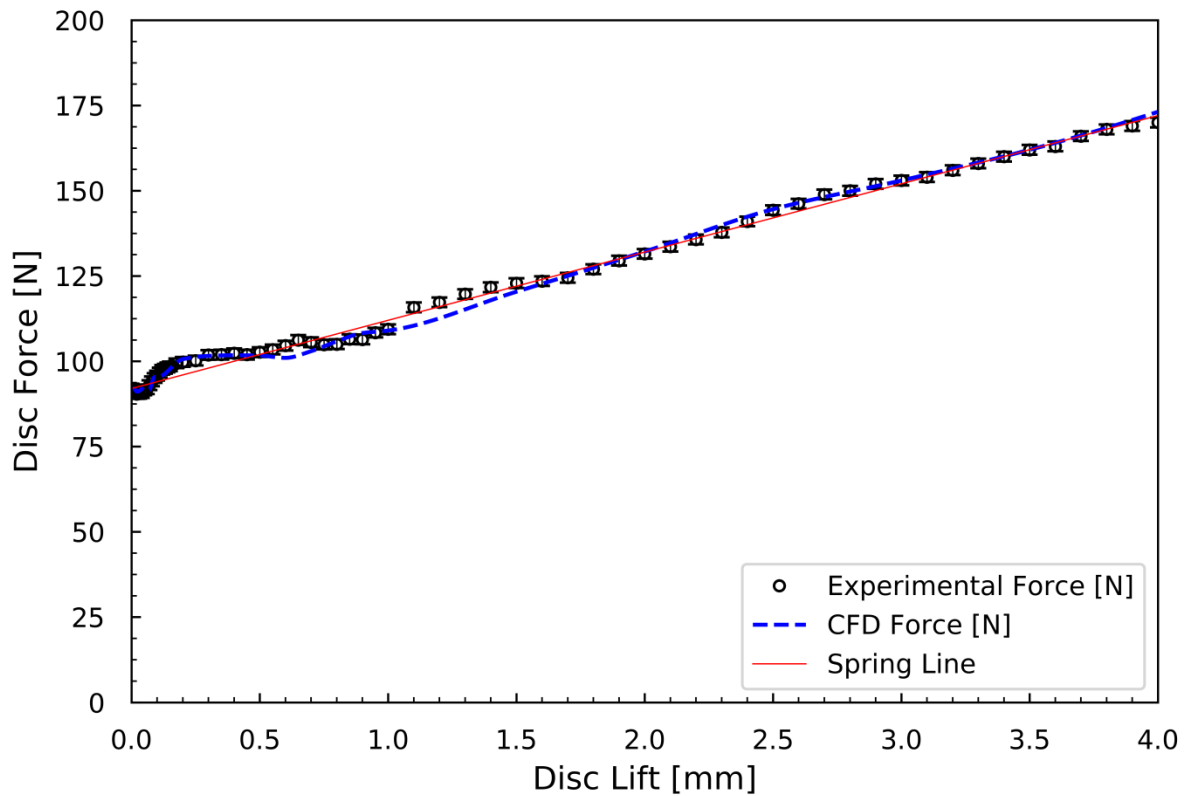


Figure 7.1 – Force-lift curve validation at 5 barg set pressure.

Figure 7.2 displays the comparison of LVDT data and displacement prediction from the LVM at 5 barg set pressure. A close match is found throughout the full operational cycle, this is expected as the force-lift curves show good agreement at the low-lift inflection point and similarly at high-lift. Table 7.1 presents the results of predicted and measured overpressure and blowdown values. The LVM predicts an overpressure at half of what was measured; this clearly indicates the sensitivity of this valve and the LVM, the blowdown is similar with the numerical model predicting a lower figure. However, all results fall within the criteria set out in the optimisation stage.

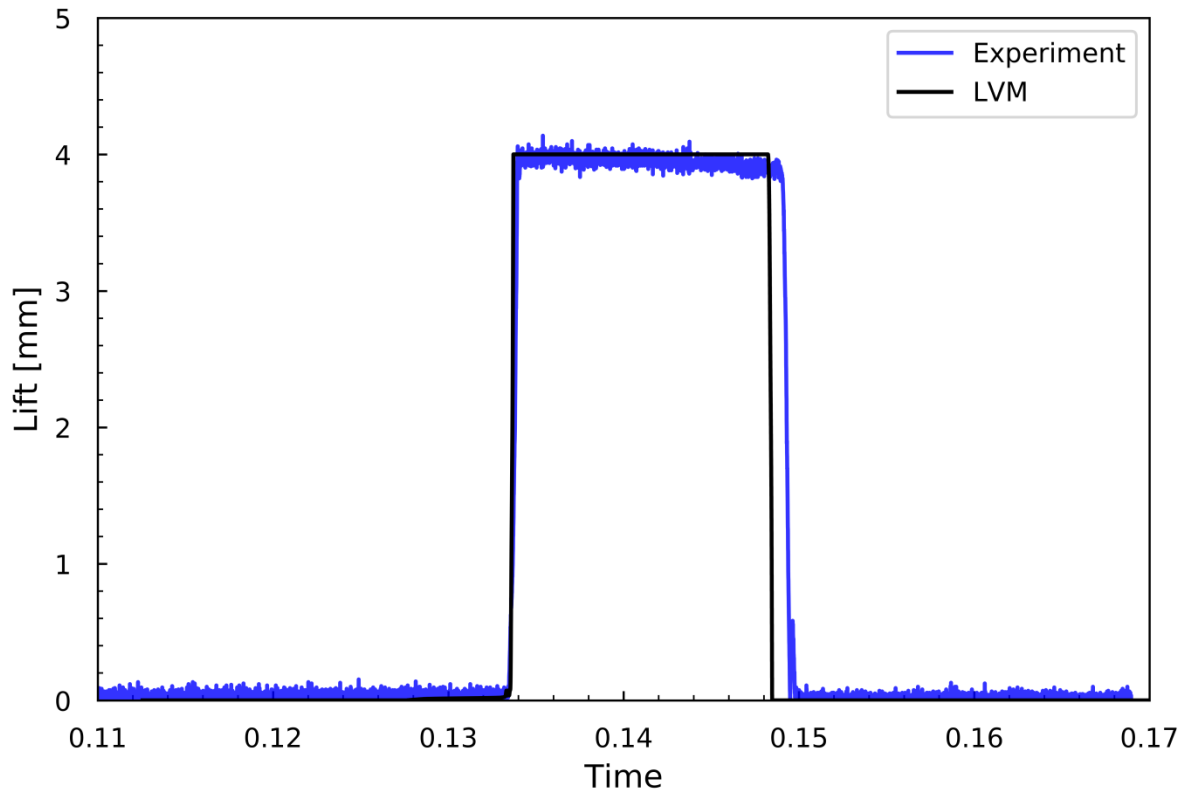


Figure 7.2 – Displacement validation at 5 barg set pressure.

	Blowdown (barg)	Blowdown (%)	Set (barg)	Overpressure (barg)	Overpressure (%)
Numerical	4.95	1.05	5.00	5.08	1.60
Physical	4.86	2.89	5.00	5.14	2.89

Table 7.1 – Comparison of results from numerical and experimental testing at 5 barg set pressure.

7.2 Validation at 9 barg set pressure.

Figure 7.3 presents the comparison of CFD and experimental force-lift curves at 9barg working set pressure. The accuracy at low-lift is acceptable with the predicted force closely following the measured disc force to around 0.6mm, this should allow for the opening

process to be modelled correctly. From 0.6mm to full lift at 4.0mm the accuracy is not as good as the 5 barg data but it is still reasonable over the length of the curve.

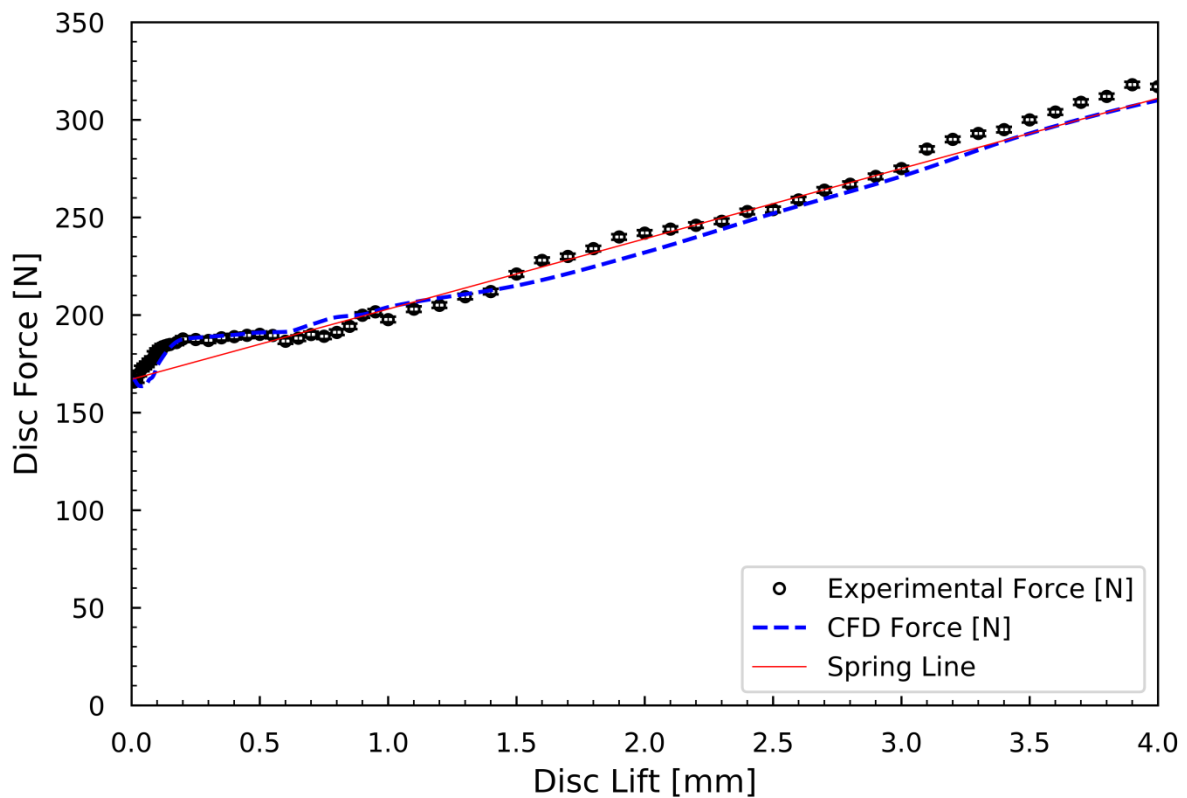


Figure 7.3 – Force-lift curve validation at 9 barg set pressure.

Figure 7.4 below displays the comparison of LVDT data and the displacement prediction of the LVM, good agreement is found throughout the full operational cycle. Table 7.2 presents the results of the predicted and measured overpressure and blowdown values. At 9 barg working pressure the LVM predicts an overpressure double what was measured - similar levels of discrepancy as 5 barg but over prediction this time. The blowdown was under predicted but as the force-lift curves were not closely matched at high lift this was expected.

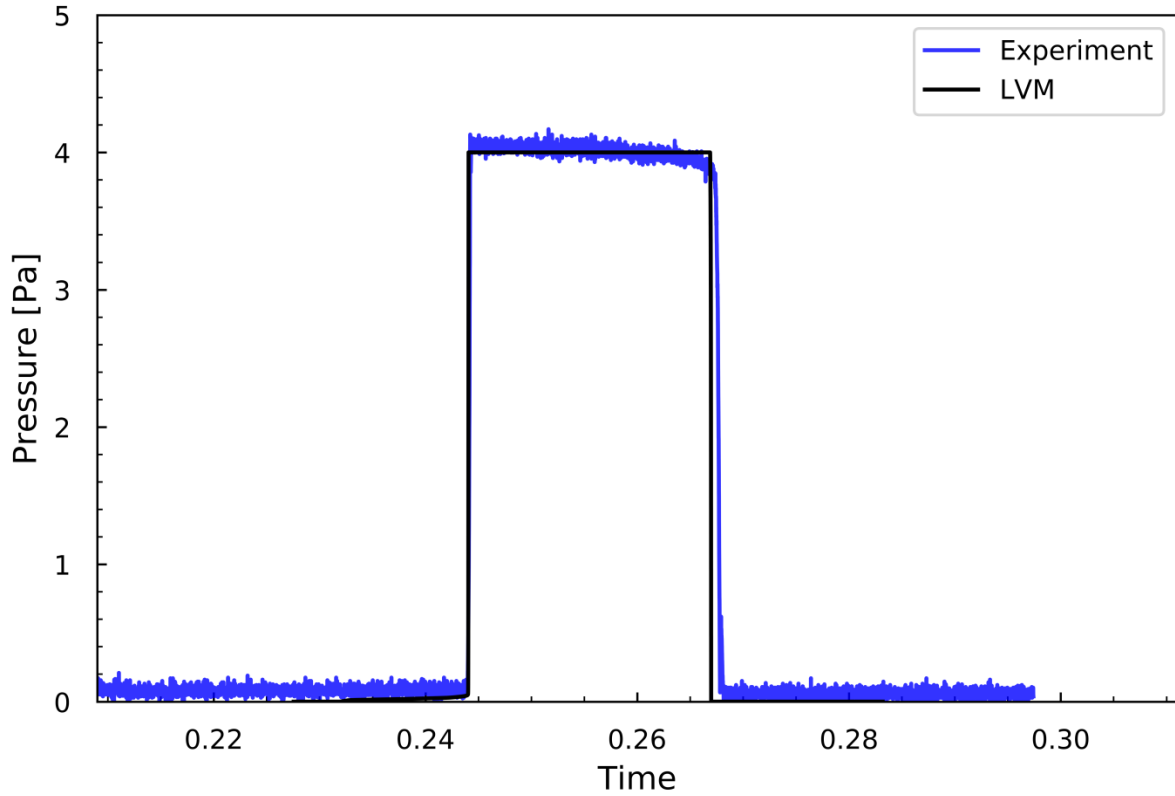


Figure 7.4 – Displacement validation at 9 barg set pressure.

	Blowdown (barg)	Blowdown (%)	Set (barg)	Overpressure (barg)	Overpressure (%)
Numerical	8.65	3.93	9.00	9.28	3.06
Physical	8.47	5.84	9.00	9.11	1.27

Table 7.2 – Comparison of results from numerical and experimental testing at 5 barg set pressure.

This current configuration for 9 barg set pressure is on the boundary of meeting ASME Section I performance criteria, an adjustment of the upper and lower ring position could improve this, an example of which is presented below in 7.3.

7.3 Assessment at a 50 barg set pressure.

This section will present the performance of the optimised valve at a working pressure of 50 barg, all figures were obtained numerically. Initially at 50 barg the SRV did not display the

necessary performance - the force lift curve is presented in figure 7.5. This clearly shows too much net force across the full length of the force-lift curve.

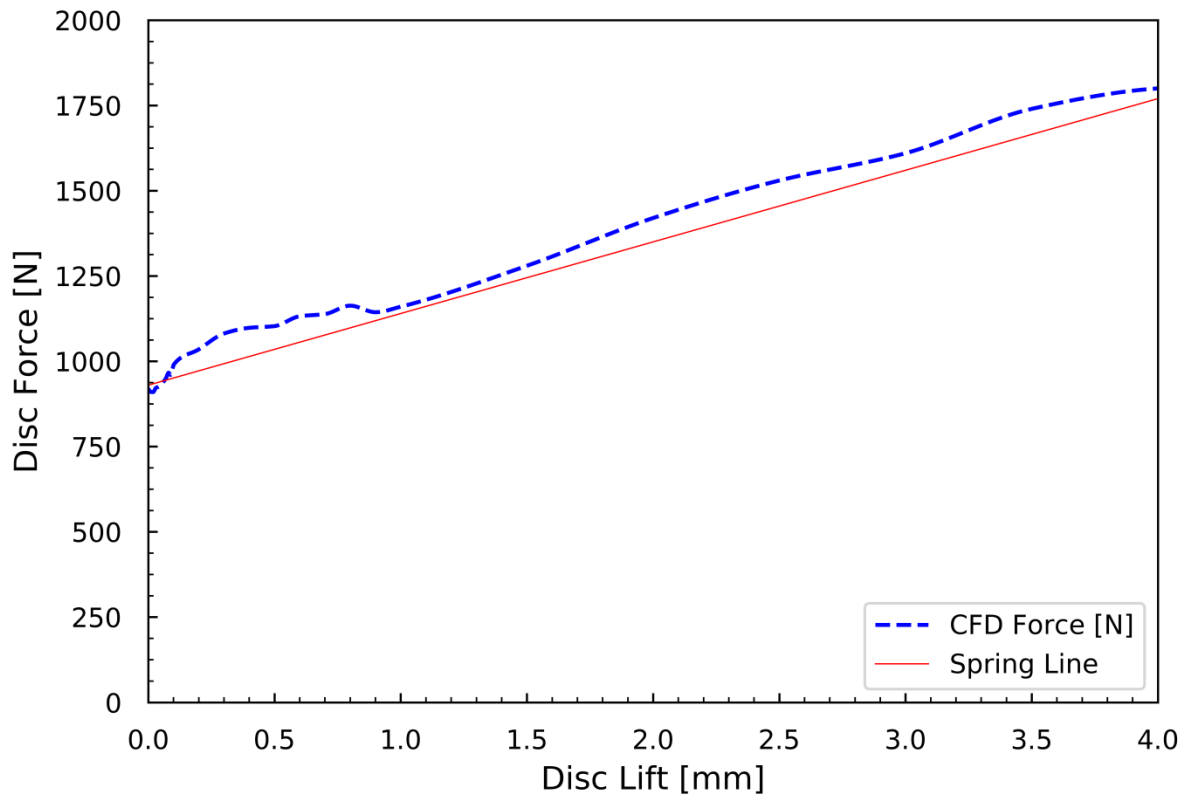


Figure 7.5 – Initial force-lift curve at 50 barg working pressure.

This result required altering the position of both adjustment rings, firstly reducing the height of the lower ring from 0.15 mm to 0.11 mm - the equivalent of one notch. Secondly, the upper ring was raised from 1.00 mm below seat level to 0.75 mm below seat level - the equivalent of five notches. This then resulted in a much more satisfactory force-lift curve which is presented in figure 7.6, much less net force is shown in this plot. Figure 7.7 displays the dynamic performance of the valve at 50 barg, clearly showing a sharp opening and closing behaviour typical of a safety relief valve.

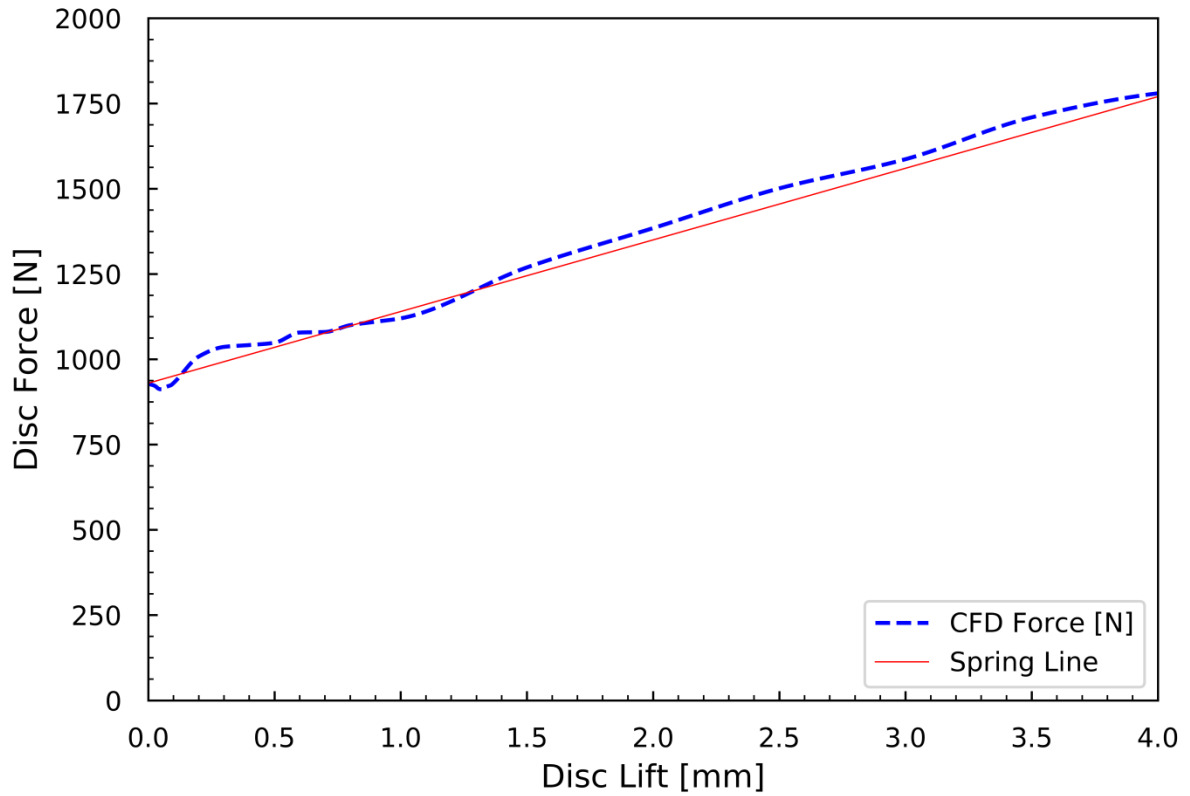


Figure 7.6 – Force-lift curve at 50 barg with adjusted setting.

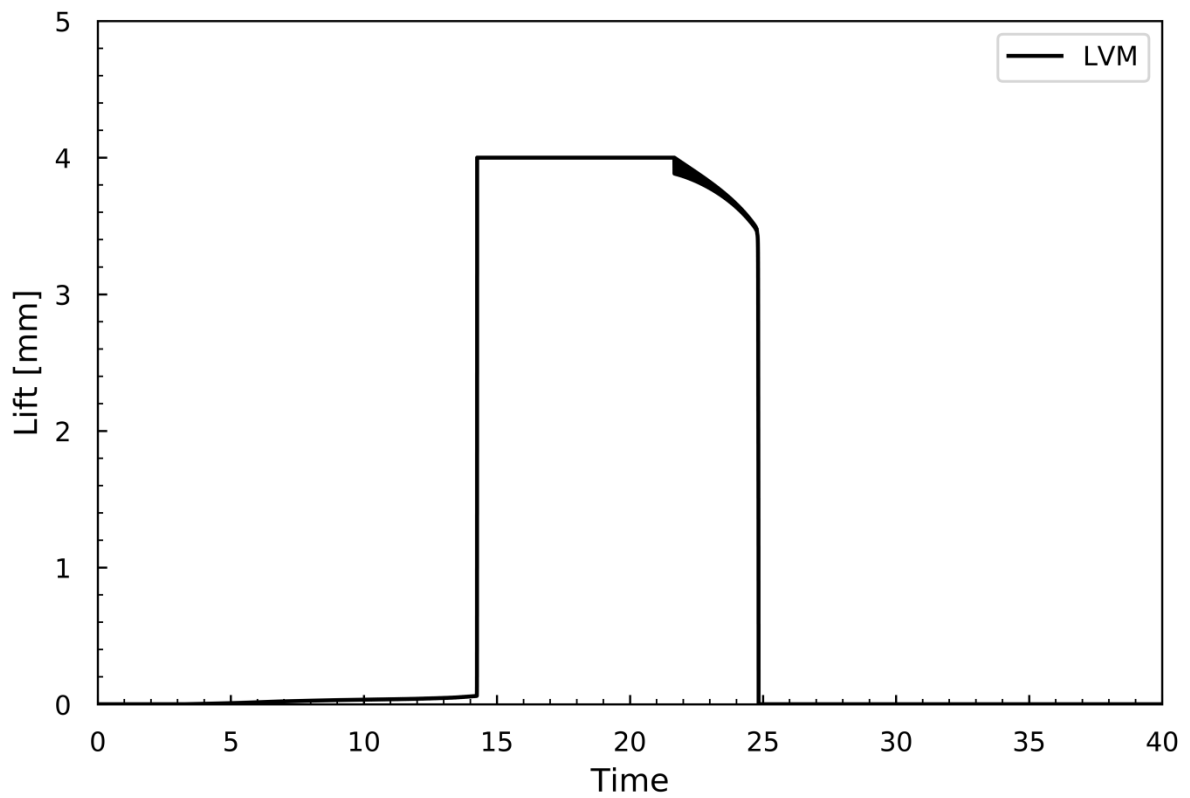


Figure 7.7 – Displacement calculated through low-order valve model using 50 barg CFD data.

Table 7.3 presents the performance results from the optimised relief valve; at this adjusted setting it was able to meet the ASME Section I performance criteria.

	Blowdown (barg)	Blowdown (%)	Set (barg)	Overpressure (barg)	Overpressure (%)
Numerical	48.67	2.67	50.00	51.18	2.35

Table 7.3 – Results from low-order valve model at 50 barg.

8. Discussion and Conclusion

The aim of this thesis was to develop a design methodology utilising mathematical optimisation to improve the performance of a safety relief valve. Throughout this investigation the capabilities of CFD modelling for ASME type SRVs was evaluated and this provided a foundation on which to evolve the design process with the inclusion of optimisation algorithms. There have been several points covered throughout this research thus this chapter shall be divided accordingly to discuss each topic further, these are based around CFD modelling, pressure scaling and optimisation.

8.1 Discussion

8.1.1 CFD Modelling

The initial stages of this thesis focused on the capabilities of CFD modelling within an ASME type SRV, the test valve was supplied by Broady Flow Control. A full verification and validation exercise was presented and through this the ability of these techniques were uncovered. Initially the force-lift curves produced through CFD were compared to those measured at the experimental facilities of Broady Flow Control. A close match was found with the accuracy generally being within 1% of the measured force, which has been classed as satisfactory as the overpressure and blowdown requirements are 3% and 4% respectively; there being a direct correspondence between desired accuracy and required % of acceptable blowdown.

Following on from this work, the CFD force data was used in a low-order valve model of the Broady test valve. Using this approach, a numerical prediction of the dynamic behaviour of

this valve was obtained. This prediction was subsequently validated against LVDT data measured through experiment, again these were found to be in good agreement. These two initial investigations were able to provide sufficient confidence in the modelling techniques and their ability to calculate the behaviour of SRVs. This was essential before building on these methods by embedding them within design optimisation algorithms.

After validation of the models further CFD calculations were carried out to study the behaviour of the reference valve and how it operates. Using a combination of contour plots and pressure distribution data, a thorough understanding of the underlying physics of the valve was obtained. In doing so a description of why the adjustment ring is able to control the valve performance was provided and this would subsequently be built upon when improving the performance through geometrical changes. The information produced throughout this section was critical in both understanding the valve behaviour but also in making decisions on what parameters to use for geometry changes. The opening and closing processes are controlled by different parts of the SRV geometry and it was during this section that their exact role was uncovered. In order to understand the opening process, disc force measurements had to be taken at the sub-millimetre level. For example, an E orifice opening cycle is typically controlled within the first 0.10mm valve lift. If no force measurements or CFD calculations were taken below this point it would be difficult to understand how the valve truly operates. The CFD data produced throughout this thesis in the region of 0-0.10mm has been instrumental in the understanding of the valve operation.

8.1.2 Pressure Scaling

From the review of the current literature on SRV design and analysis, certain issues with pressure scaling techniques were found. Published research on the topic highlighted 2 separate circumstances where the industrial pressure scaling methods may not hold true. These were at both low and high-lift conditions thus it was essential to undertake a study on the Broady test valve to discover how these effects occur in this type of SRV.

Firstly, low-lift conditions were studied; this consisted of CFD calculations from 1-40 barg at a valve lift from 0-1.00mm. The force-lift curve shape was found to alter as the working pressure increased, however the non-dimensionalised force effectively became invariant as the pressure approached 40 barg. To gain a deeper understanding of the physics involved, a geometry simplification was undertaken to remove any effects from the adjustment ring and disc notches. Throughout this study it was found that the normalised pressure distribution is not constant over the pressure range and that the fluid flow field is fundamentally different, there are shocks present at 40 bar that are non-existent at lower pressures. Thus, the effects will have to be controlled to maintain valve performance; this can be achieved through the adjustment ring present in these types of relief valves.

The pressure scaling study then moved on to the effects at high lift conditions. It was found that at elevated pressures the outlet flange can act as a secondary nozzle and become choked, this results in a back-pressure build-up within the valve body itself. Ultimately this will result in additional force acting on the rear face of the disc holder and aid the spring in closing the valve. This would lead to lower lift and a reduced flow rate – which could have potentially catastrophic results for a pressurised system. From the investigation undertaken it was found that once the exit flange had become fully choked traditional pressure scaling

methods became valid; however, until this stage they are not accurate enough. It was recommended that CFD tools be used to aid the selection of springs for higher flow rates.

From this investigation it is suspected that if a build-up of backpressure occurs, the valve will begin to close slightly which would result in a lower flow rate. This reduction in flow rate could lead to the exit flange becoming un-choked again but this postulation should be checked via a full transient 3D calculation at these conditions.

8.1.3 Optimisation

The optimisation process was undertaken in two stages; initially the force-lift curve used in the low-order valve model was optimised. This resulted in a force-lift curve that would meet the performance requirements of ASME Section I. This curve was then used as a target in the second stage of the optimisation which altered the internal trim components of the SRV geometry to match this target force characteristic.

The geometrical optimisation process used a surrogate modelling approach as this is able to reduce the number of calculations needed when undertaking the optimisation. It was found that undertaking the geometrical optimisation process in two stages would further reduce the number of calculations needed when exploring the solution space. As shown in table 6.3 the number of individual force-lift curves to explore 5 separate parameters is 243 (3^5), however undertaking this exploration by focusing on 2 then 3 parameters this was reduced to 36 (3^2 & 3^3) individual force-lift curves. Using this approach, the design space exploration phase was able to be completed using a standard desktop PC over the space of a few weeks.

Once the design space data was obtained the optimisation process using an interior point algorithm in conjunction with a surrogate model took only a few minutes.

This resulted in an SRV trim geometry that could meet the disc force-lift characteristics obtained during the primary optimisation. A full force-lift curve of this geometry was produced using CFD calculations and found to be in satisfactory agreement with the requirements. The main area of focus to obtain the opening performance is the initial dip at low-lift conditions and this was found to be closely matched, thus the outcome was classed a success.

A validation of the results was undertaken, this was initially at 5 barg working pressure as this was the pressure used throughout the design optimisation stage, then pressures of 9 and 50 barg were also used to check the capabilities at different conditions. As with the validation exercise used previously in this thesis, the results were validated using disc force measurements, LVDT data and overpressure and blowdown figures. No data at 50 barg could be obtained thus that configuration could not be validated.

The validation exercise began using the 5 barg set pressure data produced during the optimisation process. When comparing the experimental force-lift curve and CFD data good agreement was found over the length of the curve, however, a slight discrepancy was found between 1.00mm and 1.50mm. To accurately predict the opening and closing process the force-lift curve must be accurate at the low-lift inflection point and also at full opening height. At these points in the curve at 5 barg the accuracy was acceptable. Unfortunately, the overpressure and blowdown predicted by the LVM model was half of that which was measured, this clearly shows the sensitivity of the LVM. Slight differences at the key points in the force-lift curve can strongly influence the SRV performance. Having both upper and

lower ring to adjust the force-lift curve allows for some manipulation of the curve shape and thus SRV performance.

The validation exercise then moved on to 9 barg set pressure, this used an identical approach to the 5 barg process. Throughout this, reasonable accuracy was found, however, the force-lift curve at high-lift conditions was slightly different. This had an effect on the system model thus the LVDT data did not exactly match the numerical opening and closing data. Overall the data was reasonably accurate, the overpressure and blowdown of both the numerical and physical were both within the ASME Section I requirements.

A final assessment focused on a working pressure of 50 barg. The initial force-lift curve was found to have a higher level of force above the spring line and as shown throughout this research a high level of net-force generally leads to poor performance. From an inspection of this curve it was known that the performance would have not been satisfactory prior to using it in the system model. This postulation was confirmed when the curve was checked and found to produce a blowdown figure well out with the performance requirements, thus an adjustment of the valve configuration was required.

Throughout this validation phase it has been recognised that the numerical modelling methods can accurately predict the performance of SRVs under a range of conditions and also that optimisation algorithms can be used successfully in the design phase of a safety relief valve. From undertaking this research one of the most important outcomes is the data produced from CFD calculations. This has been essential in explaining the operation of this type of SRV. Without this understanding it would not have been possible to make the necessary decisions on design parameters during the optimisation process. Understanding

the physics behind the operation of the lower adjustment ring was critical in choosing what dimensions to alter during the optimisation.

As this technique has now been developed it is expected that it could now be used to greatly increase the speed at which safety relief valves are designed. Using these methods should be able to produce high performing valves in a shorter time than traditional methods. Currently it is expected that one new valve design could be obtained within six weeks, this would consist of all CAD work, design space exploration and final CFD check of new design. Another two weeks to allow for manufacture of components would bring the total up to eight weeks from initial concept to be ready to test. It is difficult to compare this to an experimental approach as this trial and error approach could require many design iterations leading to a long lead time. The other main issue with a purely experimental approach is the inability to understand the flow physics inside the valve. Using CFD, the flow field data produced provides information that would be impossible to obtain any other way and is key to understanding how the device operates. Coupling CFD modelling with the optimisation process can progress a design to an optimal and removes the need for a significant amount of manufacture. Thus not only does this design tool help reduce lead time of products it reduces material costs, man hours in manufacture and energy costs for creating components.

8.2 Conclusion and Recommendations for Future Work

8.2.1 Conclusion

The main objective was to develop a design methodology for safety relief valves utilising mathematical modelling and optimisation algorithms. This was achieved using numerical methods and subsequently validated using the experimental facilities at Broady Flow Control. The outcome of this validation was that the numerical and experimental figures were in good agreement thus the procedure can be classed a success. The geometry calculated by the optimisation method was able to achieve ASME Section I performance over a range of pressures. The levels of adjustment included in the produced geometry was found to provide good levels of control over the force-lift curve and was critical in obtaining performance at a working pressure of 50 barg.

It is worth noting the value of the data produced by CFD calculations, this was critical in making design decisions and was key in producing an explanation of the fluid mechanics over the operational cycle of the Broady 3500 test valve. Without the pressure distribution data and the pressure and Mach number contour plots it would have been extremely difficult to achieve the same level of understanding as produced with CFD. If the design process was only utilising CFD modelling alone without any optimisation processes this data would be extremely valuable for making informed design decisions. Although experimental testing is still required, numerical modelling plays a critical role in the design process. Thus, it is recommended to utilise these tools whenever possible in the design and analysis of safety relief valves.

The resolution of measurements also highlighted non-smooth behaviour of forces as the valve opens. Consulting literature on safety relief valves would suggest that the disc force increases gradually as the valve opens. However, throughout this research the disc force has been shown to display different behaviour - even disc force reductions were also found throughout operational cycle. The initial force reduction at low lift was key to understanding the opening process and the effects that the lower ring had.

8.2.2 Recommendations for Future Work

From this research a number of issues were uncovered that should be given more attention in future, principally around pressure scaling.

- Firstly, the effects of high pressure flows in large valves needs to be studied by a transient CFD analysis to uncover the effects of built-up back pressure on the disc lift. It is postulated that the choking process will cause partial valve closure and reduced flow rate thus could lead to the outlet becoming un-choked. A transient analysis would provide more detail on this process. This could ultimately show that the choking process still leads to a pressure build-up upstream of an SRV taking the system pressure above the MAWP.
- Secondly the effects of high pressure flows in the type of SRV geometry used during the optimisation process should be studied. As this type of geometry has a second adjustment ring thus a rear chamber, it could be unaffected by built-up back pressure due to the disc holder rear face being isolated from the valve body.

- During the optimisation stage, a spring rate was chosen and used by the LVM to optimise the shape of the driving force-lift curve. In future an investigation into using the spring rate as a design parameter would be possible, this could improve the overall performance and stability of the LVM.
- Also, during the optimisation stage, the shape of the curve could have constraints applied to it, this would allow for more control over the shape of the final curve.
- It would also be beneficial to undertake an optimisation process at higher pressures, this could uncover a geometry that is more suitable for a range of pressures.
- It was also evident that for an optimised force lift curve the net forces acting on the valve disc becomes smaller and reduces to the accuracy of the CFD calculation. This sensitivity to the accuracy of CFD modelling is appreciated and the robustness in the optimisation process could be questioned. Further investigation is recommended.
- Finally, undertaking the optimisation validation at higher pressures would also be of benefit to this design methodology, this data could also be used for any further investigations into the built-up back pressure phenomena presented in chapter 4.

9. References

- ANSYS Inc. (2017), 'Release 18.2- Fluent Theory Guide'.
- API. (2015) 'RP 520 P1, Sizing, Selection and Installation of Pressure-Relieving Devices in Refineries; Part I – Sizing and Selection'.
- API. (2015) 'RP 520 P1, Sizing, Selection and Installation of Pressure-Relieving Devices in Refineries; Part II – Installation'.
- API. (2017) 'RP 526: Flanged Steel Pressure Relief Valves'.
- ASME. (2019) 'Boiler and Pressure Vessel Code Section I: Rules for Construction of Power Boilers'.
- ASME. (2017) 'Boiler and Pressure Vessel Code Section VIII: Rules for Construction of Pressure Vessels'.
- ASME. (2017) 'Pipe Flanges and Flanged Fittings: NPS ½ through NPS 24 Metric/Inch Standard'.
- ASME. (2016) 'V&V 20-2009, Standard for Verification and Validation in Computational Fluid Dynamics and Heat Transfer'.
- ASME. (2014) 'PTC 25 – 2014, Pressure Relief Devices'.
- Aldeeb, A.A., Darby, R. and Arndt, S. (2014) 'The dynamic response of pressure relief valves in vapor or gas service. Part II: Experimental investigation'. *Journal of Loss Prevention in the Process Industries*, 31, pp. 127-132.
- Bassi, F., Crivellini, A., Dossena, V., Franchina, N. and Savini, M. (2014) 'Investigation of flow phenomena in air–water safety relief valves by means of a discontinuous Galerkin solver'. *Computers & Fluids*, 90, pp. 57-64.
- Bazso, C., Champneys, A.R. and Hos, C.J. (2014) 'Bifurcation Analysis of a Simplified Model of a Pressure Relief Valve Attached to a Pipe'. *SIAM Journal on Applied Dynamical Systems*, 13 (2), pp. 704-721.
- Bazsó, C. and Hős, C. (2012) A CFD study on the stability of a hydraulic pressure relief valve.
- Bazsó, C. and Hős, C.J. (2013) 'An experimental study on the stability of a direct spring loaded poppet relief valve'. *Journal of Fluids and Structures*, 42, pp. 456-465.
- Beune, A. (2009) 'Analysis of high-pressure safety valves'. A Catalogue Record is Available from the Eindhoven University of Technology Library, ISBN, pp. 978-990.
- Beune, A., Kuerten, J.G.M. and van Heumen, M.P.C. (2012) 'CFD analysis with fluid–structure interaction of opening high-pressure safety valves'. *Computers & Fluids*, 64, pp. 108-116.
- Bhosekar, A. and Ierapetritou, M. (2018) 'Advances in surrogate based modelling, feasibility analysis, and optimization: A review'. *Computers & Chemical Engineering*, 108, pp. 250-267.
- Byrd, R.H., Gilbert, J.C. and Nocedal, J. (2000) 'A trust region method based on interior point techniques for nonlinear programming'. *Mathematical Programming*, 89 (1), pp. 149-185.
- Cartwright, S. (2003) 'University of Sheffield, Introduction to Experimental Error'. [online] Available at: https://www.sheffield.ac.uk/polopoly_fs/1.14221!/file/IntroToExperimentalErrors_y2.pdf, [Accessed on 04/05/19].

- Chabane, S., Plumejault, S., Pierrat, D. and Couzinet, A., (2009) Published. 'Vibration and chattering of conventional safety relief valve under built up back pressure'. 3rd IAHR International Meeting of the Work Group on Cavitation and Dynamic Problems in Hydraulic Machinery and Systems, Oct, 2009. pp. 14-16.
- Chen, F., Qian, J., Chen, M. and Zhang, M., (2018) 'Turbulent compressible flow analysis on multi-stage high pressure reducing valve'. *Flow Measurement and Instrumentation*, 61, pp. 26-37.
- Coleman, H.W. and Stern, F. (1997) 'Uncertainties and CFD Code Validation'. *Journal of Fluids Engineering*, 119 (4), pp. 795-803.
- Couckuyt, I., Dhaene, T. and Demeester, P. (2014) 'ooDACE toolbox: a flexible object-oriented Kriging implementation'. *The Journal of Machine Learning Research*, 15 (1), pp. 3183-3186.
- Couckuyt, I. Forrester, A., Gorissen, D. and Turck, F. (2012) 'Blind Kriging: Implementation and Performance Analysis'. *Advances in Engineering Software*, 49, pp.1-13.
- Couckuyt, I., Koziel, S. and Dhaene, T. (2012) 'Surrogate modeling of microwave structures using kriging, co-kriging, and space mapping'. *International Journal of Numerical Modelling: Electronic Networks, Devices and Fields*, 26 (1), pp. 64-73.
- Darby, R. (2013) 'The dynamic response of pressure relief valves in vapor or gas service, part I: Mathematical model'. *Journal of Loss Prevention in the Process Industries*, 26 (6), pp. 1262-1268.
- Darby, R. and Aldeeb, A.A. (2014) 'The dynamic response of pressure relief valves in vapor or gas service. Part III: Model validation'. *Journal of Loss Prevention in the Process Industries*, 31, pp.133-141.
- Dempster, W., Lee, C.K. and Deans, J. (2006) 'Prediction of the Flow and Force Characteristics of Safety Relief Valves'. (47543), pp. 93-99.
- Dempster, W. and Alshaikh, M. (2015) An Investigation of the Two Phase Flow and Force Characteristics of a Safety Valve.
- Dempster, W., Taggart, S. and Doyle, C. (2018) 'Limitations in the Use of Pressure Scaling for Safety Relief Valve Design'. (51623), pp. V03AT03A002.
- Dong, Z., Pan, Y., Zhang, Z. and Dong, Y., (2017) 'Model-free adaptive control law for nuclear superheated-steam supply systems'. *Energy*, 135, pp. 53-67.
- Dossena, V., Marinoni, F., Bassi, F., Franchina, N. and Savini, M. (2013) 'Numerical and experimental investigation on the performance of safety valves operating with different gases'. *International Journal of Pressure Vessels and Piping*, 104, pp. 21-29.
- Dossena, V. (2013) 'von Karman Institute for Fluid Dynamics, Lecture series 2013-08: Flow Characteristics and Performance of Safety Valves.'
- El Bouzidi, S., Hassan, M. and Ziada, S. (2018) 'Self-excited vibrations of spring-loaded valves operating at small pressure drops'. *Journal of Fluids and Structures*, 83, pp. 72-90.
- Erdödi, I. and Hős, C. (2017) 'Prediction of quarter-wave instability in direct spring operated pressure relief valves with upstream piping by means of CFD and reduced order modelling'. *Journal of Fluids and Structures*, 73, pp. 37-52.
- Föllmer, B. and Schnettler, A. (2003) 'Challenges in designing API safety relief valves'. *Valve World*, 10, pp. 39-43.
- Forrester, A.I.J. and Keane, A.J. (2009) 'Recent advances in surrogate-based optimization'. *Progress in Aerospace Sciences*, 45 (1), pp. 50-79.

- Gorissen, D., Couckuyt, I., Demeester, P. and Dhaene, T. (2010) 'A surrogate modelling and adaptive sampling toolbox for computer based design'. *Journal of Machine Learning Research*, 11 (Jul), pp. 2051-2055.
- Hellemans, M. (2009) *The safety relief valve handbook: design and use of process safety valves to ASME and International codes and standards*. Elsevier.
- Tu, J., Yeoh, G. and Liu, C. (2012). 'Computational Fluid Dynamics: A Practical Approach'. Butterworth-Heinemann
- Hou, C.-W., Qian, J.-Y., Chen, F.Q., Jiang, W.K. and Jin, Z.-J. (2018) 'Parametric analysis on throttling components of multi-stage high pressure reducing valve'. *Applied Thermal Engineering*, 128, pp. 1238-1248.
- Hős, C., Bazsó, C. and Champneys, A. (2015) 'Model reduction of a direct spring-loaded pressure relief valve with upstream pipe'. *IMA Journal of Applied Mathematics*, 80 (4), pp. 1009-1024.
- Hős, C. and Champneys, A.R. (2012) 'Grazing bifurcations and chatter in a pressure relief valve model'. *Physica D: Nonlinear Phenomena*, 241 (22), pp. 2068-2076.
- Hős, C.J., Champneys, A.R., Paul, K. and McNeely, M. (2014) 'Dynamic behaviour of direct spring loaded pressure relief valves in gas service: Model development, measurements and instability mechanisms'. *Journal of Loss Prevention in the Process Industries*, 31, pp. 70-81.
- Hős, C.J., Champneys, A.R., Paul, K. and McNeely, M. (2015) 'Dynamic behaviour of direct spring loaded pressure relief valves in gas service: II reduced order modelling'. *Journal of Loss Prevention in the Process Industries*, 36, pp. 1-12.
- Hős, C.J., Champneys, A.R., Paul, K. and McNeely, M. (2016) 'Dynamic behaviour of direct spring loaded pressure relief valves: III valves in liquid service'. *Journal of Loss Prevention in the Process Industries*, 43, pp. 1-9.
- Hős, C.J., Champneys, A.R., Paul, K. and McNeely, M. (2017) 'Dynamic behaviour of direct spring loaded pressure relief valves connected to inlet piping: IV review and recommendations'. *Journal of Loss Prevention in the Process Industries*, 48, pp. 270-288.
- Iuliano, E., Pérez, E.A.S. (2016) *Application of surrogate-based global optimization to aerodynamic design* / [internet resource]. Cham : Springer.
- Koziel, S. (2016) *Simulation-driven design by knowledge-based response correction techniques* / [internet resource]. Switzerland : Springer.
- Kramer, O. (2017) 'Genetic algorithm essentials', Springer.
- Lauder, B.E. and Spalding, D.B. (1974) 'The numerical computation of turbulent flows'. *Computer Methods in Applied Mechanics and Engineering*, 3 (2), pp. 269-289.
- Leifsson, L., Koziel, S. and Bekasiewicz, A. (2014a) 'Fast Low-fidelity Wing Aerodynamics Model for Surrogate-based Shape Optimization'. *Procedia Computer Science*, 29, pp. 811-820.
- Leifsson, L., Koziel, S. and Bekasiewicz, A. (2014b) 'Fast Low-fidelity Wing Aerodynamics Model for Surrogate-based Shape Optimization'. *Procedia Computer Science*, 29, pp. 811-820.
- Lochbaum, D. (2015) 'When Safety Relief Valves Fail to Provide Safety or Relief at Nuclear Plants', [online] Available at: <https://allthingsnuclear.org/dlochbaum/when-safety-relief-valves-fail-to-provide-safety-or-relief-at-nuclear-plants>. [Accessed 04/05/2019].
- Li, J.L., Chen, L.Z. and Song, X.G. (2015) 'Multi-objective Design Optimization of a Pressure Safety Valve for Raped Opening and Reclosing'. *Procedia Engineering*, 130, pp. 113-124.

- Liu, B., Koziel, S. and Zhang, Q. (2016) 'A multi-fidelity surrogate-model-assisted evolutionary algorithm for computationally expensive optimization problems'. *Journal of Computational Science*, 12, pp. 28-37.
- Menter, F. (1992a) 'Performance of popular turbulence model for attached and separated adverse pressure gradient flows', 22nd Fluid Dynamics, Plasma Dynamics and Laser Conference.
- Menter, F. (1992b) 'Performance of popular turbulence model for attached and separated adverse pressure gradient flows', 22nd Fluid Dynamics, Plasma Dynamics and Laser Conference.
- Menter, F. (1993) 'Zonal Two Equation k-w Turbulence Models For Aerodynamic Flows'. 23rd Fluid Dynamics, Plasmadynamics, and Lasers Conference. American Institute of Aeronautics and Astronautics.
- Menter, F.R. (2009) 'Review of the shear-stress transport turbulence model experience from an industrial perspective'. *International Journal of Computational Fluid Dynamics*, 23 (4), pp. 305-316.
- Mitchell, M. (1998) *An Introduction to Genetic Algorithms*. MIT Press.
- Moncalvo, D., Friedel, L., Jorgensen, B., Hohne, T., (2009) 'Sizing of Safety Valves Using ANSYS CFX-Flo'. *Chemical Engineering & Technology*, 32 (2), pp. 247-251.
- Narabayashi, T., Nagasaka, H., Niwano, M. and Ohtsuki, Y. (1986) *Safety Relief Valve Performance for Two-Phase Flow*.
- Nocedal, J. and Wright, S. (2006) 'Numerical optimization', Springer Science & Business Media.
- Richardson, L.F. (1910) On the approximate arithmetical solution by finite differences of physical problems involving differential equations, with an application to the stresses in a masonry dam'. *Proceedings of the Royal Society of London. Series A*, 83 (563), pp. 335.
- Ouderkirk, R. (2002) 'Rigorously size relief valves for supercritical fluids'. *Notes*, 4 5.
- Parker, G.J. (1985) 'Pop' safety valves: a compressible flow analysis'. *International Journal of Heat and Fluid Flow*, 6 (4), pp. 279-283.
- Perez-Segarra, C.-D., Lehmkuhl-Barba, O., Jaramillo-Ibarra, J.E., Colomer-Rey, G. and Oliva-Llena, A. (2018) *Turbulence Modelling and Numerical Issues: from RANS to DNS and LES*.
- Peters, J. (2003) 'Research Report 162, Assessment of valve failures in the offshore oil & gas industry'. TUV NEL.
- Qian, J.-Y., Wei, L., Zhang, M., Chen, F.-Q., Chen, L.-L., Jiang, W.-K. and Jin, Z.-J. (2017) 'Flow rate analysis of compressible superheated steam through pressure reducing valves'. *Energy*, 135, pp. 650-658.
- Roache, P.J. (1998) 'Verification and validation in computational science and engineering'. Hermosa
- Roache, P.J. (2008) Published. 'Validation: Definitions or descriptions'. 3rd Workshop on CFD Uncertainty Analysis. Lisbon, 2008. Citeseer.
- Robere, R. (2012) 'Interior point methods and linear programming'. University of Toronto.
- Schmidt, J, Egan, S. (2009). 'Case Studies of Sizing Pressure Relief Valves for Two-Phase Flow', *Chemical Engineering & Technology*. 32. 263 - 272. 10.1002/ceat.200800572.
- Scuro, N.L., Angelo, E., Angelo, G. and Andrade, D.A. (2018) 'A CFD analysis of the flow dynamics of a directly-operated safety relief valve'. *Nuclear Engineering and Design*, 328, pp. 321-332.

- Shapiro, J. (2001) 'Genetic Algorithms in Machine Learning'. Advanced Lectures. Berlin, Heidelberg: Springer Berlin Heidelberg, pp. 146-168.
- Shyy, W., Cho, Y.-C., Du, W., Gupta, A., Tseng, C.-C. and Sastry, A.M. (2011) 'Surrogate-based modeling and dimension reduction techniques for multi-scale mechanics problems'. *Acta Mechanica Sinica*, 27 (6), pp. 845-865.
- Slater, J.W., (2008) 'Overview of CFD Verification and Validation', [online] Available at: <https://www.grc.nasa.gov/www/wind/valid/tutorial/overview.html>. [Accessed on 04/05/2019].
- Song, X., Cui, L., Cao, M., Cao, W., Park, Y. and Dempster, W.M. (2014a) 'A CFD analysis of the dynamics of a direct-operated safety relief valve mounted on a pressure vessel'. *Energy Conversion and Management*, 81, pp. 407-419.
- Song, X., Cui, L., Cao, M., Cao, W., Park, Y. and Dempster, W.M. (2014b) 'A CFD analysis of the dynamics of a direct-operated safety relief valve mounted on a pressure vessel'. *Energy Conversion and Management*, 81, pp. 407-419.
- Song, X.-G., Park, Y.-C. and Park, J.-H. (2013) 'Blowdown prediction of a conventional pressure relief valve with a simplified dynamic model'. *Mathematical and Computer Modelling*, 57 (1), pp. 279-288.
- Srikanth, C. and Bhasker, C. (2009) 'Flow analysis in valve with moving grids through CFD techniques'. *Advances in Engineering Software*, 40 (3), pp. 193-201.
- Steinberg, S. and Roache, P.J. (1985a) 'Symbolic manipulation and computational fluid dynamics'. *Journal of Computational Physics*, 57 (2), pp. 251-284.
- Steinberg, S. and Roache, P.J. (1985b) 'Symbolic manipulation and computational fluid dynamics'. *Journal of Computational Physics*, 57 (2), pp. 251-284.
- van der Herten, J., Couckuyt, I., Deschrijver, D. and Dhaene, T. (2016) 'Adaptive classification under computational budget constraints using sequential data gathering'. *Advances in Engineering Software*, 99, pp. 137-146.
- Versteeg, H.K. and Malalasekera, W. (2007) *An introduction to computational fluid dynamics: the finite volume method*. Pearson Education.
- Waltz, R.A., Morales, J.L., Nocedal, J. and Orban, D. (2006) 'An interior algorithm for nonlinear optimization that combines line search and trust region steps'. *Mathematical Programming*, 107 (3), pp. 391-408.
- Wilcox, D.C. (1988) 'Reassessment of the scale-determining equation for advanced turbulence models'. *AIAA Journal*, 26 (11), pp. 1299-1310.
- Wright, S. and Nocedal, J. (1999) 'Numerical optimization'. *Springer Science*, 35 (67-68), pp. 7.
- Wu, Y., Zhao, H., Zhang, C., Wang, L. and Han, J. (2018) 'Optimization analysis of structure parameters of steam ejector based on CFD and orthogonal test'. *Energy*, 151, pp. 79-93.
- Yang, L., Wang, Z., Dempster, W., Yu, X. and Tu, S.-T. (2017) 'Experiments and transient simulation on spring-loaded pressure relief valve under high temperature and high pressure steam conditions'. *Journal of Loss Prevention in the Process Industries*, 45, pp. 133-146.
- Yu, X., Zhang, J., Zhao, S., Yu, X., Yu, X. and Liu, H. (2018) 'An investigation into the effect of gas adsorption on safety valve set pressure variations'. *Chemical Engineering Science*, 188, pp. 170-178.
- Zhang, J., Yang, L., Dempster, W., Yu, X., Jia, J. and Tu, S.-T. (2018) 'Prediction of blowdown of a pressure relief valve using response surface methodology and CFD techniques'. *Applied Thermal Engineering*, 133, pp. 713-726.

Zhao, X.a., Huang, B., Chen, T., Wang, G., Gao, D. and Zhao, J. (2017) 'Numerical simulations and surrogate-based optimization of cavitation performance for an aviation fuel pump'. *Journal of Mechanical Science and Technology*, 31 (2), pp. 705-716.

10. Appendices

A.1 Low-lift Design Space Exploration

This section presents the force data obtained when exploring the design space for the low lift optimisation. The lettering refers to each design parameter which was presented in chapter 5, the size after the letter states the dimension for that parameter. As an example, A-8.40_B-0_C-0 is the force-lift data obtained with parameter A at 8.40 mm, parameter B at 0.00 mm and parameter C at 0.00 mm.

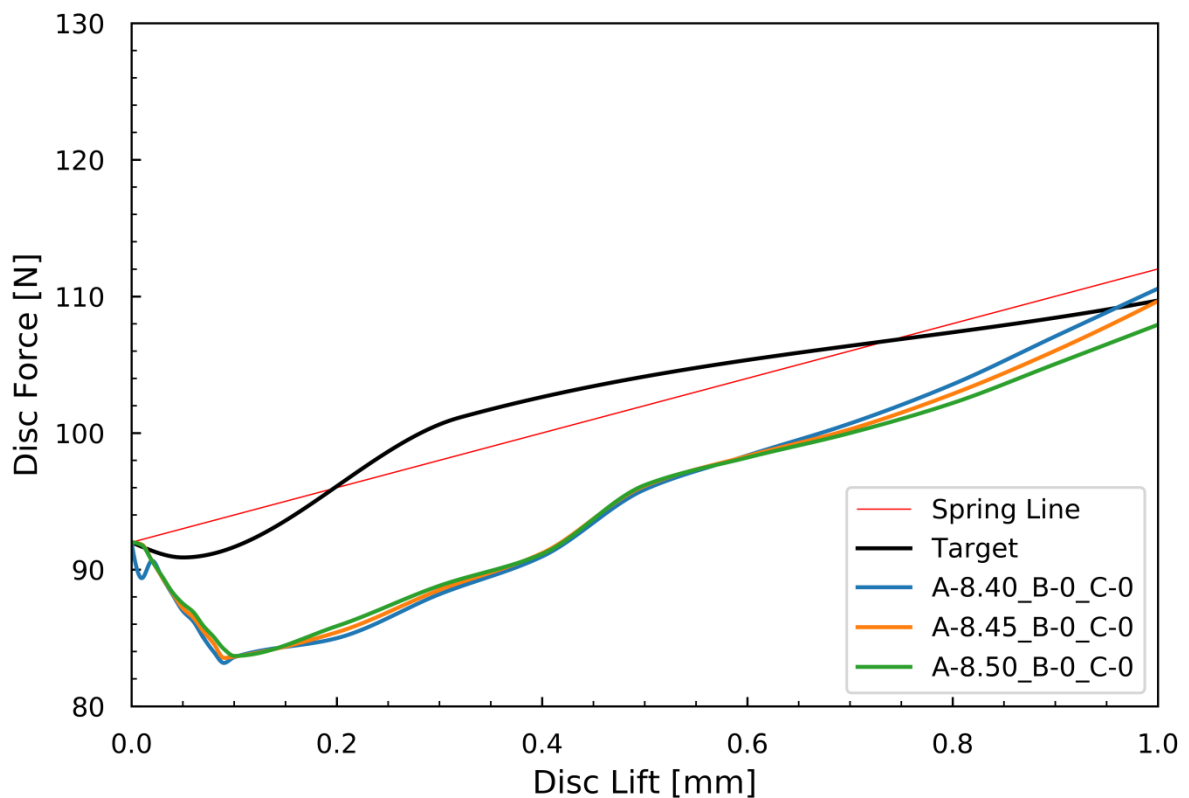


Figure A1.1 – Parameter A 8.40-8.50, B 0.00, C 0.00.

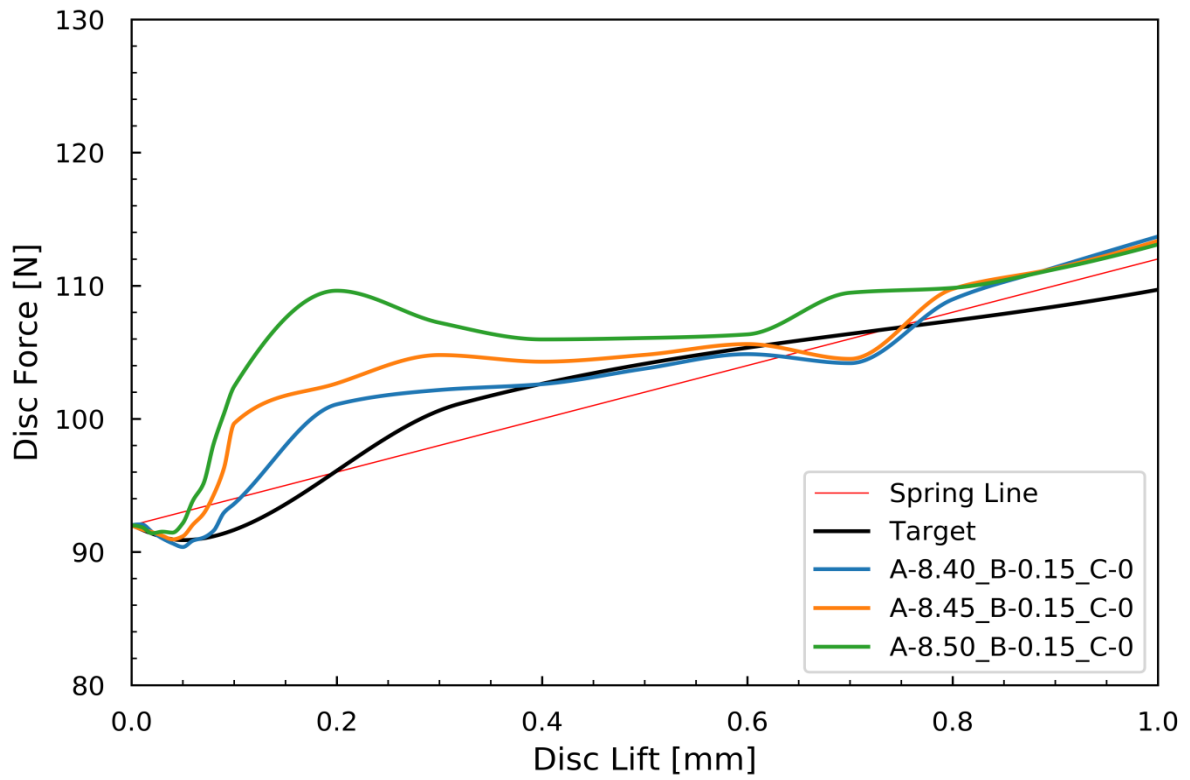


Figure A1.2 - Parameter A 8.40-8.50, B 0.15, C 0.00.

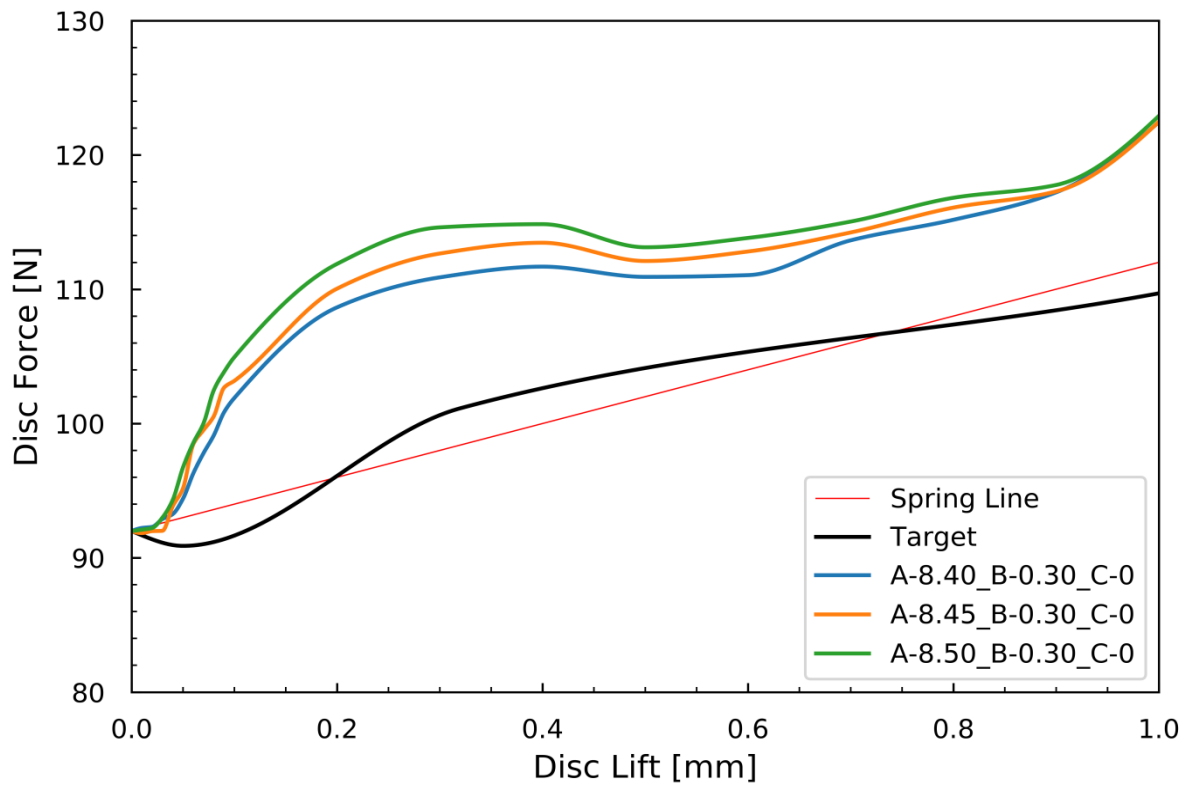


Figure A1.3 - Parameter A 8.40-8.50, B 0.30, C 0.00.

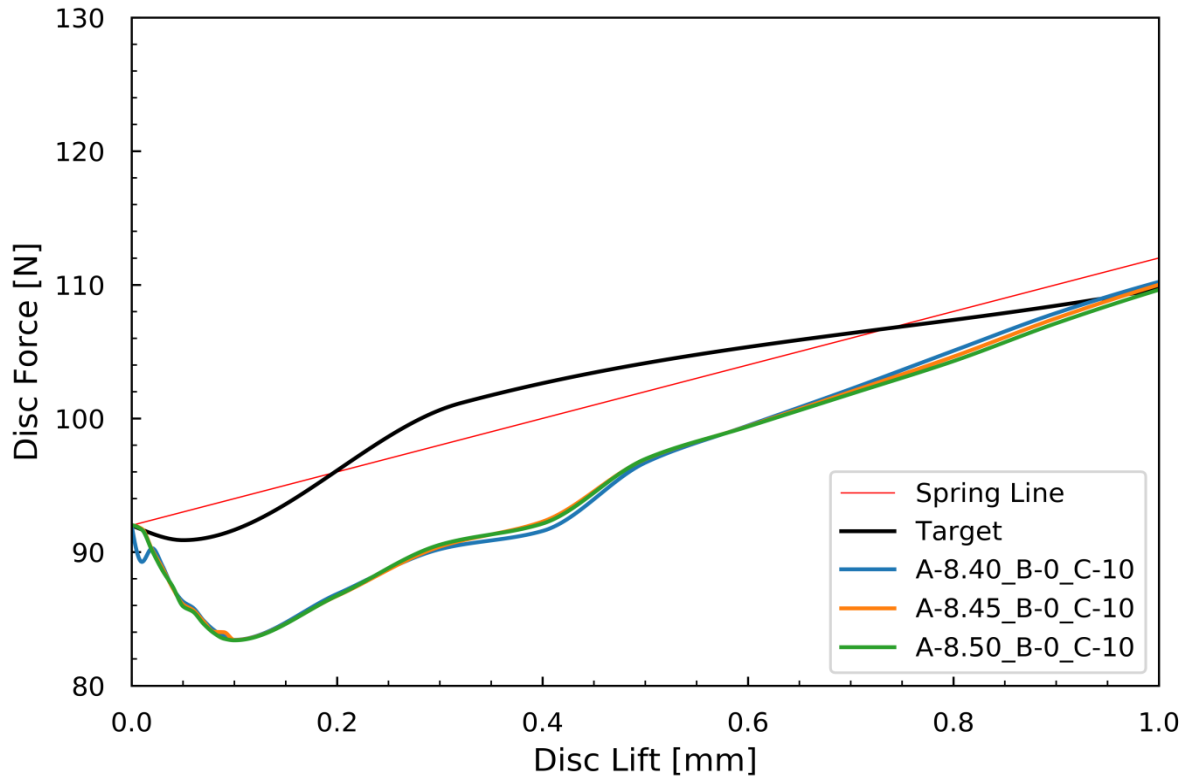


Figure A1.4 - Parameter A 8.40-8.50, B 0.00, C 0.10.

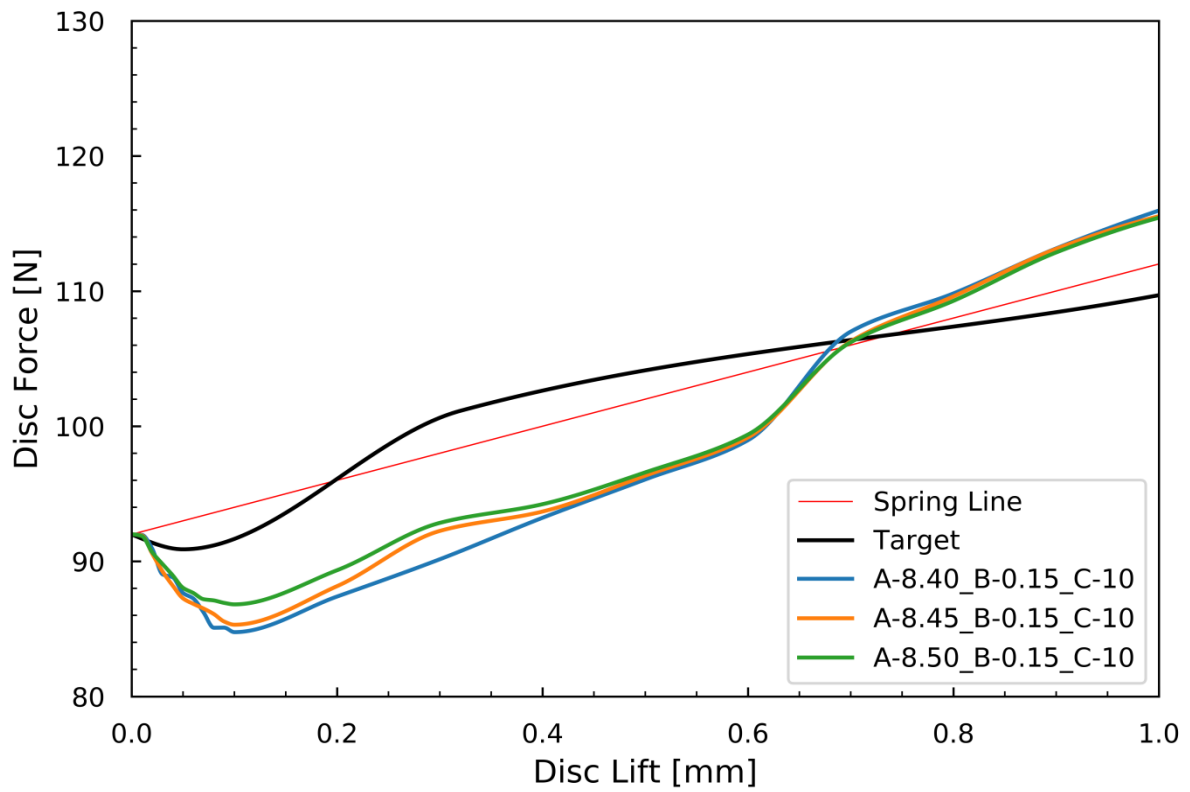


Figure A1.5 - Parameter A 8.40-8.50, B 0.15, C 0.10.

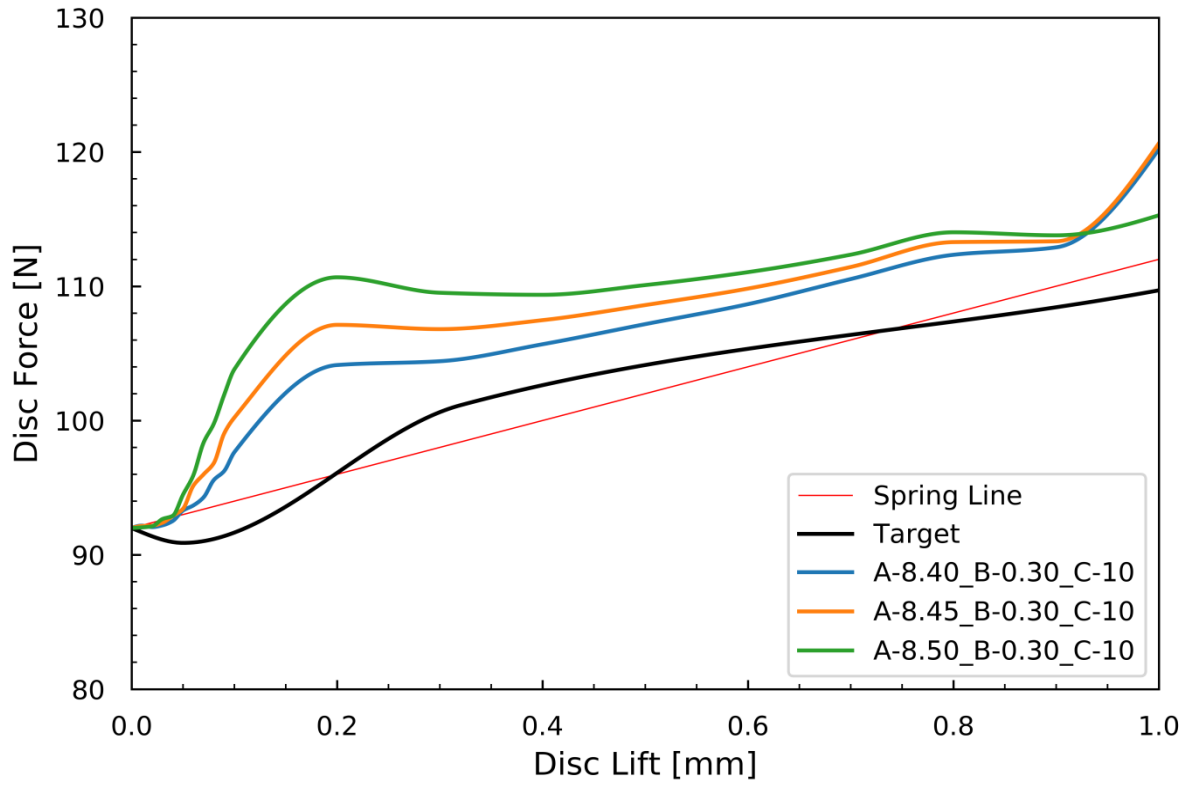


Figure A1.6 - Parameter A 8.40-8.50, B 0.30, C 0.10.

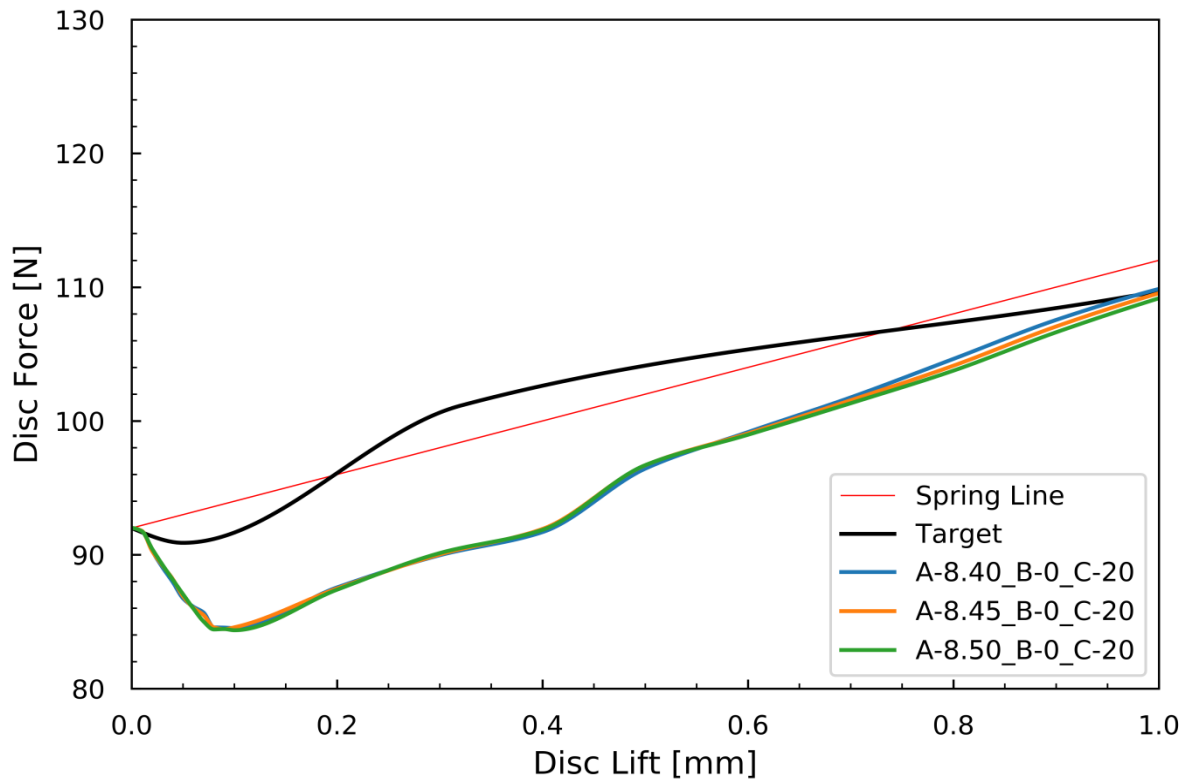


Figure A1.7 - Parameter A 8.40-8.50, B 0.00, C 0.20.

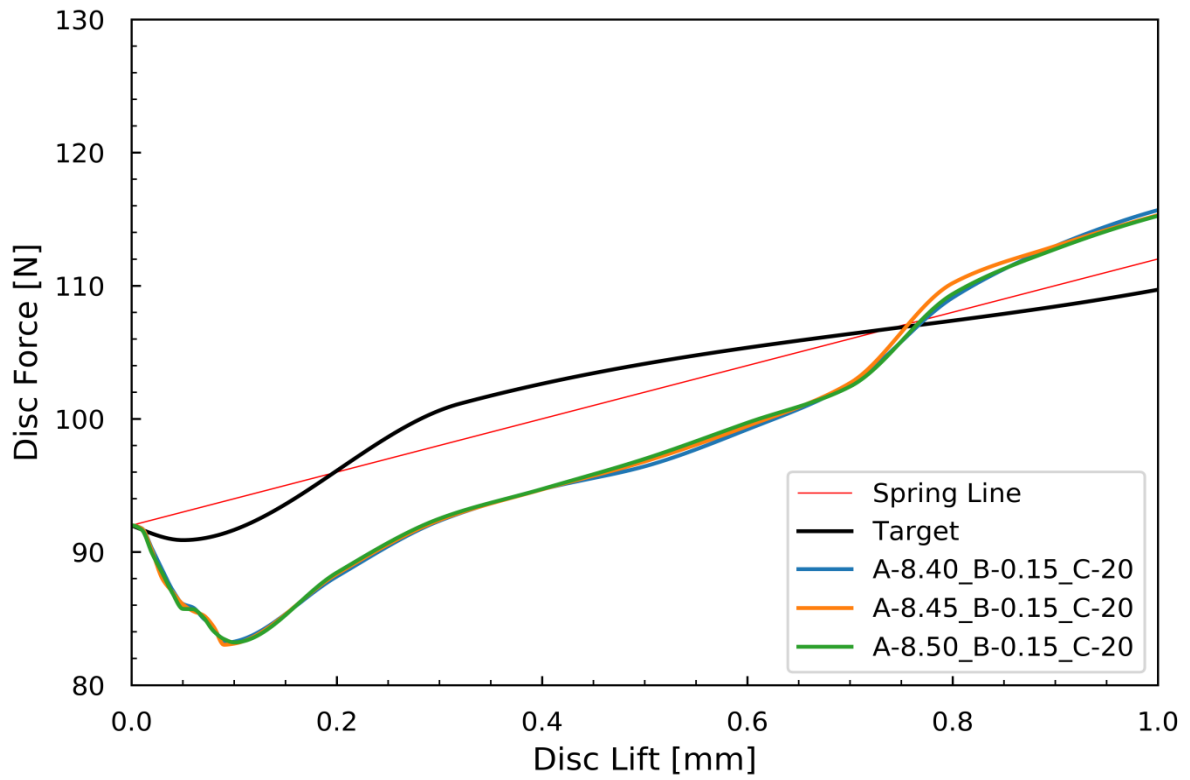


Figure A1.8 - Parameter A 8.40-8.50, B 0.15, C 0.20.

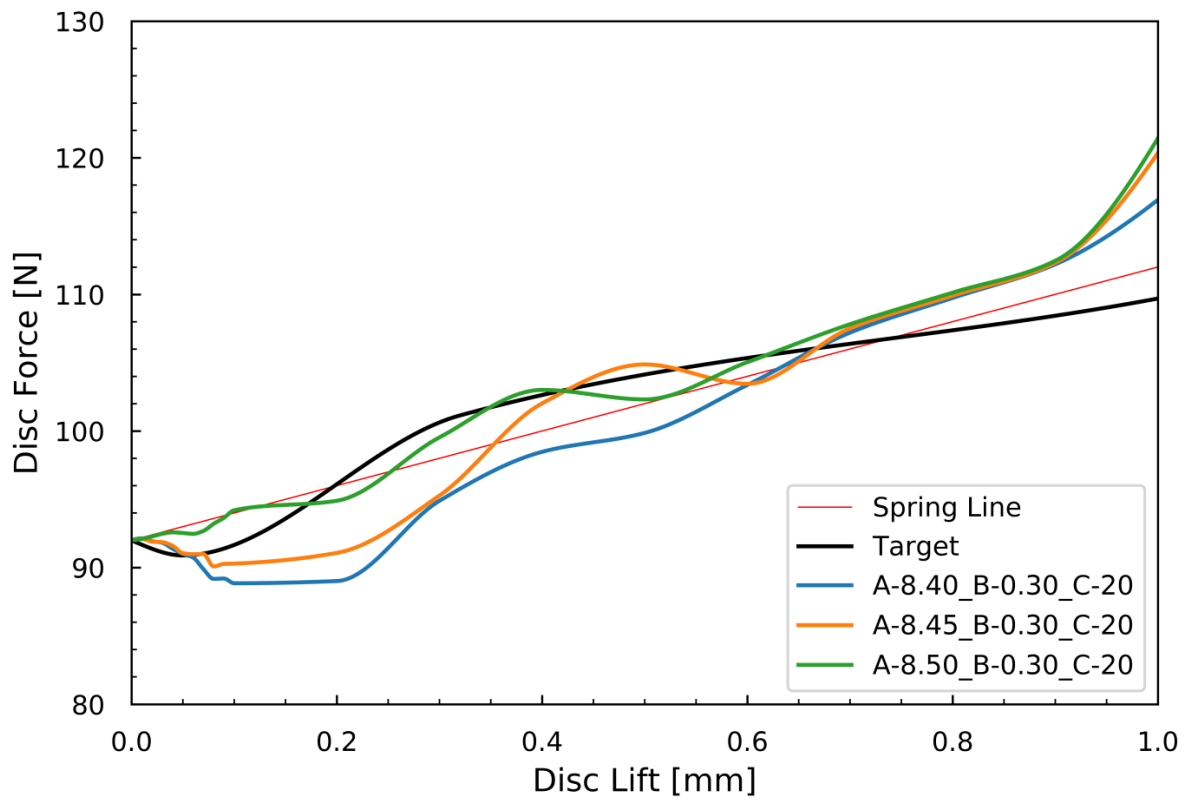


Figure A1.9 - Parameter A 8.40-8.50, B 0.30, C 0.20.

A.2 High-lift Design Space Exploration

This section presents the force data obtained when exploring the design space for the high lift optimisation. The lettering refers to each design parameter which was presented in chapter 5.

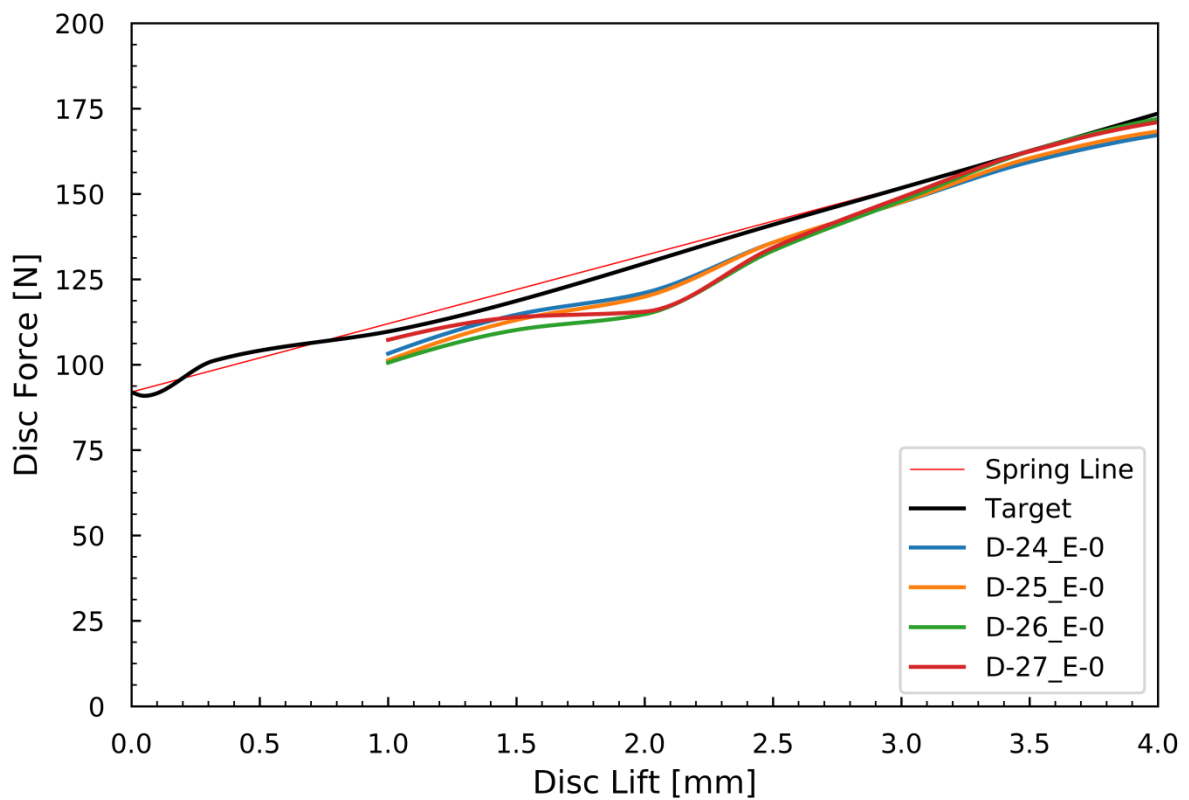


Figure A2.1 - Parameter D 24.0-27.0, E 0.00.

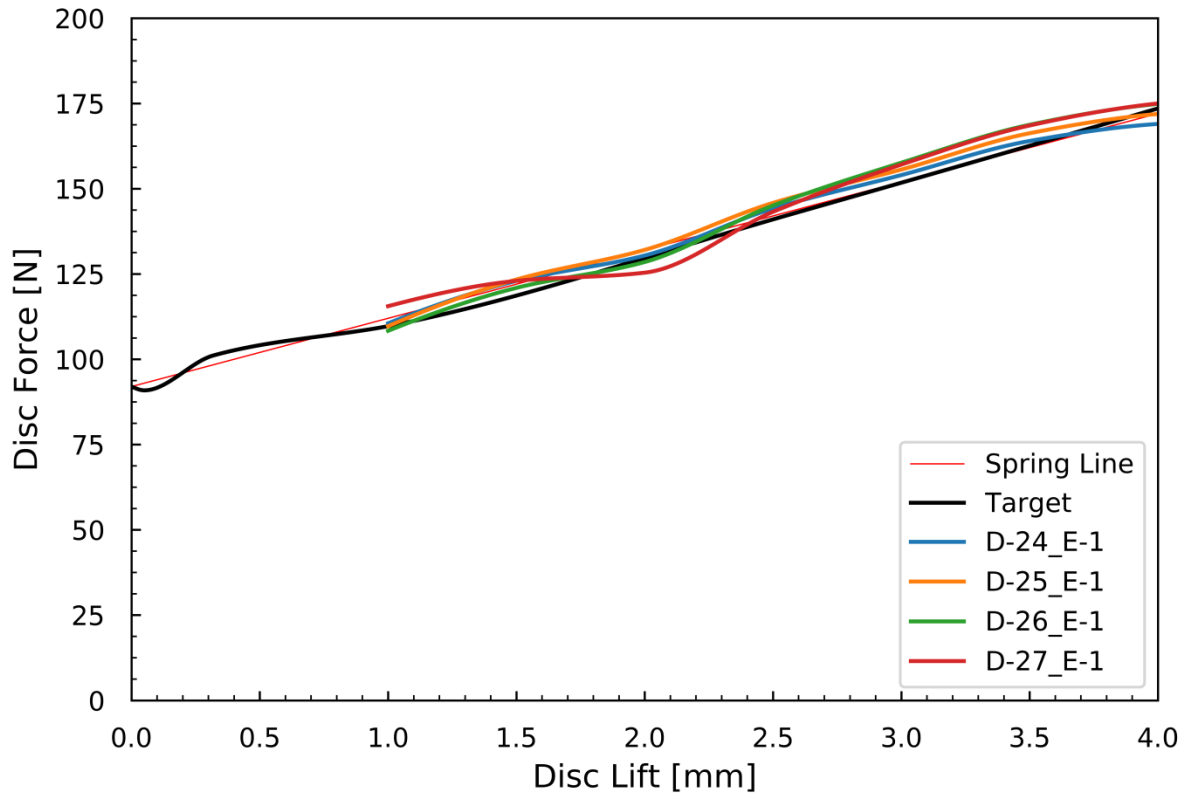


Figure A2.2 - Parameter D 24.0-27.0, E 1.00.

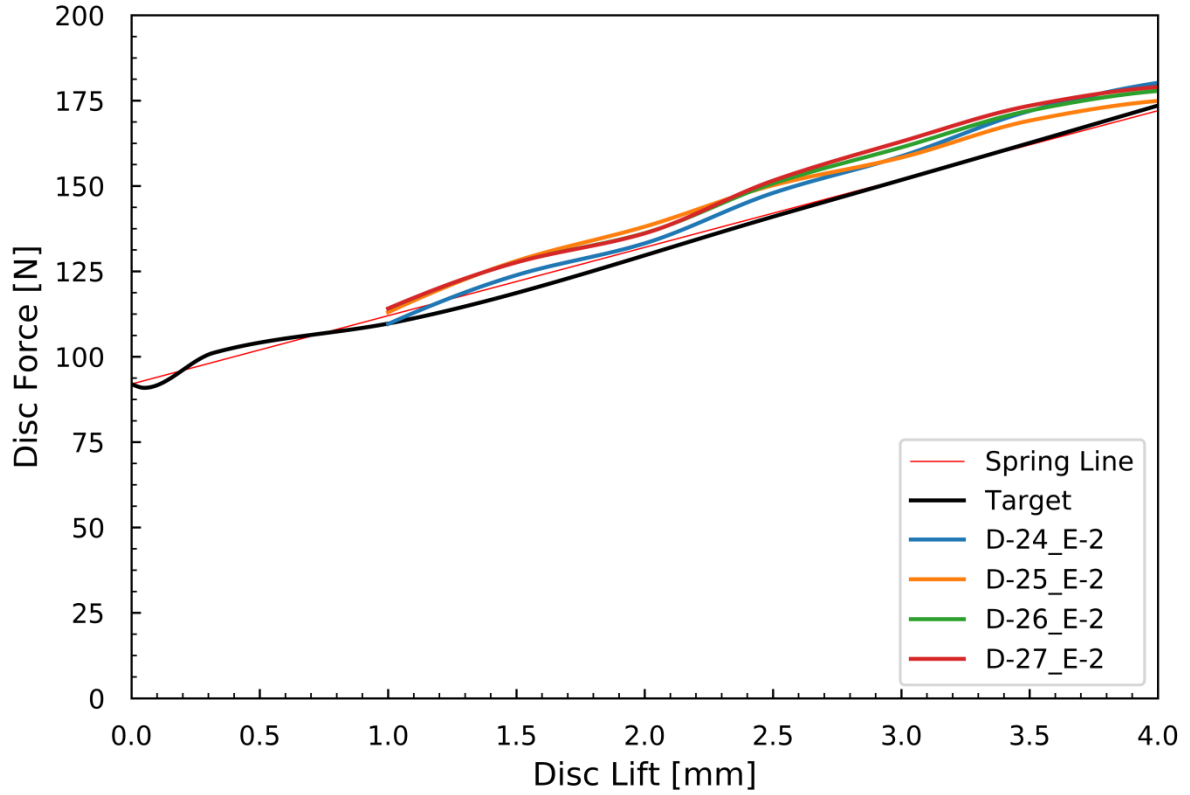


Figure A2.3 - Parameter D 24.0-27.0, E 2.00.

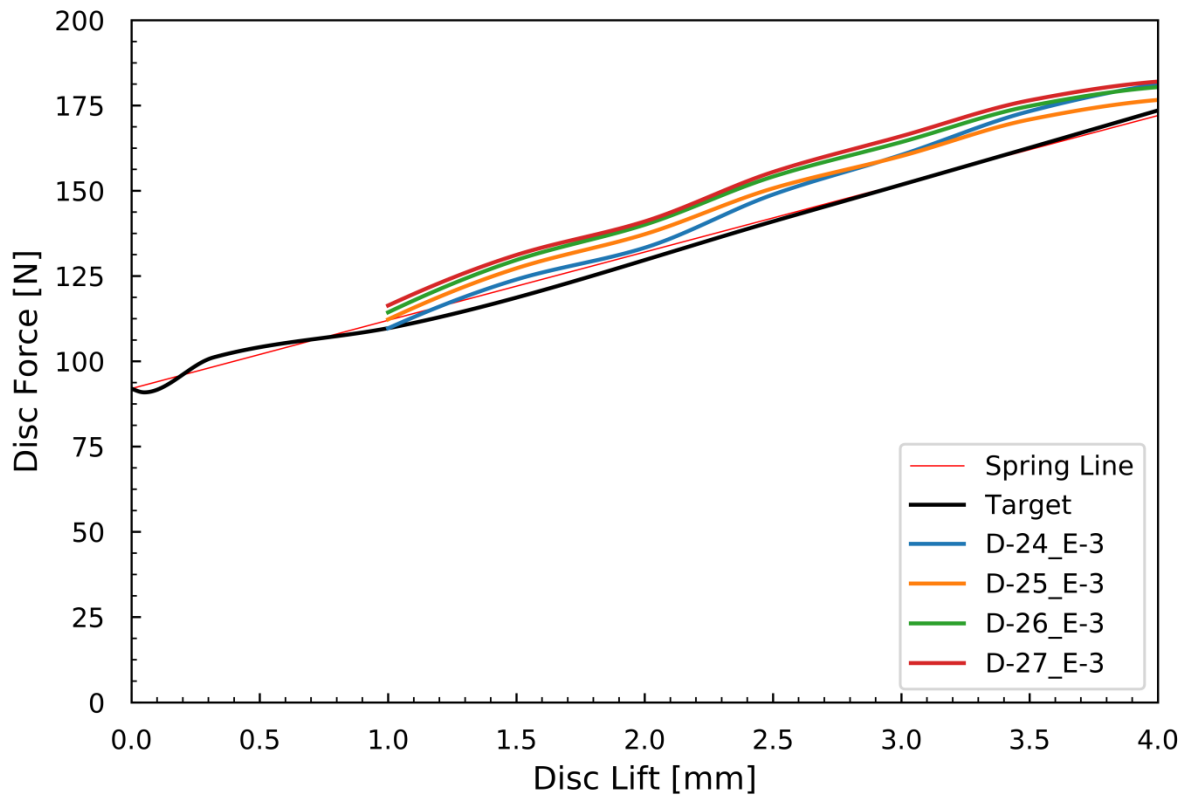


Figure A2.4 - Parameter D 24.0-27.0, E 3.00.

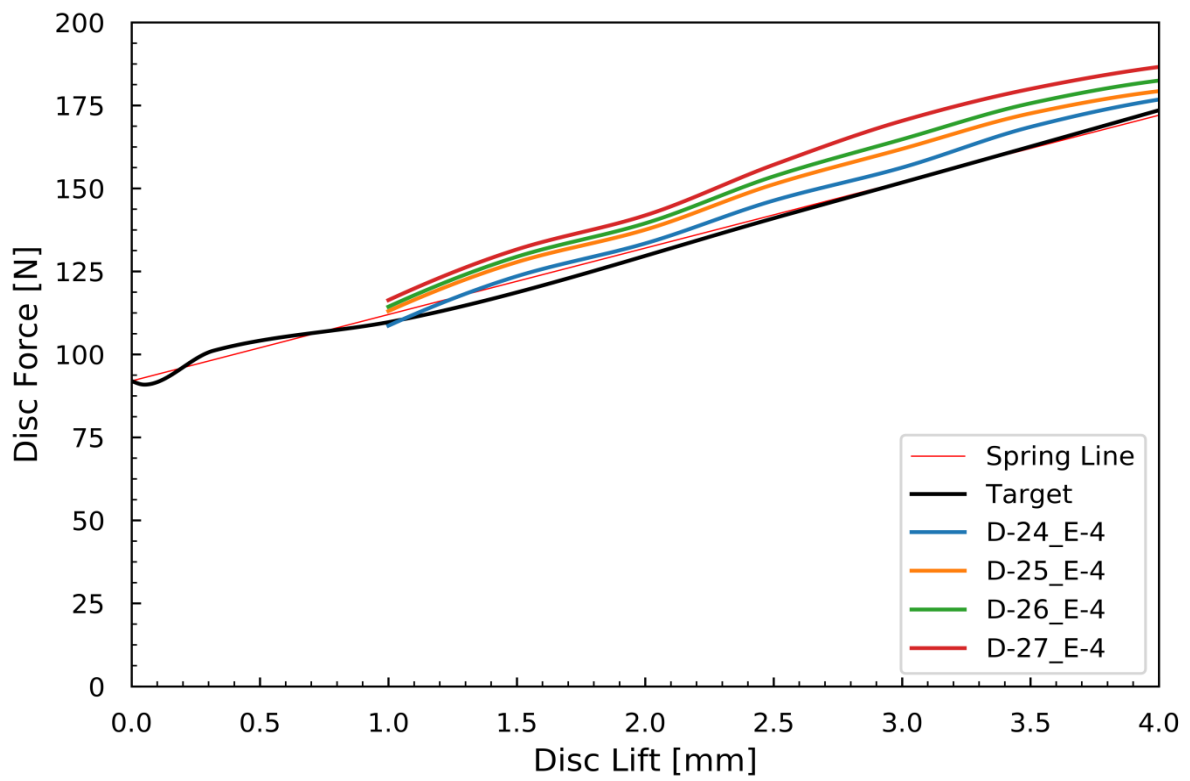


Figure A2.5 - Parameter D 24.0-27.0, E 4.00.

A.3 Low-order Valve Model Matlab Code

```
function [OP, BD] = broady_3500

    tspan=[0,40];
    ic=[4.95e6,296,0,0,0,0,60];
    options=odeset('AbsTol',1e-8,'RelTol',1e-11,'InitialStep',0.00000001);
    [t,y]=ode45(@(t,y) 50barg (t,y(1),y(2),y(3),y(4),y(5),y(6),tspan(2)),tspan,ic,options);

    %Output vector read
    p = y(:,1);
    x = y(:,5);

    %Blowdown calculation.
    BD = ((5e6 - (p(end)))/ 5e6)*100;

    %Overpressure calculation.
    OP = ((max(p) - 5e6) / 5e6)*100;

    csvwrite('p.txt',p);
    csvwrite('t.txt',t);
    csvwrite('x.txt',x);

    %Blowdown & overpressure print out.
    fprintf ('\n');
    fprintf ('Blowdown : %.3f',BD);
    fprintf ('\n');
    fprintf ('Overpressure : %.3f', OP);
    fprintf ('\n');

    %Lift graph
    figure('color','w')
    plot(t,y(:,5),'-k')
    grid on
    grid minor
    xlabel('Time (s)')
    ylabel('Lift (m)')
    title(' lift vs Time' )

    % Pressure Graph
    figure
    hold on
    plot(t,y(:,1),'-k')
    grid on
    grid minor
    xlabel('Time (s)')
    ylabel('Pressure (Pa)')
    title(' Pressure vs Time' )
    hold off

end

function y = 50barg(t,P,T,~,~,x,ve,tfinal)

    % Timer
    fprintf('TIME: %.3f of %.3f\n',t,tfinal)

    % Model constants
    V = 1.5;           %% tank volume
    g = 9.81;         %% gravitational constant
    R=287;            %% ideal gas constant
    Cp=1005;         %% specific heat capacity of air
    gamma=1.4;       %% heat capacity ratio
    d=0.01393;       %% Inlet diameter
```

```

A_i=pi*(d/2)^2; %% Inlet area
P_atm=101000; %% atmospheric pressure
P_set=5e6; %% set pressure
T_atm=293; %% atmospheric temperature
T_o=288; %% Inlet gas temperature
ma=0.651; %% mass of moving parts
k=210000; %% spring stiffness
c=1; %%Damping coefficient

% Discharge coefficient and flow area

CD=0.2;
A=3.14*d*x;
if A>A_i
    A=A_i;
end

if A < 0
    A = 0;
end

% Choked/subsonic conditions

if P_atm/P>0.5283
    P_prime=P_atm;
    T_prime=T_atm;
else
    P_prime=0.5283*P;
    T_prime=0.833*T;
end

% Mass flow rate(algebraic_eqn)

m_e=A*CD*(P_prime/(R*T_prime))*(2*Cp*T*(1-(P_prime/P)^((gamma-1)/gamma)))^0.5;

if (1-P_prime/P)<=0
    m_e=0;
end

m_i=0.2;
if t>14.3
    m_i=0;
end

% Mass rate of change of vessel
m_v=m_i-m_e;

% ODEs
dP=(1/V)*(Cp*(gamma-1)*(m_i*T_o-m_e*T)); %% change in pressure of the vessel
dT=(T/P)*dP-((R*T^2)/(P*V))*(m_v); %% change in temperature of the vessel
dm_e=m_e; %% amount of mass to leave vessel
dm_v=m_v; %% mass change of vessel
dx=ve; %% rate of change of disc position

% Valve opening and closing limits.
if x>0.004
    if dx>0
        dx=0;
    end
end

if x<1e-10
    if dx<0
        dx=0;
    end
end

% Force constants.
% Inputs from physical data, x_1 vector comprises of the x-components of the
% force/lift plot measured in the lab, y_1 vector is the corresponding y
% components. Y values (forces) have been non-dimensionalised with respect
% to the inlet pressure.

x_1 = [0 ... 0.004];
y_1 = [0.000186000000 ... 0.000355932000];

```

```

% pchip interpolation
% Cubic interpolation function used to obtain the force component over the
% full range of opening of the valve.

f_1 = pchip(x_1,y_1,x);

% Disc force
% Disc force comprises of the flow force minus the preload on the disc. The
% preload is the first component in the y_1 vector i.e. the force value at
% 0mm lift.

F=(f_1*P)-930;

% Net force acting on the disc.
nf = F;

% Rate of change of disc velocity with limits.

dve=(F-c*ve-k*x)/(ma);

if x < 1e-10
    if dve < 0
        dve = 0;
    end
end

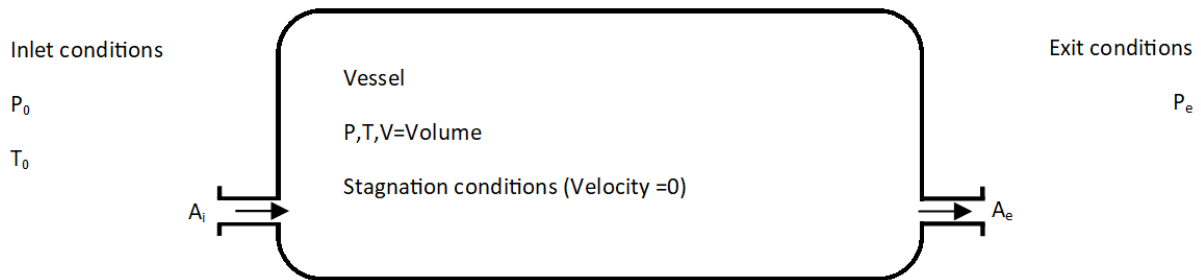
% Output vector
y=[dP;dT;dm_e;dm_v;dx;dve;nf];

end

```

A.4 Quasi-Steady Flow

In certain applications with short ducts a flow can be treated as steady state even if the flow properties are varying with time. Such flows are termed quasi-steady flow and can be analysed by using steady flow equations in combination with the laws of thermodynamics.



The inflow and outflow are via short ducts where the flow is assumed to be quasi-steady. Due to the much larger flow area inside the vessel the gas is assumed to have negligible velocity and the fluid conditions are uniform at any given instant. Assuming that the inlet and outlet are convergent nozzles the isentropic efficiency will be accounted for by using a coefficient of discharge C_D .

Applying the 1st law of thermodynamics gives

$$\begin{array}{ccccccc} E & + & E & = & E & + & E & + & \text{Work done} \\ \text{Initially} & & \text{Entering} & & \text{Finally in} & & \text{Leaving with} & & \\ \text{in Vessel} & & \text{with Inflow} & & \text{Vessel} & & \text{Outflow} & & \end{array}$$

Where E is energy

$$\text{Thus} \quad \left(\frac{dE}{dt}\right)_V = \dot{m}_i h_o - \dot{m}_e h_v - p \frac{dV}{dt}$$

Where $\left(\frac{dE}{dt}\right)_V$ is the rate of change of internal energy within the volume V, \dot{m}_i is the mass flow rate into the vessel volume V and \dot{m}_e is the mass flow rate leaving the vessel.

Giving

$$\frac{d(m_v C_v T)}{dt} = \dot{m}_i C_p T_o - \dot{m}_e C_p T - p \frac{dV}{dT}$$

Since

$$PV = m_v RT$$

$$m_v C_v T = \frac{PVC_v}{R} = \frac{PV}{(\gamma - 1)}$$

Hence

$$\frac{1}{\gamma-1} \left[V \frac{dP}{dt} + P \frac{dV}{dt} \right] = \dot{m}_i C_p T_o - \dot{m}_e C_p T - p \frac{dV}{dt} \quad (1)$$

$$\frac{dP}{dt} = \frac{1}{V} \left[C_p (\gamma - 1) (\dot{m}_i T_o - \dot{m}_e T) - \gamma P \frac{dV}{dt} \right]$$

Using $PV = m_v RT$

$$\frac{dT}{dt} = \frac{T}{V} \frac{dV}{dt} + \frac{T}{P} \frac{dP}{dt} - \frac{RT^2}{V} \frac{dm_v}{dt} \quad (2)$$

The vessel volume change will be known as a function of time thus

$$\frac{dV}{dt} = f_v(t) \quad (3)$$

The inflow is given as

$$\dot{m}_i = \left(\frac{dm}{dt} \right)_i = A_i C_{Di} \frac{P'_i}{RT'_i} \left[2C_p T_o \left(1 - \left(\frac{P'_i}{P_o} \right)^{\frac{\gamma-1}{\gamma}} \right) \right]^{\frac{1}{2}} \quad (4)$$

Where P'_i and T'_i are the pressure and temperature at the outlet plane of the nozzle. If the flow at the outlet is subsonic then $P'_i = P$ and T'_i is obtained from the isentropic relationship. If the Mach number is unity at the exit then P'_i can be different from P and P'_i is obtained using P_o and the critical pressure ratio.

Thus

$$P'_i = P \text{ if } \frac{P}{P_o} > r_{p \text{ critical}}$$

And

$$P'_i = P_o r_{p \text{ critical}} \text{ if } \frac{P}{P_o} \leq r_{p \text{ critical}}$$

For outflow

$$\dot{m}_e = \left(\frac{dm}{dt} \right)_e = A_e C_{De} \frac{P'_e}{RT'_e} \left[2C_p T \left(1 - \left(\frac{P'_e}{P} \right)^{\frac{\gamma-1}{\gamma}} \right) \right]^{\frac{1}{2}} \quad (5)$$

With

$$P'_e = P_e \text{ if } \frac{P_e}{P} > r_{p \text{ critical}}$$

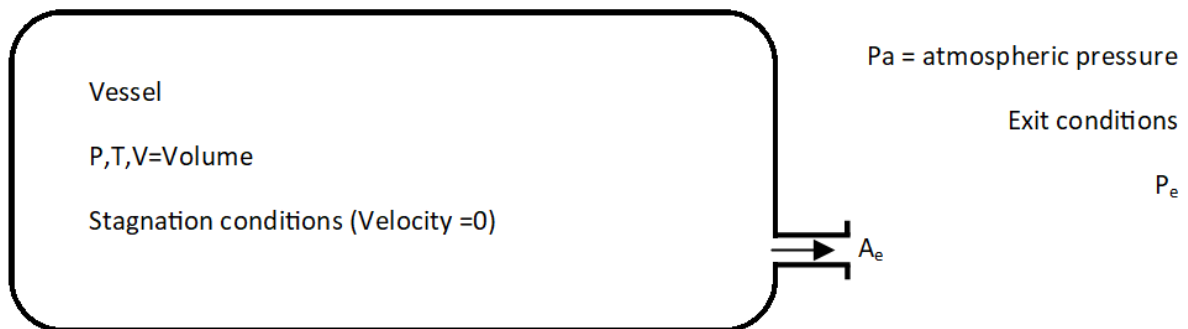
And

$$P'_e = P r_{p \text{ critical}} \text{ if } \frac{P_e}{P} \leq r_{p \text{ critical}}$$

And for conservation of mass

$$\left(\frac{dm}{dt}\right)_V = \left(\frac{dm}{dt}\right)_i - \left(\frac{dm}{dt}\right)_e \quad (6)$$

Modelling the blowdown of a vessel the equations become



$$\frac{dP}{dt} = \frac{1}{V} [C_p(\gamma - 1)(-\dot{m}_e T)]$$

$$\frac{dT}{dt} = \frac{T}{P} - \frac{RT^2}{PV} \frac{dm_v}{dt}$$

$$\dot{m}_e = \left(\frac{dm}{dt}\right)_e = A_e C_{De} \frac{P'_e}{RT'_e} \left[2C_p T \left(1 - \left(\frac{P'_e}{P}\right)^{\frac{\gamma-1}{\gamma}} \right) \right]^{\frac{1}{2}}$$

With

$$P'_e = P_a \text{ if } \frac{P_a}{P} > 0.5283$$

And

$$P'_e = P 0.5283 \text{ if } \frac{P_a}{P} \leq 0.5283$$